



UNIVERSITÀ DEGLI STUDI DI SALERNO



UNIVERSITÀ DEGLI STUDI DI SALERNO
Dipartimento di Farmacia

PhD Program
in **Drug Discovery and Development**
XXX Cycle — Academic Year 2017/2018

PhD Thesis in

***PGI products of Campania region:
chemical and biological investigation of
edible parts and by-products as potential
sources of functional ingredients for
herbal, nutraceutical and cosmetic
formulations.***

Candidate

Antonietta Cerulli

Supervisor(s)

Prof. *Sonia Piacente*

PhD Program Coordinator: Prof. Dr. *Gianluca Sbardella*

Table of contents

Introduction..... 1

Chapter 1: Phytochemical investigation of *Corylus avellana* cv. Tonda di Giffoni leaves

1.1. Giffonins A-P, Antioxidant Cyclic Diarylheptanoids from the Leaves of Corylus avellana cv. Tonda di Giffoni

1.1.1 LC-ESI/LTQOrbitrap/MS/MSⁿ analysis..... 13

1.1.2. Results and discussion..... 17

1.1.3 Biological activity 57

1.2. Metabolite profiling of “green” extracts of Corylus avellana leaves by 1H NMR spectroscopy and multivariate statistical analysis

1.2.1 Results and discussion..... 63

1.3 Conclusion 82

1.4. Experimental section..... 83

References 100

Chapter 2: Byproducts of *Corylus avellana* cv. Tonda di Giffoni: phytochemical study of flowers, green leafy covers and shells

2.1 Quali-quantitative analysis of the phenolic fraction of the flowers of Corylus avellana, cv. Tonda di Giffoni: isolation of antioxidant diarylheptanoids

2.1.1. Results and discussion..... 108

2.1.2. Biological activity 123

2.2. Cyclic Diarylheptanoids from Corylus avellana cv. Tonda di Giffoni Green Leafy Covers: Determination of Their Absolute Configurations and Evaluation of Their Antioxidant and Antimicrobial Activities

2.2.1 LC-ESI/LTQOrbitrap/MS/MSⁿ analysis..... 126

2.2.2. Results and discussions 127

2.2.3. Biological assay 145

2.3. LC-MS profiling highlights Hazelnut (cv. Tonda di Giffoni PGI) shells as a byproduct rich in antioxidant phenolics.

2.3.1. Results and discussions 154

2.3.2. Biological assay. 172

2.4. Conclusion 172

2.5. *Experimental section* 173

References..... 188

Chapter 3: Multi-class polar lipid profiling of fresh and roasted hazelnut (*Corylus avellana* cv. Tonda di Giffoni) by LC-ESI/LTQOrbitrap/MS/MSⁿ

3.1. *Results and discussion*..... 196

3.2. *Conclusion*..... 237

3.3. *Experimental section* 238

References..... 240

Chapter 4: Byproducts of *Castanea sativa* source of the Italian PGI Product “Marrone di Roccadaspide”: phytochemical investigation of leaves and shells

4.1. *Phenolics from *Castanea sativa* leaves and their effects on UVB-induced damage*

4.1.1. *Results and discussion* 249

4.1.2. *Biological activity*..... 254

4.2. *Evaluation of the biological activity of the MeOH extract of the different parts (leaves, burs, green burs, shells, chestnut) of *C. sativa*, cv. Marrone di Roccadaspide*..... 258

4.3. *Phytochemical investigation of MeOH extract of *C. sativa* cv. Marrone di Roccadaspide shells*.

4.3.1. *Results and discussions*..... 262

4.4. *Conclusion*..... 284

4.5. *Experimental section* 285

References..... 296

General experimental procedures..... 303

Conclusion..... 311

Publication list 313

Introduction

The current world production of fruits and vegetables is placed at 429 and 596 million tonne, respectively¹. The waste generated by fruit and vegetable processing industries includes both solids and liquids. In particular, the food waste, can be classified into the following six categories: (a) crop waste and residues; (b) fruit and vegetables by-products; (c) sugar, starch and confectionary industry by-products; (d) oil industry by-products; (e) grain and legume by-products; and (f) distilleries' and breweries' by-products.

The byproducts production is estimated to be approximately 30% of the processed material² (table 1).

Table 1. Percentage of food wastes and by-products in fruit and vegetable production.

Production Process	Waste and by-Products (%)
White wine production	20–30
Red wine production	20–30
Fruit and vegetable juice production	30–50
Fruit and vegetable processing and preservation	5–30
Vegetable oil production	40–70
Sugar production from sugar beet	85

This percentage is due to the global intensification of food production that has led to the creation of large quantities of wastes; generally the disposal of waste materials requests huge price by the industries and farmers.

For this reason, during the last years, the research has developed a great interest for the efficient reutilization of agricultural industry residues; in particular, fruit and vegetable processing by-/co-products are promising sources of valuable substances such as phytochemicals (carotenoids, phenolics, and flavonoids), antioxidants, antimicrobials, vitamins, or dietary fats that possess favorable

technological activities or nutritional properties. Moreover, fruit and vegetable processing residues have traditionally been used in animal nutrition as the main feed ingredients and their effect on animal performance has been extensively studied².

Byproducts of Protected Geographical Indication (PGI) products of Campania region: “Nocciola di Giffoni” and “Marrone di Roccadaspide”.

Horticulture in Campania is a major economic resource with an extremely varying range of products and many valued typical varieties. Typical products are characterized by a strong identification with the land they come from. PDO (Protected Designation of Origin), PGI (Protected Geographical Indication) and TSG (Traditional Specialities Guaranteed) labels in Campania contribute significantly to agricultural economy since producers and consumers have developed a strong sensibility to quality.

In Campania region there are currently 16 registered agriculture products, among which the PGI products “Nocciola di Giffoni” (*Corylus avellana* L.) and “Marrone di Roccadaspide”³ (*Castanea sativa* Mill.).

- “Nocciola di Giffoni”. The Protected Geographical Indication "Nocciola di Giffoni" refers to one of the most appreciated Italian varieties: Tonda di Giffoni.



The distinctive characteristics of the "Nocciola di Giffoni" PGI are represented from the perfectly round shape of the seed (which is the shelled hazelnut), which has a white flesh, consistent, with an aromatic flavor, and a thin and easily detachable perisperm (internal film). "Nocciola di Giffoni" is particularly suitable for roasting, peeling; moreover it is strongly requested by the industries for the production of pasta and grain, as well as, as a raw material, for the preparation of high-quality confectionery specialties.

"Nocciola di Giffoni" production is limited to the Salerno province around the Picentini Mountains and Irno valley⁴. Being a medium-early cultivar, the harvesting of the fruits usually begins as early as the third decade of August, after which the hazelnuts are dried, they are deposited in cool and ventilated places, without odors and humidity³.

- "Marrone di Roccadaspide" has been recognised as a PGI (Protected Geographical Indication) product in 2008.



The distinctive characteristics of the "Marrone di Roccadaspide " are represented by a medium size of the fruit (80-85 fruits per Kg) of a prevalently semi-spherical shape, sometimes roundish. For the valuable characteristics of the fruit, "Marrone di Roccadaspide " is among the few varieties of chestnuts in Campania to be defined botanically "brown type" and is therefore particularly required for industrial processing (over 90% of the commercial destination), infact the industry uses them mainly for the production of marron glacés, jams, chestnuts with rum, and purees³.

"Marrone di Roccadaspide" is considered, together with "Castagna di Montella" PGI and "Castagna di Serino", among the best chestnuts produced in Campania, not only for the quality, but also for the soil and the favorable climate³.

The production area of "Marrone di Roccadaspide PGI" is located in the province of Salerno and in particular in the Alburni area³. The harvesting is carried out during the first decade of November.

The PGI products of Campania region are not only extensively used in the local gastronomy but also represent the Italian products abroad. Italy is the second producer of hazelnut with over 13% after Turkey. Campania is the first Italian

region in the hazelnut production, and in Salerno 90% of the production is given by “Nocciola di Giffoni”. Italy is the leading producer of chestnuts: in Campania, the growing area of PGI “Marrone di Roccadaspide” is very large, and represents about 50% of the production of Salerno province.

The high importance of these products is evident, considering that only the 10-15% of the nuts are used fresh while the remaining part is for the food industry. Even if the nutritive features of these PGI products are well known, in some cases very little is known about their metabolome. A deeper insight on the chemical composition of this PGI products has the purpose to protect the reputation of the regional foods, to promote rural and agricultural activity, to help producers to obtain a premium price for their authentic products, and to eliminate the unfair competition and misleading of consumers by non-genuine products, which may be of inferior quality.

In particular, attention has been focused on the parts of the plants not edible, which result waste products and represent a large amount of the total biomass of the products. The PGI “Nocciola di Giffoni” hazelnut skin, hazelnut green leafy cover, and hazelnut tree leaf, by-products of roasting, cracking, shelling/hulling, and harvesting processes, respectively, don’t have any commercial value and represent a huge amount of discarded material; also the by-products of the PGI “Marrone di Roccadaspide” such as shell, resulting from the fruit peeling process, wood and leaves represent waste material.

The aim of the present PhD project has been the definition of the metabolome of byproducts and of the edible parts of the selected PGI branded products; particular attention has been paid to the study of waste products as potential sources of bioactive molecules, in order to highlight the occurrence of phytochemicals to use as functional ingredients for nutraceutical, herbal and cosmetic formulations.

Specifically, the objectives achieved during PhD are the following:

- definition of the chemical profile of the different parts of the selected plant species *Corylus avellana* L. cv. Tonda di Giffoni and *Castanea sativa* Mill. cv. Marrone di Roccadaspide;
- development of methods for the qualitative and quantitative analysis of extracts obtained from the different parts of the selected plant species;
- definition of the bioactivity profile of extracts and pure compounds.

Experimental plan

Extraction of the selected parts of plant.

Plant tissue metabolites are highly diverse. Several critical factors must be considered during extraction, such as the ratio of solvent and plant material, solvent characteristics, the time of extraction, the temperature and the choice of an appropriate method for the desired goals. The choice of a solvent is extremely important for the achievement of reliable results because it needs to be adequate for the metabolites targeted for extraction and for the analytical method.³ For this reason, a specific extraction protocol has been developed for each plant raw material, by using traditional extraction procedure or in some cases innovative extraction methods like Naviglio extraction.

Qualitative and quantitative analysis.

Following a qualitative approach (untargeted metabolomics), the extracts obtained from the different parts of the plants have been analyzed by liquid chromatography coupled to mass spectrometry (LC-MS) which is a very useful tool in phytochemistry and food chemistry, allowing to determine in a single analysis a large number of different molecules and, with the utilization of suitable fragmentation experiments and protocols, to obtain information about the structures. In particular LC coupled with electrospray multicollisional Ion trap

(IT) mass spectrometry (LC-ESI(IT)MSⁿ), due to its capacity to rapidly separate, fragment and detect a broad range of small molecules, can be considered a powerful approach for structural characterization in metabolite fingerprinting. Spectrometer with an ion trap analyser allow to run experiments of tandem mass spectrometry and MSⁿ, increasing the number of information obtained by a single LC-MS experiment.

According to this, a high-resolution mass spectrometer has been used (i. e. Orbitrap).

To characterize unequivocally all components of the extracts, off-line isolation protocols have been performed by carrying out sequential fractionating steps with the aid of different chromatographic preparative or semi-preparative techniques. The selection of the different chromatographic protocol depends on the physical-chemical properties of the extracts and the compounds to isolate. The same analytical protocols, when performed in semi-preparative or preparative scale on a partially purified extract can lead to a fast isolation of interesting compounds.

The structural determination of pure compounds has been performed by Mass Spectrometry (MS) and spectroscopic methods like CD, UV, IR but mainly by NMR.

The NMR structural assignment of metabolites has been obtained by 1D-(¹H and ¹³C) and 2D-NMR (DQF-COSY, HSQC, HMBC, TOCSY, ROESY).

In particular, the NMR structural assignment of plant metabolites has been carried out acquiring scalar coupling homonuclear spectra (1D-TOCSY, 2D-TOCSY, COSY) for the determination of the molecule spin-systems, heteronuclear spectra (HSQC, HMBC) for the identification of the substitution pattern and for the assembly of the molecule moieties, dipolar coupling homonuclear spectra (NOESY, ROESY) for a further assessment of the substructures contained in the molecule and for the definition of the configurational orientations particularly in those cases with well-defined conformational properties. Moreover, to determine

the relative configuration a combined QM (quantum mechanical)/NMR approach, has been followed in the frame of collaborations.

In some cases, metabolite profiling analysis has been followed by quantitative analyses based on mass spectrometry targeted approach. In particular, LC-ESI/QqQ/MS/MS, with a very sensitive and selective mass tandem experiment such as Multiple Reaction Monitoring (MRM), has been used.

Evaluation of the biological activity of the PGI product extracts and of the pure compounds.

On the basis of the chemical composition of the PGI products, biological assays have been carried out on extracts and pure compounds considering the chemical nature of the isolated metabolites. Preliminarily, in the frame of collaborations, the cytotoxicity has been evaluated to highlight the non-toxic concentration; successively different biological assays have been performed, mainly aimed at evidencing the antioxidant potential of the extracts and pure compounds.

References

1. Waliaveetil, E.; Ramesh, R. *Handbook of Postharvest Technology* (book), **2003**, 819-844.
2. Kasapidou, E.; Sossidou, E.; Mitlianga, P Fruit and Vegetable Co-Products as Functional Feed Ingredients in Farm Animal Nutrition for Improved Product Quality. *Agriculture* **2015**, 5, 1020-1034
3. www.agricolture.regione.campania.it
4. Petriccione, M.; Ciarmiello, L. F.; Boccacci, P.; De Luca, A.; Piccirillo, P., Evaluation of 'Tonda di Giffoni' hazelnut (*Corylus avellana* L.) clones. *Scientia Horticulturae* **2010**, 124, 153-158.

Chapter 1

Phytochemical investigation of *Corylus avellana* cv.

Tonda di Giffoni leaves

Introduction

Hazelnut (*Corylus avellana* L.), belonging to the Betulaceae family, is a tree which may grow up to 6 m, exhibiting deciduous leaves which are rounded, 6–12 cm long, softly hairy on both surfaces, and with a double-serrate margin; hazelnut is one of the most popular tree nuts on a worldwide basis and ranks second in tree nut production after almond. Italy is the second largest producer of hazelnut (13%) after Turkey; the main products of *C. avellana* are kernels, nutritious food with a high content of healthy lipids¹, used by the confectionary industry, consumed raw (with skin) or preferably roasted (without skin). The leaves of *C. avellana* are used in traditional medicine for the treatment of varicose veins and hemorrhoidal symptoms and also for their mild antimicrobial effects². Antioxidant activity has been reported for hazelnuts and leaves of *C. avellana*¹. Previous phytochemical investigations on the leaves resulted in the isolation of phenolic constituents, such as flavonoids, caffeic acid, and linear diarylheptanoid derivatives³.

The Italian “Nocciola di Giffoni”, also known as “Tonda di Giffoni”, is a labeled PGI (Protected Geographical Indication) product of the Campania region, representing an important economic resource.



“Nocciola di Giffoni” trees

Although the nutritive features of the PGI “Nocciola di Giffoni” hazelnut are well known^{4,5}, no studies are reported on the chemical composition of the leaves of *C. avellana*, source of the PGI hazelnut. As part of an ongoing effort to search for

new bioactive compounds from *C. avellana*^{6, 7}, the MeOH extract of the leaves was investigated.

The phytochemical investigation of *C. avellana* cv. Tonda di Giffoni leaves allowed us to isolate and characterize, by 1D and 2D NMR experiments, 16 new cyclic diarylheptanoids and diaryletherheptanoids, some of which highly hydroxylated, named giffonins A-P. Cyclic diarylheptanoids are characterized by a C-C bond between C-1 and C-2 positions of the two aromatic rings, while cyclic diaryletherheptanoids are characterized by an ether linkage between C-1 and C-17 of the two aromatic moieties. In particular, in this chapter the following topics are reported:

- isolation and structural elucidation of giffonins A-I, some of which characterized by the presence of only one stereogenic centre on the heptyl moiety; for these compounds (giffonins B, C and E-H) the absolute configuration has been established through the application of the modified Mosher's method.
- isolation and structural elucidation of giffonins J-P, possessing at least two stereogenic centres on the heptyl unit; in this case a combined QM/NMR approach has been used to establish the relative configurations.
- evaluation of the effects of giffonins A-P on oxidative damage of human plasma lipids, induced by H_2O_2 and H_2O_2/Fe^{2+} .

1.1. Giffonins A-P, Antioxidant Cyclic Diarylheptanoids from the Leaves of *Corylus avellana* cv. Tonda di Giffoni

1.1.1 LC-ESI/LTQOrbitrap/MS/MSⁿ analysis

The leaves of *C. avellana* cv. Tonda di Giffoni (910 g) have been dried and extracted at room temperature using solvents of increasing polarity.

High-performance liquid chromatography coupled to multiple-stage linear ion-trap and orbitrap high-resolution mass spectrometry in negative electrospray ionization mode (LC-ESI/LTQOrbitrap/MS/MSⁿ) analysis, of the MeOH extract of *C. avellana* leaves allowed us to obtain a preliminary plant metabolite profiling.

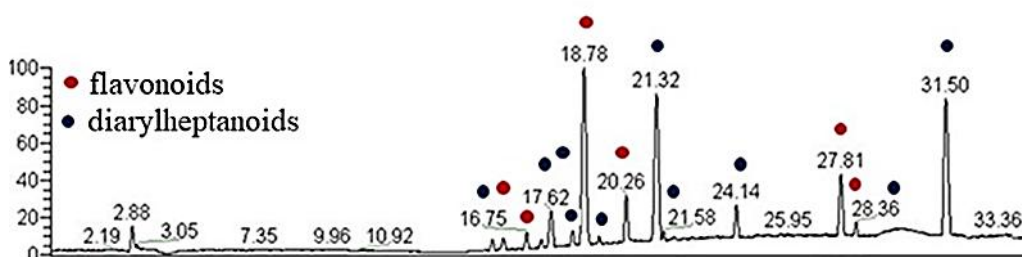


Figure 1.1. LC-MS profile of the MeOH extract of *C. avellana* leaves.

LC-MS profile of the MeOH extract highlighted peaks with m/z values corresponding to a wide range of phenolic compounds. In particular, the LC-MS spectrum showed ions characterized by typical fragmentation patterns of flavonoids, and further peaks suggesting the occurrence of diarylheptanoid derivatives (fig. 1.1).

Diarylheptanoids

Since the first diarylheptanoid isolated in 1815, more than 500 diarylheptanoids have been identified. Diarylheptanoids occur frequently in plants belonging to the Betulaceae family; they represent a class of natural products based on the 1,7-diphenylheptane skeleton that are mainly found in terrestrial plants.

They can be divided into linear or cyclic compounds. There is a smaller number¹² of cyclic diarylheptanoids that are formed from the corresponding linear type by phenolic oxidative coupling, either C-C coupling leading to meta,meta-bridged biaryls or C-O coupling leading to bridged diaryl ethers (fig. 1.2). So, they can be classified into three subgroups, namely linear diarylheptanoids, cyclic diaryletherheptanoids, and cyclic diarylheptanoids (fig. 1.2)¹².

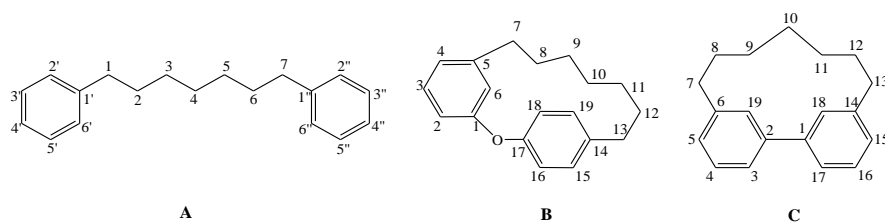
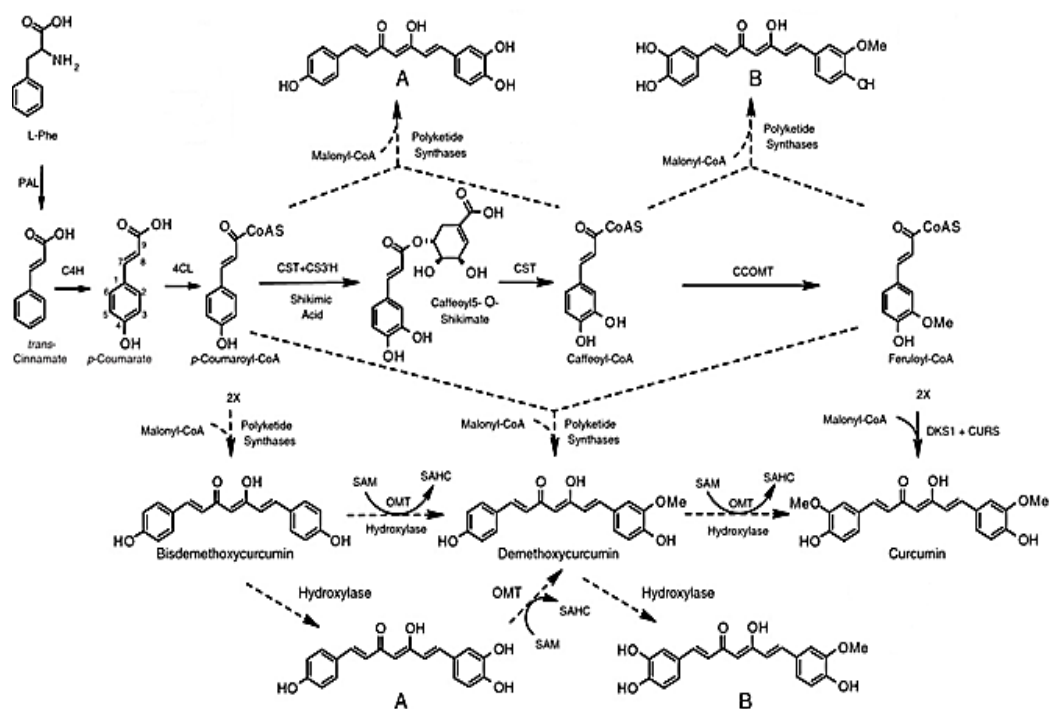


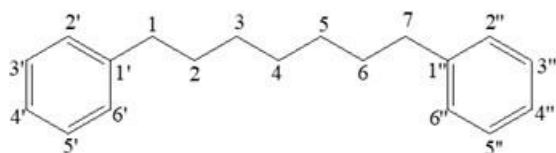
Figure 1.2. A) linear diarylheptanoids; B) macrocyclic diaryletherheptanoids; C) macrocyclic diarylheptanoids.

The biosynthesis of diarylheptanoids starts from L- phenylalanine; which thanks to the action of phenylalanine-ammonia-lyase (PAL) loses the amine group leading to cinnamic acid. The subsequent action of the cinnamate 4-hydroxylase (C4H) converts cinnamate into *p*-coumarate. At this point the concatenated actions of the 4-cumarate CoA ligase (4CL), of the *p*-cumaroyl shikimate transferase (CST) combined with the action of *p*-cumaroyl 5-*O*-shikimate 3'-hydroxylase (CS3'H), leads to the synthesis of caffeoyl-CoA. Finally, the caffeoyl-CoA O-methyltransferase (CCOMT) leads to the feruloyl-CoA, which represents the starting point for the synthesis of most of the diarylheptanoids

known today¹³. The combination of two phenylpropanoid moieties in the form of CoA-esters with malonyl-CoA generates a diarylheptanoid derivative.



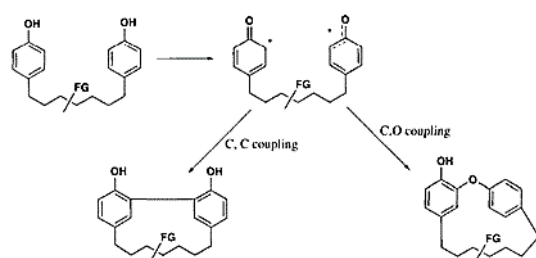
Linear diarylheptanoids are abundant in plants of the genera *Curcuma*, *Zingiber*, *Alpinia* (Zingiberaceae), *Alnus* and *Betula* (Betulaceae). Cyclic diarylheptanoids are distributed in *Myrica* (Myricaceae), *Acer* (Aceraceae), *Garuga* (Burseraceae), *Corylus*, *Betula*, *Carpinus* (Betulaceae), and *Juglans* (Juglandaceae) species¹³.



linear diarylheptanoid

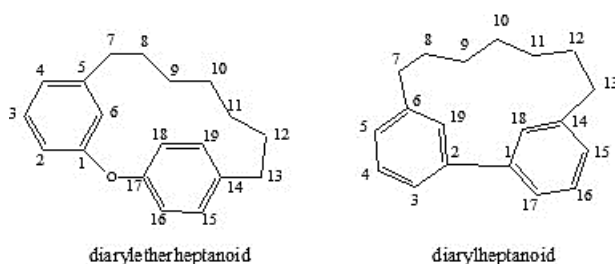
The aromatic rings of linear diarylheptanoids are often hydroxylated or methoxylated. C-4' and C-4'' hydroxyl groups can be acetylated or glycosylated. Natural occurring molecules with unsubstituted aromatic rings are scarce. The aliphatic C-7 chain is either saturated or can have up to three double bonds. Further possibility is the presence of carbonyl groups at C-3 and/or C-5. On the heptane chain hydroxyl groups can be present that may be free or engaged in another function: methyl, acetyl, sulfate or glycosyl groups can be attached. Diarylheptanoids can occur as mono-, di- or triglycosides. The sugar moieties may be further substituted by phenol carboxylic acids. Diarylheptanoids can also possess flavonoid (e.g. chalcone, flavanone) moieties at C-5 or C-7. Dimeric compounds with antiproliferative activity were also isolated from *Alpinia* species, additionally, a chalcone moiety can also be attached to the dimeric diarylheptanoid skeleton¹³.

The co-occurrence of cyclized diarylheptanoids with their corresponding acyclic counterpart in plant such as *A. japonica*, and *Acer Nikoense* provided indication of their biosynthetic relationship.



Intramolecular phenolic oxidative coupling of linear diarylheptanoids, would predict that biphenylcyclophane will be meta, meta bridged in nature, while diphenylether type cyclophane be

meta, para bridged. Such a structural pattern were indeed found in natural products¹³.



Cyclized diarylheptanoids are reported in few species of Betullaceae family, such as *Carpinus cordata*⁸, *Alnus sieboldiana*^{9, 10}, and *Ostryopsis nobilis*¹¹. Cyclic diaryletherheptanoids and cyclic diarylheptanoids show different oxidation pattern on heptanoid chain, characterized by alcoholic and chetonic funtions and cis or trans olefinic bonds; moreover, some cyclic diarylheptanoids show one or more methoxy groups on aromatic ring.

1.1.2 Results and discussion

Isolation and characterization of cyclic diarylheptanoids in the MeOH extract of C. avellana cv. Tonda di Giffoni leaves.

In order to unambiguously elucidate the compounds corresponding to the unknown peaks occurring in the LC-ESI/LTQOrbitrap/MS/MSⁿ spectrum, the MeOH extract was purified by size exclusion chromatography, followed by

further purification steps by reversed-phase using high-performance liquid chromatography equipped with refractive index (HPLC-RI), to obtain 16 compounds. Their structures were established by 1D and 2D-NMR experiments along with ESIMS and ESI/LTQORBITRAP/MS analysis.

The ESI/LTQORBITRAP/MS of **1** (m/z 377.1369 $[M+Na]^+$, calcd for $C_{21}H_{22}O_5Na$, 377.1365) and the ^{13}C NMR data supported a molecular formula of $C_{21}H_{22}O_5$. The IR spectrum showed a band at 1705 cm^{-1} indicative of the presence of a ketocarbonyl group.

The 1H NMR spectrum displayed signals for five aromatic protons ascribable to two aromatic rings: a signal at δ 4.41 (s), typical of the proton of a penta substituted aromatic ring and signals at δ 7.41 (2H, d, $J = 8.3$ Hz) and 7.01 (2H, d, $J = 8.3$ Hz), due to the proton of a 1,4-disubstituted aromatic ring. The 1H NMR data displayed further signals due to a di-substituted trans-olefinic group at δ 6.34 (d, $J = 15.7$ Hz) and 5.20 (dt, $J = 8.0, 15.7$ Hz) and four methylene groups at δ 2.32 (2H, m), 2.44 (2H, t, $J = 5.5$ Hz), 2.86 (2H, t, $J = 5.5$ Hz), and 3.03 (2H, t, $J = 5.5$ Hz) (fig. 1.3 and table 1.1). Moreover, two signals for two methoxy groups at δ 4.00 and 3.67 were evident.

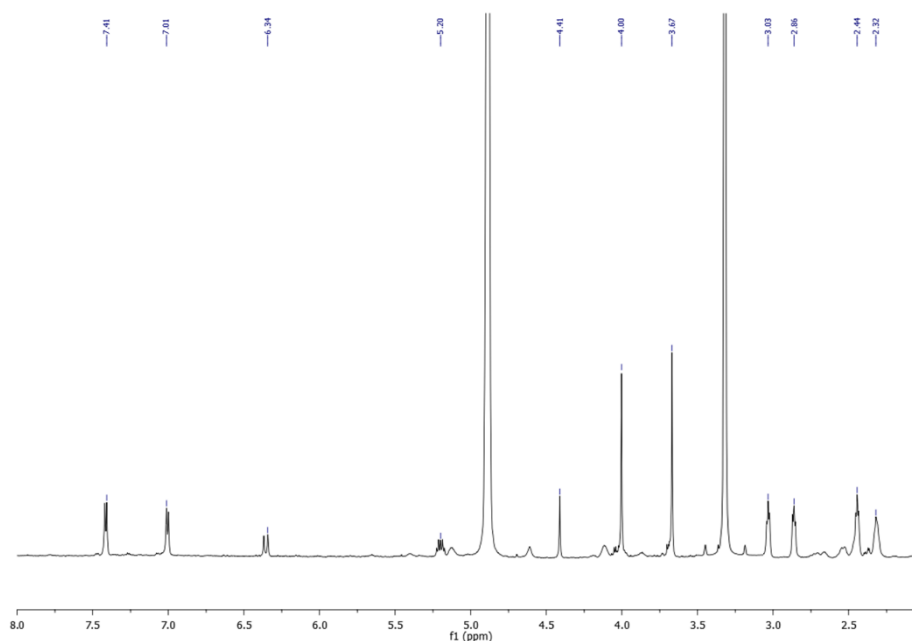


Figure 1.3. ^1H NMR spectrum (600 MHz, CD_3OD) of giffonin A (**1**).

The ^{13}C NMR spectrum of **1** showed 21 carbon signals (table 1.1), typical of diaryletherheptanoid derivatives¹⁴⁻¹⁶, comprising a signal at δ 211.1, ascribable to a ketocarbonyl group. The signal at δ 4.41 was attributed to H-6, which generally resonates at an abnormally high field, due to the anisotropic effect of the A ring in diaryletherheptanoids¹⁵. This observation together with the ROESY correlations of H-6 at δ 4.41 with H-18 (δ 7.01) and H.16 (δ 5.20) suggested the ether linkage between C-1 and C-17 of the aryl moieties. The HMBC correlations of H-6 (δ 4.41) with the ^{13}C NMR resonances at δ 152.7 (C-1), 136.9 (C-2), 140.4 (C-4), 127.8 (C-5), and 125.5 (C-7) suggested the 1,2,3,4-tetrahydroxylation of the A ring. The disposition of the heptanoid chain and the position of the keto group were determined by HSQC, HMBC, and COSY experiments. (fig 1.4-1.6)

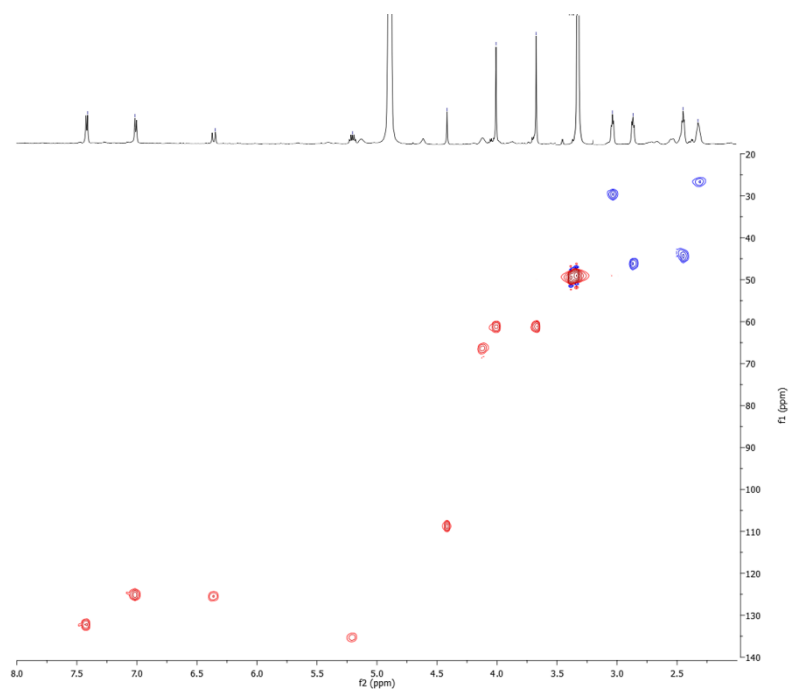


Figure 1.4. HSQC spectrum (CD₃OD) of giffonin A (1).

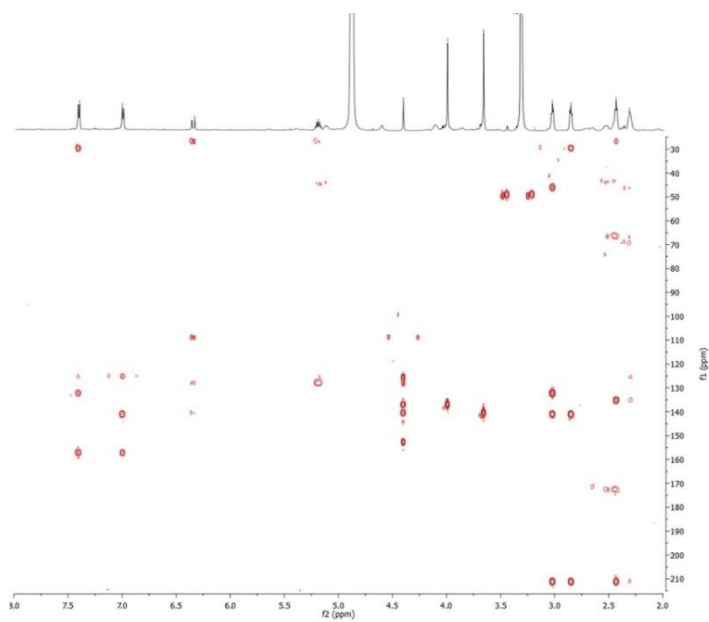


Figure 1.5. HMBC spectrum (CD₃OD) of giffonin A (1).

In the HMBC spectrum of **1**, the methylene protons at δ 3.03 were assigned to C-13 on the basis of their correlations with the ^{13}C NMR resonances at δ 132.2 (C-15 and C-19), 141.0 (C-14), 46.2 (C-12), and 211.1 (C-11) as showed in figures 1.5. The COSY correlation between the methylene protons at δ 3.03 and 2.86 allowed the latter methylene group to be located at C-12, and therefore the keto group to be located at C-11. The HMBC correlations of the proton at δ 6.34 (H-7) with the ^{13}C NMR resonances of the B ring at δ 140.4 (C-4), 127.8 (C-5), and 109.0 (C-6) and the linear connectivity observed in the COSY spectrum from H-7 to H-10 were used to assign the heptanoid chain (fig. 1.6).

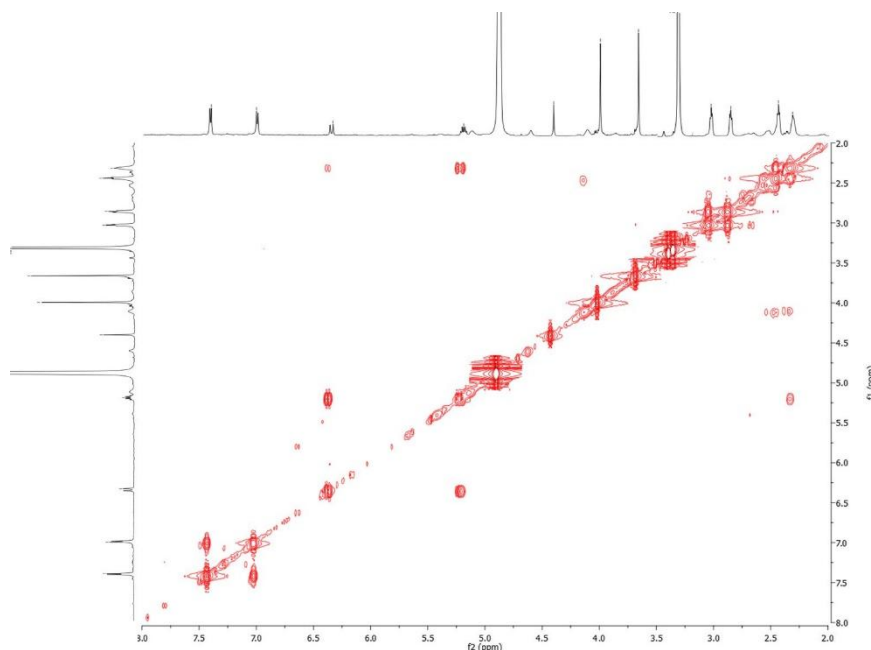


Figure 1.6. COSY spectrum (CD_3OD) of giffonin A (**1**).

Finally, the HMBC correlations between the protons at δ 4.00 and 3.67 with the ^{13}C NMR resonances at δ 136.9 (C-2) and 140.4 (C-4), respectively, allowed the methoxy groups to be located at C-2 and C-4 of the A ring. The foregoing spectroscopic data allowed the structure of compound **1**, named giffonin A, to be assigned as shown (fig. 1.7).

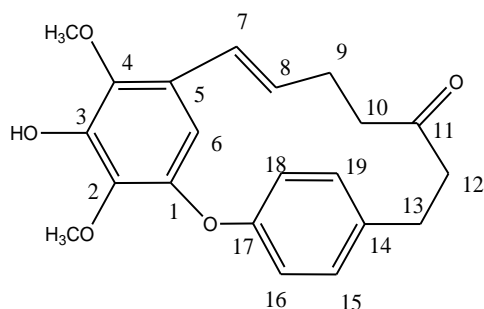


Figure 1.7. giffonin A.

The ESI/LTQORBITRAP/MS of **2** (m/z , 393.1318 $[M+Na]^+$, calcd for $C_{21}H_{22}O_6Na$, 393.1314) and the ^{13}C NMR data supported a molecular formula of $C_{21}H_{22}O_6$. The 1H NMR spectrum displayed five aromatic proton signals, which suggested the occurrence of a penta-substituted [δ 4.39 (s)] and a 1,4-disubstituted aromatic ring [δ 7.70 (dd, $J = 8.3, 1.9$ Hz), 7.45 (dd, $J = 8.3, 1.9$ Hz), 7.16 (dd, $J = 8.3, 1.9$ Hz), 7.00 (dd, $J = 8.3, 1.9$ Hz)] (table 1.1), as in **1**.

The NMR data of **2** revealed that it differed from **1** by the presence of a secondary hydroxy group suggested by a signal at δ 5.23 (dd, $J = 5.4, 8.9$ Hz) (table 1.1). The HMBC correlations of the proton at δ 5.23 with the ^{13}C NMR resonances at δ 131.4 (C-15), 128.4 (C-19), 143.4 (C-14), 54.2 (C-12), and 209.5 (C-11) suggested the secondary hydroxy group to be located at C-13. The presence of hydroxy groups on the heptane moiety causes the different chemical shifts for the corresponding protons on the aromatic ring (H-15 and H-19; H-16 and H-18)¹¹.

The ROESY spectrum showed correlations between H-6 at δ 4.39 and H-8 (δ 5.14). The aromatic proton H-19 at δ 7.70 showed a correlation with the methylene protons H-9 (δ 2.00), and H-13 at δ 5.23 showed a strong correlation with H-15 (δ 7.45).

The absolute configuration at C-13 of compound **2** was determined through the application of the modified Mosher's method¹². Mosher derivatization was performed on compound **2**, which was treated with (*R*)- and (*S*)-MTPA chloride to

form (*S*)-MTPA and (*R*)-MTPA esters, respectively. To determine the absolute configuration of C-13 in **2**, the $\Delta\delta$ ($\delta_S - \delta_R$) values were observed for signals of the protons close to C-13, revealing a $13S$ configuration for **2** (Fig. 1.8). Thus, on the basis of the above data the structure of **2**, named giffonin B, was determined as reported (fig. 1.8).

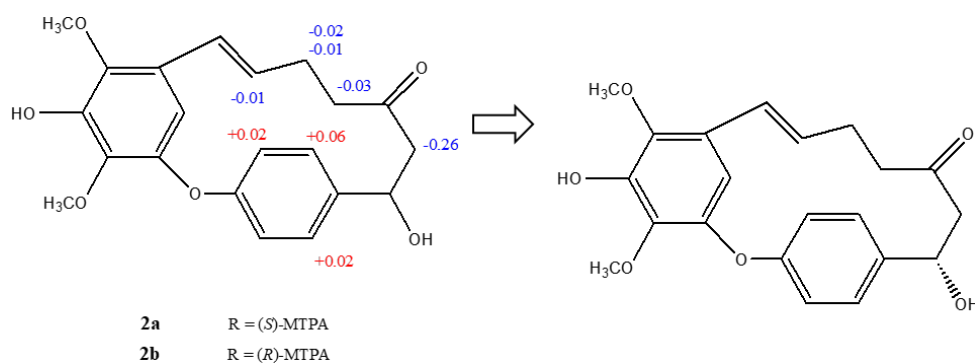


Figure 1.8. giffonin B.

The positive-ion ESI/LTQORBITRAP/MS data of **3** showed a pseudo-molecular ion at m/z 379.1524 $[M+Na]^+$ (calcd for $C_{21}H_{24}O_5Na$, 379.1521), which in combination with the ^{13}C NMR data supported a molecular formula of $C_{21}H_{24}O_5$.

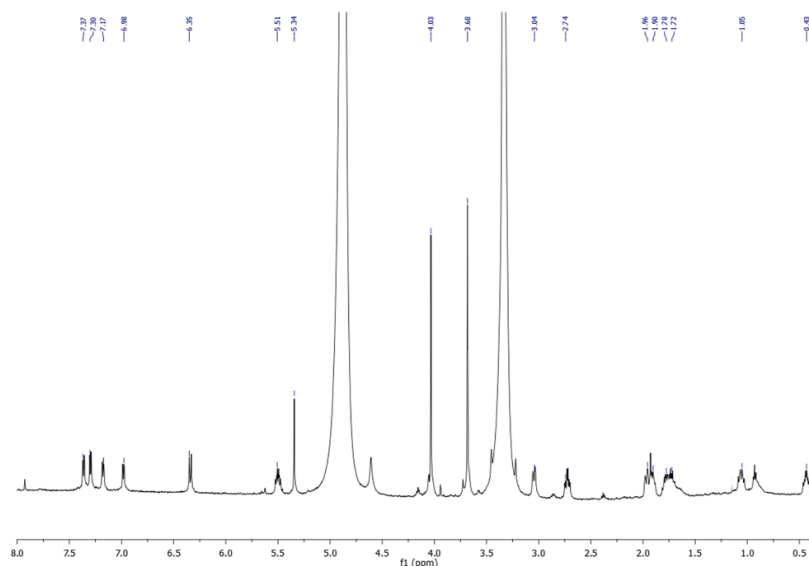


Figure 1.9. 1H NMR spectrum (600 MHz, CD_3OD) of giffonin C (**3**).

Comparison of the ^1H NMR spectrum of **3** in the aromatic region with that of giffonin B (**2**) suggested that they share the same aromatic substitution patterns (table 1.1). Moreover, the ^1H NMR spectrum displayed signals due to a disubstituted *cis* olefinic function at δ 6.35 (d, $J = 11.4$ Hz) and 5.51 (ddd, $J = 11.4, 7.3, 7.3$ Hz), a proton linked to an oxymethine carbon at δ 3.31, and two methoxy groups at δ 4.03 (s) and 3.68 (s) (fig. 1.9 and table 1.1). On the basis of the COSY experiment (fig. 1.10), the connectivity from H-7 to H-13 was established and the hydroxy group was located at C-11 (δ 72.6).

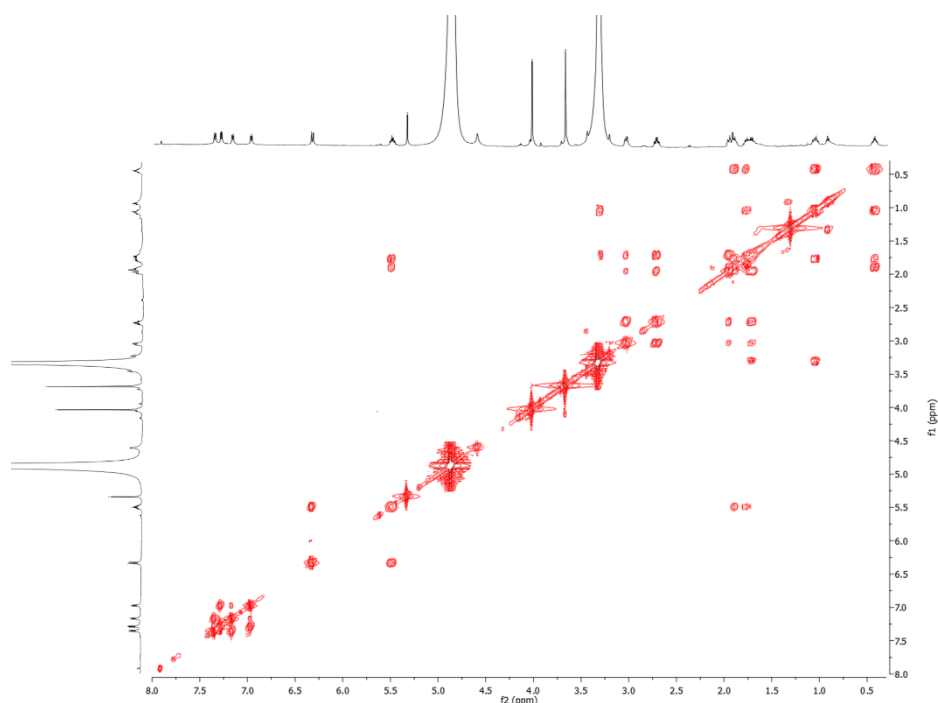


Figure 1.10. COSY spectrum (CD_3OD) of giffonin C (**3**).

The methoxy groups were placed at C-2 and C-4 via the HMBC correlations between the protons at δ 4.03 and 3.68 with the ^{13}C NMR resonances at δ 137.5 and 141.6, respectively (fig. 1.11 and fig 1.12).

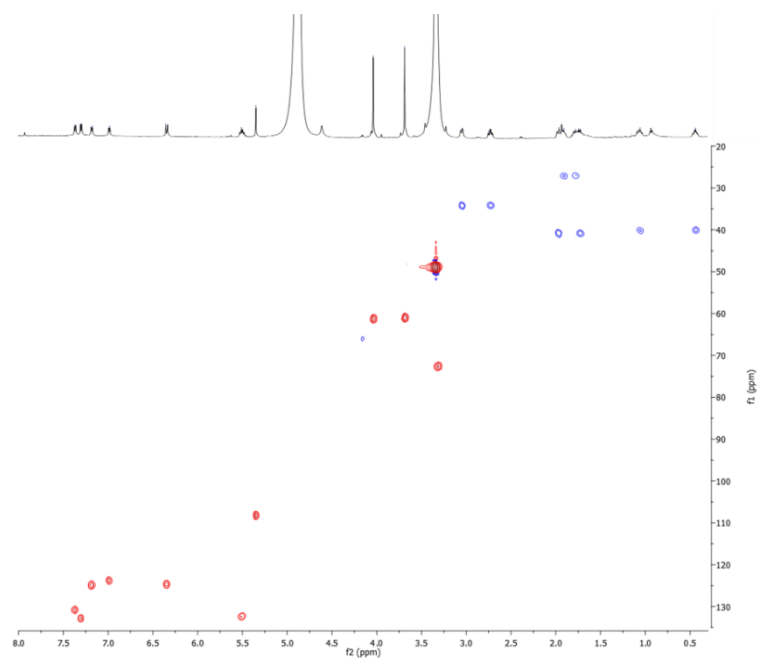


Figure 1.11. HSQC spectrum (CD_3OD) of giffonin C (**3**).

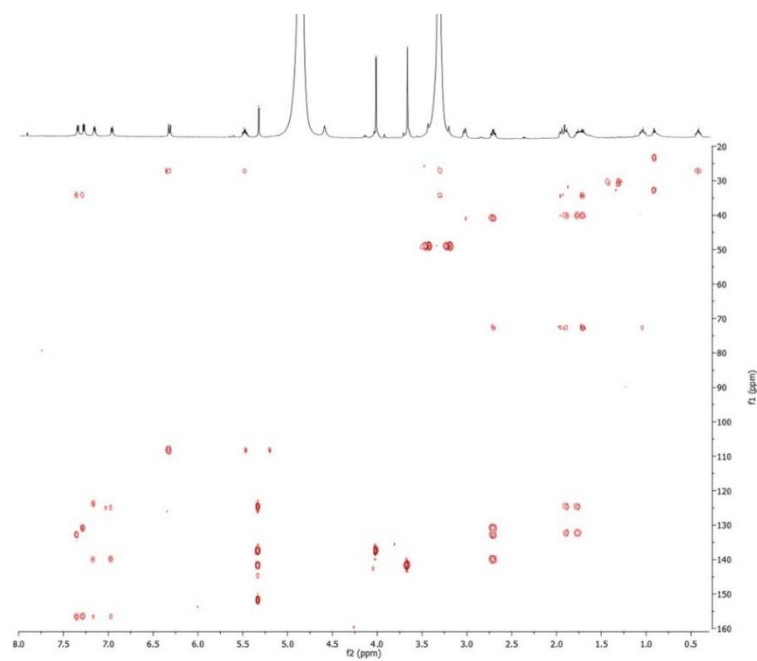


Figure 1.12. HMBC spectrum (CD_3OD) of giffonin C (**3**).

The hydroxy group at C-11, bulkier than a hydrogen atom, should be directed away from the inside of the macrocyclic ring¹⁶.

The ROE correlations between H-15 (δ 7.37) and H-13 β (δ 3.04) and between H-19 (δ 7.30) and H 13 α (δ 2.74) and H-11 (δ 3.31) were observed (fig. 1.13).

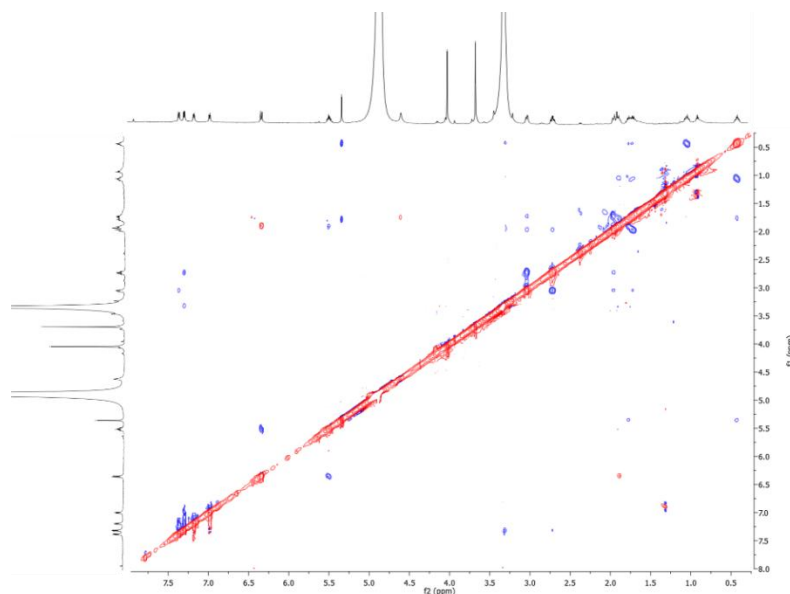


Figure 1.13. ROESY spectrum (CD_3OD) of giffonin C (**3**).

Mosher derivatization was performed on compound **3**, which was treated with (*R*)- and (*S*)-MTPA chloride to form (*S*)-MTPA and (*R*)-MTPA esters, respectively. Analysis of the $\Delta\delta$ ($\delta_S - \delta_R$) values of the protons close to the oxygenated methane according to the Mosher model¹² allowed the assignment of the 11*R* absolute configuration of **3** (fig. 1.14). Thus, the structure of compound **3**, named giffonin C, was elucidated as depicted.

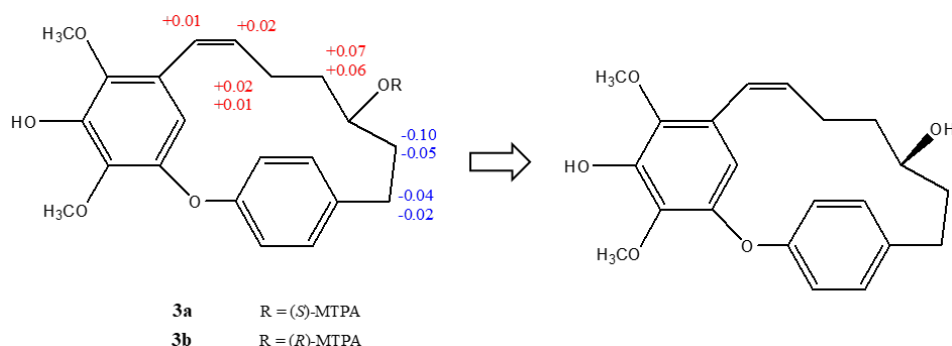


Figure 1.14. giffonin C.

The ^{13}C NMR and ESI/LTQORBITRAP/MS data of **4** (m/z 377.1367 $[\text{M}+\text{Na}]^+$, calcd for $\text{C}_{21}\text{H}_{22}\text{O}_5\text{Na}$, 377.1365) supported a molecular formula of $\text{C}_{21}\text{H}_{22}\text{O}_5$. The IR spectrum showed a band at 1713 cm^{-1} for the presence of a ketocarbonyl group. The NMR data of compound **4** were comparable to those of giffonin C (**3**) except for the presence of a carbonyl group replacing the secondary hydroxy group in **3**. Analyses of HMBC and COSY experiments confirmed the presence of a carbonyl group at C-11 (δ 213.9). Notably, the absence of the hydroxy group on the heptanoid chain induced similar chemical shifts of H-15 and H-19 (each, δ 7.26, d, $J = 8.3\text{ Hz}$) and H-16 and H-18 (each, δ 7.06, d, $J = 8.3\text{ Hz}$) (table 1.1). On the basis of the reported data the structure of **4**, named giffonin D, was deduced as depicted (fig. 1.15).

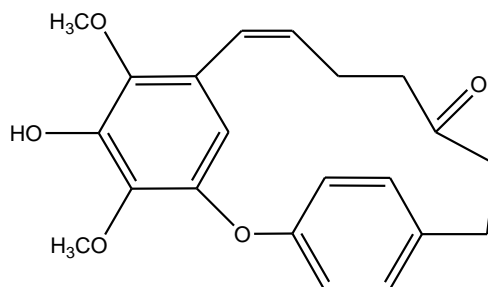


Figure 1.15. giffonin D.

Table 1.1. ^{13}C and ^1H NMR Data (J in Hz) of compounds **1-4** (600 MHz, δ ppm, in MeOH- d_4).

	1		2		3		4	
	δ_{C}	δ_{H} (J in Hz)	δ_{C}	δ_{H} (J in Hz)	δ_{C}	δ_{H} (J in Hz)	δ_{C}	δ_{H} (J in Hz)
1	152.7	-	152.7	-	151.8	-	151.8	-
2	136.9	-	137.0	-	137.5	-	137.6	-
3	144.3	-	144.1	-	144.7	-	145.0	-
4	140.4	-	140.6	-	141.6	-	141.9	-
5	127.8	-	128.0	-	124.7	-	125.7	-
6	109.0	4.41, s	109.2	4.39, s	108.3	5.34, s	108.0	5.18, s
7	125.5	6.34, d (15.7)	125.6	6.36, d (15.7)	124.6	6.35, d (11.4)	125.9	6.40, d (11.4)
8	135.5	5.20, dt (8.0, 15.7)	135.5	5.14, ddd (15.7, 10.8, 4.0)	132.5	5.51, ddd (11.4, 7.3, 7.3)	131.0	5.48, dt (11.4, 8.0)
9	26.7	2.32, (2H) m	26.1	2.52, m 2.00, m	27.0	1.90, m 1.78, m	23.0	1.94, (2H) m
10	44.3	2.44, (2H) t (5.5)	45.2	2.57, dt (17.0, 3.0) 2.29, ddd (3.0, 11.0, 12.0)	40.1	1.05, m 0.43, m	46.5	1.94, (2H) m
11	211.1	-	209.5	-	72.6	3.31, overlapped	213.9	-
12	46.2	2.86, (2H) t (5.5)	54.2	3.04, (2H) t (5.5)	40.9	1.96, m 1.72, m	45.0	2.66, (2H) t (6.8)
13	29.8	3.03, (2H) t (5.5)	71.2	5.23, dd (5.4, 8.9)	34.2	3.04, dt (12.8, 3.7) 2.74, td (12.8, 5.0)	33.6	3.03, (2H) t (6.8)
14	141.0	-	143.4	-	140.0	-	138.6	-
15	132.2	7.41, d (8.3)	131.4	7.45, dd (8.3, 1.9)	130.8	7.37, dd (8.3, 1.9)	131.8	7.26, d (8.3)
16	125.2	7.01, d (8.3)	124.4	7.00, dd (8.3, 1.9)	124.9	7.17, dd (8.3, 1.9)	124.5	7.06, d (8.3)
17	155.8	-	158.5	-	156.3	-	157.0	-
18	125.2	7.01, d (8.3)	125.8	7.16, dd (8.3, 1.9)	123.8	6.98, dd (8.3, 1.9)	124.5	7.06, d (8.3)
19	132.2	7.41, d (8.3)	128.4	7.70, dd (8.3, 1.9)	132.8	7.30, dd (8.3, 1.9)	131.8	7.26, d (8.3)
2- OCH ₃	61.7	4.00, s	61.6	4.00, s	61.3	4.03, s	61.4	4.02, s
4- OCH ₃	61.2	3.67, s	61.0	3.66, s	61.0	3.68, s	61.2	3.69, s

Table 1.2. ^{13}C and ^1H NMR Data (J in Hz) of compounds **5-8** (600 MHz, δ ppm, in $\text{MeOH-}d_4$).

	5		6		7		8	
	δ_{C}	δ_{H} (J in Hz)	δ_{C}	δ_{H} (J in Hz)	δ_{C}	δ_{H} (J in Hz)	δ_{C}	δ_{H} (J in Hz)
1	151.9	-	152.1	-	150.4	-	155.6	-
2	137.6	-	138.3	-	136.7	-	136.9	-
3	144.5	-	145.2	-	144.2	-	151.7	-
4	141.6	-	142.4	-	140.4	-	110.8	6.30, d (1.7)
5	125.7	-	124.7	-	125.1	-	133.5	-
6	108.5	5.11, s	108.3	4.89, s	110.0	5.46, s	109.6	5.51, d (1.7)
7	123.0	6.33, d (11.6)	124.9	6.46, d (12.0)	124.5	6.36, d (11.4)	129.9	6.09, d (11.2)
8	136.8	5.32, dd (11.6, 8.6)	132.2	5.31, dd (12.0, 8.8)	129.0	6.01, dd (11.4, 9.2)	128.8	5.94, t (11.2)
9	69.5	3.86 ddd (12.1, 8.6, 3.6)	65.3	4.33, t (9.8)	126.6	5.67, dd (15.4, 9.2)	126.8	5.68, dd (15.4, 11.2)
10	39.0	1.32, m	51.3	2.49, m	139.9	5.64, dd (15.4, 8.6)	140.1	5.63, dd (15.4, 8.6)
11	22.9	0.31, br t (12.1)	215.4	1.74, br s	73.2	4.07, dt (8.6, 3.3)	73.2	4.09, dt (8.6, 3.4)
12	30.5	1.78, q (10.8)	44.7	-	42.3	2.05, dq (14.2, 3.3)	42.5	2.05, dq (14.2, 3.4)
		2.11, m		2.84, td (12.5, 5.6)		1.66, tt (14.2, 3.3)		1.67, tt (14.2, 3.4)
		1.30, m		2.51, m		3.04, dt (12.8, 3.0)	34.6	3.04, dt (13.0, 3.3)
13	36.3	3.05, m	32.9	3.08, m	34.3	2.71, td (12.8, 3.0)		2.72, td (13.0, 3.3)
		2.47, td (12.7, 5.4)		3.03, td (12.1, 5.6)				
14	140.1	-	138.6	-	139.3	-	140.9	-
15	130.9	7.40, dd (8.3, 1.9)	130.5	7.52, dd (8.3, 1.9)	132.8	7.33, dd (8.3, 1.9)	133.2	7.36, dd (8.3, 1.9)
16	124.9	7.15, dd (8.3, 1.9)	125.0	7.20, dd (8.3, 1.9)	122.8	7.20, dd (8.3, 1.9)	123.0	7.19, dd (8.3, 1.9)
17	155.8	-	156.9	-	155.2	-	156.7	-
18	123.2	7.00, dd (8.3, 1.9)	123.8	6.98, dd (8.3, 1.9)	125.6	7.01, dd (8.3, 1.9)	126.3	7.03, dd (8.3, 1.9)
19	134.0	7.39, dd (8.3, 1.9)	134.0	7.12, dd (8.3, 1.9)	130.5	7.42, dd (8.3, 1.9)	130.7	7.44, dd (8.3, 1.9)
2-OCH ₃	61.4	4.03, s	61.2	4.03, s	61.2	4.05, s	60.0	4.03, s
4-OCH ₃	61.2	3.71, s	61.2	3.71, s	61.0	3.69, s		

The molecular formula of **5** was established as $\text{C}_{21}\text{H}_{24}\text{O}_5$ by ESI/LTQORBITRAP/MS (m/z 379.1526 $[\text{M}+\text{Na}]^+$, calcd for $\text{C}_{21}\text{H}_{24}\text{O}_5\text{Na}$, 379.1521) and ^{13}C NMR data. The ^1H NMR spectrum of **5** displayed signals at δ 7.40 (dd, $J = 8.3, 1.9$ Hz), 7.39 (dd, $J = 8.3, 1.9$ Hz), 7.15 (dd, $J = 8.3, 1.9$ Hz), 7.00 (dd, $J = 8.3, 1.9$ Hz), 5.11 (s), 4.03 (s), and 3.71 (s), ascribable to the two aryl

moieties with the same substitution pattern as in **3** (table 1.2). Further signals of a disubstituted cis-olefinic function at δ 6.33 (d, $J = 11.6$ Hz) and 5.32 (dd, $J = 11.6, 8.6$ Hz) and of a proton linked to an oxymethine carbon at δ 3.86 (ddd, $J = 12.1, 8.6, 3.6$ Hz) (table 1.2) were observed. The position of the hydroxy group was determined by COSY and HMBC correlations. In the HMBC spectrum, correlations between the proton signals at δ 6.33 (H-7) and the ^{13}C NMR resonances at δ 141.6 (C-4), 125.7 (C-5), 108.5 (C-6), 136.8 (C-8), and 69.5 (C-9) were observed. In the COSY spectrum the correlation between the proton at δ 6.33 (H-7) and the proton at δ 5.32 (H-8), which in turn correlated with the proton at δ 3.86 (H-9), allowed the hydroxy group to be located at C-9. The ^1H and ^{13}C NMR chemical shifts of the heptene moiety and the coupling constant of the proton of the secondary hydroxy function (δ 3.86, ddd, $J = 12.1, 8.6, 3.6$ Hz) of compound **5** were almost superimposable to those of 3,5'-dihydroxy-4'-methoxy-3',4''-oxy-1,7-diphenyl-1-heptene, isolated from *Betula platyphylla* var. *japonica*¹⁷.

The absolute configuration of compound **5** was determined through the application of the Mosher methodology¹⁸. The $\Delta\delta$ ($\delta_S - \delta_R$) values observed for signals of the protons close to C-9 in compounds **5a** and **5b** revealed a 9S configuration for **5**. On the basis of these observation, the structure of **5**, named giffonin E, was determined as depicted (fig. 1.16).

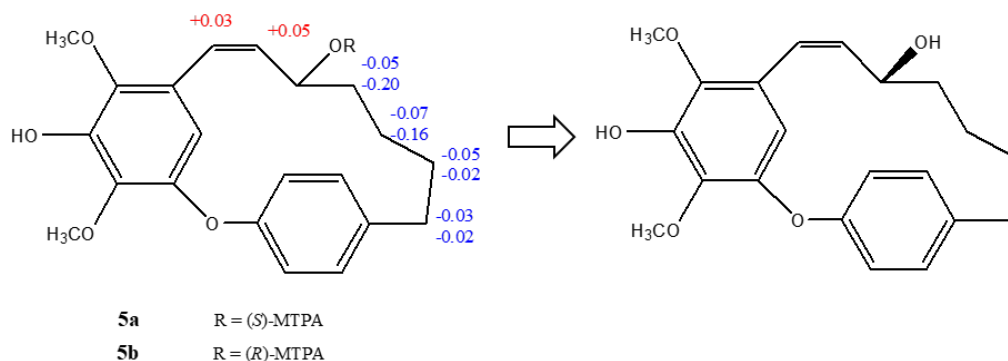


Figure 1.16. giffonin E.

The ^{13}C NMR and ESI/LTQORBITRAP/MS data of **6** (m/z 393.1319 $[\text{M}+\text{Na}]^+$, calcd for $\text{C}_{21}\text{H}_{22}\text{O}_6\text{Na}$, 393.1314) supported a molecular formula of $\text{C}_{21}\text{H}_{22}\text{O}_6$. The IR spectrum showed a band at 1710 cm^{-1} for the presence of a carbonyl group. The NMR data of compound **6** were similar to those of giffonin E (**5**) except for the presence of the resonance of a carbonyl group (δ 215.4). The location of the carbonyl group at C-11 was confirmed by the HMBC correlations of the proton signals at δ 3.08 and 3.03 (H-13) and δ 4.33 (H-9) with the carbon resonance at δ 215.4.

Mosher derivatization was performed on compound **6**, which was treated with (*R*)- and (*S*)-MTPA chloride to form (*S*)-MTPA and (*R*)-MTPA esters, respectively. Analysis of the $\Delta\delta$ ($\delta_S - \delta_R$) values of the protons neighboring the oxygenated methine according to the Mosher model¹⁸ allowed the assignment of the *9S* configuration of **6**. (fig. 1. 17). Accordingly, the structure of compound **6**, named giffonin F, was determined as shown.

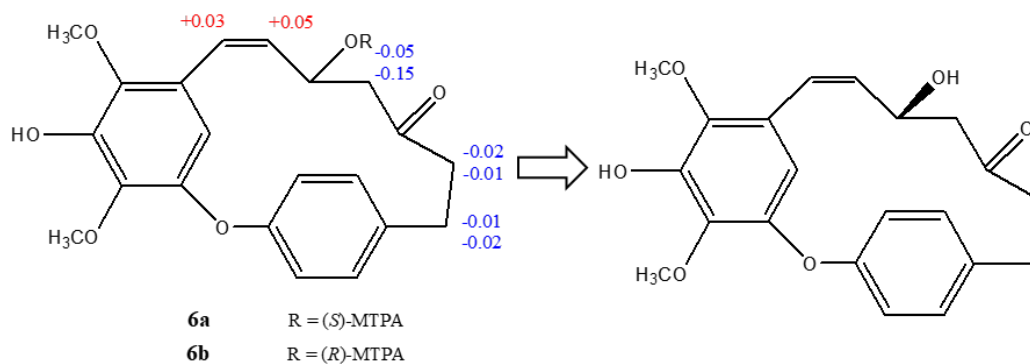


Figure 1.17. giffonin F.

The molecular formula of **7** was established as $\text{C}_{21}\text{H}_{22}\text{O}_5$ by ESI/LTQORBITRAP/MS (m/z 377.1367 $[\text{M}+\text{Na}]^+$, calcd for $\text{C}_{21}\text{H}_{22}\text{O}_5\text{Na}$, 377.1365) and the ^{13}C NMR data. Comparison of the ^1H NMR spectrum of **7** with those of **1–6** suggested that they share the same aromatic substitution patterns.

Furthermore, the ^1H NMR spectrum displayed four signals at δ 6.36 (d, $J = 11.4$ Hz), 6.01 (dd, $J = 11.4, 9.2$ Hz), 5.67 (dd, $J = 15.4, 9.2$ Hz), and 5.64 (dd, $J = 15.4, 8.6$ Hz), ascribable to *Z*- and *E* olefinic protons, respectively, and a signal at δ 4.07 (dt, $J = 8.6, 3.3$ Hz), corresponding to a proton linked to an oxymethine carbon (table 1.2). The COSY experiment showed the connectivity from H-7 to H-10, allowing a conjugated diene system (C-7/C-10) flanked by a hydroxy group at C-11 (δ 4.07) to be identified. ROESY experiment showed correlations of H-15 (δ 7.33) with H-13 β (δ 3.04) and of H-19 (δ 7.42) with H-13 α (δ 2.71) and H-11 (δ 4.07).

To determine the absolute configuration of C-11 in **7**, (*S*)- and (*R*)-MTPA esters of **7** were synthesized. The $\Delta\delta$ ($\delta_S - \delta_R$) values observed for signals of the protons close to C-11 revealed an 11*S* configuration for **7**. On the basis of the reported data, the structure of compound **7**, named giffonin G, was determined as depicted (fig. 1.18).

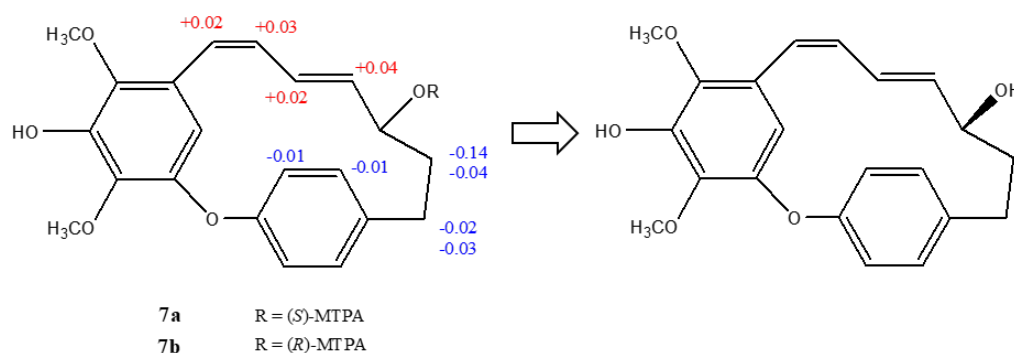


Figure 1.18. giffonin G.

The ^{13}C NMR and ESI/LTQORBITRAP/MS data of **8** (m/z 347.1261 [$\text{M}+\text{Na}$] $^+$, calcd for $\text{C}_{20}\text{H}_{20}\text{O}_4\text{Na}$, 347.1259) supported a molecular formula of $\text{C}_{20}\text{H}_{20}\text{O}_4$. The ^1H NMR data for the heptadiene moiety were comparable to those of **7**, while differences were observed for signals due to an aryl moiety. In particular, the ^1H NMR spectrum showed aromatic signals at δ 7.44 (dd, $J = 8.3, 1.9$ Hz, H-19),

7.36 (dd, $J = 8.3, 1.9$ Hz, H-15), 7.19 (dd, $J = 8.3, 1.9$ Hz, H-16), and 7.03 (dd, $J = 8.3, 1.9$ Hz, H-18), corresponding to the 1,4-disubstituted aromatic ring, and at δ 6.30 (d, $J = 1.7$ Hz, H-4) and 5.51 (d, $J = 1.7$ Hz, H-6), corresponding to a 1,2,3,5-tetrasubstituted aromatic ring (table 1.2). Moreover, a signal at δ 4.03 (s), typical of a methoxy group, was observed. The HMBC correlation between the proton signal at δ 4.03 and the carbon resonance at δ 136.9 allowed the methoxy group to be placed at C-2.

Mosher derivatization was performed on compound **8**, which was treated with (*R*)- and (*S*)-MTPA chloride to form (*S*)-MTPA and (*R*)-MTPA esters, respectively. Analysis of the $\Delta\delta$ ($\delta_S - \delta_R$) values of the protons neighboring the oxygenated methine according to the Mosher model¹⁸ allowed the assignment of an 11*S* configuration of **8**. Therefore, the structure of compound **8**, named giffonin H, was defined as shown (fig. 1.19).

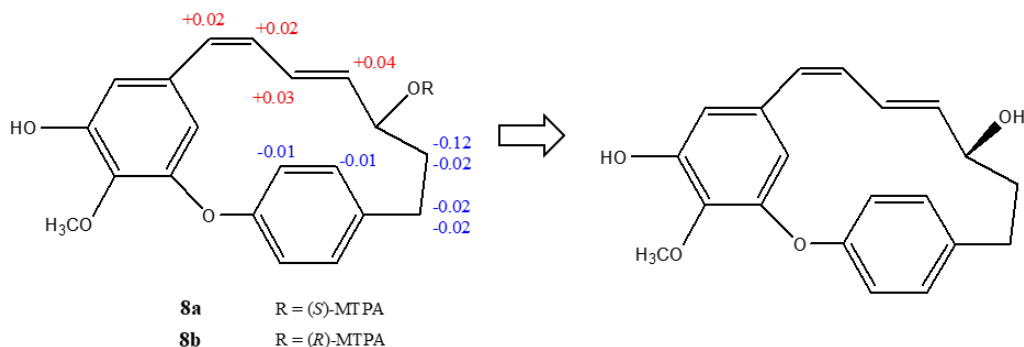


Figure 1.19. giffonin H.

The ^{13}C NMR and ESI/LTQORBITRAP/MS data of **9** (m/z 611.2107 $[\text{M}+\text{Na}]^+$, calcd for $\text{C}_{30}\text{H}_{36}\text{O}_{12}\text{Na}$, 611.2104) supported a molecular formula of $\text{C}_{30}\text{H}_{36}\text{O}_{12}$. The ^{13}C NMR spectrum of **9** showed 30 carbon signals, of which 19 were assigned to a diaryl heptanoid moiety¹⁷ and 11 to two sugar units (table 1.3).

Table 1.3. ^{13}C and ^1H NMR Data (J in Hz) of compound **9** (600 MHz, δ ppm, in $\text{MeOH-}d_4$).

9		
δ_{C}	δ_{H} (J in Hz)	
1	127.4	-
2	127.5	-
3	152.4	-
4	117.6	6.83, d (8.0)
5	128.9	7.04, dd (8.0, 2.2)
6	137.6	-
7	30.4	3.17, (2H) m
8	40.6	2.83, (2H) m
9	203.0	-
10	134.6	6.62, d (15.6)
11	150.4	7.10, dt (15.6, 7.6)
12	36.2	2.62, (2H) m
13	33.8	2.93, (2H) br t (5.5)
14	133.4	-
15	129.3	7.03, dd (8.0, 2.2)
16	116.4	6.76, d (8.0)
17	153.2	-
18	136.0	6.92, d (2.2)
19	134.2	7.02, d (2.2)
α -Ara (at C-3)		
1	93.5	5.14, d (3.7)
2	73.7	3.38, dd (8.0, 3.7)
3	74.5	3.69, dd (8.0, 3.0)
4	72.7	3.81, m
5	62.7	3.87, dd (12.5, 3.0)
β -Glc (at C-17)		
1	97.9	4.51, d (7.8)
2	76.0	3.15, dd (9.0, 7.8)
3	77.7	3.37, dd (9.0, 9.0)
4	71.6	3.31, dd (9.0, 9.0)
5	77.7	3.31, m
6	62.5	3.80, dd (12.0, 2.5)

The ^1H NMR spectrum (fig. 1.20) showed signals ascribable to two 1,2,4 trisubstituted aromatic rings at δ 7.04 (dd, $J = 8.0, 2.2$ Hz), 7.03 (dd, $J = 8.0, 2.2$ Hz), 7.02 (d, $J = 2.2$ Hz), 6.92 (d, $J = 2.2$ Hz), 6.83 (d, $J = 8.0$ Hz), 6.76 (d, $J = 8.0$ Hz), and signals due to a disubstituted *trans*-olefinic function at δ 6.62 (d, $J = 15.6$ Hz) and 7.10 (dt, $J = 7.6, 15.6$ Hz).

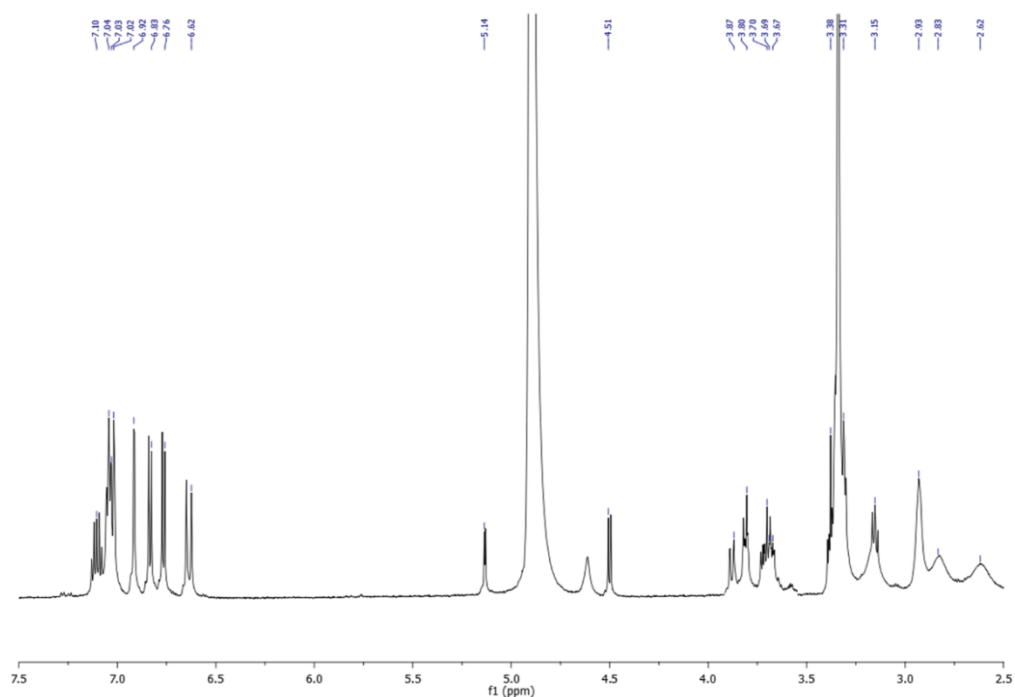


Figure 1.20. ^1H NMR spectrum (600 MHz, CD_3OD) of giffonin I (**9**).

The structure of the heptanoid moiety was readily deduced from HSQC, HMBC and COSY correlations (fig. 1.21, 1.22 and 1.23). Thus, the aglycone of **9** was established as alnusone, a natural compound previously isolated from *Alnus japonica* and also available via total synthesis^{14,15}. The ^1H NMR spectrum displayed in the sugar region signals corresponding to two anomeric protons at δ 5.14 (d, $J = 3.7$ Hz) and 4.51 (d, $J = 7.8$ Hz). The NMR data (HSQC, HMBC, COSY, and 1D-TOCSY) indicated the presence of an α -arabinopyranosyl unit (δ 5.14) and a β -glucopyranosyl unit (δ 4.51).

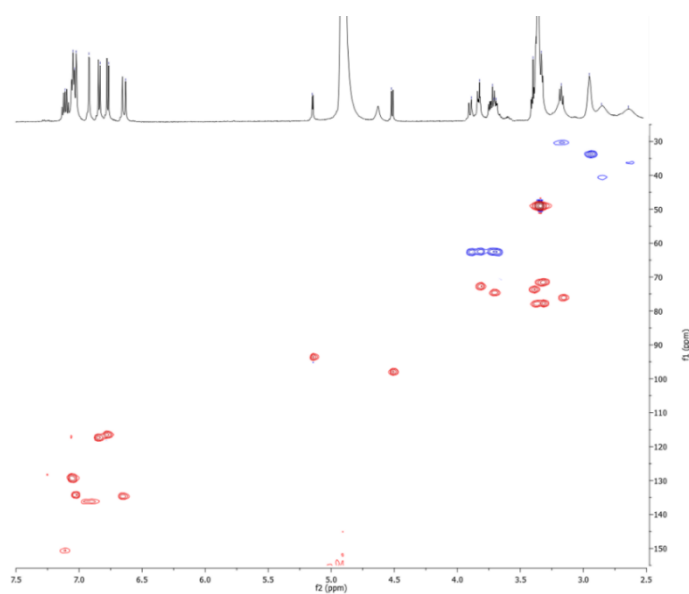


Figure 1.21. HSQC spectrum (CD_3OD) of giffonin I (**9**).

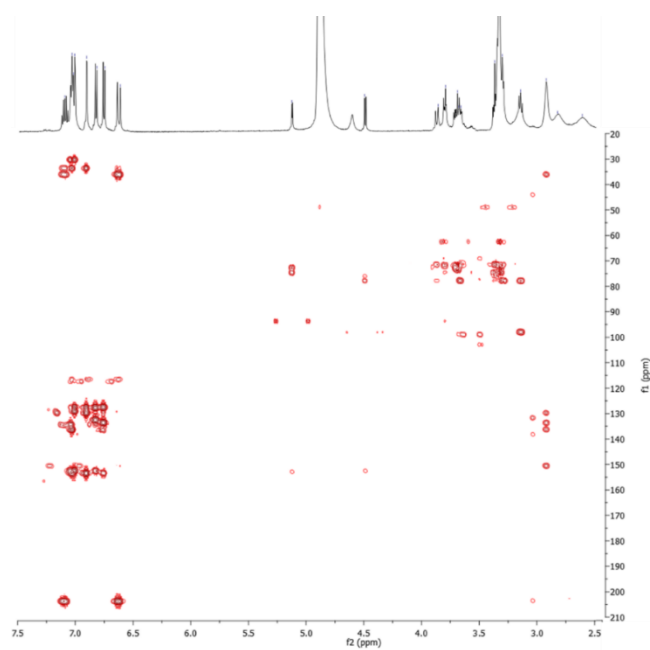


Figure 1.22. HMBC spectrum (CD_3OD) of giffonin I (**9**).

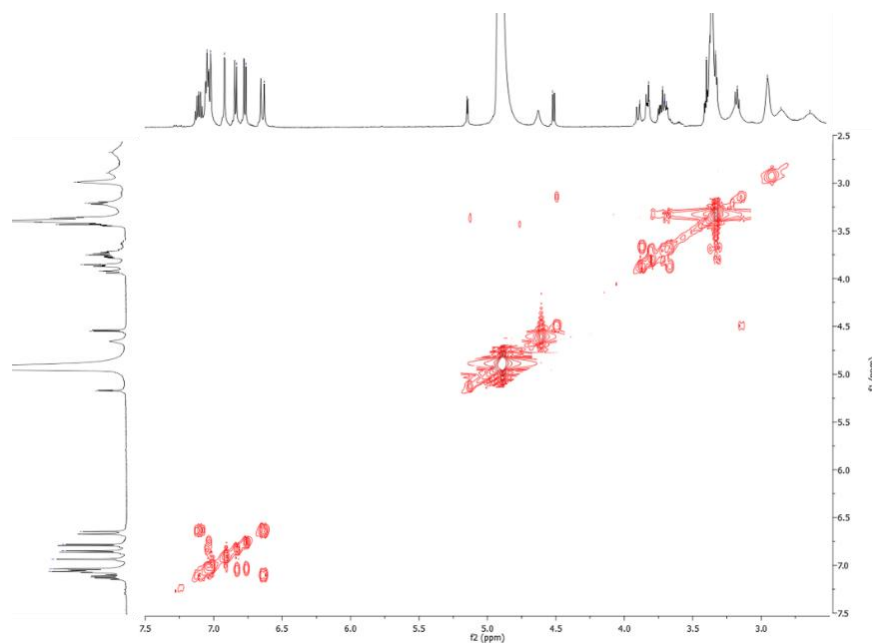


Figure 1.23. COSY spectrum (CD_3OD) of giffonin I (**9**).

The configurations of the arabinose and glucose units were established as L and D, respectively, after hydrolysis of **9** with 1 N HCl, trimethylsilylation and GC analysis¹⁶. The linkage sites of the sugar units on the diaryl heptanoid moiety were obtained from the HMBC spectrum, which showed correlations between H-1_{ara} (δ 5.14) and the ¹³C NMR resonance of C-3 (δ 152.4), and between H-1_{glc} (δ 4.51) and C-17 (δ 153.2). On the basis of the reported data, the structure of compound **9**, named giffonin I, was established as shown (fig. 1.24).

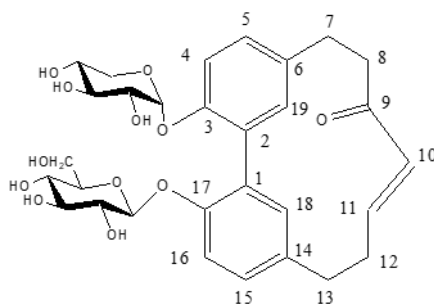


Figure 1.24. giffonin I.

Moreover, the isolation and the structural elucidation of giffonins J-P, possessing at least two stereogenic centres on the heptyl unit was carried out. These data resembled those reported for giffonins A-H, as characterized by the signal of H-6 being considerably upfield shifted, due to the anisotropic effect of the A-ring in diaryletherheptanoids. In particular, the ESI/LTQORBITRAP/MS of **10** (m/z 395.1475 $[M+Na]^+$, calcd for $C_{21}H_{24}O_6Na$, 395.1471) and the ^{13}C NMR data supported a molecular formula of $C_{21}H_{24}O_6$. The 1H NMR spectrum displayed signals for five aromatic protons ascribable to two aromatic rings: a signal at δ 5.32 (s), typical of the proton of a pentasubstituted aromatic ring and signals at δ 7.65 (dd, $J = 8.2, 1.9$ Hz), 7.32 (dd, $J = 8.2, 1.9$ Hz), 7.29 (dd, $J = 8.2, 1.9$ Hz), 6.99 (dd, $J = 8.2, 1.9$ Hz) (fig. 1.25 and table 1.4), due to the protons of a 1,4-disubstituted aromatic ring.

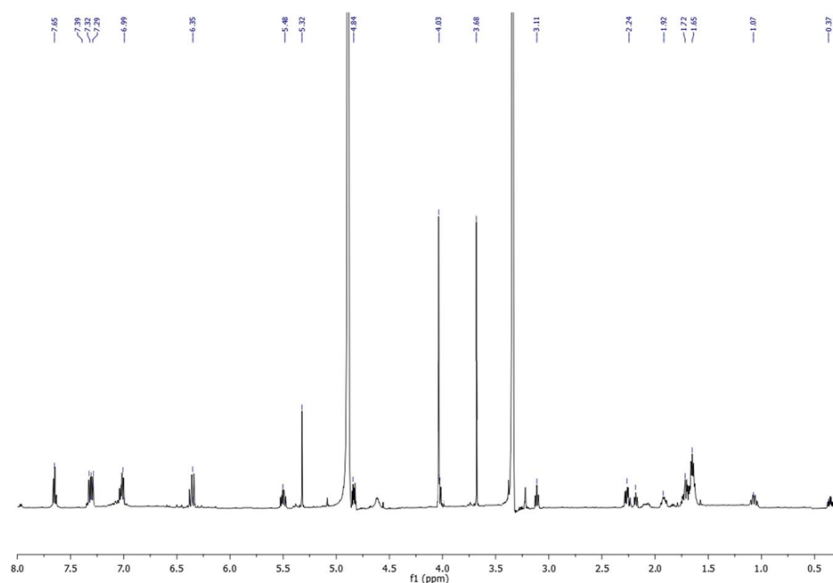


Figure 1.25. ^1H NMR spectrum (600 MHz, CD_3OD) of giffonin J (**10**).

The ^1H NMR data displayed further signals due to a disubstituted *cis*-olefinic group at δ 6.35 (d, $J = 12.0$ Hz) and 5.48 (dt, $J = 12.0, 6.0$ Hz), and for two protons linked to an oxymethine carbon at δ 4.84 (dd, $J = 10.7, 5.6$ Hz) and 3.11 (tt, $J = 9.0, 2.0$ Hz) (table 1.4). Moreover, two signals for two methoxy groups at δ 4.03 and 3.68 were evident. The ^{13}C NMR spectrum of **10** showed 21 carbon signals (table 1.4), typical of a diaryletherheptanoid derivative.

Table 1.4. ^{13}C (150 MHz) and ^1H NMR Data (600 MHz, CD_3OD , δ ppm, J in Hz) of compounds **10** and **11**.

	10		11	
	δ_{C}	δ_{H} (J in Hz)	δ_{C}	δ_{H} (J in Hz)
1	150.1	-	151.8	-
2	136.2	-	138.0	-
3	143.1	-	144.8	-
4	141.1	-	141.9	-
5	123.6	-	125.3	-
6	108.0	5.32, s	110.3	5.44, s
7	124.9	6.35, d (12.0)	125.2	6.37, d (11.4)
8	132.2	5.48, dt (12.0, 6.0)	129.1	6.03, dd (11.4, 9.2)
9	27.3	1.72, 1.92, m	127.0	5.62, dd (15.4, 9.2)
10	39.5	0.36, 1.07, m	139.2	5.59, dd (15.4, 8.6)
11	69.4	3.11, tt (9.0, 2.0)	71.3	3.84, m
12	50.1	1.65, 2.24, m	50.6	2.25, 1.72, m
13	73.5	4.84, dd (10.7, 5.6)	73.7	4.83 ^a
14	141.8	-	143.0	-
15	130.2	7.32, dd (8.2, 1.9)	127.9	7.65, dd (8.4, 1.8)
16	123.1	6.99, dd (8.2, 1.9)	126.5	7.30, dd (8.3, 1.9)
17	156.4	-	157.6	-
18	125.4	7.29, dd (8.2, 1.9)	122.2	7.04, dd (7.9, 2.2)
19	127.9	7.65, dd (8.2, 1.9)	131.0	7.44, dd (8.3, 1.9)
OCH ₃ -2	61.3	4.03, s	61.3	4.06, s
OCH ₃ -4	61.3	3.68, s	61.2	3.69, s

The HMBC correlations of H-6 (δ 5.32) with the ^{13}C NMR resonances at δ 150.1 (C-1), 136.2 (C-2), 141.1 (C-4), 123.6 (C-5) and 124.9 (C-7), suggested the 1,2,3,4 tetrahydroxylation of the A-ring (fig. 1.26 and 1.27).

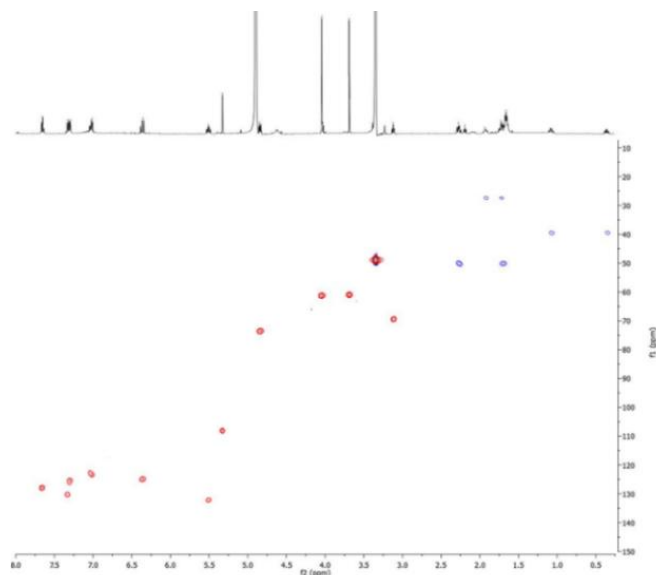


Figure 1.26. HSQC spectrum (CD_3OD) of giffonin J (**10**).

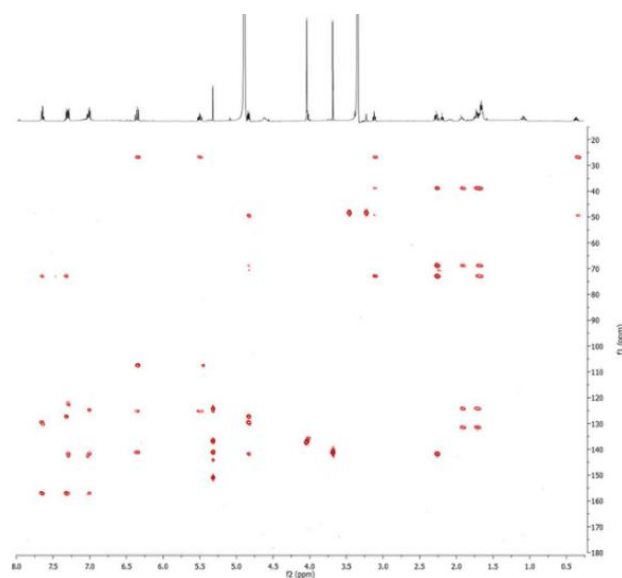


Figure 1.27. HMBC spectrum (CD_3OD) of giffonin J (**10**).

A secondary hydroxy group was assigned to C-13 on the basis of the correlations of the proton signal at δ 4.84 with the ^{13}C NMR resonances at δ 130.2 (C-15), 127.9 (C-19), and 141.8 (C-14). The HMBC correlations of the proton at δ 6.35 (H-7) with the ^{13}C NMR resonances of the B ring at δ 141.1 (C-4), 123.6 (C-5) and 108.0 (C-6), and the linear connectivity observed in the COSY spectrum (fig. 1.28) from H-7 to H-13 were used to assign the heptanoid chain allowing the further secondary hydroxy group to be located at C-11 (69.4).

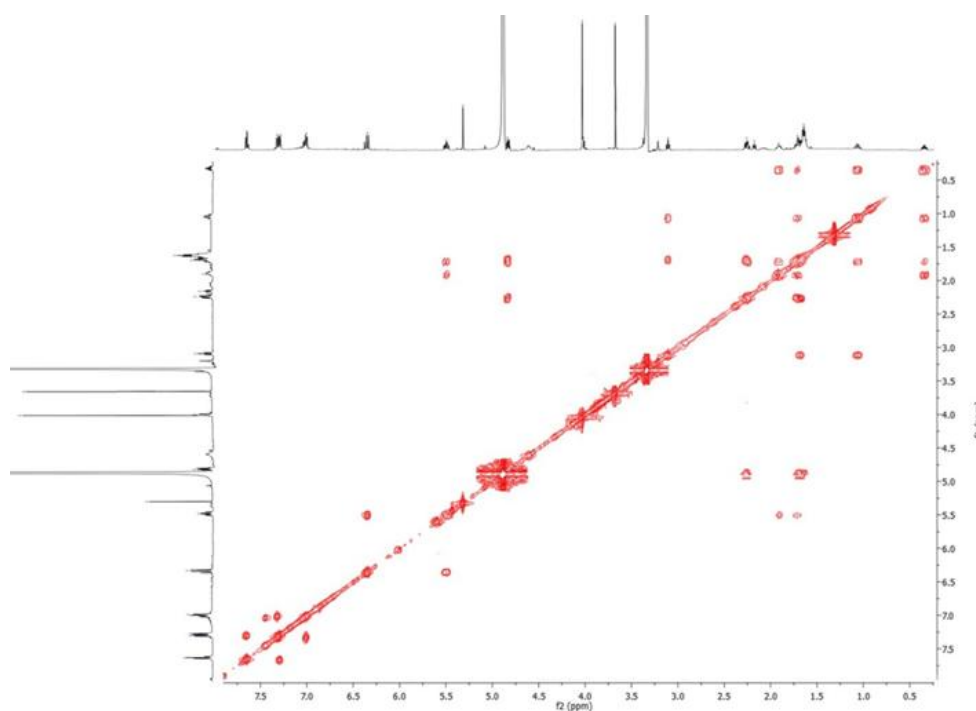


Figure 1.28. COSY spectrum (CD_3OD) of giffonin J (**10**).

Finally, the HMBC correlations between the protons at δ 4.03 and 3.68 with the ^{13}C NMR resonances at δ 136.2 (C-2) and 141.1 (C-4), respectively, suggested that the methoxy groups are located at C-2 and C-4 of the B ring. Thus, on the basis of the above data, the planar structure of **10**, named giffonin J, was determined as shown (fig. 1.29).

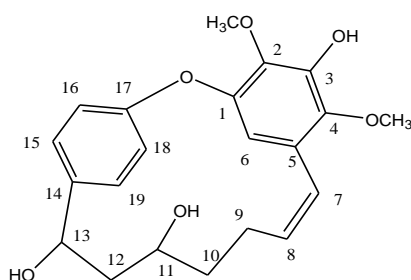


Figure 1.29. planar structure of giffonin J.

The molecular formula of **11** was established as $C_{21}H_{22}O_6$ by ESI/LTQORBITRAP/MS and the ^{13}C NMR data. HSQC data confirmed the same aromatic substitution patterns as in **10** (table 1.4). Furthermore, the 1H NMR spectrum displayed four signals at δ 6.37 (d, $J = 11.4$ Hz), 6.03 (dd, $J = 11.4, 9.2$ Hz), 5.62 (dd, $J = 15.4, 9.2$ Hz), 5.59 (dd, $J = 15.4, 8.6$ Hz), ascribable to *Z*- and *E*-olefinic protons, respectively, and two signals at δ 4.83 (overlapped) and 3.84 (m), corresponding to protons linked to oxymethine carbons (table 1.4). The NMR data revealed that compound **11** differed from **10** for the presence of an additional double bond. The COSY, HSQC, and HMBC experiments supported a conjugated diene system (C-7/C-10) and the two hydroxy groups at C-11 (δ 71.3) and C-13 (δ 73.7). The foregoing spectroscopic data allowed the planar structure of compound **11** (giffonin K) to be assigned as shown (fig. 1.30).

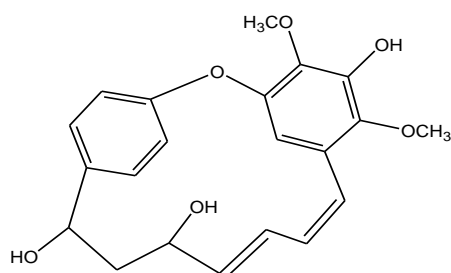


Figure 1.30. planar structure of giffonin K.

The ^1H and ^{13}C NMR spectra of compounds **12-16** showed signals ascribable to a diaryl heptanoid moiety. In particular, for compound **12**, the ^1H NMR spectrum showed signals attributable to two 1,2,4 trisubstituted aromatic rings at δ 7.04 (dd, $J = 8.2, 1.8$ Hz), 7.01 (dd, $J = 8.2, 1.8$ Hz), 6.94 (d, $J = 1.8$ Hz), 6.81 (d, $J = 8.2$ Hz), 6.80 (d, $J = 8.2$ Hz), and 6.77 (d, $J = 1.8$ Hz) (table 1.5).

A detailed analysis of their NMR data showed that compounds **12-16** differed in terms of the occurrence of secondary hydroxy groups and carbonyl functions at various positions on the heptanoid chain (tables 1.5 and 1.6). A combination of HSQC, HMBC and COSY experiments permitted the determination of the linear connectivity from H-7/C-7 to H-13/C-13 of the heptanoid chain in compounds **12-16**.

Table 1.5. ¹H NMR Data (600 MHz, CD₃OD, δ ppm, *J* in Hz) of compounds 12-16.

	12	13	14	15	16
1	-	-	-	-	-
2	-	-	-	-	-
3	-	-	-	-	-
4	6.81, d (8.2)	6.78, d (8.1)	6.77, d (8.2)	6.84, d (8.2)	6.84, d (8.2)
5	7.01, dd (8.2, 1.8)	7.00, dd (8.1, 2.1)	7.02, dd (8.2, 1.8)	7.07 dd (8.2, 1.8)	7.08, dd (8.2, 1.8)
6	-	-	-	-	-
7	2.70, dd (15.9, 11.2)	3.19, dd (15.4, 3.6)	3.32, dd (15.2, 3.5)	3.02, dd (16.0, 11.2)	2.97, dd (16.4, 3.2)
	3.13, dd (15.9, 2.8)	2.56, dd (15.4, 11.4),	2.63, dd (15.2, 11.4),	3.08, dd (16.0, 3.8)	3.04, m
8	4.21, td (11.2, 2.8)	4.63, m	4.69, m	4.73, dd (11.2, 3.8)	4.77, dd (11.3, 3.2)
9	2.59, dd (15.2, 11.2)	2.46, dd (14.5, 11.6)	2.47, dd (14.6, 11.6)	4.83 ^a	4.09, brs
	1.56, dd (15.2, 10.8),	1.60, td (11.6, 3.4)	1.77, td (11.6, 3.2)		
10	4.40, brd (10.8)	4.43, dd (11.9, 3.4)	4.64, m	-	4.19, d (10.1)
11	4.12, brs	-	-	2.35, dd (13.3, 9.4)	4.04, d (10.1)
				3.65, d (13.3)	
12	4.80, dd (11.4, 3.5)	2.91, 3.50, m	2.95, 3.53, m	4.52, m	4.27, brdd (9.9, 6.1)
13	3.02, dd (16.6, 11.4)	2.89, 3.16, m	2.85, dd (16.4, 3.6)	2.79, dd (16.6, 11.2)	3.05, m
	2-.97, dd (16.6, 3.5),		3.16, m	3.18, dd (16.6, 2.5)	
14	-	-	-	-	-
15	7.04, dd (8.2, 1.8)	7.08, dd (8.1, 2.1)	7.06, dd (8.2, 1.8)	7.07, dd (8.2, 1.8)	7.07, dd (8.2, 1.8)
16	6.80, d (8.2)	6.82, d (8.1)	6.80, d (8.2)	6.84, d (8.2)	6.80, d (8.2)
17	-	-	-	-	-
18	6.94, d (1.8)	6.56, d (1.8)	6.57, d (1.8)	6.90, d (1.8)	6.76, d (1.8)
19	6.77, d (1.8)	6.71, d (1.8)	6.68, d (1.8)	7.07, d (1.8)	6.82, d (1.8)
		-	β-Glc (at C-8)	-	-
1	-	-	4.46, d (8.0)	-	-
2	-	-	3.26, dd (9.0, 8.0)	-	-
3	-	-	3.42, dd (9.0, 9.0)	-	-
4	-	-	3.24, dd (9.0, 9.0)	-	-
5	-	-	3.39, m	-	-

6	-	-	3.87, dd (12.0, 2.5)	-	-
			3.62, dd (12.0, 4.5)		

^aOverlapped with the H₂O peak in CD₃OD.

Table 1.6. ^{13}C NMR Data (150 MHz, CD_3OD , δ ppm) of compounds 12-16.

	12	13	14	15	16
1	127.6	127.0	128.0	128.9,	128.7
2	128.0	127.7	127.0	128.7	128.7
3	153.8	153.8	154.0	153.9	152.8
4	117.3	117.0	117.2	117.2	116.8
5	129.8	130.0	130.2	130.3	130.3
6	131.4	130.1	134.0	130.1	130.3
7	40.4	40.9	37.0	36.7	34.7
8	68.9	67.6	75.2	69.5	70.0
9	42.8	42.1	40.3	76.1	68.8
10	78.7	76.1	75.2	210.3	79.2
11	70.9	217.4	219.3	46.5	68.8
12	69.7	36.6	36.7	68.0	69.7
13	35.3	24.8	24.7	40.7	36.2
14	130.6	130.8	130.6	129.3	131.4
15	129.8	129.3	129.3	130.3	130.3
16	117.3	117.1	117.2	117.2	116.8
17	153.9	153.1	153.1	153.7	152.8
18	134.5	134.3	134.2	135.1	135.4
19	134.8	134.3	134.2	135.1	135.2
-	-	-	β -Glc (at C-8)	-	-
1	-	-	102.3	-	-
2	-	-	74.9	-	-
3	-	-	77.9	-	-
4	-	-	72.2,	-	-
5	-	-	77.7	-	-
6	-	-	63.6	-	-

The ^{13}C NMR and ESI/LTQORBITRAP/MS data of **12** supported a molecular formula of $\text{C}_{19}\text{H}_{22}\text{O}_6$. The ^1H NMR spectrum of this compound showed signals corresponding to four protons linked to oxymethine carbons at δ 4.80, 4.40, 4.21, and 4.12, which were assigned to C-12 (δ 69.7), C-10 (δ 78.7), C-8 (δ 68.9) and C-11 (δ 70.9), respectively, as supported by HMBC and COSY correlations. Thus, the planar structure of compound **12** (giffonin L) was elucidated as depicted (fig. 1.31).

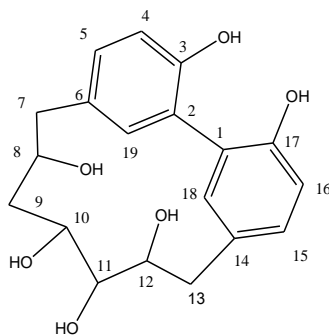


Figure 1.31. planar structure of giffonin L.

The ESI/LTQORBITRAP/MS data of **13** in combination with the ^{13}C NMR data supported a molecular formula of $\text{C}_{19}\text{H}_{20}\text{O}_5$. The IR spectrum showed a band at 1720 cm^{-1} for the presence of a ketocarbonyl group. As with **12**, HSQC data confirmed a diarylheptanoid core structure with oxymethine (δ 4.63, 4.43) proton resonances correlating with carbons at δ 67.6 (C-8) and 76.1 (C-10), respectively. The carbonyl group could be located at C-11 (δ 217.4), on the basis of the HMBC correlations between H-10 (δ 4.43), H₂-12 (δ 3.50, 2.91), H₂-13 (δ 3.16, 2.89), and H₂-9 (δ 2.46, 1.60) with the carbon resonance at δ 217.4. Accordingly, the planar structure of compound **13** (giffonin M) was determined as shown (fig. 1.32).

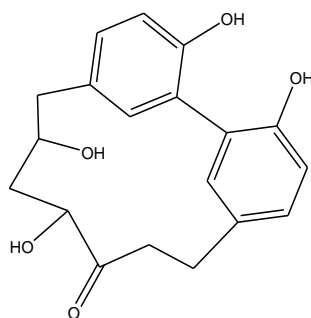


Figure 1.32. planar structure of giffonin M.

The molecular formula of **14** was established as $C_{25}H_{30}O_{10}$ by ESI/LTQORBITRAP/MS and the ^{13}C NMR data. The NMR data of **14** revealed that it differed from **13** by the presence of a β -glucopyranosyl unit ($H-1_{glc} = \delta$ 4.46) (fig. 1.33 and tables 1.5 and 1.6).

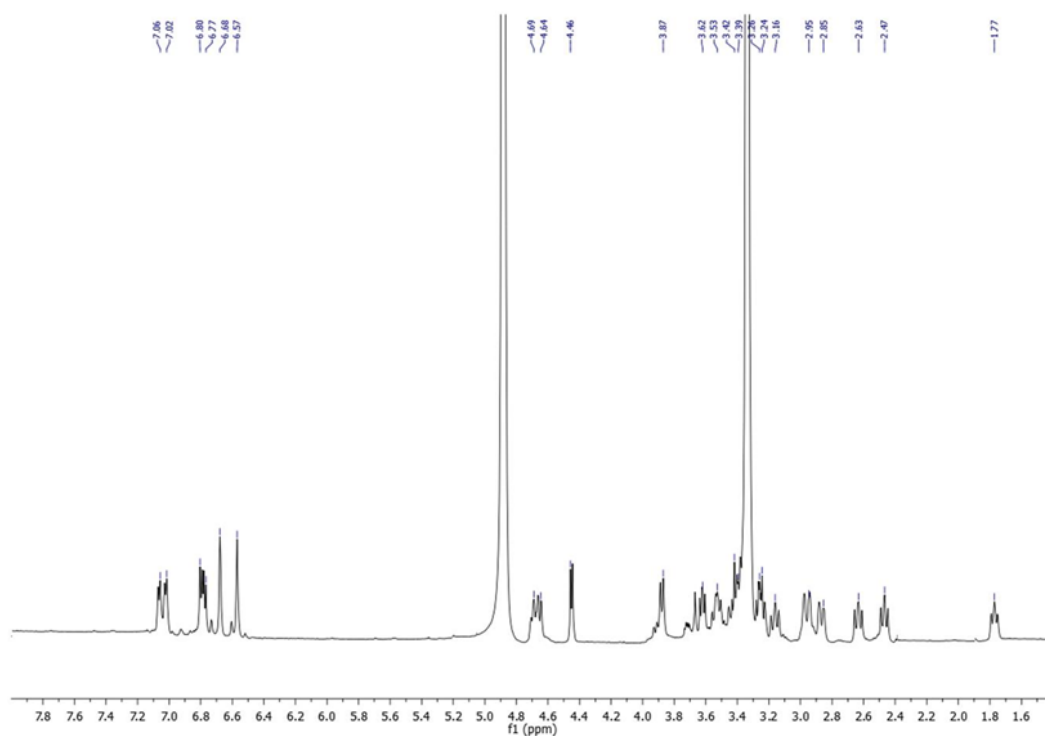


Figure 1.33. 1H NMR spectrum (600 MHz, CD_3OD) of giffonin N (**14**).

The configuration of the glucose unit was established as D, after hydrolysis of **14** with 1 N HCl, trimethylsilation and GC analysis¹⁹. The sugar unit was located at C-8 on the basis of the HMBC correlation (fig. 1.34) between H-1_{glc} (δ 4.46) and C-8 (δ 75.2), downfield shifted if compared with compound **13** (δ 67.6, C-8).

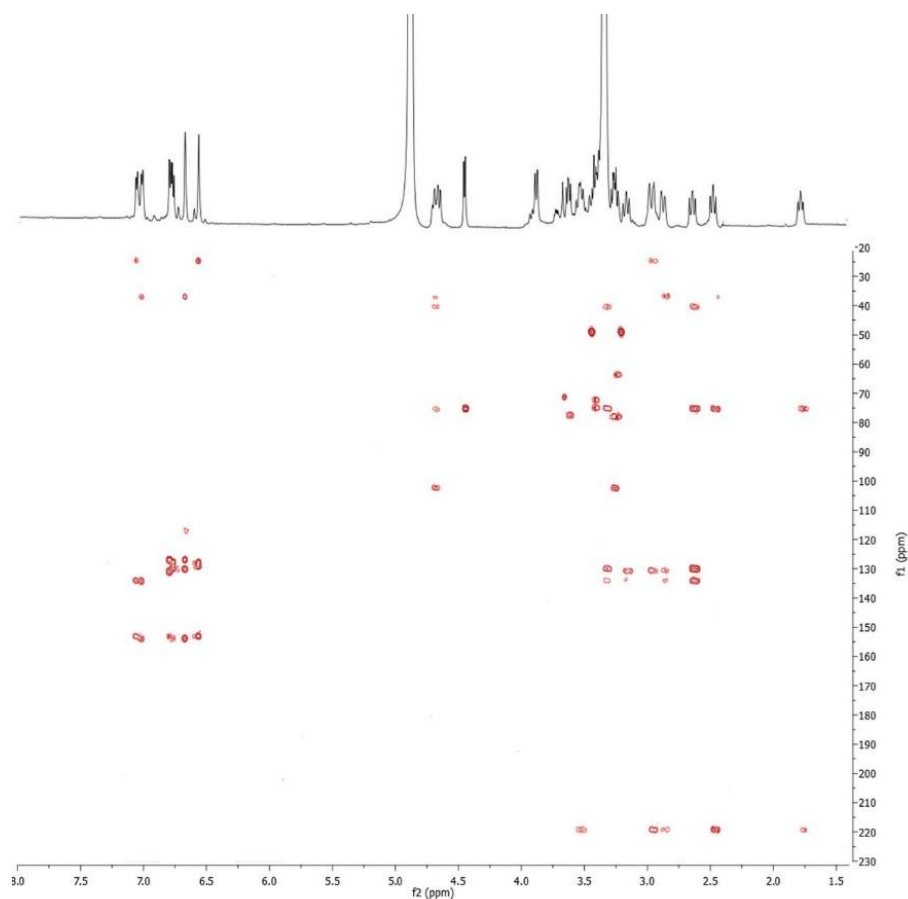


Figure 1.34. HMBC spectrum (CD₃OD) of giffonin N (**14**).

On the basis of the data measured, the planar structure of compound **14** (giffonin N) was established as shown (fig. 1.35).

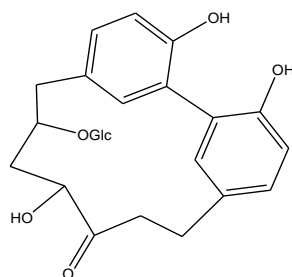
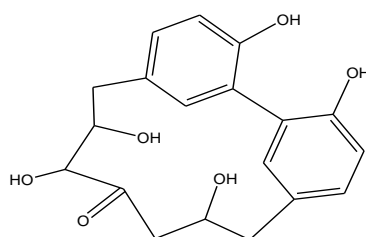


Figure 1.35. planar structure of giffonin N.

The molecular formula of **15** was established as $C_{19}H_{20}O_6$ by ESI/LTQORBITRAP/MS and the ^{13}C NMR data. For the heptanoid chain, the NMR data showed the presence of three secondary hydroxy groups at C-8 (δ_H 4.73/ δ_C 69.5), C-9 (δ_H 4.83/ δ_C 76.1), and C-12 (δ_H 4.52/ δ_C 68.0). Similar to **13**, the heptanoid chain contained a carbonyl group (δ_C 210.3), as suggested by an absorption peak at 1725 cm^{-1} in the IR spectrum. This was assigned at C-10 on the basis of the HMBC correlations between H-9 (δ 4.83), H-8 (δ 4.73), H-12 (δ 4.52), and H₂-11 (δ 3.65, 2.35) with the carbon resonance at δ 210.3. Therefore, the planar structure of compound **15** (giffonin O) was defined as shown (fig. 1.36).



giffonin O

Figure 1.36. planar structure of giffonin O.

The ^{13}C NMR and ESI/LTQORBITRAP/MS data of **16** allowed a molecular formula of $\text{C}_{19}\text{H}_{22}\text{O}_7$ to be established. The proton sequence (δ 4.77, 4.09, 4.19, 4.04, and 4.27), as deduced from the COSY experiment was located at C-8 (δ 70.0), C-9 (δ 68.8), C-10 (δ 79.2), C-11 (δ 68.8) and C-12 (δ 69.7), on the basis of HSQC and HMBC experiments, revealing the presence of a highly hydroxylated heptanoid chain. Thus, on the basis of the above performed data the planar structure of **16** (giffonin P) was determined as reported (fig. 1.37).

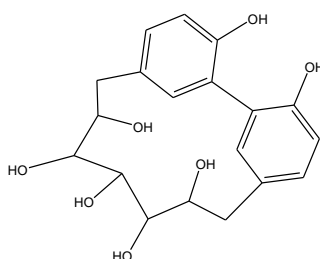


Figure 1.37. planar structure of giffonin P.

In addition, four known flavonoid derivatives, myricetin 3-*O*- α -L-rhamnopyranoside²⁰ (**17**), quercetin 3-*O*- α -L-rhamnopyranoside²⁰ (**18**), kaempferol 3-*O*- α -L-rhamnopyranoside²⁰ (**19**), and kaempferol 3-*O*-(4''-*trans-p*-coumaroyl)- α -L-rhamnopyranoside²¹ (**20**) were also isolated from the leaves of *C. avellana* in the present investigation.

Relative configurations of the diarylheptanoids 10-16

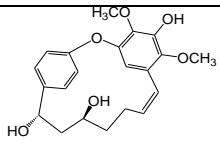
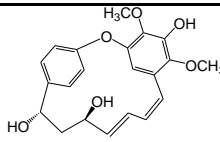
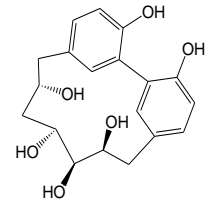
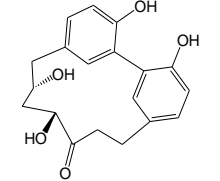
In collaboration with Prof. Giuseppe Bifulco (Department of Pharmacy, University of Salerno), the relative configurations of the reported compounds **10-16** were assigned. In particular, a combined QM/NMR approach, comparing the experimental $^{13}\text{C}/^1\text{H}$ NMR chemical shift data and the related predicted values was used. This procedure was employed, since the chemical shifts are the most diagnostic parameters of the local chemical and magnetic environment and the most reliably addressable by quantum chemical calculations²².

For each compound considered, a proper sampling of the conformations was performed in order to attain a close agreement between calculated and experimental NMR parameters. For these reasons, an extensive conformational search at the empirical level (molecular mechanics, MM) for all the possible diastereoisomers of each investigated compound was carried out, combining Monte Carlo Molecular Mechanics (MCMC), Low-Mode Conformational Sampling (LMCS), and Molecular Dynamics (MD). Subsequently, the selected non-redundant conformers were submitted further to a geometry and energy optimization step at the density functional level (DFT). After the optimization of the geometries at the QM level, the newly selected conformers were used for the subsequent computation of the ^{13}C and ^1H NMR chemical shifts.

In detail, the conformational analysis revealed many degrees of freedom in the heptanoid chains connecting the two phenyl moieties, determining different geometries to be accounted in the final Boltzmann distribution. Furthermore, similar conformers differing in the presence/absence of intramolecular H-bonds between the hydroxy groups placed on adjacent carbons on the heptanoid chains were weighted energetically in the Boltzmann distribution according to the protic solvent (MeOH) “continuum model” considered in the QM calculations. The diaryl moieties also affected the conformational sampling, leading to various conformers specifically differing for the dihedral angles between the two aromatic groups and their final arrangements on the heptanoid chain.

Starting from the selected conformers, the ^{13}C and ^1H NMR chemical shifts for each investigated diastereoisomer were computed at the density functional level (DFT). Afterwards, for each atom of the investigated molecules, a comparison of the experimental and calculated ^{13}C and ^1H NMR chemical shifts was performed by computing the $\Delta\delta$ parameter. Finally, the relative configuration of each investigated compound was determined by calculating and comparing the mean absolute errors (MAEs) for all the possible diastereoisomers (table 1.7).

Table 1.7. $^{13}\text{C}/^1\text{H}$ MAE (ppm) Values Reported for all the Possible Relative Stereoisomers for Compounds **10-16**.^a

# of stereogenic centers	# of possible relative stereoisomers	stereoisomer	relative configuration	# of sampled conformers	^{13}C MAE (ppm)	^1H MAE (ppm)	proposed structure	
10	2		10a	12 <i>S</i> *,14 <i>S</i> *	24	1.63	0.22	
			10b	12 <i>R</i> *,14 <i>S</i> *	25	1.73	0.28	
11	2		11a	12 <i>S</i> *,14 <i>S</i> *	19	1.85	0.25	
			11b	12 <i>R</i> *,14 <i>S</i> *	18	1.71	0.17	
12	4	8	12a	8 <i>S</i> *,10 <i>R</i> *,11 <i>R</i> *,12 <i>R</i> *	16	4.37	0.36	
			12b	8 <i>S</i> *,10 <i>R</i> *,11 <i>R</i> *,12 <i>S</i> *	17	2.77	0.34	
			12c	8 <i>S</i> *,10 <i>R</i> *,11 <i>S</i> *,12 <i>R</i> *	15	2.25	0.23	
			12d	8 <i>S</i> *,10 <i>R</i> *,11 <i>S</i> *,12 <i>S</i> *	17	2.05	0.34	
			12e	8 <i>S</i> *,10 <i>S</i> *,11 <i>R</i> *,12 <i>R</i> *	18	1.70	0.25	
			12f	8 <i>S</i> *,10 <i>S</i> *,11 <i>R</i> *,12 <i>S</i> *	15	1.37	0.16	
			12g	8 <i>S</i> *,10 <i>S</i> *,11 <i>S</i> *,12 <i>R</i> *	17	3.00	0.28	
			12h	8 <i>S</i> *,10 <i>S</i> *,11 <i>S</i> *,12 <i>S</i> *	18	3.07	0.21	
13	2		13a	8 <i>S</i> *,10 <i>S</i> *	27	2.62	0.30	
			13b	8 <i>S</i> *,10 <i>R</i> *	28	2.08	0.19	

14	2	2	14a	8 <i>S</i> *,10 <i>S</i> *	35	2.79	0.16	
			14b	8 <i>S</i> *,10 <i>R</i> *	34	2.50	0.14	
15	3	4	15a	8 <i>S</i> *,9 <i>R</i> *,12 <i>S</i> *	18	3.21	0.31	
			15b	8 <i>S</i> *,9 <i>R</i> *,12 <i>R</i> *	20	1.50	0.18	
			15c	8 <i>S</i> *,9 <i>S</i> *,12 <i>S</i> *	18	2.06	0.23	
			15d	8 <i>S</i> *,9 <i>S</i> *,12 <i>R</i> *	20	2.61	0.35	
16	4	8	16a	8 <i>S</i> *,9 <i>R</i> *,11 <i>R</i> *,12 <i>R</i> *	19	3.56	0.34	
			16b	8 <i>S</i> *,9 <i>R</i> *,11 <i>R</i> *,12 <i>S</i> *	22	2.40	0.31	
			16c	8 <i>S</i> *,9 <i>R</i> *,11 <i>S</i> *,12 <i>R</i> *	21	3.67	0.23	
			16d	8 <i>S</i> *,9 <i>R</i> *,11 <i>S</i> *,12 <i>S</i> *	22	3.57	0.24	
			16e	8 <i>S</i> *,9 <i>S</i> *,11 <i>R</i> *,12 <i>R</i> *	20	2.80	0.29	
			16f	8 <i>S</i> *,9 <i>S</i> *,11 <i>R</i> *,12 <i>S</i> *	21	2.98	0.23	
			16g	8 <i>S</i> *,9 <i>S</i> *,11 <i>S</i> *,12 <i>R</i> *	19	2.28	0.18	
			16h	8 <i>S</i> *,9 <i>S</i> *,11 <i>S</i> *,12 <i>S</i> *	21	3.04	0.37	

584 total
sampled
conformers

^a**MAE** = $\Sigma[|(\delta_{\text{exp}} - \delta_{\text{calcd}})|]/n$, summation through n of the absolute error values (difference of the absolute values between corresponding experimental and ¹³C/¹H chemical shifts), normalized to the number of the chemical shifts. The predicted relative configurations are highlighted in green.

In this way, the relative configurations of compounds **10-16**, shown in figure 1.38, were assigned selecting the related diastereoisomers showing the lowest $^{13}\text{C}/^1\text{H}$ MAE errors (table 1.7).

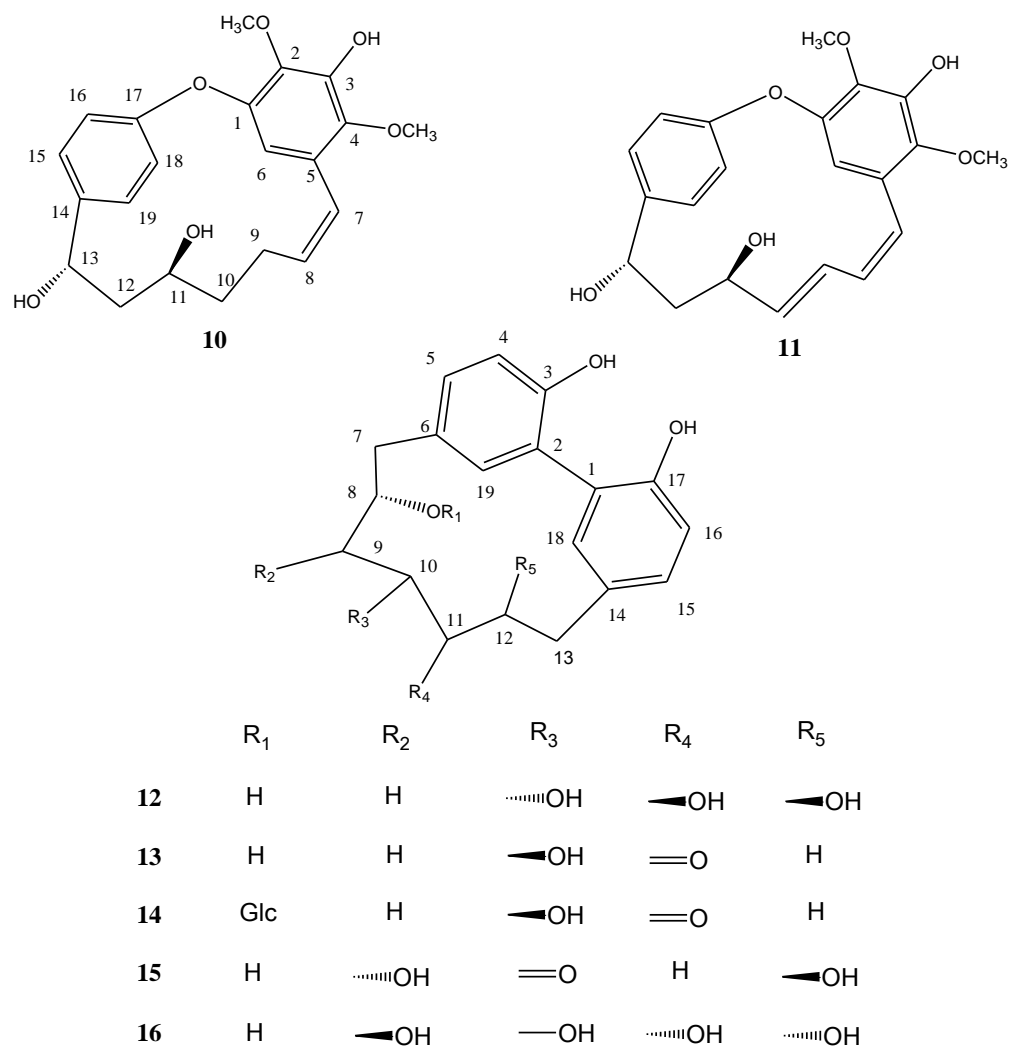


Figure 1.38. relative configuration of compounds **10-16**.

1.1.3 Biological activity

Diarylheptanoids have been reported by numerous studies to possess diverse bioactivities including anti-inflammatory, antioxidant, anticancer, estrogenic, leishmanicidal, melanogenesis, hepatoprotective and neuroprotective activities²³.

In vitro and *in vivo* cytotoxicity against human cancer cell lines of diarylheptanoids has been reported²³. *In vivo* cytotoxicity of oregonin has been proved in the B16 murine melanoma model.

In the diarylheptanoid class, curcumin, the well known polyphenolic molecule isolated from the rhizome of *Curcuma longa* (Zingiberaceae), appears as a promising chemopreventive compound able to reverse, inhibit or prevent the development of cancer and to affect molecular events implicated in inflammation²⁴.

Evaluation of cytotoxicity of MeOH extract of leaves and giffonins

Preliminarily, , in collaboration with Dr. G. L. Russo (ISA, CNR, Avellino), the cytotoxic activities of compounds **1-16** and curcumin, used as a reference compound, were evaluated against two cancer cell lines, namely U2Os and SAOs cells. The two cell lines were selected based on the following criteria: (1) both cell lines have a common origin (human osteosarcoma) and they are resistant to apoptotic stimuli; (2) they are characterized by a different genetic background relatively to p53 gene, being SAOs p53 mutated and U2Os p53 wild-type; and (3) both cell lines have been employed in previous studies to assess the biological activity of naturally occurring phenolic compounds. The results obtained showed that all the tested compounds exhibited EC₅₀ values higher than 150 µM at 24-48 h, indicating the absence of cytotoxicity against both cell lines.

Evaluation of antioxidant activity of MeOH extract of leaves and giffonins

The diarylheptanoids isolated from plants belonging to the Betulaceae family have been reported to possess various biological activities including antioxidant²; moreover, the antioxidant activity has been reported for hazelnuts and leaves of *C. avellana*¹. Therefore, in collaboration with the research group of Prof. Beata Olas (University of Lodz, Poland), peroxidation induced by H₂O₂ and H₂O₂/Fe²⁺ has been evaluated, by measuring the concentration of TBARS (Thiobarbituric Acid Reactive Substances).

2-ThioBarbituric Acid Reactive Substances (TBARS) are naturally present in biological specimens and include lipid hydroperoxides and aldehydes which increase in concentration as a response to oxidative stress. TBARS assay values are usually reported in malonaldehyde (malondialdehyde, MDA) equivalents, a compound that results from the decomposition of polyunsaturated fatty acid lipid peroxides. The TBARS assay is a well-recognized, established method for quantifying these lipid peroxides; this assay is based on the reaction of a chromogenic reagent, 2-thiobarbituric acid, with MDA at 25°C. One molecule of MDA reacts with 2 molecules of 2-thiobarbituric acid via a Knoevenagel-type condensation to yield a chromophore with absorbance maximum at 532 nm²⁵, as shown below in figure 1.39.

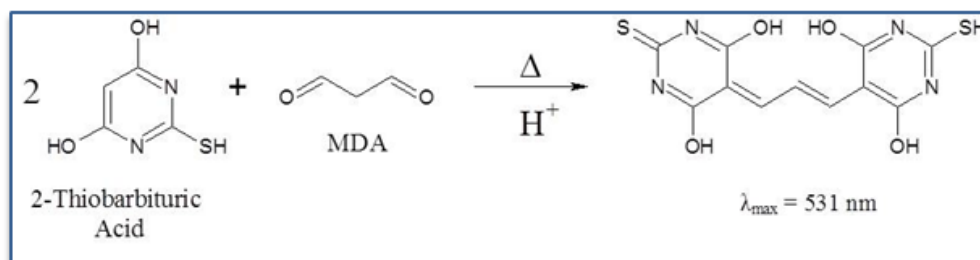


Figure 1.39.

In our case, the MeOH extract, compounds **1-16**, and curcumin, used as reference compound, were tested at doses ranging from 0.1 to 100 $\mu\text{g}/\text{mL}$ and from 0.1 to 100 μM , respectively. The tested compounds, curcumin, and the plant extract did not exert any effect on autoperoxidation of human plasma (data not shown). The MeOH extract of leaves at 10 $\mu\text{g}/\text{mL}$ reduced by about 38 % plasma lipid peroxidation stimulated by H_2O_2 or $\text{H}_2\text{O}_2/\text{Fe}^{2+}$. Giffonin D (**4**) and giffonin H (**8**) at 10 μM reduced both H_2O_2 and $\text{H}_2\text{O}_2/\text{Fe}^{2+}$ induced lipid peroxidation by more than 60 and 50 %, respectively, being more active than curcumin (fig. 1.41).

Among the 16 compounds, the weakest activity was displayed by compounds **2, 6, and 9** (fig. 1.40. and 1.41, and table 1.8), which exerted a protective action against oxidative stress induced by H_2O_2 or $\text{H}_2\text{O}_2/\text{Fe}^{2+}$, similar to that shown by curcumin

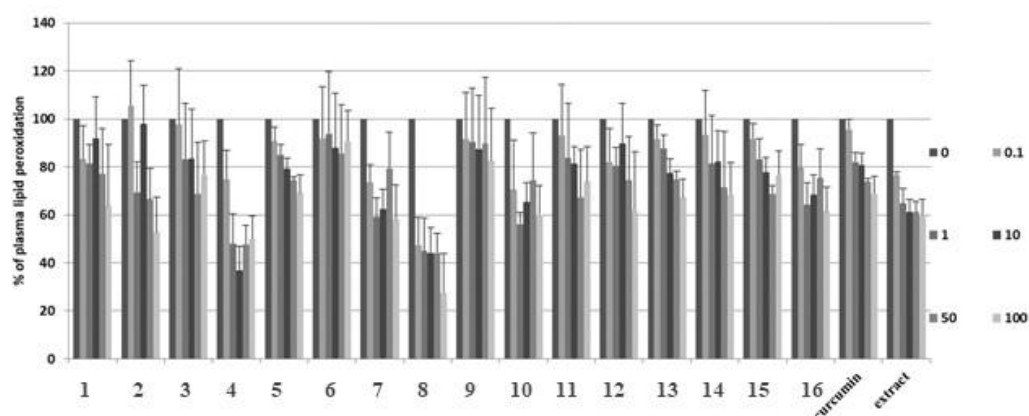


Figure 1.40. Effects of MeOH extract (0.1 – 100 $\mu\text{g}/\text{mL}$; 30 min), giffonins A-P (**1-16**) (0.1 – 100 μM ; 30 min) and curcumin (0.1 – 100 μM ; 30 min) on plasma lipid peroxidation induced by H_2O_2 . The results are representative of three independent experiments, and are expressed as means \pm SD. The effect of five different concentrations of tested compounds (0.1, 1, 10, 50 and 100 μM) and tested extract (0.1, 1, 10, 50 and 100 $\mu\text{g}/\text{mL}$) was statistically significant according to ANOVA I test, $p < 0.05$ (for compounds **1, 5, 7** and curcumin); $p < 0.02$ (for compounds **4, 8, 13, 16** and extract); $p > 0.05$ (for compounds **2, 3, 6, 9, 10-12** and **14-15**).

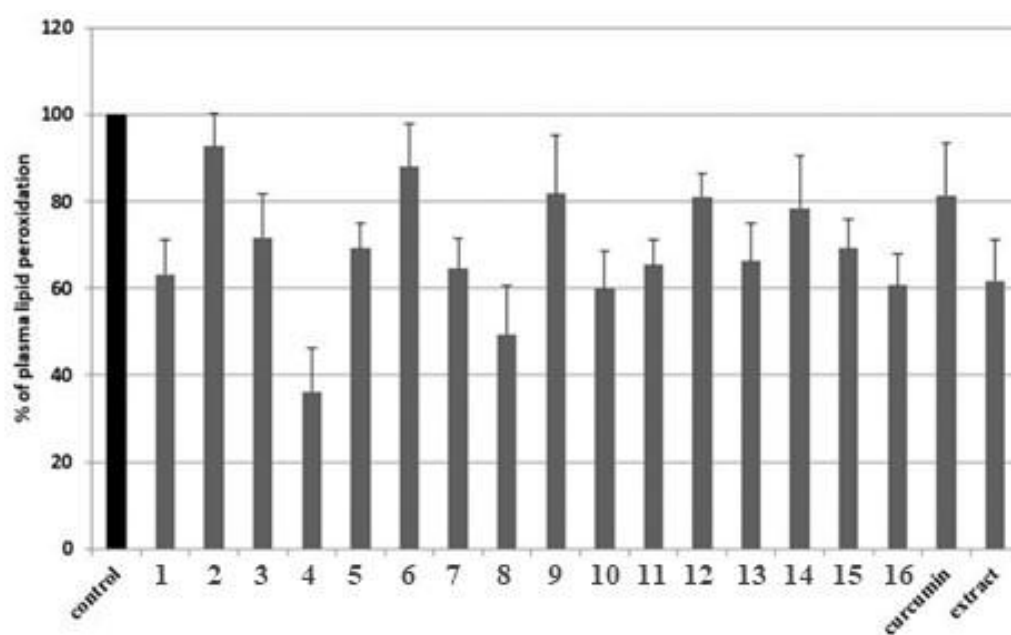


Figure 1.41. Effects of MeOH extract (10 $\mu\text{g}/\text{mL}$; 30 min), giffonins A-P (**1-16**) (10 μM ; 30 min) and curcumin (10 μM ; 30 min) on plasma lipid peroxidation induced by $\text{H}_2\text{O}_2/\text{Fe}^{2+}$. The results are representative of three independent experiments, and are expressed as means \pm SD. The statistical significances were confirmed with the paired Student's t-test.

Table 1.8. Inhibitory Effects of the Extract (10 µg/mL; 30 min), compounds **1-16** (10 µM; 30 min) and Curcumin (10 µM; 30 min) on Plasma Lipid Peroxidation Induced by H₂O₂ or H₂O₂/Fe²⁺.

compound	Inhibition of lipid peroxidation induced by H ₂ O ₂ (%)	Inhibition of lipid peroxidation induced by H ₂ O ₂ /Fe ²⁺ (%)
1	8.1 ± 3.6 (p<0.05)	36.8 ± 8.8 (p<0.02)
2	2.2 ± 2.4 (p>0.05)	7.3 ± 3.8 (p>0.05)
3	16.4 ± 3.9 (p<0.05)	28.2 ± 4.9 (p<0.05)
4	64.3 ± 14.5 (p<0.002)	63.2 ± 10.7 (p<0.002)
5	20.8 ± 5.1 (p<0.05)	30.8 ± 6.8 (p<0.02)
6	12.1 ± 4.9 (p<0.05)	12.0 ± 5.2 (p<0.05)
7	37.6 ± 7.7 (p<0.02)	35.5 ± 7.6 (p<0.02)
8	55.8 ± 13.9 (p<0.01)	50.6 ± 14.5 (p<0.01)
9	12.6 ± 4.5 (p<0.05)	18.1 ± 4.8 (p<0.05)
10	65.4 ± 8.0 (p<0.05)	59.9 ± 8.7 (p<0.05)
11	81.3 ± 7.1 (p<0.05)	65.5 ± 5.8 (p<0.05)
12	89.7 ± 16.9 (p<0.05)	81.1 ± 5.3 (p<0.05)
13	77.3 ± 6.1 (p<0.02)	66.3 ± 8.7 (p<0.02)
14	82.4 ± 12.5 (p<0.05)	78.5 ± 12.1 (p<0.05)
15	77.6 ± 6.2 (p<0.05)	69.3 ± 6.5 (p<0.05)
16	68.4 ± 8.3 (p<0.02)	60.7 ± 7.3 (p<0.02)
curcumin	19.2 ± 4.4 (p<0.05)	18.6 ± 5.1 (p<0.05)
extract	38.8 ± 6.1 (p<0.02)	38.3 ± 7.2 (p<0.02)

1.2. Metabolite profiling of “green” extracts of *Corylus avellana* leaves by ^1H NMR spectroscopy and multivariate statistical analysis

Introduction

In traditional medicine the leaves of *C. avellana* are used for their mild antimicrobial effects and also for the treatment of varicose veins and hemorrhoidal symptoms. They are claimed for their beneficial properties, are widely distributed in on-line market and suggested to be used in infusion preparations. To the best of our knowledge, there are no study on the chemical composition of extracts of the leaves obtained by infusion. Thus a further objective of the present project was the investigation of the infusion of the leaves of *C. avellana* cv. Tonda di Giffoni with the aim to highlight their chemical composition and to evidence the occurrence of phytochemicals with health benefits. Each extraction method has its own advantages and disadvantages, but the main goal of the chosen method is the achievement of complete extraction of the compounds of interest and avoidance of their chemical modification. The chemical investigation was carried out also on extracts obtained by “eco-friendly” procedures in order to explore their potential use as functional ingredients for nutraceutical, herbal and cosmetic formulations.

NMR metabolomics is considered an invaluable tool in plant science since it is a robust, quick, reproducible, non-destructive and relatively easy to use analytical platform that does not require laborious sample preparation and can simultaneously identify diverse groups of secondary metabolites. NMR metabolomics is widely used to study the plant metabolite composition influenced by extraction methods²⁶. Metabolomic analysis generates huge datasets that make it necessary the application of chemometric methods.

Herein NMR metabolomics with multivariate data analysis (MVDA) were used to identify the metabolite variation among the “green” extracts obtained by

maceration, infusion and SLDE-Naviglio methods. Moreover the total phenolic and antioxidant capacities of the obtained extracts were measured by colorimetric assays, respectively Folin–Ciocalteu, DPPH and ABTS assay and the most active extracts were studied by an *in vitro* antioxidant test to validate the phytomedicinal properties of the significant metabolites identified from the NMR analysis.

1.2.1. Results and discussion

Choice of the best parameters for the extraction by maceration

The leaves of *C. avellana* cv. Tonda di Giffoni were extracted by maceration in a beaker at room temperature. Parameters such as time of extraction, solid-solvent ratio and mixture ethanol-water as solvent of extraction were modified in order to choose the best conditions for a higher phenolic content. Preliminarily, the extraction time has been evaluated using 50% ethanol-water and 1:20 solid-solvent ratio at different time extraction (30 min, 60 min, 90 min, 2 h, 4 h, 8 h, 10 h, 14 h and 18 h)^{27,28}.

The choice of the best extraction time was given by the phenolics content, assayed by the Folin-Ciocalteu method that showed as the phenolic extraction yield increased during the time. The best result was at 10h (216.49 mg GAE/g DW), but no significant difference was observed after 10h.

In fact, two stages of extractions could be observed, an initial increase of the concentration of polyphenols in the beginning of the process followed by slow extraction (after 10 h) characterized by a low enhancement of polyphenol content with the progress of extraction. The decrease in the extraction yield, observed with the progression of the time extraction may be due to the degradation of polyphenols²⁹. The optimization of the extraction was further monitored at 2 h, 4 h, 8 h and 10 h, changing other parameters. In fact, other two different solid-solvent ratio (1:10, 1:30) were examined to test the effect of the solid-solvent

ratio, using 50% ethanol-water. The highest phenolic content was measured for the 1:30 solvent ratio at 10 h (608.10 mg GAE/g DW). The results are in agreement with the previous findings that higher solid-solvent ratio leads to the higher yield of polyphenols²⁸. It should be noted that higher solid-solvent ratio generate a decrease in the consumption of plant material and decrease in the cost of extraction.

In order to investigate the effects of different solvents on the extraction efficiency, ethanol at concentration of 70% and 80% were also used. The results revealed that the yield of phenolic content was maximized at 50% of ethanol (608.10 mg GAE/g DW) as shown in Table 1.9 So, water can play an important role in swelling of plant material, whereas ethanol is responsible for disrupting the bonding between the solutes and plant matrix, thus enabling better mass transfer of the compounds. Therefore, the mixture of water and ethanol as solvent agent shows a synergistic effect which facilitates phenolic extraction³⁰.

Table 1.9. Phenolic content evaluated by Folin–Ciocalteu method.

Maceration (% ethanol-water, time of extraction)* 1:30*	Total phenolics content (mg GAE/g DW)
50% 2 h	306.37±0.01
50% 4 h	496.99±0.01
50% 8 h	573.53±0.01
50% 10 h	608.10±0.01
70% 2 h	255.01±0.01
70% 4 h	409.58±0.01
70% 8 h	443.65±0.01
70% 10 h	466.86±0.01
80% 2 h	298.47±0.01
80% 4 h	329.58±0.02
80% 8 h	403.65±0.01
80% 10 h	430.32±0.01
Infusion**	
1:100	19.95±0.01
5:100	60.44±0.01
10:100	170.57±0.01
SLDE-Naviglio***	
6.5	322.66±0.01
8.0	471.80±0.01
12.0	322.17±0.01

*1:30 solid– solvent ratio; **solid:solvent ratio; ***time of each cycle (min)

Choice of the best parameters for the extraction by infusion

According to Pharmacopoeia XII, three different infusions were obtained using 1:100, 5:100 and 10:100 solid:solvent ratios at 100 °C. For each infusion the phenolic content activity has been evaluated through the Folin-Ciocalteu method and the results showed the better phenolic content of 170.57 mg GAE/g DW for the 10:100 solid:solvent ratio (table 1.9). These experimental results showed that the increase of the solid:solvent ratio improve the yield of polyphenols, but significantly differences were observed between these three infusion and the extract obtained with ethanol:water, probably because the only water is not able to extract all the polyphenolic components.

Choice of the best parameters for the extraction by solid–liquid dynamic extractor (SLDE)-Naviglio

To select the most suitable extractive cycle, three different conditions have been tested. Extractions with 20 extractive cycles have been used, that differed from each other for the time of each cycle, 6.5 min 8 min and 12 min, respectively. The Folin-Ciocalteu assay revealed a higher phenolic content for the extraction performed by SLDE-Naviglio with a time of cycle of 8.0 min (table 1.9). The decrease in yield extract, observed with longer time of cycle may be due to the degradation of polyphenols with progressing time extraction.

Antioxidant activity by DPPH and TEAC assays

The antioxidant activity of the extracts exhibiting the higher phenolic content (50% 1:30 10 h macerate, 10:100 infusion and SLDE-Naviglio 8 min) were tested by DPPH and TEAC assays.

For DPPH assay, expressed as $\mu\text{g/mL}$ of antioxidant required to decrease the initial DPPH[•] concentration by 50% (EC_{50}), the highest antioxidant activity was displayed by SLDE-Naviglio with cycles of 8.0 min ($\text{EC}_{50} = 100.33$), as shown in

table 1.10. This extract in the TEAC assay showed the highest antioxidant activity (TEAC value 1.62 mg/mL), defined as the concentration of a standard Trolox solution with the same antioxidant capacity as a 1 mg/mL of the tested extract, and compared to quercetin 3-*O*- β -D-glucopyranoside, used as reference compound (table 1.10).

Table 1.10. free radical scavenging activity evaluated by TEAC and DPPH assay.

<i>C. avellana</i> cv. Tonda di Giffoni leaves	free radical scavenging activity (mg/mL \pm SD) ^a	free radical scavenging activity (EC50, μ g/mL \pm SD) ^b
Maceration (EtOH:H ₂ O 50%, solid-solvent ratio 1.30, 10h)	1.26 \pm 0.007	129.34 \pm 0.009
Infusion (solid-solvent ratio 10:100)	1.15 \pm 0.006	195.08 \pm 0.014
SLDE-Naviglio (8.0 min)	1.62 \pm 0.004	100.33 \pm 0.012
quercetin ^c	1.79 \pm 0.008	
Vitamin C ^d		4.40 \pm 0.012

^aDetermined by TEAC assay Range of tested concentrations (0.25–1.00 mg/mL). ^bDetermined by DPPH test. Range of tested concentrations (50–200 μ g/mL). ^cPositive control for TEAC assay. ^dPositive control for DPPH assay.

Targeting metabolomics analysis by ¹H NMR spectra

A detailed analysis of the metabolite profile of *C. avellana* leaves “green extract” was performed using 1D and 2D NMR spectra. The ¹H NMR spectrum was crowded, with several overlapping peaks. Therefore, an accurate analysis of the proton spectrum was carried out to assign unambiguously a key signal characteristic of an individual metabolite. Based on the NMR data, a total of 28 metabolites, including 8 primary metabolites and 20 phenolic compounds were detected. *C. avellana* leaves extracted by different processes exhibited quantitative variation rather than qualitative variation in the metabolite content. The resonance values selected to detect each compound are shown in table 1.10 with a wide

range of metabolites, including amino acids, carbohydrates, cyclic diarylheptanoids and flavonoids.

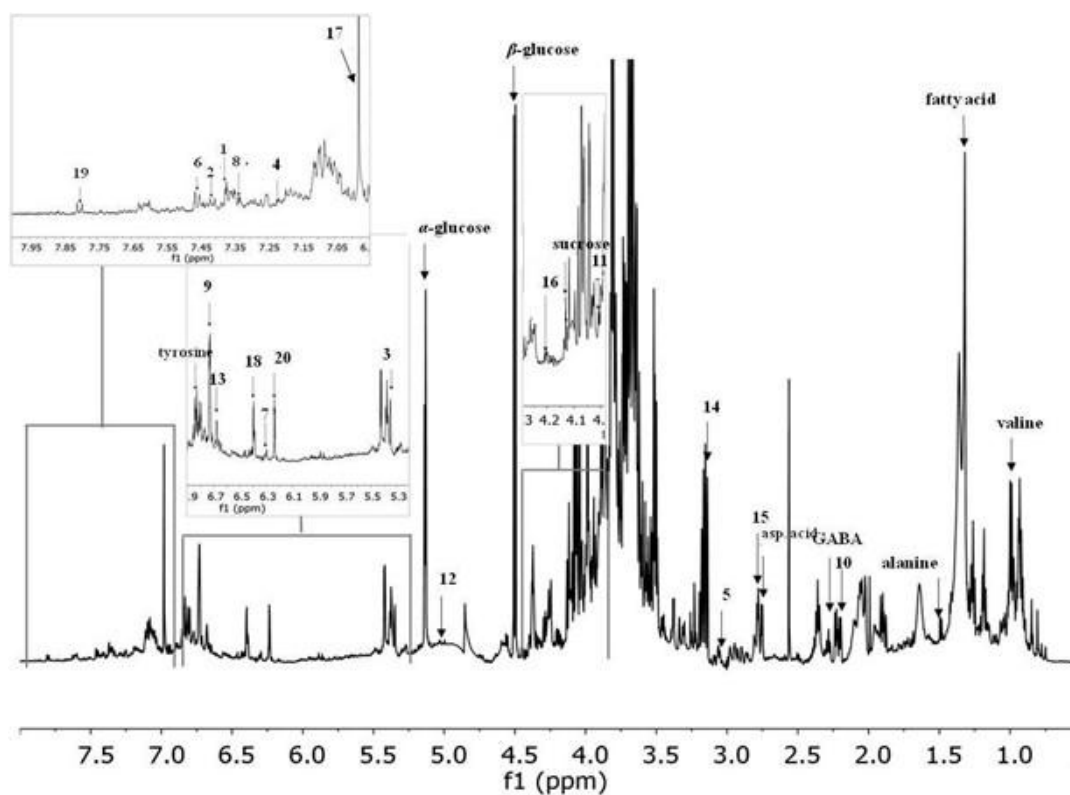


Figure 1.42. ^1H NMR spectra with annotations of identified metabolites detected in *C. avellana* leaves macerate at 10 hours, 50% ($\text{H}_2\text{O}:\text{EtOH}$), 1:30 (solid.: solvent): valine, alanine, giffonin J (**10**), GABA, aspartic acid, giffonin O (**15**), giffonin E (**5**), giffonin N (**14**), giffonin K (**11**), sucrose, giffonin P (**16**), β -glucose, giffonin L (**12**), α -glucose, giffonin C (**3**), kaempferol 3-*O*-(4''-*trans-p*-coumaroyl)- α -L-rhamnopyranoside (**20**), giffonin G (**7**), quercetin 3-*O*- α -L-rhamnopyranoside (**18**), giffonin M (**13**), giffonin I (**9**), tyrosine, myricetin 3-*O*- α -L-rhamnopyranoside (**17**), giffonin D (**4**), giffonin H (**8**), giffonin A (**1**), giffonin B (**2**), giffonin F (**6**), kaempferol 3-*O*- α -L-rhamnopyranoside (**19**).

Table 1.11. Characteristic ^1H NMR peaks identified in *C. avellana* leaves extracts.

compound	δ_{H} (J in Hz)
valine	1.0 (d, 1.0)
alanine	1.49 (d, 7.1)
giffonin J (10)	2.24 m
GABA	2.30 (t, 7.5)
aspartic acid	2.75 (dd, 8.8, 17.3)
giffonin O (15)	2.79 (dd, 11.2, 16.6)
giffonin E (5)	3.05 m
giffonin N (14)	3.53 m
giffonin K (11)	4.06 s
sucrose	4.13 (d, 8.7)
giffonin P (16)	4.27 (brdd, 6.1, 9.9)
β - glucose	4.50 (d, 7.9)
giffonin L (12)	4.80 (dd, 3.5, 11.4)
α - glucose	5.14 (d, 3.6)
giffonin C (3)	5.34 s
kaempferol 3- <i>O</i> -(4''- <i>trans-p</i> -coumaroyl)- α -L-rhamnopyranoside (20)	6.24 (d, 2.1)
giffonin G (7)	6.36 (d, 11.4)
quercetin 3- <i>O</i> - α -L-rhamnopyranoside (18)	6.42 (d, 2.0)
giffonin M (13)	6.71 (d, 1.8)
giffonin I (9)	6.76 (d, 8.1)
tyrosine	6.86 m
myricetin 3- <i>O</i> - α -L-rhamnopyranoside (17)	6.98 s
giffonin D (4)	7.26 (d, 8.1)
giffonin H (8)	7.36 (dd, 1.8, 8.1)
giffonin A (1)	7.41 (d, 8.1)
giffonin B (2)	7.45 (dd, 1.8, 8.1)
giffonin F (6)	7.52 (dd, 1.8, 8.1)
kaempferol 3- <i>O</i> - α -L-rhamnopyranoside (19)	7.81 (d, 8.1)

Amino acids occurring in the *C. avellana* leaves include valine, alanine, GABA, aspartic acid in the low to mid frequency region of the ^1H NMR spectrum and tyrosine in the region of higher frequency²⁶. A typical signal at δ 2.30 (t, $J = 7.5$) corresponding to γ -aminobutyric acid²⁶ (GABA) was also evident. The presence of fatty acids was suggested by specific resonances at δ 1.27 and δ 1.64, along with overlapping triplets with coupling constants around 7.0 Hz within 0.8-0.95 ppm.

The mid to low-field region from 3.5 to 5.5 ppm showed peaks mainly due to carbohydrate. The ^1H NMR spectrum displayed signals of sugars ascribable to sucrose at δ 4.13 (d, $J = 8.7$ Hz), and two anomeric protons related to β -glucose at δ 4.50 ppm (d, $J = 7.9$ Hz) and α -glucose at δ 5.14 (d, $J = 3.6$ Hz).

A large number of phenolic compounds were present in the ^1H NMR spectrum, mainly represented by diarylheptanoid and flavonoid derivatives. The analysis of the NMR spectrum at low-field region suggested the presence of different signals ascribable to cyclic diarylheptanoids typical of *C. avellana*; in particular, five aromatic signals at δ 7.26, 7.36, 7.41, 7.45, 7.52 due to the protons H_{15} of giffonins D, H, A, B, F, respectively, and other aromatic signals related to different protons of the 1,2,4-trisubstituted aromatic rings of giffonin M at δ 6.71 (d, $J = 1.8$ Hz) and giffonin I at δ 6.76 (d, $J = 8.0$ Hz) were observed. The region 6.8-7.5 ppm showed other overlapping signals, due to the presence of other giffonins (as further confirmed by 2D NMR experiments). So, for these compounds other signals located in different regions of the spectrum were chosen, to unequivocally assign the molecule structures. Thus, the protons linked to the oxymethine carbons of the heptanoid chain related to giffonin P at δ 4.27 (brdd, $J = 6.1$ and 9.9 Hz), giffonin L at δ 4.80 (dd, $J = 3.5$ and 11.4 Hz) and giffonin C at δ 5.34 (s) were considered. In the aliphatic region, signals related to CH_2 of the heptanoid chain of giffonins J at δ 2.24 (m), giffonin O at δ 2.79 (dd, $J = 11.2$ and 16.6 Hz), giffonin E at δ 3.05 (m) and giffonin N at δ 3.53 (m), were detected.

The presence of flavonoids was suggested by their characteristic signals in the aromatic regions, in particular the signal at δ 7.81 (2H, d, $J = 8.6$ Hz) was relative to H-2' and H-6' of the kaempferol 3-*O*- α -L-rhamnopyranoside, the proton signal at δ 6.98 (s) corresponded to myricetin 3-*O*-rhamnopyranoside while the signals at δ 6.24 (d, $J = 2.1$ Hz) and 6.42 (d, $J = 2.0$ Hz) were ascribable to H-8 of the kaempferol 3-*O*- α -L-(4''-trans-*p*-coumaroyl) rhamnopyranoside and quercetin 3-*O*- α -L-rhamnopyranoside, respectively.

The presence of all the metabolites suggested by the ^1H NMR spectra was further confirmed by their peaks in the bidimensional experiments HSQC, HMBC and COSY.

Multivariate Data analysis

With the aim to investigate the impact of the preparation method on the metabolite profile of *C. avellana* leaves, PCA, PLS-DA and PLS methods were carried out. Specifically, exploratory data analysis was performed by principal component analysis (PCA) while two different projection to latent structures partial least squares-discriminant analysis (PLS-DA) and partial least squares (PLS)-based methods were applied to discriminate the samples.

While PCA is a well-known technique used in multivariate data analysis, the PLS-based approach is a robust regression technique used to investigate the relationships existing between two blocks of data, usually called X- and Y-block and has predictive applications. In the present study, in a first step discriminant classification was carried out using partial least squares-discriminant analysis (PLS-DA), a method based on the PLS regression algorithm, that use arbitrary classes as the Y for the regression. In a second step the quantitative determination of phenolic content was used as Y and correlated to the data matrix obtained by NMR metabolomics data.

To this extent, PCA was performed by measuring the selected peak area for each identified metabolite in the $^1\text{H-NMR}$ dataset and a matrix was obtained by using these areas (variables), while the columns of the matrix were the different “green” extracts obtained through the use of “eco-friendly” procedures (observations). The exploratory principal component analysis (PCA) was employed in order to acquire a general insight and visualize any relation (trends, outliers) among the observations (samples). The PCA score plot shows the separation of samples into clusters (observations), while the loading plot highlights the metabolites that contribute to the separation (variables).

In this study, $^1\text{H NMR}$ derived data set were subjected to PCA to understand the clustering characteristic of the extracts obtained with different extraction protocols, and to determine the compounds responsible for their discrimination. The resulted model, obtained after scaling data by Pareto scaling, showed good fitness and the absence of outliers. The extracts of the leaves obtained with the four different extraction methods (maceration with methanol, maceration with ethanol:water, infusion and SLDE-Naviglio) appeared separated into four clusters. In figure 1.43, the extracts obtained with MeOH, used only in a comparative way respect of “eco-friendly” procedures, appear located in a section of the score plot different from those of the “green extracts”. PC1 contributed to 49.3% of the variance followed by PC2, which contributed to 11.9%. Hence, the first two PCs exhibited a total variance of 61.2%. Therefore, the extracts were well discriminated each other. Specifically, in the PCA model the extracts obtained by infusions (in triplicate, I1-3, J1-3 and K1-3) were separated from extracts obtained by maceration (in triplicate, A1-3, B1-3, C1-3, D1-3) and SLDE-Naviglio (in triplicate, E1-3, F1-3, G1-3) along the second principal component (PC2), resulting the extraction solvent as the main differentiating factor. In the PCA model a clear difference between the extractions carried out with SLDE-Naviglio with cycle of 12 minutes and those of 6.5-8 minutes, was evident, probably due to

a very long and hard extraction that affect the metabolite content; for this reason the extracts obtained by SLDE-Naviglio, with a cycle of 12 min were not considered during successive steps. Figure 1.43 B shows the loading scatter plot relative to this model. The contribute of variables under investigation for the discrimination of MeOH extract samples, appearing in the low right square of the plot, is not evaluable by loading plot.

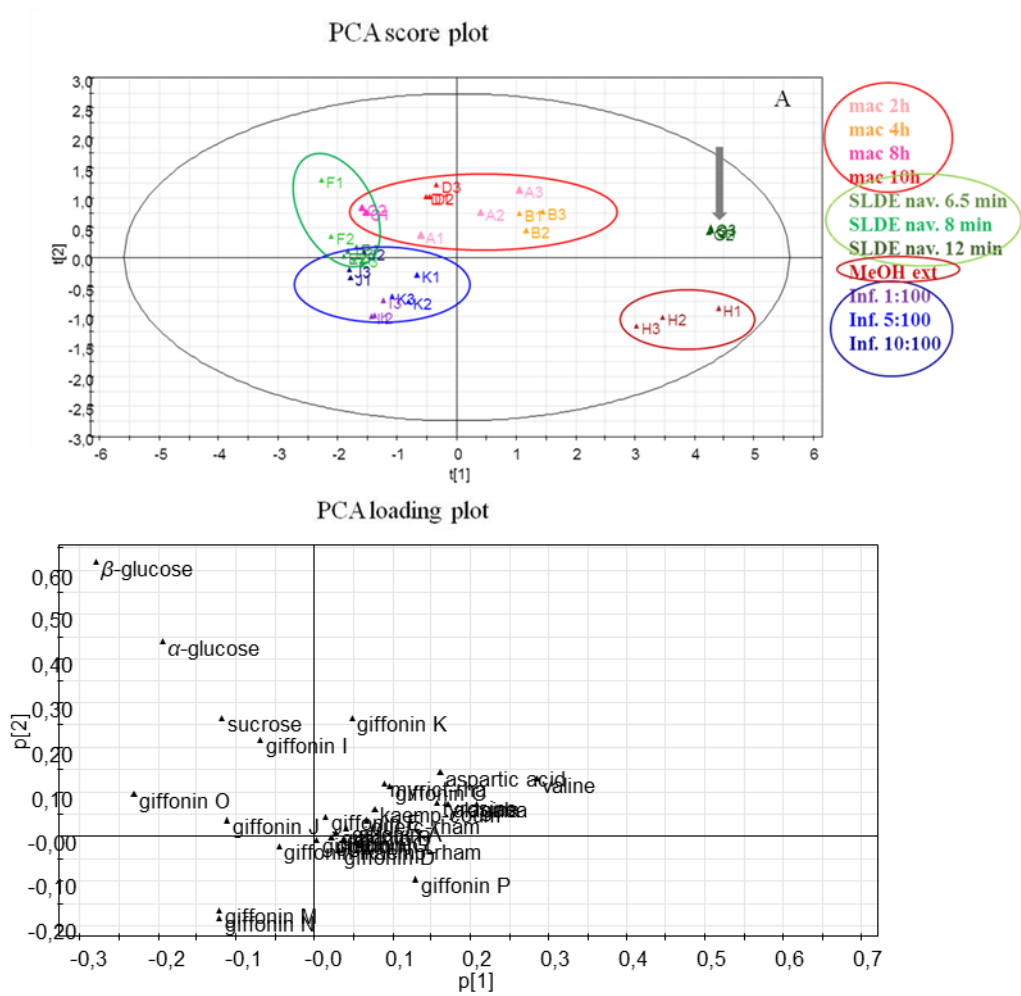


Figure 1.43. A) PCA score scatter plot, B) PCA loading plot.

Figure 1.44 shows the comparative PLS-DA analysis of extracts obtained by infusion, macerations and SLDE-Naviglio (except that with cycle of 12 min), with the PLS-DA score plot with component one explaining 22% of the variation and component two accounting for 36% of the variation, exhibiting a good separation between these groups. The PLS-DA analysis showed a distinct separation (R^2Y , 0.84) and good predictability (Q^2 , 0.71) and was validated by permutation test which proved the model was credible and robust.

PLS-DA showed a main separation among extracts obtained by infusion and those obtained by maceration along the first principal component (PC1). Only the extracts achieved by Naviglio (E1-3: with a cycle of 8 min and F1-3: with a cycle of 6.5 min) were separated in the plot by the second principal component (PC2) but not by PC1 component (fig. 1.44A). In figure 1.44B the loading scatter plot shows potentially significant metabolites based on contributions and reliability to the separation observed in the score scatter plot. Metabolites in the loading plot that are distant from the origin, can be considered as markers of the extraction procedures as a confirmation of their different distribution in different samples. In addition the specific contribute of single variables to the principal component 1 (PC1) is reported in figure 1.44C. The metabolites marked below the baseline are present in lower concentrations in the extracts obtained by maceration as compared to those obtained by infusions. Maceration protocol determine higher concentrations of primary metabolites as amino acids (valine, aspartic acid and GABA), sugars (α -glucose, β -glucose and sucrose) and of some secondary metabolites [(giffonins C, I, K, P, kaempferol 3-*O*-(4''-trans-*p*-coumaroyl)- α -L-rhamnopyranoside and myricetin 3-*O*- α -L-rhamnopyranoside)].

Moreover, a PLS correlation of ^1H NMR data matrix with phenolic content (measured by Folin-Ciocalteu method) used as Y, was performed. PLS analysis model was validated as described above, resulting in a predictive Q^2 value of 0.67 and in a correlation R^2Y value of 0.82.

Score scatter plot of PLS model (fig. 1.45A) showed principally a separation of observations along the first principal component (PC1). In detail, the infusions and the extracts obtained by maceration were located, respectively, in the left and right of the score scatter plot; only the extracts achieved by Naviglio (E1-3: with a cycle of 8 min and F1-3: with a cycle of 6.5 min) were separated in the plot by the second principal component (PC2) but not by PC1 component. By means of PLS variable graphs (fig. 1.45B) it has been possible to highlight the metabolites mainly responsible of these differences, in particular the flavonoids kaempferol 3-*O*-(4''-trans-*p*-coumaroyl)- α -L-rhamnopyranoside and myricetin 3-*O*- α -L-rhamnopyranoside and the diarylheptanoid giffonin I mainly contribute to phenolic content of extracts obtained by maceration.

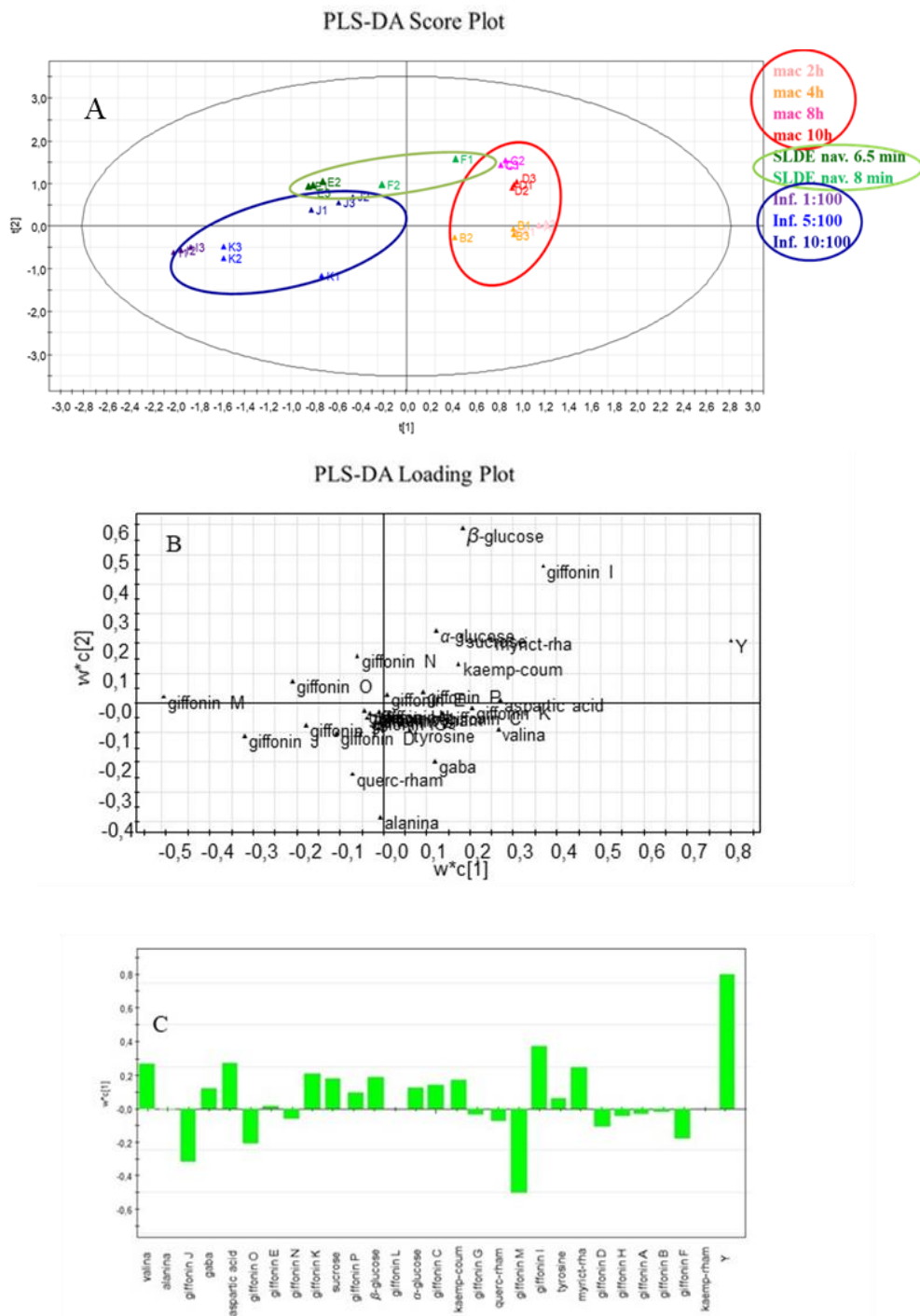


Figure 1.44. A) PLS-DA score scatter plot, B) PLS-DA loading plot, C) PLS DA single variables to the principal component 1 (PC1).

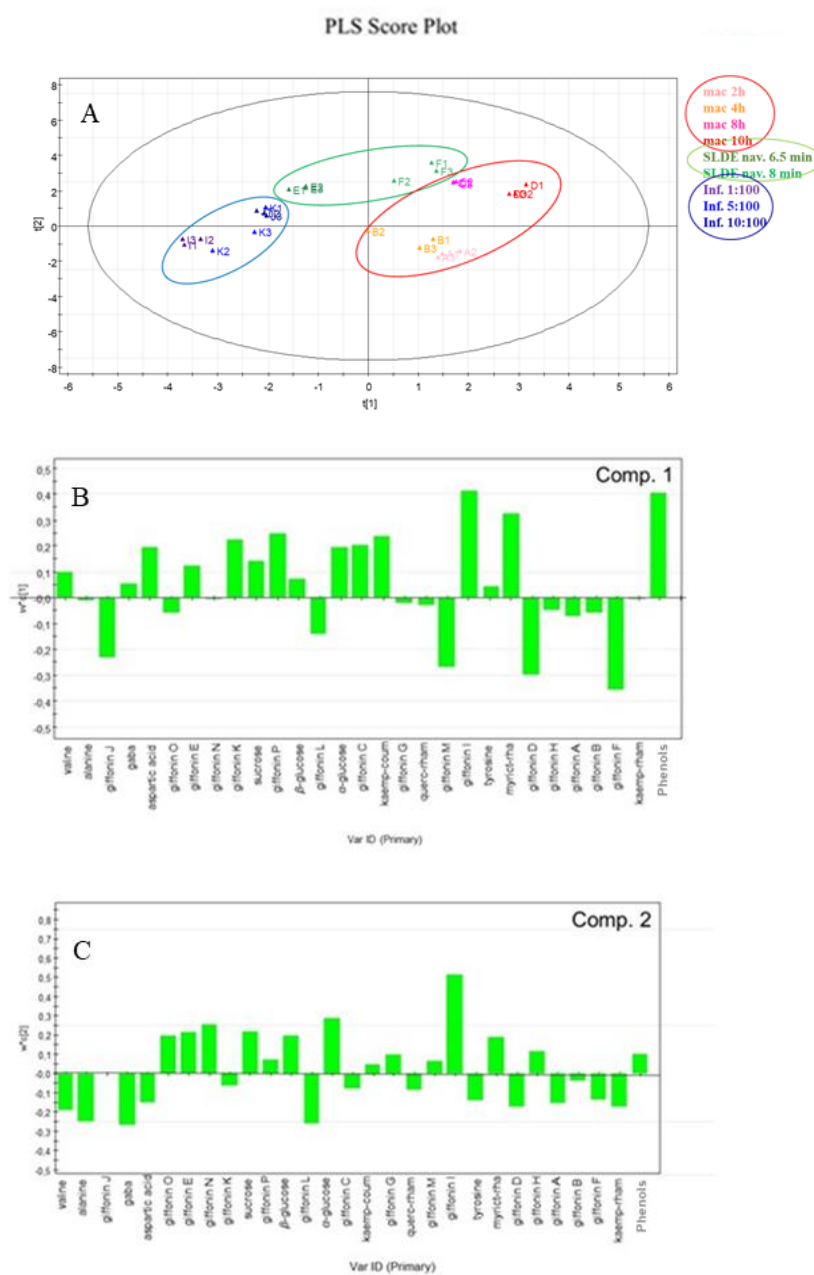


Figure 1.45. PLS correlation of ^1H NMR data matrix with phenolic content (measured by Folin-Ciocalteu method). A) PLS Score Plot, B) single variables to the principal component 1 (Comp. 1), Y= phenols. C) single variables to the principal component 2 (Comp. 2), Y= phenols

Cytotoxicity by WST-1 assay.

During my period abroad at the University of Veterinary and Pharmaceutical Sciences of Brno, the cytotoxicity of the extracts that showed the highest total phenolic content (1:30, 50% 10h and Naviglio 6.5 min) and their ability to inhibit proliferation were investigated by WST-1 assay using the cell line THP-1 with the aim of finding a nontoxic concentration for subsequent *in vitro* experiments. The amount of formazan formed by reduction of the tetrazolium salt WST-1 corresponds directly to the number of viable cells with active mitochondrial reductases. Clearly non-toxic concentrations of the tested extracts were chosen for subsequent studies on cell cultures (5 µg/mL).

Evaluation of Influence of the extracts tested on the formation of ROS

Successively, the antioxidant effects of the tested extracts were confirmed by the evaluation of cellular ROS production stimulated by pyocyanin.

The pyocyanin, a toxin produced and secreted by the Gram negative bacterium *Pseudomonas aeruginosa*, causes the intracellular generation of ROS, which is one possible reason for cytotoxicity and the development of inflammation³¹.

Role of Oxidative Stress in Pyocyanin's Toxicity

Oxidative stress is a major contributing factor to the cytotoxicity displayed by PCN a reversible redox active compound with its effects seen in figure 1.46 below PCN's induction of oxidative stress is, at least in part, due to its ability to increase intracellular levels of reactive oxygen species (ROS), in particular superoxide (O_2^-) and hydrogen peroxide (H_2O_2). These increases are mediated by dismutase and under aerobic conditions, H_2O_2 and O_2^- are formed by cyclic non enzymatic reduction by NAD(P)H with PCN accepting electrons from NAD(P)H. The intracellular ROS formed after PCN exposure cause free radical damage resulting in oxidative damage to components of the cell cycle, as well as direct damage to

DNA, NAD(P)H depletion and enzyme inhibition with the main target, the mitochondria of cells³¹.

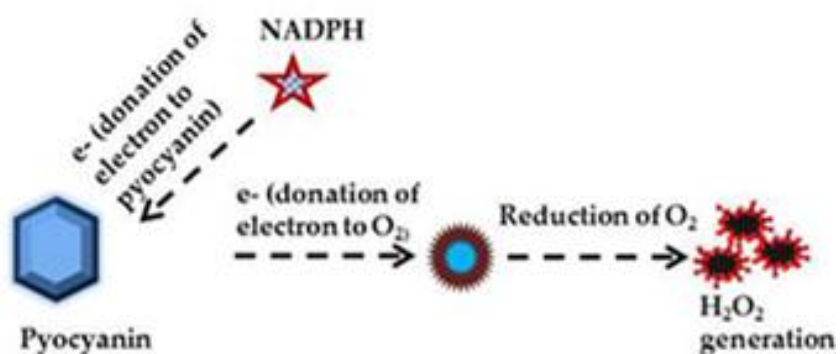


Figure 1.46. Mechanism of PCN-induced oxidative stress.

In this study the tested extracts produced antioxidant effects by reducing intracellular ROS levels. In particular, at 5 $\mu\text{g/mL}$, the extract obtained by maceration (1:30, 50% at 10h) and by Naviglio (6.5 min) showed a reducing intracellular ROS levels of about 31% and 42% (fig. 1.47 and table 1.12).

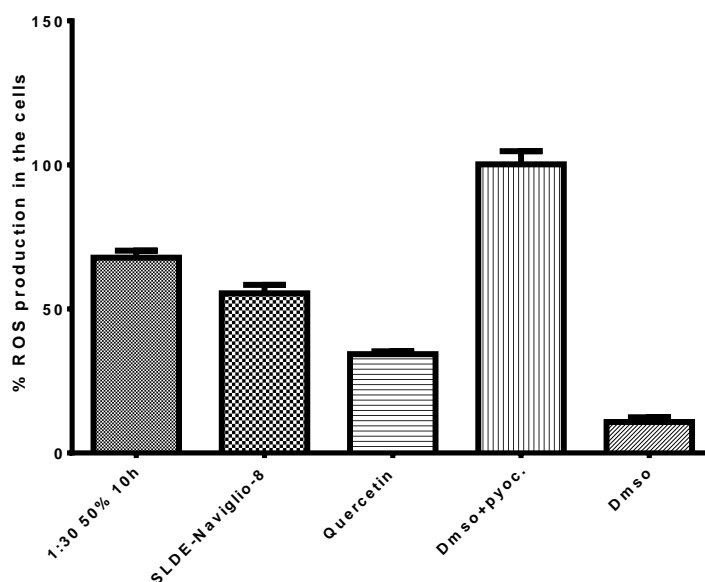


Figure 1.47. Antioxidant activity of tested extract by *in vitro* assay.

Table 1.12. Antioxidant activity evaluated by *in vitro* ROS- Pyocyanin assay.

“Tonda di Giffoni“ PGI leaves extracts 5 $\mu\text{g/mL}$)	inhibition of ROS induced by pyocyanin (%)
Maceration (EtOH:H ₂ O 50%, solid-solvent ratio 1.30, 10h)	30.92 \pm 4.08**
SLDE-Naviglio (8.0 min)	42.41 \pm 2.59**
Quercetin*	65.89 \pm 0.94**
DMSO	89.47 \pm 4.00**

* 5 μM ; ** $p < 0.05$

1.3. Conclusion

The phytochemical investigation of the MeOH extract of *C. avellana*, cv. Tonda di Giffoni leaves allowed us to isolate and characterize 16 new compounds belonging to diarylheptanoid class, some of which preventing the oxidative damages of human plasma lipids, induced by H₂O₂ and H₂O₂/Fe²⁺. Noteworthy, giffonins A–P differ from the compounds reported in the leaves of *C. avellana* collected in Turkey, because they represent cyclized diarylheptanoids, revealing the cultivar Tonda di Giffoni as a source of both cyclic diarylheptanoids and diaryletherheptanoids.

Herein NMR metabolomics with multivariate data analysis (MVDA) was used to identify the metabolite variation among the “green” extracts obtained by macerations, infusions and SLDE-Naviglio extraction of the leaves of *C. avellana*. The three different “eco-friendly” extraction methods contribute to the variation of phenolic content, as well as to the antioxidant activity. By means of the ¹H NMR analysis followed by multivariate data analysis of *C. avellana* leaves it is evident that no qualitative variation occur in the extracts obtained by maceration, infusion and SLDE-Naviglio. The obtained results demonstrate that the maceration procedure with 50% ethanol:water for 10 h is the most suitable method to extract *C. avellana* leaves, affording the highest amount of phenolic

compounds. The ^1H NMR-based metabolomics reveals the metabolite variation among the leaves subjected to different extraction methods and correlates the phenolic content to the specific phytochemicals occurring in the extracts. So, the constituents that mainly contribute to the phenolic content of the extract obtained by with 50% ethanol:water for 10 h result to be kaempferol 3-*O*-(4''-*trans-p*-coumaroyl)- α -L-rhamnopyranoside , myricetin 3-*O*- α -L-rhamnopyranoside and the diarylheptanoid giffonin I.

Therefore, this study demonstrates the potential benefits of *C. avellana* leaves as a rich source of phenolic compounds and reinforces the notion of the antioxidant capacity of *C. avellana* leaves extracts. In particular, it can be suggested that the maceration in the indicated conditions appears as the best procedure to obtain an extract rich in antioxidant phenolics. All these finding represent a real way to give an interesting and economically feasible opportunity to recycle the leaves of the PGI product *C. avellana*.

1.4. Experimental section

Plant Material

The leaves of the *C. avellana* cv. Tonda di Giffoni were collected at Giffoni, Salerno, Italy, in November 2012 and identified by V. De Feo (Department of Pharmacy, University of Salerno, Italy). A voucher specimen has been deposited in this Department.

Extraction and Isolation

The leaves of *C. avellana* cv. Tonda di Giffoni (910 g) were dried and extracted at room temperature using solvents of increasing polarity, inclusive of as *n*-hexane (2.5 L for 3 days, three times), CHCl_3 (2.5 L for 3 days, three times), and MeOH (2.5 L for 3 days, three times). After filtration and evaporation of the solvent to

dryness in vacuo, 30 g of crude MeOH extract were obtained. The dried MeOH extract (3.0 g) was fractionated on a Sephadex LH-20 (Pharmacia) column (100 x 5 cm), using MeOH as mobile phase, affording 88 fractions (8 mL), which were monitored by TLC. Fractions 30-31 (36.9 mg) were chromatographed by semi-preparative HPLC using MeOH- H₂O (12:8) as mobile phase (flow rate 2.5 mL/min) to yield compounds **10** (1.7 mg, $t_R = 9.2$ min) and **11** (2.1 mg, $t_R = 10.0$ min). Fractions 34-35 (56.5 mg) were chromatographed by semipreparative HPLC using MeOH-H₂O (3:2) as mobile phase (flow rate 2.5 mL/min) to yield compounds **2** (1.8 mg, $t_R = 11.1$ min), **6** (1.5 mg, $t_R = 19.5$ min), **3** (2.9 mg, $t_R = 30.2$ min), and **5** (1.6 mg, $t_R = 52.2$ min). Fractions 36-40 (90.0 mg) were chromatographed by semipreparative HPLC using MeOH- H₂O (13:7) as mobile phase (flow rate 2.5 mL/min) to yield compounds **8** (2.4 mg, $t_R = 18.0$ min), **1** (2.0 mg, $t_R = 19.2$ min), **7** (3.5 mg, $t_R = 20.5$ min), and **4** (4.1 mg, $t_R = 21.2$ min). Fraction 41 (13.5 mg) was chromatographed by semipreparative HPLC using MeOH- H₂O (9:11) as mobile phase (flow rate 2.5 mL/min) to yield compound **9** (2.5 mg, $t_R = 20.0$ min). Fractions 42-43 (27.0 mg) were chromatographed by semi-preparative HPLC using MeOH- H₂O (4:6) as mobile phase (flow rate 2.5 mL/min) to yield compound **14** (2.5 mg, $t_R = 18.4$ min). Fractions 48-50 (31.0 mg) were chromatographed by semi-preparative HPLC using MeOH-H₂O (2:3) as mobile phase (flow rate 2.5 mL/min) to yield compounds **16** (3.2 mg, $t_R = 9.2$ min), **12** (1.8 mg, $t_R = 18.2$ min), **15** (1.0 mg, $t_R = 19.5$ min), and **13** (1.0 mg, $t_R = 21.6$ min). Fractions 52-53 (29.0 mg) were chromatographed by semi-preparative HPLC using MeOH-H₂O (1:1) as mobile phase (flow rate 2.5 mL/min) to yield compound **19** (3.0 mg, $t_R = 28.8$ min). Fractions 54-56 (70.0 mg) were chromatographed by semi-preparative HPLC using MeOH-H₂O (9:11) as mobile phase (flow rate 2.5 mL/min) to yield compound **18** (10.0 mg, $t_R = 29.6$ min). Fractions 59-62 (82.0 mg) were chromatographed by semi-preparative HPLC using MeOH-H₂O (2:3) as mobile phase (flow rate 2.5 mL/min) to yield

compound **17** (15.0 mg, $t_R = 10.8$ min). Fractions 71-73 corresponded to compound **20** (13.6 mg).

Giffonin A (1): amorphous white solid; IR (KBr) ν_{\max} 3440, 2935, 1705, 1660 cm^{-1} ; ^1H and ^{13}C NMR (MeOH- d_4 , 600 MHz) data, see table 1.1; ESI/LTQORBITRAP/MS $[\text{M}+\text{Na}]^+$ m/z 377.1369 (calcd for $\text{C}_{21}\text{H}_{22}\text{O}_5\text{Na}$, 377.1365).

Giffonin B (2): amorphous white solid; $[\alpha]_{\text{D}}^{25}$ -14 (c 0.1 MeOH); IR (KBr) ν_{\max} 3430, 2940, 1705, 1660 cm^{-1} ; ^1H and ^{13}C NMR (MeOH- d_4 , 600 MHz) data, see table 1.1; ESI/LTQORBITRAP/MS $[\text{M}+\text{Na}]^+$ m/z 393.1318 (calcd for $\text{C}_{21}\text{H}_{22}\text{O}_6\text{Na}$, 393.1314).

Giffonin C (3): amorphous white solid; $[\alpha]_{\text{D}}^{25}$ -28 (c 0.03 MeOH); IR (KBr) ν_{\max} 3450, 2940, 1655 cm^{-1} ; ^1H and ^{13}C NMR (MeOH- d_4 , 600 MHz) data, see table 1.1; ESI/LTQORBITRAP/MS $[\text{M}+\text{Na}]^+$ m/z 379.1524 (calcd for $\text{C}_{21}\text{H}_{24}\text{O}_5\text{Na}$, 379.1521).

Giffonin D (4): amorphous white solid; IR (KBr) ν_{\max} 3425, 2930, 1713, 1665 cm^{-1} ; ^1H and ^{13}C NMR (MeOH- d_4 , 600 MHz) data, see table 1.1; ESI/LTQORBITRAP/MS $[\text{M}+\text{Na}]^+$ m/z 377.1367 (calcd for $\text{C}_{21}\text{H}_{22}\text{O}_5\text{Na}$, 377.1365).

Giffonin E (5): amorphous white solid; $[\alpha]_{\text{D}}^{25}$ -28 (c 0.03 MeOH); IR (KBr) ν_{\max} 3430, 2935, 1665 cm^{-1} ; ^1H and ^{13}C NMR (MeOH- d_4 , 600 MHz) data, see table 1.2; ESI/LTQORBITRAP/MS $[\text{M}+\text{Na}]^+$ m/z 379.1526 (calcd for $\text{C}_{21}\text{H}_{24}\text{O}_5\text{Na}$, 379.1521).

Giffonin F (6): amorphous white solid; $[\alpha]_{\text{D}}^{25}$ -24 (c 0.03 MeOH); IR (KBr) ν_{\max} 3432, 2940, 1710, 1665 cm^{-1} ; ^1H and ^{13}C NMR (MeOH- d_4 , 600 MHz) data, see table 1.2; ESI/LTQORBITRAP/MS $[\text{M}+\text{Na}]^+$ m/z 393.1319 (calcd for $\text{C}_{21}\text{H}_{22}\text{O}_6\text{Na}$, 393.1314).

Giffonin G (7): amorphous white solid; $[\alpha]_D^{25}$ -71 (*c* 0.1 MeOH); IR (KBr) ν_{\max} 3430, 2930, 1620 cm^{-1} ; ^1H and ^{13}C NMR (MeOH- d_4 , 600 MHz) data, see table 1.2; ESI/LTQORBITRAP/MS $[\text{M}+\text{Na}]^+$ m/z 377.1365 (calcd for $\text{C}_{21}\text{H}_{22}\text{O}_5\text{Na}$, 377.1365).

Giffonin H (8): amorphous white solid; $[\alpha]_D^{25}$ -22 (*c* 0.03 MeOH); IR (KBr) ν_{\max} 3430, 2930, 1620 cm^{-1} ; ^1H and ^{13}C NMR (MeOH- d_4 , 600 MHz) data, see table 1.2; ESI/LTQORBITRAP/MS $[\text{M}+\text{Na}]^+$ m/z 347.1261 (calcd for $\text{C}_{20}\text{H}_{20}\text{O}_4\text{Na}$, 347.1259).

Giffonin I (9): amorphous white solid; $[\alpha]_D^{25}$ -4 (*c* 0.1 MeOH); IR (KBr) ν_{\max} 3425, 2920, 1710 cm^{-1} ; ^1H and ^{13}C NMR (MeOH- d_4 , 600 MHz) data, see table 1.3; ESI/LTQORBITRAP/MS $[\text{M}+\text{Na}]^+$ m/z 611.2107 (calcd for $\text{C}_{30}\text{H}_{36}\text{O}_{12}\text{Na}$, 611.2104).

Giffonin J (10): amorphous white solid; $[\alpha]_D^{25}$ -15 (*c* 0.1 MeOH); IR (KBr) ν_{\max} 3440, 2945, 1655 cm^{-1} ; ^{13}C and ^1H NMR (MeOH- d_4 , 600 MHz) data, see table 1.4; ESI/LTQORBITRAP/MS $[\text{M}+\text{Na}]^+$ m/z 395.1475 (calcd for $\text{C}_{21}\text{H}_{24}\text{O}_6\text{Na}$, 395.1471).

Giffonin K (11): amorphous white solid; $[\alpha]_D^{25}$ -5 (*c* 0.1 MeOH); IR (KBr) ν_{\max} 3435, 2930, 1625 cm^{-1} ; ^{13}C and ^1H NMR (MeOH- d_4 , 600 MHz) data, see table 1.4; ESI/LTQORBITRAP/MS $[\text{M}+\text{Na}]^+$ m/z 393.1317 (calcd for $\text{C}_{21}\text{H}_{22}\text{O}_6\text{Na}$, 393.1314).

Giffonin L (12): amorphous white solid; $[\alpha]_D^{25}$ + 10 (*c* 0.1 MeOH); IR (KBr) ν_{\max} 3440, 3010, 2941, 655 cm^{-1} ; ^1H and ^{13}C NMR (MeOH- d_4 , 600 MHz) data, see tables 1.5 and 1.6, respectively; ESI/LTQORBITRAP/MS $[\text{M}+\text{Na}]^+$ m/z 369.1317 (calcd for $\text{C}_{19}\text{H}_{22}\text{O}_6\text{Na}$, 369.1314).

Giffonin M (13): amorphous white solid; $[\alpha]_D^{25}$ - 14 (*c* 0.1 MeOH); IR (KBr) ν_{\max} 3430, 2930, 1720, 1665 cm^{-1} ; ^{13}C and ^1H NMR (MeOH- d_4 , 600 MHz) data, see

tables 1.5 and 1.6, respectively; ESI/LTQORBITRAP/MS $[M+Na]^+$ m/z 351.1211 (calcd for $C_{19}H_{20}O_5Na$, 351.1208).

Giffonin N (14): amorphous white solid; $[\alpha]_D^{25} +6$ (*c* 0.03 MeOH); IR (KBr) ν_{max} 3420, 2925, 1665 cm^{-1} ; ^{13}C and 1H NMR (MeOH- d_4 , 600 MHz) data, see tables 1.5 and 1.6, respectively; ESI/LTQORBITRAP/MS $[M+Na]^+$ m/z 513.1740 (calcd for $C_{25}H_{30}O_{10}Na$, 513.1737).

Giffonin O (15): amorphous white solid; $[\alpha]_D^{25} +27$ (*c* 0.1 MeOH); IR (KBr) ν_{max} 3430, 2930, 1725, 1665 cm^{-1} ; ^{13}C and 1H NMR (MeOH- d_4 , 600 MHz) data, see tables 1.5 and 1.6, respectively; ESI/LTQORBITRAP/MS $[M+Na]^+$ m/z 367.1161 (calcd for $C_{19}H_{20}O_6Na$, 367.1158).

Giffonin P (16): amorphous white solid; $[\alpha]_D^{25} -37$ (*c* 0.1 MeOH); IR (KBr) ν_{max} 3430, 2920, 1615 cm^{-1} ; ^{13}C and 1H NMR (MeOH- d_4 , 600 MHz) data, see tables 1.5 and 1.6, respectively; ESI/LTQORBITRAP/MS $[M+Na]^+$ m/z 385.1266 (calcd for $C_{19}H_{22}O_7Na$, 385.1263).

Preparation of (S)- and (R)-MTPA esters of 2, 3 and 5–8

(R)-(-) and (S)-(+)-MTPA-Cl (15 μ L) and a catalytic amount of DMAP were separately added to two different aliquots of **2** (each 1.5 mg) in anhydrous pyridine. The resulting mixtures were maintained at room temperature under vigorous stirring overnight, and then 1H NMR spectra were recorded. The related proton signals were assigned by analyzing COSY spectra. By the same procedure, the (S)- and (R)-MTPA esters of **3**, **5–8** were prepared, and the related proton signals were also assigned by analyzing COSY spectra.

(S)-MTPA ester of **2** (**2a**): selected 1H NMR values (600 MHz, MeOH- d_4) δ_H 7.80 (dd, $J = 8.5, 1.9$ Hz, H-19), 7.74 (dd, $J = 8.5, 1.9$ Hz, H-15), 7.29 (dd, $J = 8.5, 1.9$ Hz, H-18), 5.79 (dd, $J = 5.4, 8.9$ Hz, H-13), 5.25 (ddd, $J = 15.5, 10.5, 4.0$, H-8),

3.17 (t, $J = 5.5$ Hz, H-12), 2.65 (dt, $J = 16.0, 3.0$ Hz, H-10), 2.60 (m, H-9), 2.15 (m, H-9).

(*R*)-MTPA ester of **2** (**2b**): selected ^1H NMR values (600 MHz, MeOH- d_4) δ_{H} 7.74 (dd, $J = 8.5, 1.9$ Hz, H-19), 7.72 (dd, $J = 8.5, 1.9$ Hz, H-15), 7.28 (dd, $J = 8.5, 1.9$ Hz, H-18), 5.79 (dd, $J = 5.4, 8.9$ Hz, H-13), 5.26 (ddd, $J = 15.5, 10.5, 4.0$, H-8), 3.43 (t, $J = 5.5$ Hz, H-12), 2.68 (dt, $J = 16.0, 3.0$ Hz, H-10), 2.61 (m, H-9), 2.17 (m, H-9).

(*S*)-MTPA ester of **3** (**3a**): selected ^1H NMR values (600 MHz, MeOH- d_4) δ_{H} 6.49 (d, $J = 11.5$ Hz, H-7), 5.65 (ddd, $J = 11.5, 7.5, 7.5$ Hz, H-8), 4.23 (m, H-11), 3.15 (dt, $J = 12.5, 3.7$ Hz, H-13), 2.85 (td, $J = 12.5, 5.2$ Hz, H-13), 2.21 (m, H-12), 2.01 (m, H-9), 1.98 (m, H-12), 1.97 (m, H-9), 1.30 (m, H-10), 0.75 (m, H-10).

(*R*)-MTPA ester of **3** (**3b**): selected ^1H NMR values (600 MHz, MeOH- d_4) δ_{H} 6.48 (d, $J = 11.4$ Hz, H-7), 5.63 (ddd, $J = 11.5, 7.5, 7.5$ Hz, H-8), 4.23 (m, H-11), 3.19 (dt, $J = 12.5, 3.7$ Hz, H-13), 2.87 (td, $J = 12.5, 5.2$ Hz, H-13), 2.31 (m, H-12), 2.00 (m, H-9), 2.03 (m, H-12), 1.95 (m, H-9), 1.24 (m, H-10), 0.68 (m, H-10).

(*S*)-MTPA ester of **5** (**5a**): selected ^1H NMR values (600 MHz, MeOH- d_4) δ_{H} 6.43 (d, $J = 11.2$ Hz, H-7), 5.20 (dd, $J = 11.2, 8.6$ Hz, H-8), 5.05 (ddd, $J = 12.0, 8.5, 3.4$ Hz, H-9), 3.07 (m, H-13), 2.45 (td, $J = 12.5, 5.4$ Hz, H-13), 2.16 (m, H-12), 1.98 (q, $J = 10.8$ Hz, H-11), 1.45 (m, H-10), 1.38 (m, H-12), 1.12 (m, H-11), 0.35 (br t, $J = 11.8$ Hz, H-10).

(*R*)-MTPA ester of **5** (**5b**): selected ^1H NMR values (600 MHz, MeOH- d_4) δ_{H} 6.40 (d, $J = 11.2$ Hz, H-7), 5.15 (dd, $J = 11.2, 8.6$ Hz, H-8), 5.05 (ddd, $J = 12.0, 8.5, 3.4$ Hz, H-9), 3.09 (m, H-13), 2.48 (td, $J = 12.5, 5.4$ Hz, H-13), 2.21 (m, H-12), 2.05 (q, $J = 10.8$ Hz, H-11), 1.65 (m, H-10), 1.40 (m, H-12), 1.28 (m, H-11), 0.40 (br t, $J = 11.8$ Hz, H-10).

(*S*)-MTPA ester of **6** (**6a**): selected ^1H NMR values (600 MHz, MeOH- d_4) δ_{H} 6.53 (d, $J = 11.8$ Hz, H-7), 5.25 (dd, $J = 11.8, 8.6$ Hz, H-8), 5.15 (t, $J = 10.0$ Hz, H-9),

3.13 (m, H-13), 3.09 (td, $J = 12.5, 5.5$ Hz, H-13), 2.90 (td, $J = 12.5, 5.5$ Hz, H-12), 2.59 (m, H-12), 2.75 (m, H-10), 1.90 (br s, H-10).

(*R*)-MTPA ester of **6** (**6b**): selected ^1H NMR values (600 MHz, MeOH- d_4) δ_{H} 6.50 (d, $J = 11.8$ Hz, H-7), 5.20 (dd, $J = 11.8, 8.6$ Hz, H-8), 5.15 (t, $J = 10.0$ Hz, H-9), 3.15 (m, H-13), 3.10 (td, $J = 12.5, 5.5$ Hz, H-13), 2.92 (td, $J = 12.5, 5.5$ Hz, H-12), 2.60 (m, H-12), 2.80 (m, H-10), 2.05 (br s, H-10).

(*S*)-MTPA ester of **7** (**7a**): selected ^1H NMR values (600 MHz, MeOH- d_4) δ_{H} 7.52 (dd, $J = 8.2, 1.9$ Hz, H-19), 7.08 (dd, $J = 8.2, 1.9$ Hz, H-18), 6.47 (d, $J = 11.4$ Hz, H-7), 6.05 (dd, $J = 11.4, 9.0$ Hz, H-8), 5.87 (dd, $J = 15.4, 8.4$ Hz, H-10), 5.69 (dd, $J = 15.4, 9.0$ Hz, H-9), 5.57 (dt, $J = 8.4, 3.3$ Hz, H-11), 3.05 (dt, $J = 12.5, 3.0$ Hz, H-13), 2.83 (td, $J = 12.5, 3.0$ Hz, H-13), 2.27 (dq, $J = 14.0, 3.3$ Hz, H-12), 1.75 (tt, $J = 14.0, 3.3$ Hz, H-12).

(*R*)-MTPA ester of **7** (**7b**): selected ^1H NMR values (600 MHz, MeOH- d_4) δ_{H} 7.53 (dd, $J = 8.2, 1.9$ Hz, H-19), 7.09 (dd, $J = 8.2, 1.9$ Hz, H-18), 6.45 (d, $J = 11.4$ Hz, H-7), 6.02 (dd, $J = 11.4, 9.0$ Hz, H-8), 5.83 (dd, $J = 15.4, 8.4$ Hz, H-10), 5.67 (dd, $J = 15.4, 9.0$ Hz, H-9), 5.57 (dt, $J = 8.4, 3.3$ Hz, H-11), 3.08 (dt, $J = 12.5, 3.0$ Hz, H-13), 2.85 (td, $J = 12.5, 3.0$ Hz, H-13), 2.41 (dq, $J = 14.0, 3.3$ Hz, H-12), 1.79 (tt, $J = 14.0, 3.3$ Hz, H-12).

(*S*)-MTPA ester of **8** (**8a**): selected ^1H NMR values (600 MHz, MeOH- d_4) δ_{H} 7.41 (dd, $J = 8.3, 1.9$ Hz, H-19), 7.30 (dd, $J = 8.3, 1.9$ Hz, H-18), 6.22 (d, $J = 11.4$ Hz, H-7), 5.98 (t, $J = 11.4$ Hz, H-8), 5.88 (dd, $J = 15.4, 8.6$ Hz, H-10), 5.79 (dd, $J = 15.4, 11.4$ Hz, H-9), 5.57 (dt, $J = 8.6, 3.5$ Hz, H-11), 3.06 (dt, $J = 13.0, 3.3$ Hz, H-13), 2.80 (td, $J = 13.0, 3.3$ Hz, H-13), 2.24 (dq, $J = 14.2, 3.4$ Hz, H-12), 1.73 (tt, $J = 14.2, 3.4$ Hz, H-12).

(*R*)-MTPA ester of **8** (**8b**): selected ^1H NMR values (600 MHz, MeOH- d_4) δ_{H} 7.42 (dd, $J = 8.3, 2.9$ Hz, H-19), 7.31 (dd, $J = 8.3, 2.9$ Hz, H-18), 6.20 (d, $J = 11.2$ Hz, H-7), 5.96 (t, $J = 11.2$ Hz, H-8), 5.84 (dd, $J = 15.4, 8.6$ Hz, H-10), 5.76 (dd, $J = 15.4, 11.2$ Hz, H-9), 5.57 (dt, $J = 8.6, 3.8$ Hz, H-11), 3.08 (dt, $J = 12.8, 3.3$ Hz,

H-13), 2.82 (td, $J = 12.8, 3.3$ Hz, H-13), 2.36 (dq, $J = 14.2, 3.8$ Hz, H-12), 1.75 (tt, $J = 14.2, 3.8$ Hz, H-12).

Computational Details

Maestro 9.6³² was used to build the chemical structures of all possible relative diastereoisomers of compounds **10-16**. Optimization of the 3D structures was performed with MacroModel 10.2³² using the OPLS force field³³ and the Polak-Ribier conjugate gradient algorithm (PRCG, maximum derivative less than 0.001 kcal/mol).

In particular, for compounds **10**, **11**, **13** and **14**, which have two stereochemical centers, two possible diastereoisomers were considered:

- **10a** (12*S**,14*S**), **10b** (12*R**,14*S**);
- **11a** (12*S**,14*S**), **11b** (12*R**,14*S**);
- **13a** (8*S**,10*S**), **13b** (8*S**,10*R**);
- **14a** (8*S**,10*S**), **14b** (8*S**,10*R**).

For compound **15**, possessing three stereochemical centers, four possible diastereoisomers were considered:

- **15a** (8*S**,9*R**,12*R**), **15b** (8*S**,9*R**,12*S**),
- **15c** (8*S**,9*S**,12*R**) and **15d** (8*S**,9*S**,12*S**).

Moreover, for compounds **12**, possessing four stereochemical centers, eight diastereoisomers were accounted:

- **12a** (8*S**,10*R**,11*R**,12*R**), **12b** (8*S**,10*R**,11*R**,12*S**),
- **12c** (8*S**,10*R**,11*S**,12*R**), **12d** (8*S**,10*R**,11*S**,12*S**),
- **12e** (8*S**,10*S**,11*R**,12*R**), **12f** (8*S**,10*S**,11*R**,12*S**),
- **12g** (8*S**,10*S**,11*S**,12*R**), **12h** (8*S**,10*S**,11*S**,12*S**);

For compound **16**, which has five stereochemical centers with one plane of symmetry, eight possible diastereoisomers were taken into account:

- **16a** (8*S**,9*R**,11*R**,12*R**), **16b** (8*S**,9*R**,11*R**,12*S**),

- **16c** (8*S**,9*R**,11*S**,12*R**), **16d** (8*S**,9*R**,11*S**,12*S**),
- **16e** (8*S**,9*S**,11*R**,12*R**), **16f** (8*S**,9*S**,11*R**,12*S**),
- **16g** (8*S**,9*S**,11*S**,12*R**), **16h** (8*S**,9*S**,11*S**,12*S**).

Starting from the obtained 3D structures, exhaustive conformational searches at the empirical molecular mechanics (MM) level with Monte Carlo Multiple Minimum (MCMM) method (50,000 steps) and Low Mode Conformational Search (LMCS) method (50,000 steps) were performed, in order to allow a full exploration of the conformational space. Furthermore, molecular dynamic simulations were performed at 450, 600, 700, 750 K, with a time step of 2.0 fs, an equilibration time of 0.1 ns, and a simulation time of 10 ns. A constant dielectric term of MeOH, mimicking the presence of the solvent, was used in the calculations to reduce artefacts.

For each diastereoisomer, all the conformers obtained from the previously mentioned conformational searches were minimized (PRCG, maximum derivative less than 0.001 kcal/mol) and compared. The “Redundant Conformer Elimination” module of Macromodel 10.2³² was used to select non-redundant conformers, excluding the conformers differing more than 13.0 kJ/mol (3.11 kcal/mol) from the most energetically favoured conformation and setting a 1.0 Å RMSD (root-mean-square deviation) minimum cut-off for saving structures.

Next, the obtained conformers were optimized at quantum mechanical (QM) level by using the MPW1PW91 functional and the 6-31G(d) basis set³⁴, and experimental solvent effects (CH₃OH) were reproduced using the integral equation formalism version of the polarizable continuum model (IEFPCM). After this step at the QM level, the newly obtained geometries were visually inspected in order to remove further possible redundant conformers, and then those selected were accounted for the subsequent computation of the ¹³C and ¹H NMR chemical shifts, using the MPW1PW91 functional and the 6-31G(d,p) basis set and MeOH IEFPCM. Final ¹³C and ¹H NMR spectra for each of the investigated

diastereoisomers were built considering the influence of each conformer on the total Boltzmann distribution taking into account the relative energies. Furthermore, calibrations of calculated ^{13}C and ^1H chemical shifts were performed following the multi-standard approach (MSTD)^{35, 36}. In particular, aromatic ^{13}C and ^1H chemical shifts were scaled using benzene as reference compound^{35, 36}. All the other ^{13}C and ^1H calculated chemical shifts were scaled to TMS (tetramethylsilane).

Then, for each atom of the investigated molecules, the comparison of the experimental and calculated ^{13}C and ^1H NMR chemical shifts was performed computing the $\Delta\delta$ parameter:

$$\Delta\delta = |\delta_{\text{exp}} - \delta_{\text{calc}}|$$

where, δ_{exp} (ppm) and δ_{calc} (ppm) are the $^{13}\text{C}/^1\text{H}$ experimental and calculated chemical shifts, respectively.

The computation and comparison of the mean absolute errors (MAEs) for all the possible diastereoisomers (see table 1.7), were used for the determination of the relative configuration of each investigated compound:

$$\text{MAE} = \sum(\Delta\delta)/n$$

specifically defined as the summation through n of the absolute error values (difference of the absolute values between corresponding experimental and $^{13}\text{C}-^1\text{H}$ chemical shifts), normalized to the number of the chemical shifts considered. All QM calculations were performed using Gaussian 09 software package³⁷.

Determination of the Sugar Configuration.

The configurations of the sugar unit of glycosylate compounds were established after hydrolysis of each compounds with 1 N HCl, trimethylsilation, and determination of the retention times by GC operating under the reported experimental conditions.

*Sample preparation for eco-friendly extracts and infusion**Maceration extraction*

To determine the factors that permit to increase polyphenols yields, experiments under selected conditions for polyphenols extraction have been performed based on the literature data^{29,30}.

In particular, maceration has been carried out in a beaker with agitation fixed on 170 rpm, at room temperature. During extraction, the solution has been protected with plastic paraffin film, to prevent solvent evaporation. Aluminum foil has been used to preserve phenolic compound against every reaction with light.

The time extraction, the solid-solvent ratio and the different percentage ratio of the two solvents chosen for extraction have been studied as factors able to change the polyphenols yield.

Preliminary, the extraction with 50% ethanol:water and 1:20 solid– solvent ratio was performed^{27,28}. The samples were collected at 30 min, 60 min, 90 min, 2 h, 4 h, 8 h, 10 h, 14 h and 18 h. The effect of the different time of extraction on yield extract has been determined by colorimetric assays.

The extraction time lower than 2 h and the extraction time of more than 10 h had no significant influence on the amount of phenolics, so the optimization of the extraction for the next experiments was monitored at 2 h, 4 h, 8 h and 10 h.

In the next set of experiments, other two different solid-solvent ratio (1:10, 1:30) and different percentage ratio of ethanol:water (70% and 80%) have been used. The effect of these factors on yield extract have been determined by colorimetric assays.

Infusion extraction

On the basis of Pharmacopea XII three different solid-solvent ratio (1:100, 5:100 and 10:100) were studied. The infusions were carried out in boiling distilled water, using moderate stirring, recovered with aluminum and protected with plastic parafilm both to permit the conservation of a stable temperature and to prevent solvent evaporation and light reaction; then filtered under reduced pressure.

The effect of different solid-solvent ratio on yield extract was determined by the Folin–Ciocalteu methods.

SLDE-Naviglio

A dynamic solid–liquid extraction was carried out using a Naviglio Extractor. To find the best extractive cycle, were tested the follow conditions: 20 extractive cycles of 6.5 min (5 min in the static phase and 1.5 min in the dynamic phase; SLDE-Naviglio-6.5), 8 min (5 min in the static phase and 3 min in the dynamic phase; SLDE-Naviglio-8), and 12 min (9 min in the static phase and 3 min in the dynamic phase; SLDENaviglio-12) each as reported in literature.³⁸

The effect of the different extractive cycle on yield extract was determined by colorimetric assays.

Determination of total penolic content, determination of DPPH and TEAC radical scavenging activity.

Reported in the section: general experimental procedures.

NMR spectroscopy

All 2D-NMR spectra were acquired in MeOH-*d*₄ (99.95%).

For the sample preparation 5 mg crude extract was transferred to Eppendorf tube before the addition of the same volume (600 μL) of both MeOH-*d*₄. The sample was then vortexed and sonicated for 15 min at controlled temperature. A 500 μL

of supernatant was transferred to NMR tube. NMR experiments were performed on a Bruker DRX-600 spectrometer (Bruker BioSpin GmbH, Rheinstetten, Germany) equipped with a Bruker 5 mm TCI CryoProbeat 300 K. The NMR tubes were labeled and immediately subjected to ^1H NMR measurements using a preset setting for all of the samples. The analysis temperature was 24 °C.

Gradient shimming was performed prior to signal acquisition and $\text{MeOH-}d_4$ was used to provide an internal lock. The proton spectra were collected with a 90° pulse width of 8.25 μs , a relaxation delay 3 s, 128 scans, 64 K data points and a spectral width of 9 ppm.

A series of 2D experiments, Heteronuclear Single-Quantum Correlation Spectroscopy (HSQC) and Heteronuclear Multiple Bond Correlation (HMBC) were implemented and permitted the assignment of the existing metabolites.

Data reduction and spectral alignment

The spectra were imported into the MestreNOVA 10 software. Phasing, baseline correction, binning (spectral buckets of 0.004 ppm), normalization to the standardized area of the reference compound and removal of unwanted resonances (residual solvent) were performed. Finally, the spectra were aligned and converted to ASCII format.

Chemometrics

Data analysis

Spectrum processing is an intermediate step between acquiring the raw spectra and data analysis. It should preserve as much as possible the variance relative to the chemical compounds contained in the NMR spectra while reducing other

types of variance induced by different sources of bias such as baseline, noise or misalignment. Generally, spectrum processing steps include baseline correction, noise elimination, alignment, data reduction and normalization prior to multivariate statistical analyses. In the present work NMR spectra were manually phased and baseline corrected. Identification of metabolites was achieved using chemical shifts known by literature for each compound. Each samples was analyzed in triplicate.

Multivariate data analysis

Chemometric techniques based on projection methods were applied for metabolomics multivariate data analysis. Specifically, exploratory data analysis was performed by principal component analysis (PCA) while a projection to latent structures (PLS-DA) based method was applied to discriminate the samples based on the extraction system. In the protocol here followed, discriminant classification was carried out using partial least squares-discriminant analysis (PLS-DA), a method based on the PLS regression algorithm giving each sample a class based on the extraction method used. Classes attributed were -1, 0 and +1 and specifically -1 to samples obtained under maceration (I,L,K) 0 to samples obtained under Naviglio extraction (E, F, G) +1 to samples obtained by water infusion(A, B, C, D), Finally a PLS correlation of data matrix with measured phenolic content was performed (using the measured value as a Y).

Projection methods in multivariate data analysis were performed by using SIMCA-P+ software (Version 12.0, Umetrics, Umeå, Sweden). The entire data matrix, after log transform and Pareto scaling, was first analyzed by PCA to define homogeneous cluster of samples (Exploratory data analysis).

Models were validated by cross-validation techniques and permutation tests according to standardized good practice to minimize false discoveries and to obtain robust statistical models. A small number of metabolites changing during

the experiment was extracted and the behavior of each single metabolite was studied by linear mixed-effects model for longitudinal studies. All the different pretreatments provided good discriminant ability in calibration and cross-validation (above 90%)³⁹.

Biological assay: materials and methods

Cytotoxicity Testing

- The U2Os and SAOs cell lines, derived from human osteosarcomas^{40, 41} were maintained in Dulbecco's modified Eagle's medium (DMEM) supplemented with 10% fetal bovine serum (FBS; Life Technologies, Monza, Italy), 1% L-glutamine, 1% penicillin, 1% streptomycin (Life Technologies) at 37 °C, in a 5% CO₂ humidified atmosphere and harvested at approximately 90% confluence.

Cell viability tests were performed plating cells in 96-multiwells plate at a density of 1×10^4 in a total volume of 0.1 mL. Cells were allowed to adhere for 24 h and subsequently incubated (in quadruplicate; $n = 2$) for 24-48 h in the presence of different concentrations of tested compounds dissolved in DMSO. Viability was determined using a crystal violet assay⁴². Briefly, medium was carefully removed and cells gently washed with phosphate buffer saline solution (PBS). After fixing with 10% formalin for 15 min at room temperature, 0.01% crystal violet (w/v) was added and cells incubated for an additional 30 min. After washing, 10% acetic acid was added to solubilize the dye and absorbance was measured spectrophotometrically at 590 nm (Microplate reader, Synergy HT BioTek, Milan, Italy). EC₅₀ values were calculated using a linear dose-response curve. Curcumin, used as reference compound, showed after 24 h EC₅₀ values of 34.4 μ M and 48.6 μ M against the U2Os and SAOs cell lines, respectively and after 48 h, EC₅₀ values of 22.8 μ M and 28.1 μ M against the U2Os and SAOs cell lines, respectively.

- THP-1 cells (floating monocytes, 500000 cells/mL) were incubated in 100 μ L of a serum-free RPMI 1640 medium and seeded into 96-well plates in triplicate at 37 °C. Measurements were taken 24 h after treatment with increasing concentrations of the test compounds dissolved in DMSO. Viability was measured by the cell proliferation reagent WST-1 (Roche, Basel, Switzerland) according to the manufacturer's manual. The amount of formazan created (which correlates to the number of metabolically active cells in the culture) was calculated as a percentage of the control cells, which were treated only with DMSO and were assigned as 100%. THP-1 cells, human monocytic leukemia cell line, (floating monocytes, 500000 cells/mL) were incubated in 100 μ L of a serum-free RPMI 1640 medium and seeded into 96-well plates in triplicate at 37 °C. Measurements were taken 24 h after treatment with increasing concentrations of the test compounds dissolved in DMSO. Viability was measured by the cell proliferation reagent WST-1 (Roche, Basel, Switzerland) according to the manufacturer's manual. The amount of formazan created (which correlates to the number of metabolically active cells in the culture) was calculated as a percentage of the control cells, which were treated only with DMSO and were assigned as 100%.

TBARS assay and Lipid Peroxidation Measurement.

Reported in the section: general experimental procedures.

Determination of intracellular reactive oxygen species (ROS) scavenging activity

To elucidate the possible pro/anti-oxidative activity of the different extracts, a dichlorofluorescein method was used. THP1-XBlue™-MD2-CD14 cells were seeded in a serum-free medium (50 000 cells/100 μ L/well) into a black 96-well plate and were incubated for 2 hours. In the following step, the solutions of tested compounds were added at the final concentration of 5 μ g/mL and the standard antioxidant quercetin was added at the final concentration of 5 μ M. After 30

minutes of the treatment of the cells with the compounds, pyocyanin was added in final concentration 100 μ M in each well (except in the group of negative control) and the cells were incubated for 30 minutes. After this incubation, DCFH-DA (5 μ g/mL) was introduced into the cell medium of all the wells and the cells were incubated for the next 30 minutes. Finally, the intracellular fluorescence of the dichlorofluorescein product was measured by Fluostar Omega Microplate Reader (BMG Labtech) using the $\lambda(\text{ex./em.}) = 480/530$ nm.

Statistical Analysis.

The statistical analysis was done by several tests. In order to eliminate uncertain data, the Q-Dixon test was performed. All the values in this study were expressed as mean \pm SD. The statistical analysis was performed with one-way ANOVA for repeated measurements. The statistically significant differences were also assessed by applying the paired Student's t-test.

References

1. Shahidi, F.; Alasalvar, C.; Liyana-Pathirana, C. M., Antioxidant phytochemicals in hazelnut kernel (*Corylus avellana* L.) and hazelnut byproducts. *J Agr Food Chem* **2007**, *55*, 1212-1220.
2. Riethmueller, E.; Alberti, A.; Toth, G.; Beni, S.; Ortolano, F.; Kery, A., Characterisation of Diarylheptanoid- and Flavonoid-type Phenolics in *Corylus avellana* L. Leaves and Bark. *Phytochem. Anal.* **2013**, *24*, 493-503.
3. Amaral, J. S.; Cunha, S. C.; Santos, A.; Alves, M. R.; Seabra, R. M.; Oliveira, B. P. P., Influence of Cultivar and Environmental Conditions on the Triacylglycerol Profile of Hazelnut (*Corylus avellana* L.). *J. Agric. Food Chem.* **2006**, *54*, 449-456.
4. Stevigny, C.; Rolle, L.; Valentini, N.; Zeppa, G., Optimization of extraction of phenolic content from hazelnut shell using response surface methodology. *J. Sci. Food Agric.* **2007**, *87*, 2817-2822.
5. De Salvador, F. R.; Proietti, G.; Lolletti, D.; Tombesi, A.; Farinelli, D.; Delfini, M.; Di Cocco, M. E., Influence of pedoclimatic conditions and orchard management on fruit quality characteristics in hazelnut cultivars 'Tonda Gentile Romana' and 'Tonda di Giffoni'. *Acta Hort.* **2009**, *845*, 599-606.
6. Kirmizibekmez, H.; Ariburnu, E.; Masullo, M.; Festa, M.; Capasso, A.; Yesilada, E.; Piacente, S., Iridoid, phenylethanoid and flavonoid glycosides from *Sideritis trojana*. *Fitoterapia* **2012**, *83*, 130-136.
7. Pereira do Amaral, F.; Napolitano, A.; Masullo, M.; Campaner dos Santos, L.; Festa, M.; Vilegas, W.; Pizza, C.; Piacente, S., HPLC-ESIMSn profiling, isolation, structural elucidation, and evaluation of the antioxidant potential of phenolics from *Paepalanthus geniculatus*. *J Nat. Prod.* **2012**, *75*, 547-556.
8. Lee, J. S.; Kim, H. J.; Park, H.; Lee, Y. S., New diarylheptanoids from the stems of *Carpinus cordata*. *Journal of Natural Products* **2002**, *65*, 1367-1370.
9. Chiba, K.; Ichizawa, H.; Kawai, S.; Nishida, T., alpha-Glucosidase Inhibition Activity by Cyclic Diarylheptanoids from *Alnus sieboldiana*. *J Wood Chem Technol* **2013**, *33*, 44-51.
10. Ibrahim, S. R. M.; Mohamed, G. A.; Khedr, A. I. M.; Aljaeid, B. M., Alnuheptanoid B: A New Cyclic Diarylheptanoid from *Alnus japonica* Stem Bark. *Rec. Nat. Prod.* **2016**, *10*, 362-368.
11. Zhang, Y. X.; Xia, B.; Zhou, Y.; Ding, L. S.; Peng, S. L., Two new cyclic diarylheptanoids from the stems of *Ostryopsis nobilis*. *Chinese Chem Lett* **2013**, *24*, 512-514.
12. Reddy, V. L. N.; Ravinder, K.; Srinivasulu, M.; Goud, T. V.; Reddy, S. M.; Srujan Kumar, D.; Rao, T. P.; Murty, U. S.; Venkateswarlu, Y., Two new

macrocyclic diaryl ether heptanoids from *Boswellia ovalifoliolata*. *Chem. Pharm. Bull.* **2003**, *51*, 1081-1084.

13. Zhu, J.; Islas-Gonzalez, G.; Bois-Choussy, M, recent progress in isolation, bioactivity evaluation and total synthesis of diarylheptanoids. *Org Prep Proced Int.* **2000**, *32*, 505-546.

14. Lee, W. S.; Kim, J.-R.; Im, K.-R.; Cho, K.-H.; Sok, D.-E.; Jeong, T.-S., Antioxidant effects of diarylheptanoid derivatives from *Alnus japonica* on human LDL oxidation. *Planta Med.* **2005**, *71*, 295-299.

15. Jin, W. Y.; Cai, X. F.; Na, M.; Lee, J. J.; Bae, K., Diarylheptanoids from *Alnus hirsuta* inhibit the NF- κ B activation and NO and TNF- α production. *Biol. Pharm. Bull.* **2007**, *30*, 810-813.

16. Martineau, L. C.; Herve, J.; Muhamad, A.; Saleem, A.; Harris, C. S.; Arnason, J. T.; Haddad, P. S., Anti-adipogenic activities of *Alnus incana* and *Populus balsamifera* bark extracts, part I: sites and mechanisms of action. *Planta Med.* **2010**, *76*, 1439-1446.

17. Fuchino, H.; Konishi, S.; Satoh, T.; Yagi, A.; Saitsu, K.; Tatsumi, T.; Tanaka, N., Chemical evaluation of *Betula* species in Japan. II. Constituents of *Betula platyphylla* var. *japonica*. *Chem. Pharm. Bull.* **1996**, *44*, 1033-1038.

18. Appendino, G.; Pollastro, F.; Verotta, L.; Ballero, M.; Romano, A.; Wyrembek, P.; Szczuraszek, K.; Mozrzymas, J. W.; Tagliabatella-Scafati, O., Polyacetylenes from Sardinian *Oenanthe fistulosa*: A Molecular Clue to risus sardonius. *J. Nat. Prod.* **2009**, *72*, 962-965.

19. Altunkeyik, H.; Gulcernal, D.; Masullo, M.; Alankus-Caliskan, O.; Piacente, S.; Karayildirim, T., Triterpene saponins from *Cyclamen hederifolium*. *Phytochemistry* **2012**, *73*, 127-33.

20. Oliveira, I.; Sousa, A.; Valentao, P.; Andrade, P. B.; Ferreira, I. C. F. R.; Ferreres, F.; Bento, A.; Seabra, R.; Estevinho, L.; Pereira, J. A., Hazel (*Corylus avellana* L.) leaves as source of antimicrobial and antioxidative compounds. *Food Chem.* **2007**, *105*, 1018-1025.

21. Sultana, N.; Sarker, S. D.; Armstrong, J. A.; Wilson, P. G.; Waterman, P. G., The coumarins of *Philotheca* sensu lato: distribution and systematic significance. *Biochem. Syst. Ecol.* **2003**, *31*, 681-691.

22. Willoughby, P. H.; Jansma, M. J.; Hoye, T. R., A guide to small-molecule structure assignment through computation of (¹H- and ¹³C-) NMR chemical shifts. *Nature Protocols* **2014**, *9*, 643-660.

23. Shanmugam, M. K.; Rane, G.; Kanchi, M. M.; Arfuso, F.; Chinnathambi, A.; Zayed, M. E.; Alharbi, S. A.; Tan, B. K.; Kumar, A. P.; Sethi, G., The multifaceted role of curcumin in cancer prevention and treatment. *Molecules* **2015**, *20*, 2728-69.

24. Teiten, M.-H.; Eifes, S.; Dicato, M.; Diederich, M., Curcumin-the paradigm of a multi-target natural compound with applications in cancer prevention and treatment. *Toxins* **2010**, *2*, 128-162.
25. Ghani, M. A.; Barril, C.; Bedgood, D. R., Jr.; Prenzler, P. D., Measurement of antioxidant activity with the thiobarbituric acid reactive substances assay. *Food Chem.* **2017**, *230*, 195-207.
26. Fotakis, C.; Tsigrimani, D.; Tsiaka, T.; Lantzouraki, D. Z.; Strati, I. F.; Makris, C.; Tagkouli, D.; Proestos, C.; Sinanoglou, V. J.; Zoumpoulakis, P., Metabolic and antioxidant profiles of herbal infusions and decoctions. *Food Chem.* **2016**, *211*, 963-971.
27. Cacace, J. E.; Mazza, G., Optimization of extraction of anthocyanins from black currants with aqueous ethanol. *J Food Sci* **2003**, *68*, 240-248.
28. d'Alessandro, L. G.; Kriaa, K.; Nikov, L.; Dimitrov, K., Ultrasound assisted extraction of polyphenols from black chokeberry. *Sep Purif Technol* **2012**, *93*, 42-47.
29. Naima, R.; Oumam, M.; Hannache, H.; Sesbou, A.; Charrier, B.; Pizzi, A.; El Bouhtoury, F. C., Comparison of the impact of different extraction methods on polyphenols yields and tannins extracted from Moroccan *Acacia mollissima* barks. *Ind Crops Prod.* **2015**, *70*, 245-252.
30. Cujic, N.; Savikin, K.; Jankovic, T.; Pljevljakusic, D.; Zdunic, G.; Ibric, S., Optimization of polyphenols extraction from dried chokeberry using maceration as traditional technique. *Food Chem.* **2016**, *194*, 135-142.
31. Hall, S.; McDermott, C.; Anoopkumar-Dukie, S.; McFarland, A. J.; Forbes, A.; Perkins, A. V.; Davey, A. K.; Chess-Williams, R.; Kiefel, M. J.; Arora, D.; Grant, G. D., Cellular effects of pyocyanin, a secreted virulence factor of *Pseudomonas aeruginosa*. *Toxins* **2016**, *8*, 236/1-236/14.
32. Schrödinger, *LLC New York NY* **2013**.
33. Jorgensen, W. L.; Tiradorives, J., The Opls Potential Functions for Proteins - Energy Minimizations for Crystals of Cyclic-Peptides and Crambin. *J Am Chem Soc* **1988**, *110*, 1657-1666.
34. Cimino, P.; Gomez-Paloma, L.; Duca, D.; Riccio, R.; Bifulco, G., Comparison of different theory models and basis sets in the calculation of ¹³C NMR chemical shifts of natural products. *Magn Reson Chem.* **2004**, *42 Spec no*, S26-33.
35. Sarotti, A. M.; Pellegrinet, S. C., A Multi-standard Approach for GIAO (¹³C) NMR Calculations. *J Org Chem.* **2009**, *74*, 7254-7260.
36. Sarotti, A. M.; Pellegrinet, S. C., Application of the Multi-standard Methodology for Calculating H-1 NMR Chemical Shifts. *J Org Chem.* **2012**, *77*, 6059-6065.
37. Frisch, M. J. T., G. W.; Schlegel, H. B.; Scuseria, G. E.; Robb, M. A.; Cheeseman, J. R.; Scalmani, G.; Barone, V.; Mennucci, B.; Petersson, G. A.;

Nakatsuji, H.; Caricato, M.; Li, X.; Hratchian, H. P.; Izmaylov, A. F.; Bloino, J.; Zheng, G.; Sonnenberg, J. L.; Hada, M.; Ehara, M.; Toyota, K.; Fukuda, R.; Hasegawa, J.; Ishida, M.; Nakajima, T.; Honda, Y.; Kitao, O.; Nakai, H.; Vreven, T.; Montgomery, J. A., Jr.; Peralta, J. E.; Ogliaro, F.; Bearpark, M.; Heyd, J. J.; Brothers, E.; Kudin, K. N.; Staroverov, V. N.; Kobayashi, R.; Normand, J.; Raghavachari, K.; Rendell, A.; Burant, J. C.; Iyengar, S. S.; Tomasi, J.; Cossi, M.; Rega, N.; Millam, J. M.; Klene, M.; Knox, J. E.; Cross, J. B.; Bakken, V.; Adamo, C.; Jaramillo, J.; Gomperts, R.; Stratmann, R. E.; Yazyev, O.; Austin, A. J.; Cammi, R.; Pomelli, C.; Ochterski, J. W.; Martin, R. L.; Morokuma, K.; Zakrzewski, V. G.; Voth, G. A.; Salvador, P.; Dannenberg, J. J.; Dapprich, S.; Daniels, A. D.; Farkas, Ö.; Foresman, J. B.; Ortiz, J. V.; Cioslowski, J.; Fox, D. J., *Gaussian 09, Revision A.02*, Gaussian, Inc., Wallingford CT, 2009.

38. Sanchez-Gomez, R.; Zalacain, A.; Alonso, G. L.; Salinas, M. R., Vine-Shoot Waste Aqueous Extracts for Re-use in Agriculture Obtained by Different Extraction Techniques: Phenolic, Volatile, and Mineral Compounds. *J Agr Food Chem.* **2014**, *62*, 10861-10872.

39. Westad, F.; Marini, F., Validation of chemometric models - A tutorial. *Anal. Chim. Acta* **2015**, *893*, 14-24.

40. Murray, E.; Provvedini, D.; Curran, D.; Catherwood, B.; Sussman, H.; Manolagas, S., Characterization of a human osteoblastic osteosarcoma cell line (SAOS-2) with high bone alkaline phosphatase activity. *J Bone Miner Res.* **1987**, *2*, 231-8.

41. Ponten, J.; Saksela, E., Two established in vitro cell lines from human mesenchymal tumours. *Int J Cancer.* **1967**, *2*, 434-47.

42. Serrano, M.; Lin, A. W.; McCurrach, M. E.; Beach, D.; Lowe, S. W., Oncogenic ras provokes premature cell senescence associated with accumulation of p53 and p16INK4a. *Cell* **1997**, *88*, 593-602.

Chapter 2

Byproducts of *Corylus avellana* cv. Tonda di Giffoni: phytochemical study of flowers, green leafy covers and shells

Introduction

During hazelnut processing, a large amount of waste material is generated such as leafy covers, skins and shells. In fact, only 10% of hazelnuts is sold in shells, while generally the hazelnuts are consumed raw or roasted ¹. The amount of hazelnut byproducts production is estimated to be approximately about 40%. A comprehensive investigation of the byproducts of the Turkish variety of *C. avellana*, known as Tombul, evaluated their antioxidant activity by different tests, revealing as hazelnut byproducts could potentially be considered as an excellent and readily available source of natural antioxidants ¹.

The discovery of cyclic diarylheptanoids, giffonins A-P, from the leaves of *C. avellana* cv. Tonda di Giffoni, some of which able to prevent oxidative damages of human plasma lipids, encouraged us to study the chemical profile of other byproducts of *C. avellana*, as well as to investigate their biological activities. Therefore, the chemical and biological investigation of the male flowers, green leafy covers and shells of *C. avellana* has been performed.

2.1 Quali-quantitative analysis of the phenolic fraction of the flowers of *Corylus avellana*, cv. Tonda di Giffoni: isolation of antioxidant diarylheptanoids

C. avellana male flowers



C. avellana flowers are produced very early in spring before the leaves, and are monoecious, with single-sex catkins; the male catkins are pale yellow and 5-12 cm long, and the female ones are very small and largely concealed in the buds, with only the bright-red, 1-to-3

mm-long styles visible.

2.1.1. Results and discussion

Qualitative analysis of MeOH extract of C. avellana, cv. Tonda di Giffoni flowers. LC-ESI/LTQOrbitrap/MS/MSⁿ analysis, in negative ionization mode, of the MeOH extract of *C. avellana* male flowers allowed us to obtain a preliminary plant metabolite profiling.

In particular, a careful analysis of the multistage mass spectra of the main peaks suggested the presence of twelve phenolic compounds (fig. 2.1).

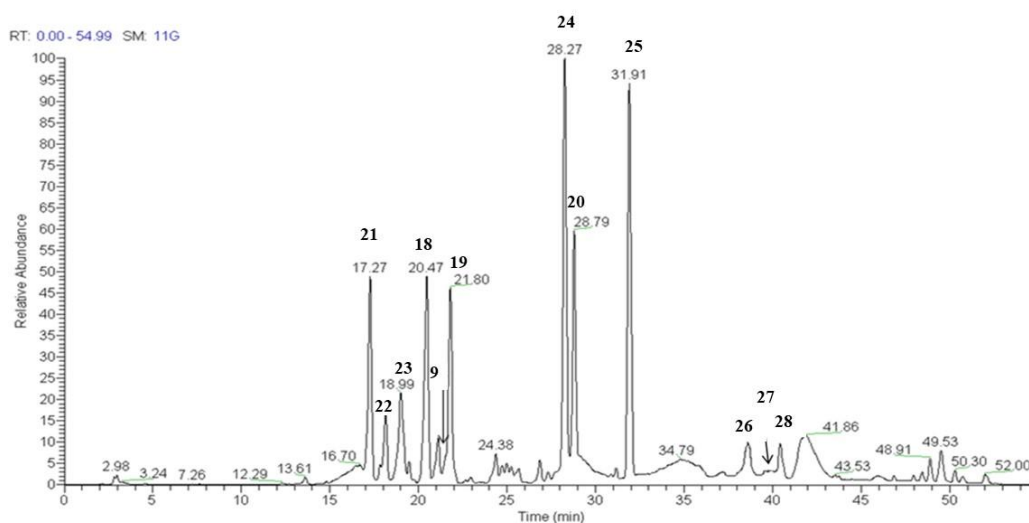


Figure 2.1. LC-ESI/LTQOrbitrap/MS profile (negative ion mode) of the MeOH extract of *C. avellana* flowers.

In order to unambiguously elucidate their structures by NMR experiments, the twelve compounds were isolated by size exclusion chromatography of the MeOH extract, followed by further purification steps by reversed-phase HPLC-RI. Their structures were established by 1D and 2D-NMR experiments along with ESIMS and ESI/LTQORBITRAP/MS analysis.

The ESI/LTQORBITRAP/MS of compound **26** (m/z 293.1182 $[M-H]^-$, calcd for $C_{19}H_{17}O_3$, 293.1178) and the ^{13}C NMR data supported a molecular formula of $C_{19}H_{18}O_3$. The IR spectrum showed a band at 1725 cm^{-1} suggesting the presence of a ketocarbonyl group. The 1H NMR spectrum showed aromatic signals at δ 7.29 (2H, d, $J=8.2$ Hz, H-15 and H-19) and 6.99 (2H, d, $J=8.2$ Hz, H-16 and H-18) typical of a 1,4-disubstituted aromatic ring, and signals at δ 6.73 (d, $J=8.2$ Hz, H-3), 6.55 (dd, $J=8.2, 1.8$ Hz, H-4) and 5.82 (d, $J=1.8$, H-6) due to the protons of a 1,2,5-trisubstituted aromatic ring (fig.2.2. and table 2.1).

Table 2.1. ^1H NMR spectroscopic data (600 MHz, J in Hz) and ^{13}C NMR data of compounds **26-28** (CD_3OD).

	26		27		28	
	δ_{C}	δ_{H} (J in Hz)	δ_{C}	δ_{H} (J in Hz)	δ_{C}	δ_{H} (J in Hz)
1	151.4	-	151.3	-	151.2	-
2	148.1	-	147.9	-	137.3	-
3	116.2	6.73, d (8.2)	117.3	6.84, d (8.2)	149.2	-
4	122.5	6.55, dd (8.2, 1.8)	125.0	6.74, dd (8.2, 1.8)	108.0	6.53, d (1.8)
5	138.9	-	129.8	-	136.8	-
6	115.8	5.76, d (1.9)	119.6	5.94, d (1.8)	114.1	5.61, d (1.8)
7	32.0	2.69, m	136.2	6.51, d (11.5)	136.8	6.52, d (11.5)
8	34.9	2.37, m	124.3	6.03, dd (11.5, 9.6)	125.6	6.05, dd (11.5, 9.6)
9	134.6	6.59, m	138.5	6.27, dd (16.2, 138.2)	138.2	6.27, dd (16.2,
10	131.8	5.82, d (16.1)	135.5	6.18, d (16.2),	136.0	6.20, d (16.2)
11	203.9	-	205.8	-	205.0	-
12	33.6	2.73, t (6.5)	43.2	2.74, d (5.6)	43.5	2.74, d (5.6)
13	44.6	3.05, t (6.5),	2.3532.8	3.07, d (5.6)	32.8	3.07, d (5.6)
14	138.6	-	140.1	-	139.5	-
15	131.5	7.29, d (8.2)	131.7	7.30, d (8.2)	131.7	7.28, d (8.2)
16	124.0	6.99, d (8.2)	124.6	7.10, d (8.2)	125.8	7.08, d (8.2)
17	156.8	-	157.6	-	157.5	-
18	124.0	6.99, d (8.2)	124.6	7.10, d (8.2)	125.8	7.08, d (8.2)
19	131.5	7.29, d (8.2)	131.7	7.30, d (8.2)	131.7	7.28, d (8.2)
OCH_3					56.5	3.89, s

Moreover, the ^1H NMR spectrum displayed signals due to a disubstituted *trans*-olefinic group at δ 6.59 (m, H-9) and 5.76 (d, $J=16.1$ Hz, H-10), and four methylene groups at δ 3.05 (t, $J=6.5$ Hz) and 2.35 (m), 2.73 (2H, t, $J=6.5$ Hz), 2.69 (2H, m), and 2.37 (2H, m).

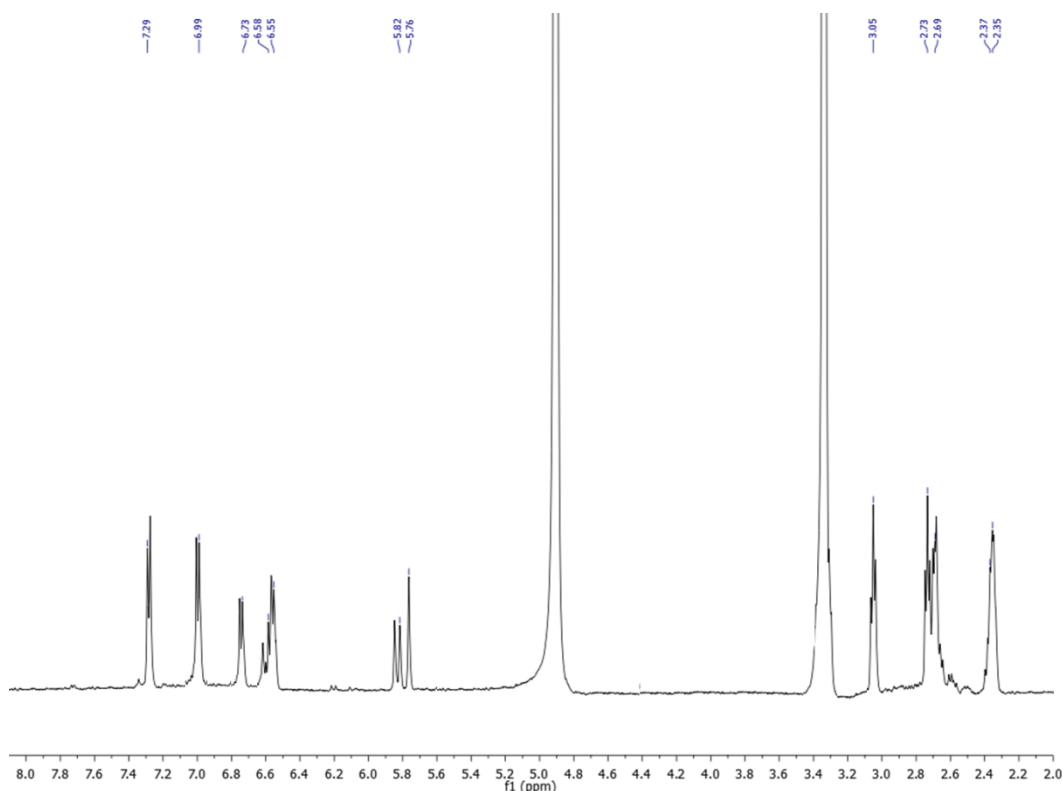


Figure 2.2. ^1H NMR spectrum (600 MHz, CD_3OD) of giffonin Q (**26**).

The ^{13}C NMR spectrum of **26** showed 19 carbon signals, typical of diaryletherheptanoid derivatives, comprising a signal at δ 203.9, ascribable to a ketocarbonyl group (table 2.1). The signal at δ 5.82 was attributed to H-6, which generally resonates at an abnormally high field, due to the anisotropic effect of the A ring in diaryletherheptanoid. This observation together with the ROESY correlation of H-6 at δ 5.82 with H-18 (δ 6.99) suggested the ether linkage between C-1 and C-17 of the aryl moieties. The HMBC correlations of H-6 (δ

5.82) with the ^{13}C NMR resonances at δ 151.4 (C-1), 148.1 (C-2), 122.5 (C-4), 138.9 (C-5) and 32.0 (C-7) and the HMBC correlations of H-4 (δ 6.55) with the ^{13}C NMR resonances at δ 148.1 (C-2), 138.9 (C-5), 115.8 (C-6) and 32.0 (C-7) suggested the 1,2, dihydroxylation of the A-ring. The disposition of the heptanoid chain, the olefinic groups and the position of the ketocarbonyl group were determined by HSQC, HMBC, and COSY (fig. 2.3.-2.5) experiments. On the basis of the HMBC correlations between H-10 (δ 5.82), H₂-12 (δ 2.73), H₂-13 (δ 3.05 and 2.35) and H-9 (δ 6.58) with the carbon resonance at δ 203.9 the carbonyl group was assigned to C-11 (fig 2.3-2.5).

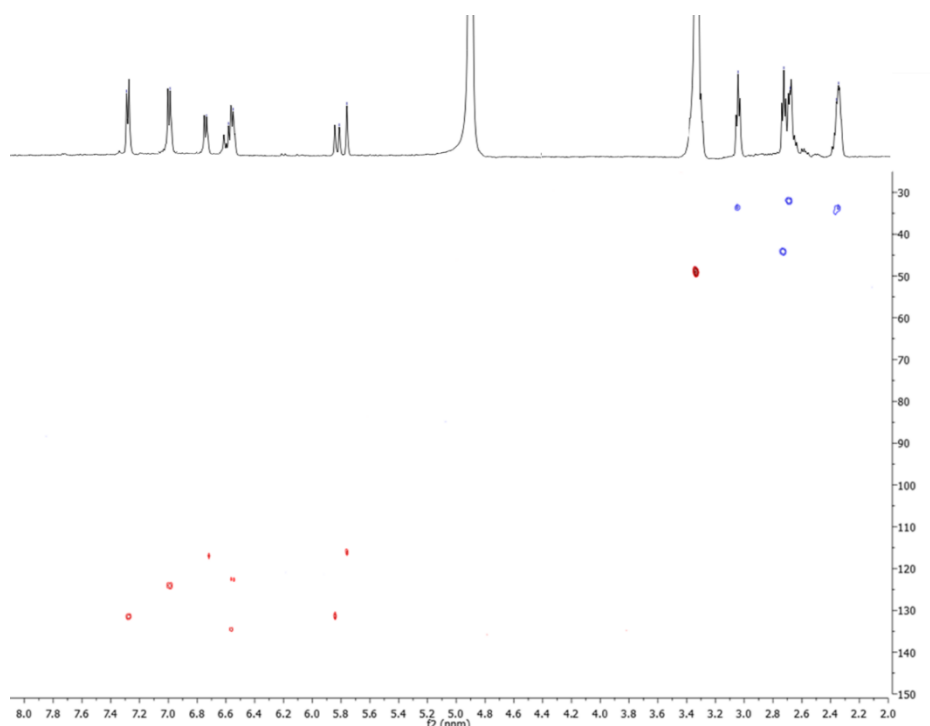


Figure 2.3. HSQC spectrum (CD_3OD) of giffonin Q (**26**).

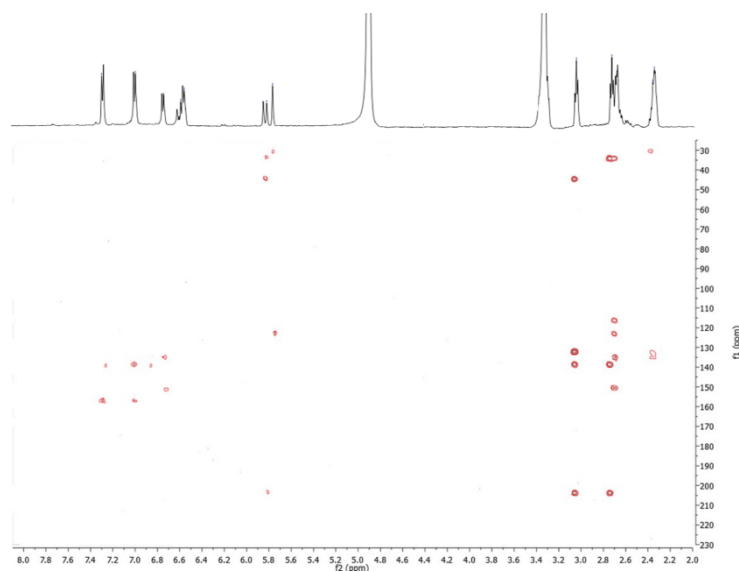


Figure 2.4. HMBC spectrum (CD₃OD) of giffonin Q (**26**).

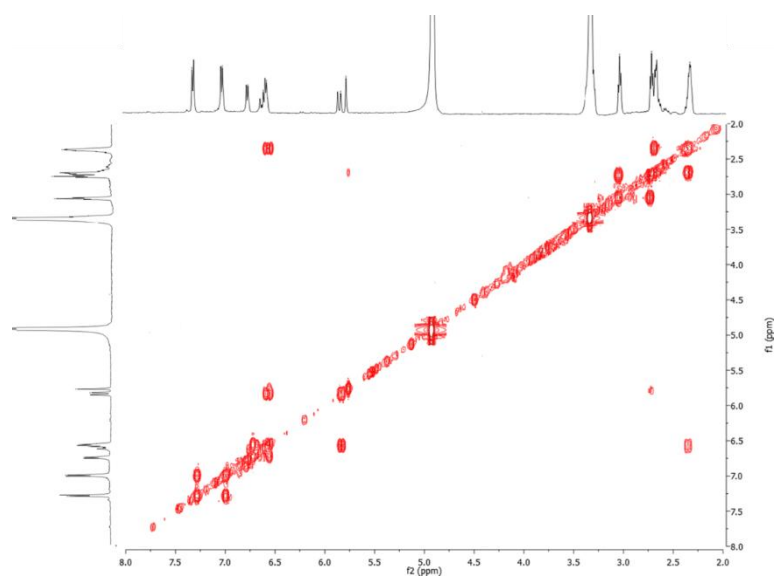


Figure 2.5. COSY spectrum (CD₃OD) of giffonin Q (**26**).

On the basis of these observations the structure of compound **26**, named giffonin Q, was elucidated as shown (fig. 2.6).

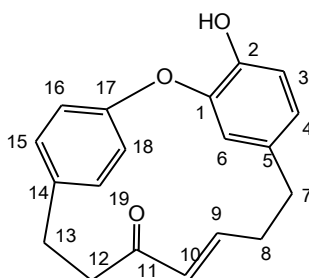


Figure 2.6. giffonin Q.

This structure is reported as an artefact formed during the acid hydrolysis of aceroside V, a diaryletherheptanoid β -glucopyranoside isolated from *Acer nikoense*². Moreover, no NMR data were reported for this artefact. So, this is the first finding of this compound as a natural product.

The ESI/LTQORBITRAP/MS of **27** (m/z 291.1026 [M-H]⁻, calcd for C₁₉H₁₅O₃, 291.1021) and the ¹³C NMR data supported a molecular formula of C₁₉H₁₆O₃. The IR spectrum showed a band at 1715 cm⁻¹ due to the presence of a ketocarbonyl group. Comparison of the ¹H NMR spectrum of **27** in the aromatic region with that of giffonin Q (**26**) suggested that they share the same aromatic substitution patterns (table 2.1). Moreover, the ¹H NMR spectrum displayed four signals at δ 6.51 (d, $J = 11.5$ Hz), 6.03 (dd, $J = 11.5, 9.6$ Hz), 6.27 (dd, $J = 16.2, 9.6$ Hz), 6.18 (d, $J = 16.2$ Hz), ascribable to *Z*- and *E*- olefinic protons, respectively. The linear connectivity observed in the COSY spectrum showed the presence of a conjugated diene system (C-7/C-10). On the basis of the HMBC correlations between H-10 (δ 6.18), H₂-12 (δ 2.74), H₂-13 (δ 3.07) and H-9 (δ 6.27) with the carbon resonance at δ 205.8 the carbonyl group was assigned to C-11 (δ 205.8). On the basis of these observation the structure of compound **27**, named giffonin R, was elucidated as shown (fig. 2.7).

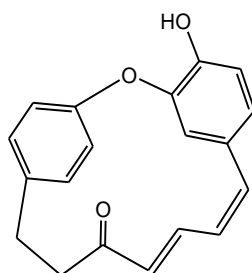


Figure 2.7. giffonin R.

The molecular formula of **28** was established as $C_{20}H_{18}O_4$ by ESI/LTQORBITRAP/MS (m/z 321.1130 $[M-H]^-$, calcd for $C_{20}H_{17}O_4$, 321.1127) and the ^{13}C NMR data. A detailed analysis of NMR data of compound **28** revealed that the heptadienone moiety was comparable to that of **28**, while differences were observed for signals due to one aryl moiety. In particular, the 1H NMR spectrum showed aromatic signals at δ 7.28 (2H, d, $J = 8.2$ Hz, H-15 and H-19) and 7.08 (2H, d, $J = 8.2$ Hz, H-16 and H-18), corresponding to the 1,4-disubstituted aromatic ring, and at δ 6.53 (d, $J = 1.8$ Hz, H-4), and 5.61 (d, $J = 1.8$, H-6), corresponding to a 1,2,3,5-tetrasubstituted aromatic ring (table 2.1). Moreover, a signal at δ 3.89 (s), typical of a methoxy group was observed. The HMBC correlation between the proton signal at δ 3.89 with the carbon resonance at δ 149.2 (C-3) allowed the methoxy group to be placed at C-3. Therefore, the structure of compound **28**, named giffonin S, was determined as reported (fig. 2.8).

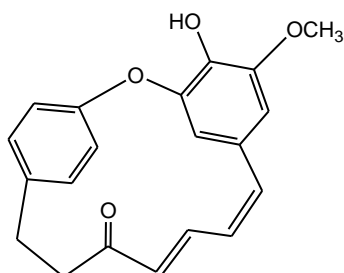


Figure 2.8. giffonin S.

Moreover, the other compounds isolated by HPLC-RI, were identified by analysis of spectroscopic data in comparison to those reported in literature as giffonin I (**9**), quercetin 3-*O*- α -L-rhamnopyranoside (**18**), kaempferol 3-*O*- α -L-rhamnopyranoside (**19**), kaempferol 3-*O*-(4''-*trans-p*-coumaroyl)- α -L-rhamnopyranoside (**20**), quercetin 3-*O*- β -D-galactopyranosyl-(1 \rightarrow 2)- β -D-glucopyranoside (**21**), kaempferol 3-*O*- β -D-glucopyranosyl-(1 \rightarrow 2)- β -D-glucopyranoside (**22**), quercetin 3-*O*- β -D-glucopyranoside (**23**), kaempferol 3-*O*-(4''-*cis-p*-coumaroyl)- α -L-rhamnopyranoside (**24**), and alnusone (**25**) (fig.2.9).

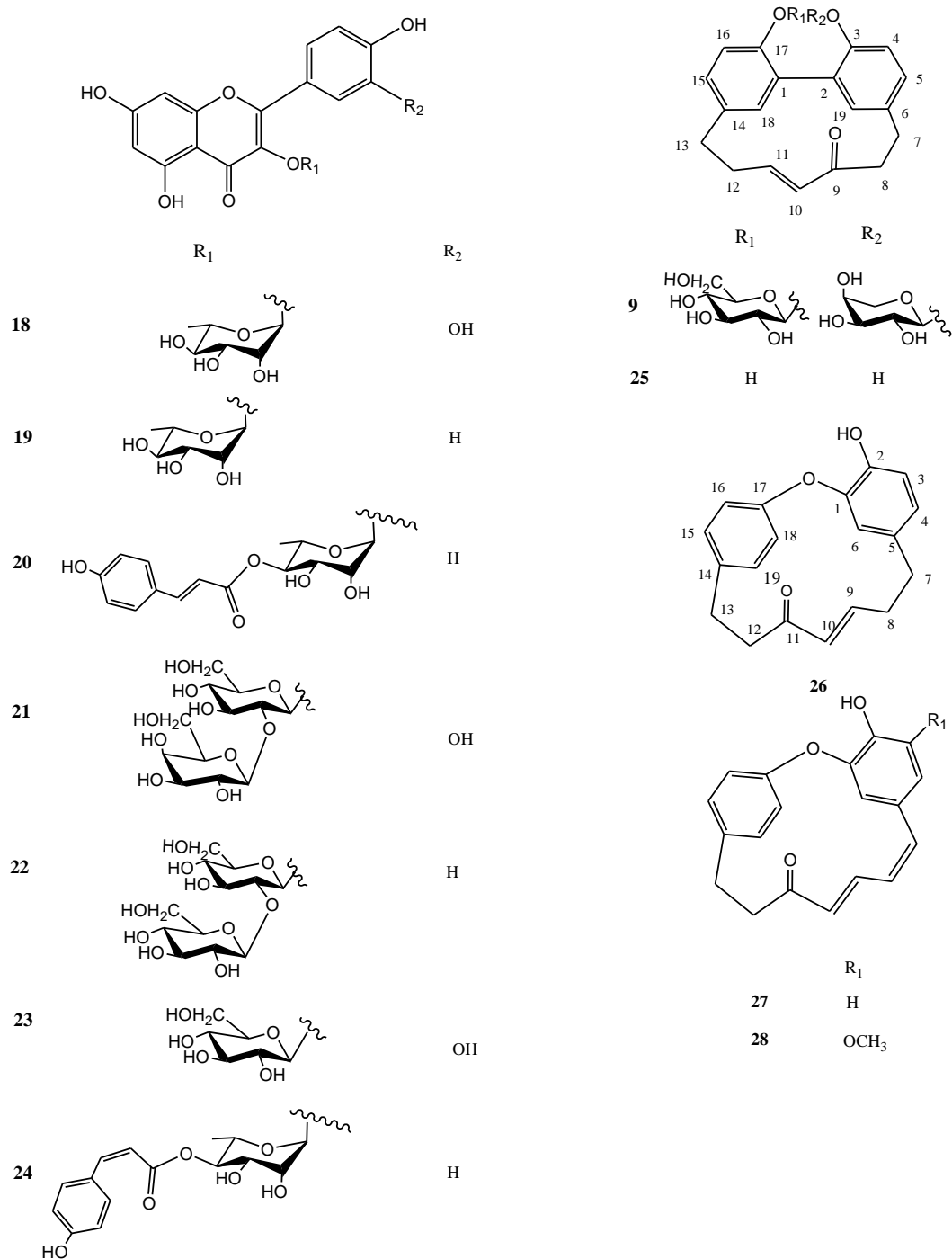


Figure 2.9. Compounds isolated from *C. avellana* flowers.

Quantitative analysis of compounds 9, and 18-28 in C. avellana flowers by LC-ESI/QqQ/MS/MS

In order to determine the amount of the main compounds occurring in the MeOH extract of *C. avellana* flowers (fig. 2.9), a quantitative determination by LC-MS was carried out. LC-ESI/QqQ/MS/MS using a very sensitive and selective mass tandem experiment such as Multiple Reaction Monitoring (MRM) is considered one of the most suitable techniques for quantification of metabolites³⁻⁷.

As reported in table 2.2, for the flavonoids quercetin 3-*O*- α -L-rhamnopyranoside (**18**), kaempferol 3-*O*- α -L-rhamnopyranoside (**19**), kaempferol 3-*O*-(4''-*trans-p*-coumaroyl)- α -L-rhamnopyranoside (**20**) quercetin 3-*O*- β -D-galactopyranosyl-(1 \rightarrow 2)- β -D-glucopyranoside (**21**), kaempferol 3-*O*- β -D-glucopyranosyl-(1 \rightarrow 2)- β -D-glucopyranoside (**22**), quercetin 3-*O*- β -D-glucopyranoside (**23**), kaempferol 3-*O*-(4''-*cis-p*-coumaroyl)- α -L-rhamnopyranoside (**24**), the loss of the sugar moiety, leading to a fragment ion [(M-sugar)-H]⁻, was the predominant fragmentation obtained from the pseudomolecular ion [M-H]⁻, thus this fragment ion was chosen for MRM analysis. The *cis* and *trans* isomers of kaempferol 3-*O*-(4''-*p*-coumaroyl)- α -L-rhamnopyranoside (**24**, **20**) showed a pseudomolecular ion [M-H]⁻ at *m/z* 577. They were characterized by the same MS/MS fragmentation pattern originating a main fragment ion [(M-146-146)-H]⁻ at *m/z* 285, due to the loss of a rhamnose and a *p*-coumaroyl unit. MRM transition of giffonin I (**9**) was characterized by the loss of both glucose and arabinose sugars originating a very intense fragment ion [(M-294)-H]⁻ at *m/z* 293. In the LC-MS/MS experiment alnusone (**25**) showed a very simple fragmentation pattern where the base peak was produced by the neutral loss of 210 amu corresponding to the diaryl moiety.

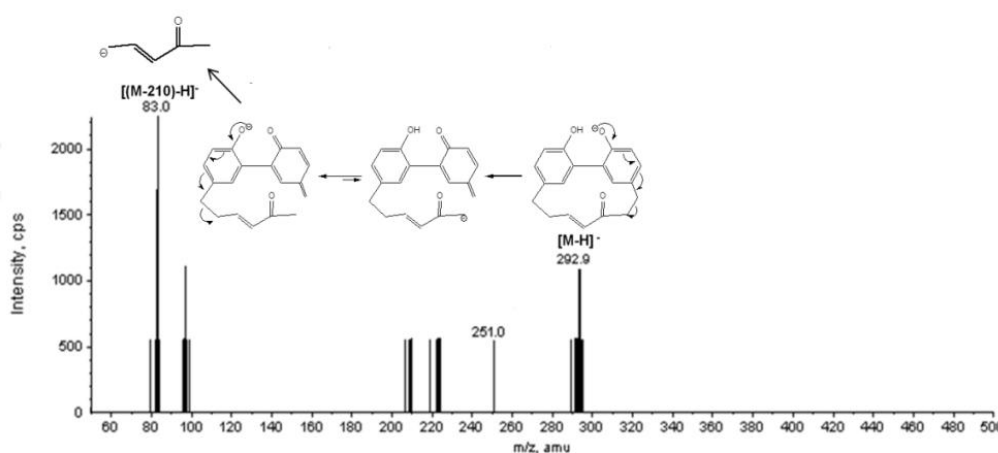


Figure 2.10. Negative ion LC-ESI/QqQ/MS/MS spectrum and proposed fragmentation pattern of alnusone occurring in the MeOH extract of *C. avellana* flowers.

This was explained by a rearrangement from the deprotonated compound and the subsequent opening of the diarylheptanoid cycle by the cleavage of the linkage between carbons 7 and 8. A subsequent cleavage of the linkage between carbons 12 and 13 originated a very intense signal at m/z 83 ascribable to a deprotonated pent-3-en-2-one fragment ion. For this reason this transition was selected for MRM experiments (fig. 2.10). Finally due to their low abundance in the MeOH extract, high quality MS/MS spectra of the new diaryletherheptanoids giffonin Q, R, S (**26-28**) were not available. According to this, pseudo-MRM (pseudomultiple reaction monitoring) was chosen as tandem mass spectrometry detection method. As in MRM, both the first and second analyzers were focused on selected masses, but the precursor and product ions are set to the same m/z values^{8,9}. Therefore, stock solutions of 1 mg/mL were prepared and properly diluted to produce known concentration solutions. To each solution an internal standard, was added. By injecting triplicates of standard solutions at different concentrations, linear regression curves were obtained for each compound with the only exception of kaempferol 3-*O*-(4''-*trans-p*-coumaroyl)- α -L-rhamnopyranoside (**20**) whose

amount was calculated by considering the regression curve of its isomer kaempferol 3-*O*-(4''-*cis-p*-coumaroyl)- α -L-rhamnopyranoside (**24**). The calibration curves were found to be linear in the range 0.0015-0.020 $\mu\text{g}\mu\text{L}^{-1}$. Finally area ratio of the internal and external standard peak were calculated and related, in a Cartesian coordinate system, to the corresponding known reference concentration. Table 2.3 shows the amount (mg/100 g) of each selected compound in *C. avellana* flowers. The quantitative results highlight that compounds are present in concentration ranges of 1.20-65.47 (mg/100 g). In particular, the flavonoids quercetin 3-*O*- β -D-galactopyranosyl-(1 \rightarrow 2)- β -D-glucopyranoside (**21**), kaempferol 3-*O*- β -D-glucopyranosyl-(1 \rightarrow 2)- β -D-glucopyranoside (**22**), kaempferol 3-*O*-(4''-*cis-p*-coumaroyl)- α -L-rhamnopyranoside (**24**) and the diarylheptanoid alnusone (**25**) exhibit the highest concentrations. In spite of this, giffonin I (**9**) and the new diaryletherheptanoids giffonin Q, R, S (**26-28**) were not quantified, since they resulted not detectable in the MeOH extract of *C. avellana* flowers (table 2.3).

Table 2.2. Quantitative data of *C. avellana* flowers extract (MRM, negative ion mode) Five-point calibration with eleven standards. MRM transitions, Limits of detection (LODs), limits of quantification (LOQs) in ng mL⁻¹.

Compound		MRM transition	R ²	Regression line	LOQ (ng mL ⁻¹)	LOD (ng mL ⁻¹)
quercetin galactopyranosyl-(1→2)-β-D-glucopyranoside (21)	3-O-β-D-	625→463	0.9912	Y=50.6x+0.0833	18.0	2.5
kaempferol glucopyranosyl-(1→2)-β-D-glucopyranoside (22)	3-O-β-D-	609→447	0.9928	Y=22.8x+0.0385	18.0	2.5
quercetin glucopyranoside (23)	3-O-β-D-	463→301	0.9968	Y=122x+0.2250	15.0	3.5
quercetin rhamnopyranoside (18)	3-O-α-L-	447→301	0.9840	Y=501x+2.4000	15.0	3.5
giffonin I (9)		587→293	0.9899	Y=603x+4.4000	18.5	4.5
kaempferol rhamnopyranoside (19)	3-O-α-L-	431→285	0.9900	Y=411x+1.4400	12.0	2.0
kaempferol coumaroyl)-α-L-rhamnopyranoside (24)	3-O-(4''-cis-p-	577→285	0.9943	Y=206x+0.2410	15.0	3.5
alnosone (25)		293→83	0.9908	Y=92.2x+0.0695	10.0	3.0
giffonin Q (26)		293→293	0.9967	Y=633x +3.3000	20.0	5.0
giffonin R (27)		291→291	0.9892	Y=891x+6.8900	20.0	4.5
giffonin S (28)		367→367	0.9916	Y=700x+5.2000	20.0	4.5

Table 2.3. Retention times (R_t), molecular formula, $[M-H]^-$, $[M+HCOOH]^-$, Δ ppm, characteristic product ions (m/z), amount (mg/100g dry weight) of compounds **9**, **18-28** occurring in the MeOH extract of *C. avellana* flowers quantified by LC-ESI/QqQ/MS/MS and identified by LC-ESI/LTQOrbitrap/MS/MSⁿ.

n°	Compound	R_t (min)	Molecular Formula	$[M-H]^-$	Δ ppm	Characteristic product ions (m/z)	mg/100g flowers \pm SD*
21	quercetin 3- <i>O</i> - β -D-galactopyranosyl-(1 \rightarrow 2)- β -D-glucopyranoside	17.27	C ₂₇ H ₃₀ O ₁₇	625.1386	-2.19	463, 445, 301	49.33 \pm 2.6 4
22	kaempferol 3- <i>O</i> - β -D-glucopyranosyl-(1 \rightarrow 2)- β -D-glucopyranoside	18.08	C ₂₇ H ₃₀ O ₁₆	609.1432	-3.01	447, 429, 285	65.47 \pm 3.6 3
23	quercetin 3- <i>O</i> - β -D-glucopyranoside	18.99	C ₂₁ H ₂₀ O ₁₂	463.0858	-2.58	301	1.36 \pm 0.21
18	quercetin 3- <i>O</i> - α -L-rhamnopyranoside	20.47	C ₂₁ H ₂₀ O ₁₁	447.0909	-2.84	301	6.53 \pm 0.92
9	giffonin I	21.14	C ₃₀ H ₃₆ O ₁₂	587.21320	1.52	455, 425, 293	**ND
19	kaempferol 3- <i>O</i> - α -L-rhamnopyranoside	21.80	C ₂₁ H ₂₀ O ₁₀	431.0962	-2.47	285	1.20 \pm 0.39
24	kaempferol 3- <i>O</i> -(4"-cis- <i>p</i> -coumaroyl)- α -L-rhamnopyranoside	28.27	C ₃₀ H ₂₆ O ₁₂	577.1324	-2.90	431, 285	53.33 \pm 11. 57
20	kaempferol 3- <i>O</i> -(4"-trans- <i>p</i> -coumaroyl)- α -L-rhamnopyranoside	28.79	C ₃₀ H ₂₆ O ₁₂	577.1328	-2.15	431, 285	17.73 \pm 3.8 4
25	alnusone	31.91	C ₁₉ H ₁₈ O ₃	293.1168	-1.39	251, 83	51.07 \pm 3.4 5
26	giffonin Q	38.08	C ₁₉ H ₁₈ O ₃	293.1178	1.97	-	**ND
27	giffonin R	39.18	C ₁₉ H ₁₆ O ₃	291.1021	1.81	-	**ND
[M+HCOOH]⁻							
28	giffonin S	40.41	C ₂₁ H ₁₉ O ₆	367.1182	1.59	-	**ND

* Values mean of triplicates for each sample.

** ND, not detected.

2.1.2. Biological activity

Cytotoxic activity

The cytotoxic activity of isolated compounds by male flowers of *C. avellana* cv. Tonda di Giffoni was tested against two cancer cell lines including A549 (human lung adenocarcinoma) and DeFew (human B lymphoma). In the range 10-100 μM , the compounds did not show a significant reduction of the cell number (data not shown), in agreement with the absence of cytotoxicity previously reported for giffonins A-P.

Biological evaluation of isolated compounds by male flowers of C. avellana in TBARS assay.

On the basis of the antioxidant activity reported for the MeOH extract of *C. avellana* leaves and for giffonins A-P, the MeOH extract and the isolated compounds (except giffonin I because tested previously) were evaluated for their inhibitory effects on human plasma lipid peroxidation induced by H_2O_2 and $\text{H}_2\text{O}_2/\text{Fe}^{2+}$, by measuring the concentration of TBARS (thiobarbituric acid reactive substances). Exposure of human plasma to strong chemical oxidants such as H_2O_2 and $\text{H}_2\text{O}_2/\text{Fe}^{2+}$ resulted in enhanced level of plasma lipid peroxidation. The MeOH extract and pure compounds were found to protect plasma against H_2O_2 and $\text{H}_2\text{O}_2/\text{Fe}^{2+}$ induced lipid peroxidation. The MeOH extract, isolated compounds, and curcumin used as reference compound were tested at doses ranging from 0.1 to 100 $\mu\text{g}/\text{mL}$ (MeOH extract) and from 0.1 to 100 μM . All tested compounds, curcumin and the MeOH extract did not exert any effect on autoperoxidation of human plasma (data not shown). The MeOH extract at 10 $\mu\text{g}/\text{mL}$ reduced by about 50 % and 25 % the plasma lipid peroxidation stimulated by H_2O_2 or $\text{H}_2\text{O}_2/\text{Fe}^{2+}$, respectively. Compounds **27** and **28** at 10 μM reduced both H_2O_2 and $\text{H}_2\text{O}_2/\text{Fe}^{2+}$ induced lipid peroxidation by more than 50 % and about 35

%, respectively, resulting more active than curcumin (fig. 2.11 and table 2.4). Among the twelve compounds, **18**, **21**, **24** and **25** (fig. 2.11 and table 2.4) exerted a protective action against oxidative stress induced by H₂O₂ or H₂O₂/Fe²⁺ similar to that shown by curcumin.

Table 2.4. Inhibitory effects of the extract (10 µg/mL; 30 min), compounds **18-28** (10 µM; 30 min) and curcumin (10 µM; 30 min) on plasma lipid peroxidation induced by H₂O₂ or H₂O₂/Fe²⁺.

compound	Inhibition of lipid peroxidation induced by H ₂ O ₂ (%)	Inhibition of lipid peroxidation induced by H ₂ O ₂ /Fe ²⁺ (%)
18	26.3 ± 8.1 (p<0.05)	28.7 ± 5.6 (p<0.05)
19	5.7 ± 3.2 (p>0.05)	20.1 ± 7.2 (p<0.05)
20	31.8 ± 9.9 (p<0.02)	39.7 ± 8.2 (p<0.02)
21	19.9 ± 5.2 (p<0.05)	18.8 ± 6.3 (p<0.05)
22	35.4 ± 9.9 (p<0.02)	14.2 ± 4.4 (p<0.05)
23	23.1 ± 5.6 (p>0.05)	9.9 ± 4.2 (p>0.05)
24	36.9 ± 10.1 (p<0.02)	29.5 ± 5.1 (p<0.05)
25	23.9 ± 7.8 (p<0.05)	31.2 ± 7.9 (p<0.02)
26	40.4 ± 12.2 (p<0.02)	38.5 ± 5.9 (p<0.02)
27	52.3 ± 17.2 (p<0.01)	33.4 ± 4.2 (p<0.02)
28	54.6 ± 15.2 (p<0.01)	36.6 ± 7.7 (p<0.02)
Curcumin	20.6 ± 8.2 (p<0.05)	23.2 ± 5.8 (p<0.05)
extract	51.1 ± 13.3 (p<0.01)	25.5 ± 7.0 (p<0.05)

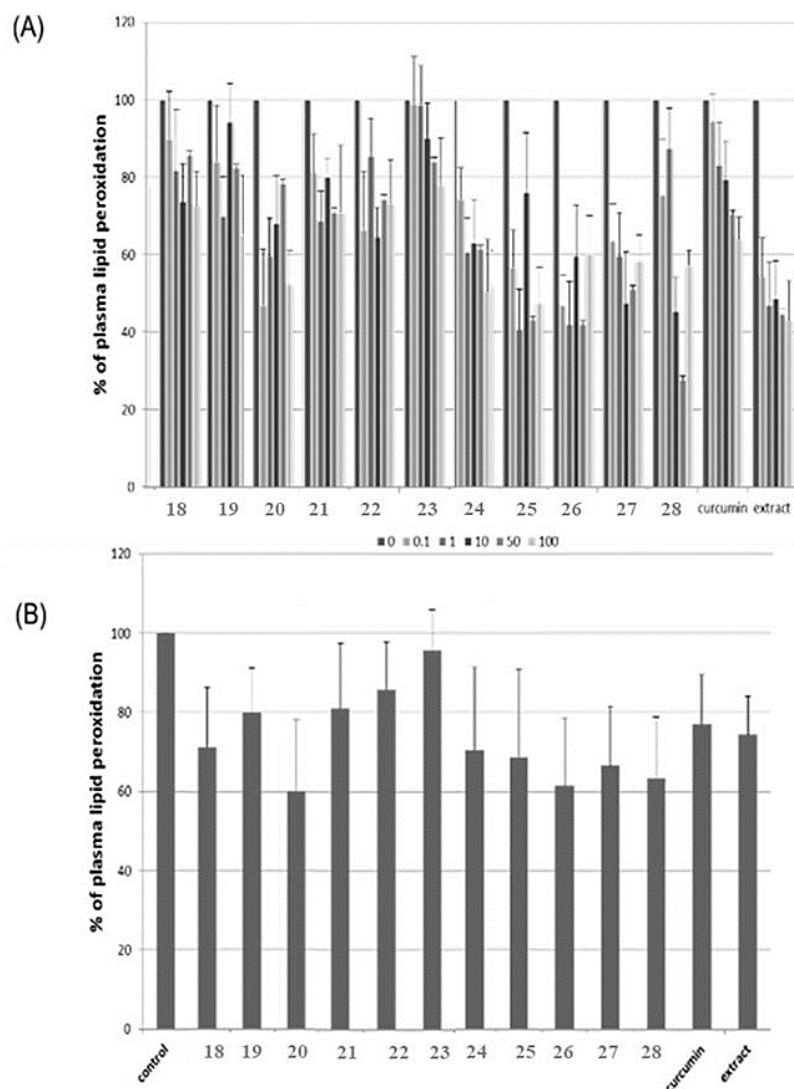


Figure. 2.11. (A). The effects of MeOH extract (0.1 – 100 µg/mL; 30 min), tested compounds) (0.1 – 100 µM; 30 min) and curcumin (0.1 – 100 µM; 30 min) on plasma lipid peroxidation induced by H₂O₂. The results are representative of 5-9 independent experiments, and are expressed as means ± SD. The effect of five different concentrations of tested compounds (0.1, 1, 10, 50 and 100 µM) and tested extract (0.1, 1, 10, 50 and 100 µg/mL) was statistically significant according to ANOVA I test ($p < 0.05$). (B). The effects of MeOH extract (10 µg/mL; 30 min), tested compounds (10 µM; 30 min) and curcumin (10 µM; 30 min) on plasma lipid peroxidation induced by H₂O₂/Fe²⁺. The results are representative of 6-9 independent experiments, and are expressed as means ± SD. The statistical significances were confirmed with the paired Student's t-test ($p < 0.05$).

2.2. Cyclic Diarylheptanoids from *Corylus avellana* cv. Tonda di Giffoni Green Leafy Covers: Determination of Their Absolute Configurations and Evaluation of Their Antioxidant and Antimicrobial Activities

C. avellana green leafy covers



Hazelnuts develop in clusters of 1-12, each separately enclosed in an involucre made up of two overlapping, leafy bracts (modified leaves) that vary considerably across the *Corylus* species in terms of length, constriction around the nut, indentation and serration at the apex, and thickness at the base. In *C. avellana* this cup of green leafy cover encloses about three quarters of the nut. The green leafy covers have no current commercial value, but are occasionally used as fertilizer for the hazelnut trees upon composting¹⁰. On the basis of the occurrence of phenolic antioxidants with potential health benefits in the leaves of *C. avellana*, a phytochemical investigation of the green leafy covers of *C. avellana* cv. Tonda di Giffoni has been carried out.

2.2.1 LC-ESI/LTQOrbitrap/MS/MSⁿ analysis

The green leafy covers of *C. avellana* cv. Tonda di Giffoni (535 g) have been dried and extracted at room temperature using solvents of increasing polarity.

LC-ESI/LTQOrbitrap/MS/MSⁿ analysis, in negative ionization mode, of the MeOH extract of *C. avellana* leaves allowed us to obtain a preliminary plant metabolite profiling.

LC-MS profile of the MeOH extract of *C. avellana* leaves highlighted peaks with m/z values corresponding to a wide range of phenolic compounds. In particular, the LC-MS spectrum showed ions characterized by typical fragmentation patterns

of flavonoids, and further peaks suggesting the occurrence of diarylheptanoid derivatives (fig. 2.12).

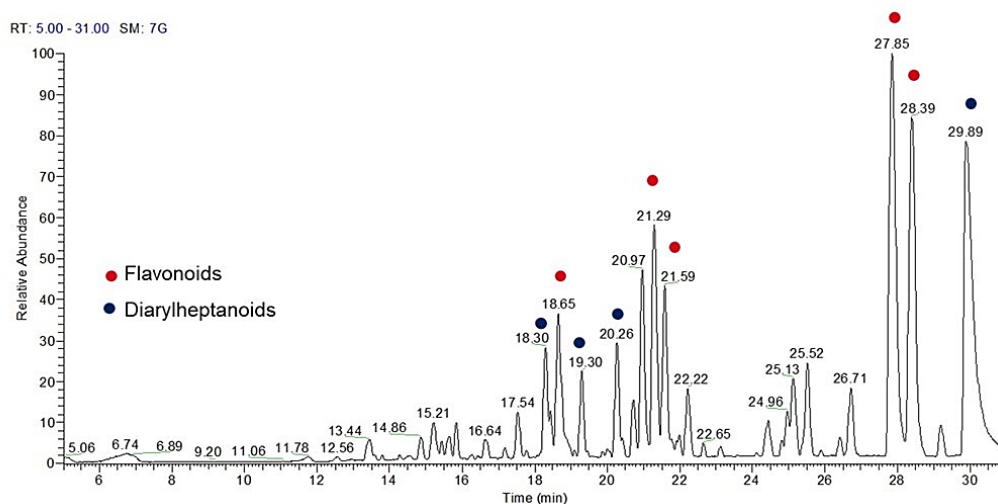


Figure 2.12. LC-ESI/LTQOrbitrap/MS profile (negative ion mode) of the MeOH extract of *C. avellana* green leafy covers.

2.2.2. Results and discussions

Qualitative analysis of MeOH extract of C. avellana, cv. Tonda di Giffoni green leafy covers.

With the aim to unambiguously elucidate the compounds corresponding to the unknown peaks occurring in LC-ESI/LTQOrbitrap/MS/MSⁿ spectrum, the MeOH extract of the leafy covers of *C. avellana* was fractionated by size-exclusion chromatography and the resulting fractions were purified by semipreparative HPLC to obtain 11 compounds. Their structures were established by 1D and 2D-NMR experiments along with ESIMS and ESI/LTQORBITRAP/MS analysis.

The ¹H and ¹³C NMR spectra of compounds **29-31** showed signals ascribable to a diaryl heptanoid moiety. A detailed analysis of their NMR data showed that these compounds differed in terms of the occurrence of secondary hydroxy groups and

carbonyl functions at various positions on the heptanoid chain (table 2.5). A combination of HSQC, HMBC and COSY experiments permitted the determination of the linear connectivity from H-7/C-7 to H-13/C-13 of the heptanoid chain in compounds **29-31**.

In particular, the ESI/LTQORBITRAP/MS data of **29** (m/z 343.1188 [M-H]⁻, calcd for C₁₉H₁₉O₆, 343.1182) in combination with the ¹³C NMR data showed the molecular formula C₁₉H₂₀O₆. In the IR spectrum an absorption maximum at 1720 cm⁻¹ due a ketocarbonyl group was evident. The ¹H NMR data showed signals ascribable to two 1,2,4 trisubstituted aromatic rings at δ 7.08 (dd, $J = 8.1, 1.8$ Hz), 7.02 (dd, $J = 8.1, 1.8$ Hz), 6.81 (d, $J = 8.1$ Hz), 6.78 (d, $J = 8.1$ Hz), 6.68 (d, $J = 1.8$ Hz) and 6.39 (d, $J = 1.8$ Hz) (fig. 2.13 and table 2.5).

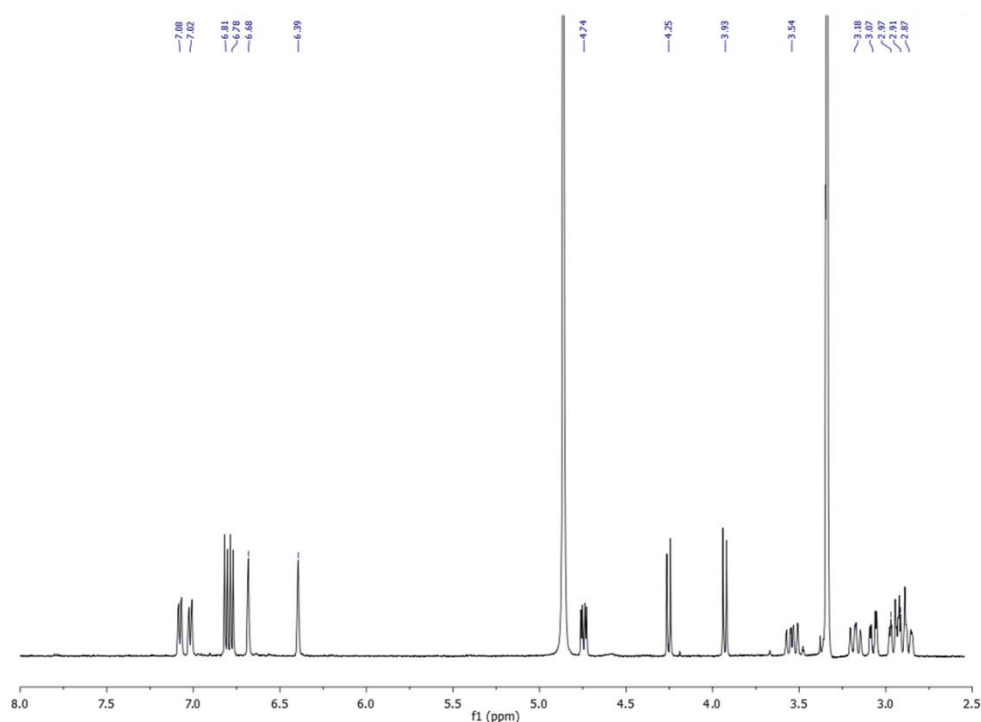


Figure 2.13. ¹H NMR spectrum (600 MHz, CD₃OD) of carpinontriol B (**29**).

Table 2.5. ¹H NMR and ¹³C NMR data of compounds **29-31** (MeOH-*d*₄).

	29		30		31	
	δ_c	δ_H (J in Hz)	δ_c	δ_H (J in Hz)	δ_c	δ_H (J in Hz)
1	127.1	-	128.4	-	126.8	-
2	127.0	-	127.7	-	128.4	-
3	153.3	-	151.9	-	153.1	-
4	117.1	6.78, d (8.1)	117.3	6.81, d (8.1)	116.8	6.81, d (8.2)
5	129.2	7.02, dd (8.1, 1.8)	130.6	7.05, dd (8.1, 1.8)	130.6	7.09, dd (8.2, 1.8)
6	130.7	-	130.2	-	130.6	-
7	37.1	2.91, d (15.8, 11.3)	37.1	2.88, dd (15.8, 12.2)	39.5	2.94, dd (16.3, 9.6)
		3.07, dd (15.8, 4.2)		3.09, dd (15.8, 4.4)		3.01, dd (16.3, 3.8)
8	68.5	4.74, dd (11.3, 4.2)	68.5	4.67, dd (12.2, 4.4)	71.9	4.22, dd (9.6, 3.8)
9	69.7	3.93, d (10.1)	69.5	3.74, d (10.1)	70.1	4.41, br s
10	78.6	4.25, d (10.1)	78.4	4.21, d (10.1)	77.6	4.35, d (5.6)
11	215.0	-	215.3	-	81.7	4.27, d (5.6)
12	37.1	2.97, ddd (19.6, 5.2, 2.0)	37.0	2.95, m	216.9	-
		3.54, ddd (19.6, 12.6, 2.0)		3.55, m		
13	24.9	2.87, ddd (16.6, 5.2, 2.0)	24.7	2.94, m	43.7	3.13, d (12.0)
		3.18, ddd (16.6, 12.6, 2.0)		3.15, ddd (17.2, 12.6, 2.0)		4.74, d (12.0)
14	130.7	-	132.8	-	129.9	-
15	129.0	7.08, dd (8.1, 1.8)	129.7	7.23, dd (8.1, 1.8)	130.1	7.06, dd (8.1, 1.8)
16	117.1	6.81, d (8.1)	115.4	7.20, d (8.1)	116.8	6.83, d (8.1)
17	152.7	-	152.6	-	153.1	-
18	134.6	6.39, d (1.8)	135.9	6.30, d (1.8)	136.9	7.25, d (1.8)
19	134.4	6.68, d (1.8)	135.8	6.54, d (1.8)	135.6	6.68, d (1.8)
				β -Glc (at C-17)		
1	-	-	102.3	5.12, d (7.6)	-	-
2	-	-	74.6	3.48, dd (9.0, 7.6)	-	-
3	-	-	78.0	3.54, dd (9.0, 9.0)	-	-
4	-	-	71.2	3.41, dd (9.0, 9.0)	-	-

5	-	77.9	3.52, m	-	-
6	-	62.3	3.73, dd (12.0, 4.5)	-	-
			3.93, dd (12.0, 2.5)		

The ^1H NMR spectrum showed further signals corresponding to three oxymethine protons at δ 4.74 (dd, $J = 11.3, 4.2$ Hz), 4.25 (d, $J = 10.1$ Hz) and 3.93 (d, $J = 10.1$ Hz). The ^{13}C NMR spectrum of compound **29** showed 19 carbon signals, typical of a cyclic diarylheptanoid¹⁰. HMBC (fig 2.15) and COSY cross-peaks and (fig. 2.16) permitted the assignment of the three hydroxy groups to C-8 (δ 68.5), C-9 (δ 69.7), and C-10 (δ 78.6).

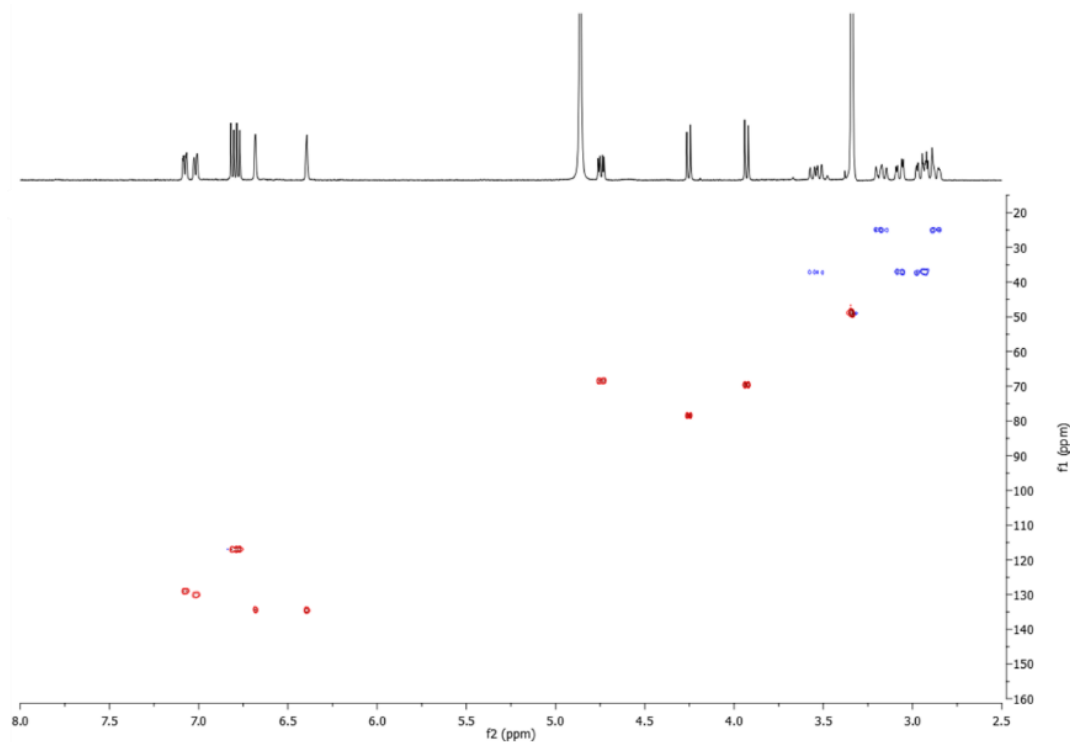


Figure 2.14. HSQC spectrum (CD_3OD) of carpinontriol B (**29**).

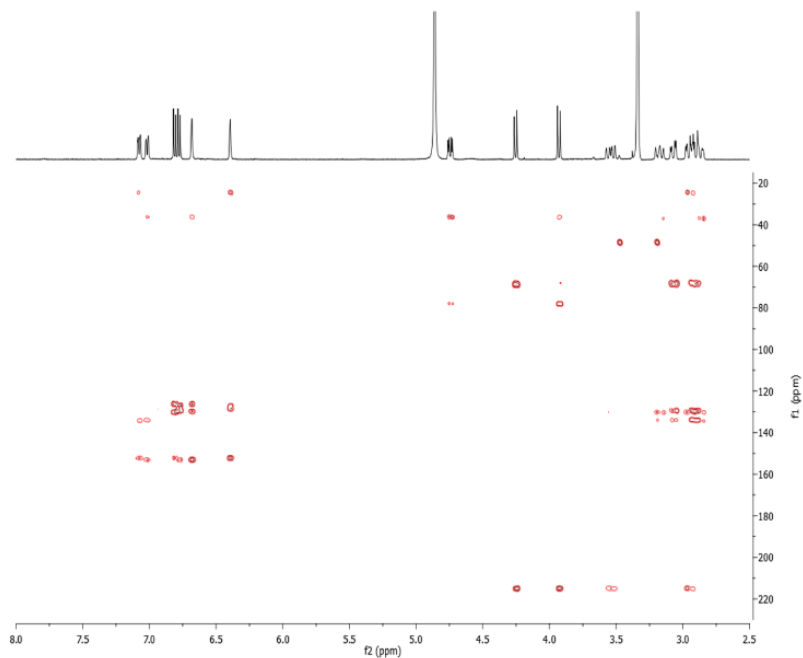


Figure 2.15. HMBC spectrum (CD_3OD) of carpinontriol B (**29**).

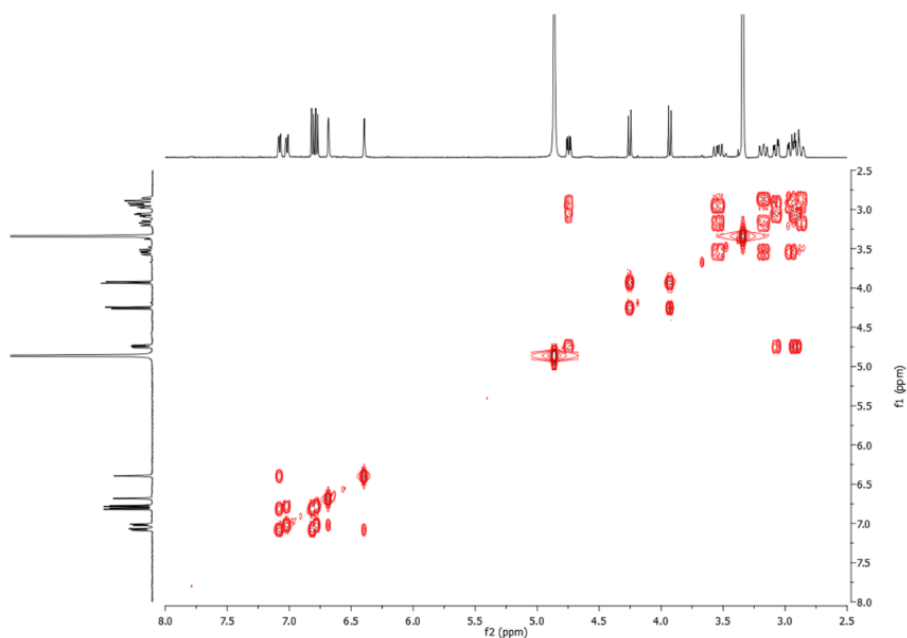


Figure 2.16. COSY spectrum (CD_3OD) of carpinontriol B (**29**).

The position of the carbonyl group was determined by 2D NMR data; in particular, the HMBC cross-peaks between the signals of H-9 (δ 3.93), H-10 (δ 4.25), H₂-12 (δ 3.54, 2.97) and H₂-13 (δ 3.18, 2.87), with the carbon resonance at δ 215.0 allowed the carbonyl group to be located at C-11 of the heptyl moiety. The ROESY experiment (fig. 2.17) showed correlations of H-19 (δ 6.68) with H-18 (δ 6.39), H-8 (δ 4.74), and H-9 (δ 3.93), as well as correlations of H-18 (δ 6.39) H₂-12 (δ 3.54) and H₂-13 (δ 3.18). Further correlations of H-8 (δ 4.74) with H-9 (δ 3.93), and H-10 (δ 4.25) were observed.

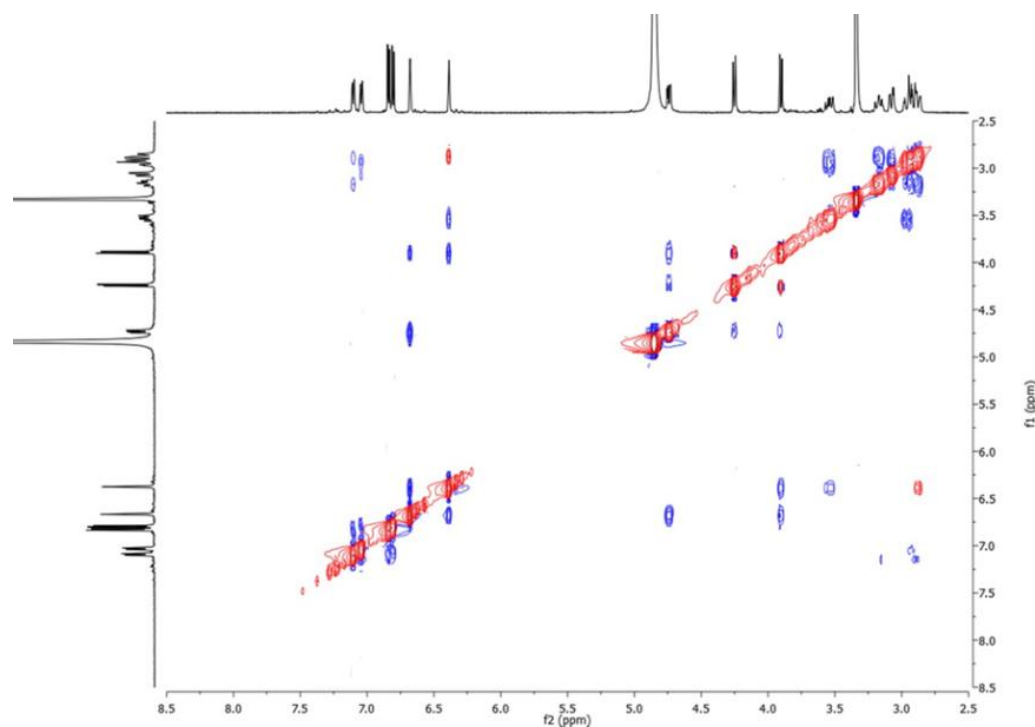


Figure 2.17. ROESY spectrum (CD₃OD) of carpinontriol B (**29**).

However, ROESY correlations cannot define the orientations of the hydroxy groups on the heptyl moiety chain because of its conformational mobility. Based on the aforementioned data, the 2D structure of compound **29** was elucidated as depicted (fig. 2.18).

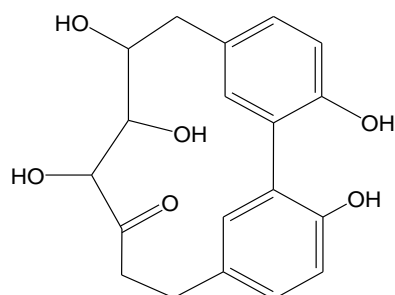


Figure 2.18. planar structure of compound **29**.

The ^1H and ^{13}C NMR spectra of compounds **30** and **31**, in comparison with those of **29**, suggested they were also diarylheptanoid derivatives.

The molecular formula of **30** was established as $\text{C}_{25}\text{H}_{30}\text{O}_{11}$ by ESI/LTQORBITRAP/MS (m/z 505.1717 $[\text{M}-\text{H}]^-$, calcd for $\text{C}_{25}\text{H}_{29}\text{O}_{11}$, 505.1710) and the ^{13}C NMR data. The NMR data of **30** revealed that it differed from **29** by the presence of a β -glucopyranosyl unit (δ 5.12) (fig. 2.19 and table 2.5).

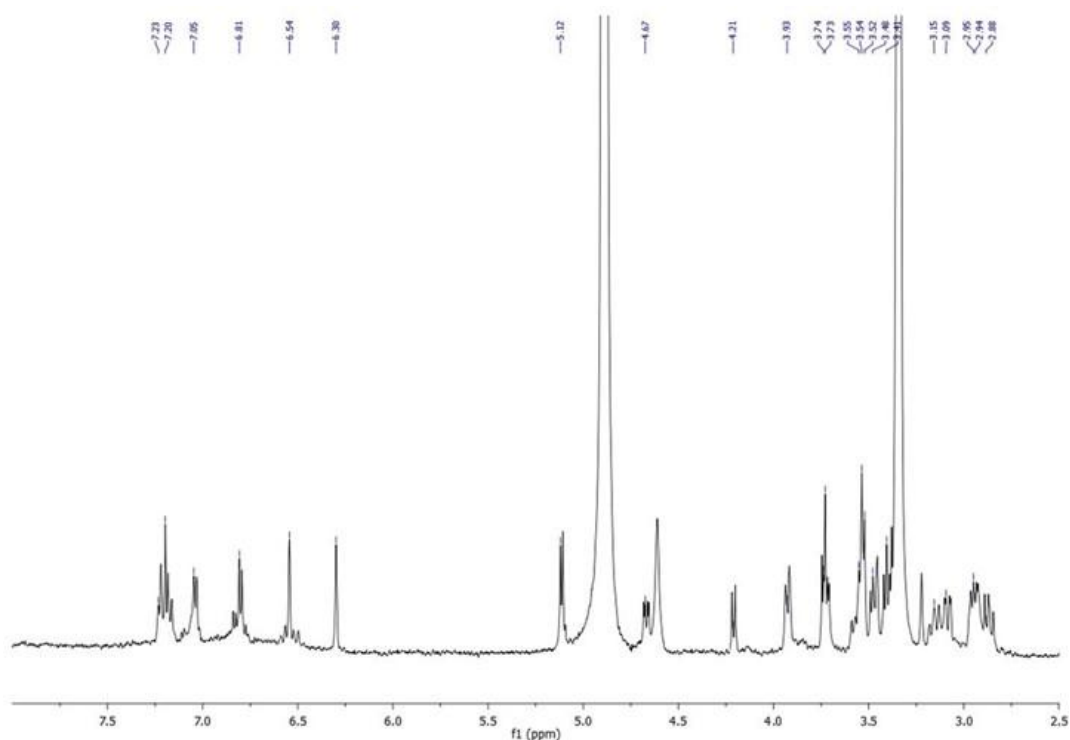


Figure 2.19. ^1H NMR spectrum (600 MHz, CD_3OD) of giffonin T (**30**).

The D-configuration of the glucose unit was established via hydrolysis of **30** with 1 N HCl, trimethylsilation, and GC analysis¹¹. The linkage site of the sugar unit on the diaryl moiety was obtained from the HMBC spectrum, which showed a cross-peak between H-1_{glc} (δ 5.12) and C-17 (δ 152.6). Thus, the 2D structure of giffonin T (**30**), was established as shown (fig. 2.20).

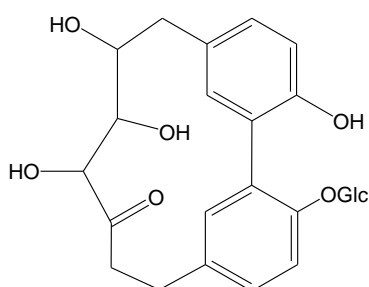


Figure 2.20. planar structure of giffonin T.

The ¹³C NMR and ESI/LTQORBITRAP/MS data of **31** (m/z 359.1136 [M-H]⁻, calcd for C₁₉H₁₉O₇, 359.1131), suggested a molecular formula of C₁₉H₂₀O₇. A carbonyl group was evident in the IR spectrum at 1730 cm⁻¹. Analysis of the NMR data showed that compound **31** differed from **29** regarding the presence of an additional secondary hydroxy group and the location of the carbonyl function (table 2.5). In particular, HSQC data confirmed a diarylheptanoid core structure with oxymethine (δ 4.41, 4.35, 4.27, 4.22) proton resonances correlating to C-9 (δ 70.1), C-10 (δ 77.6), C-11 (δ 81.7), and C-8 (δ 71.9), respectively (table 2.5). The carbonyl group was located at C-12 (δ 216.9), on the basis of the HMBC cross-peaks between H₂-13 (δ 4.74, 3.13), H-10 (δ 4.35) and H-11 (δ 4.27) with the carbonyl resonance at δ 216.9. In the ROESY spectrum correlations of H-18 (δ 7.25) with H-19 (δ 6.68) and H-10 (δ 4.35), and of H-8 (δ 4.22) with H-9 (δ 4.41), H-10 (δ 4.35), and H-7 (δ 2.94) were observed. The 2D structure of giffonin U (**31**) was thus established as shown (fig. 2.21).

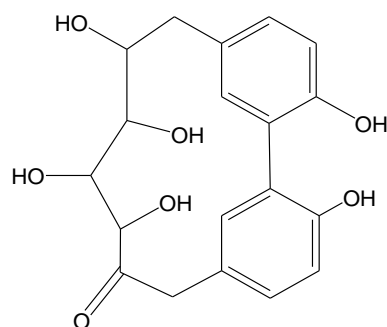


Figure 2.21. planar structure of giffonin U.

Relative configurations of the diarylheptanoids 29-31

These compounds, possessing at least two stereogenic centres on the heptyl unit, therefore, as realized previously for giffonins J-P, in collaboration with Prof. Giuseppe Bifulco (Department of Pharmacy, University of Salerno) a combined QM/NMR approach has been used to establish the relative configurations of compounds **29-31**. In the present investigation, the QM/NMR approach was employed to determine the relative configurations of compounds **29-31** through the comparison of the experimental $^{13}\text{C}/^1\text{H}$ NMR chemical shift data and the related predicted values. The latter data were computed on all the possible diastereoisomers¹²⁻¹⁷, also taking into account the atropisomers arising from the hindered rotation along the biaryl axis. Specifically, QM/NMR calculations were performed for compounds **29** and **31**, since the experimental data revealed that **30** differs from **29** by the presence of a β -D-glucopyranosyl unit, while maintaining the same relative configuration. Firstly, the experimental NMR data for compound **29** showed a high similarity with those reported for carpinontriol B from *Carpinus cordata*¹⁸. In this case, the QM/NMR combined approach was used for confirming the established relative configuration, while additional stereochemical information arising from the preferred atropisomeric forms were reported. Moreover, the absolute configurations of **29** and **31** were established by comparing the calculated and experimental ECD spectra.

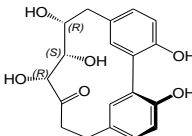
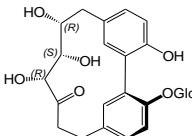
As previously described for analogous compounds¹⁰, an extensive conformational search related to all the possible diastereoisomers of **29** and **31** was required for the subsequent phases of computation of the NMR parameters. Firstly, the conformational search was performed at the empirical level (molecular mechanics, MM), combining Monte Carlo Molecular Mechanics (MCMM), Low-Mode Conformational Sampling (LMCS), and Molecular Dynamics (MD) simulations. The accurate analysis of these representative conformers highlighted a significant conformational variability mainly due to the flexible heptyl moieties, and the distribution of intramolecular H-bonds between the hydroxy groups on adjacent carbons rather influenced the energy of the related conformers weighted in the Boltzmann distribution. Also, the hypothesized hindered rotation along the *o*-disubstituted biaryl axis determines one preferential arrangement of the two phenyl moieties (*aR* or *aS* absolute configuration) giving rise to atropisomerism^{19, 20}. Importantly, the starting MM sampling generated conformers for both groups of possible atropisomers for each diastereoisomer, that were subsequently submitted to geometry and energy optimization steps at the density functional level of theory (DFT). After the optimization of the geometries, the conformers were visually inspected in order to avoid further possible redundant conformers. DFT calculations were employed for predicting the rotational energy barrier related to the interconversion between the atropisomers (Experimental Section), specifically on the *aR**/*aS** atropisomers of *8S**,*9R**,*10R**-**29** as representative system for all the investigated compounds. The difference between the energy of the most energetically favoured conformer and the related energy of the transition state indicated $\Delta G^\ddagger = 20.7$ kcal/mol, thus suggesting hindered rotation about the biphenyl bond¹⁹.

Specifically, this parameter was calculated for the *aR**,*8S**,*9R**,*10R** (**29a**)/*aS**,*8S**,*9R**,*10R** (**29b**) atropisomers of compound **29** as representative system for all the investigated diastereoisomers, and showed $\Delta G^\ddagger = 20.7$ kcal/mol

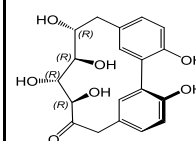
for **29a** and $\Delta G^\ddagger = 16.6$ kcal/mol for **29b** (difference between the energy of the most energetically favoured conformers of **29a** and **29b** and the related energy of the transition state). The high rotational barrier calculated for **29a** ($\Delta G^\ddagger = 20.7$ kcal/mol) indicated the hindered rotation about the biphenyl bond¹⁹ corroborating the presence of atropisomerism and the related hindered interconversion to the **29b** isomer. On the other hand, **29b** showed a lower predicted energy barrier ($\Delta G^\ddagger = 16.6$ kcal/mol) that would allow its interconversion to the energetically more favoured and stable **29a** isomer.

For each considered compound, the NMR chemical shift data were computed for all the possible diastereoisomers featuring a specific relative configuration at the stereogenic centers and at the biaryl axis (*aR**/*aS** atropisomeric forms). For each of them, the weighted averages of the predicted ¹³C and ¹H NMR chemical shifts were computed at the density functional level of theory (DFT), accounting the energies of the sampled conformers on the final Boltzmann distribution. Also, a first set of ¹³C and ¹H NMR chemical shift data were obtained with TMS as reference compound; afterwards, the “multi-standard” approach^{21, 22} was also employed obtaining a second set of values, using TMS as reference only for sp³ ¹³C and ¹H atoms, and benzene as reference for sp² ¹³C and ¹H atoms. For each atom of the investigated molecules, experimental and calculated ¹³C and ¹H NMR chemical shifts were compared, and afterwards the mean absolute errors (MAEs) for all the possible diastereoisomers were computed (table 2.6).

Table 2.6. $^{13}\text{C}/^1\text{H}$ MAE (ppm) Values, and DP4+ Data Reported for the Possible Stereoisomers of compounds **29** and **31**; Stereochemistry of compound **30** was Considered the Same as **29**, Since They Differ by the Presence of a β -D-glucopyranosyl Unit. In the Last Two Columns, the Predicted Absolute Configurations and the Related Chemical Structures of **29-31** are Reported.

# of stereogenic centers	# of possible relative stereoisomer	Stereoisomer	Relative configuration	# of sampled conformers	^{13}C MAE (ppm)	^1H MAE (ppm)	DP4+ probability ^c			Absolute configuration ^d	Proposed structure
							all	^{13}C data	^1H data		
29	3, plus one axis of chirality	29a	$aR^*,8S^*,9R^*,10R^*$	7	2.9	0.1	0.0	0.0	0.00		
			$aS^*,8S^*,9R^*,10R^*$	5	4.1	0.3	0.0	0.0	0.00		
		29c	$aR^*,8S^*,9R^*,10S^*$	11	2.3	0.1	99.0	99.3	100.0		$aS,8R,9S,10R$
			$aS^*,8S^*,9R^*,10S^*$	4	4.3	0.4	0.0	0.0	0.00		
		29e	$aR^*,8S^*,9S^*,10R^*$	10	2.7	0.2	0.0	0.0	0.00		
			$aS^*,8S^*,9S^*,10R^*$	2	4.1	0.3	0.0	0.0	0.00		
		29g	$aR^*,8S^*,9S^*,10S^*$	6	2.8	0.1	0.5	0.0	0.00		
			$aS^*,8S^*,9S^*,10S^*$	4	4.1	0.2	0.0	0.0	0.00		
30	3, plus one axis of chirality	30a	$aR^*,8S^*,9R^*,10R^*$								
			$aS^*,8S^*,9R^*,10R^*$								
		30c	$aR^*,8S^*,9R^*,10S^*$								
			$aS^*,8S^*,9R^*,10S^*$								
		30e	$aR^*,8S^*,9S^*,10R^*$								

		30f	a <i>S</i> [*] ,8 <i>S</i> [*] ,9 S [*] ,10 <i>R</i> [*]							
		30g	a <i>R</i> [*] ,8 <i>S</i> [*] ,9 S [*] ,10 <i>S</i> [*]							
		30h	a <i>S</i> [*] ,8 <i>S</i> [*] ,9 S [*] ,10 <i>S</i> [*]							
31	4, plus 16 one axis of chirality	31a	a <i>R</i> [*] ,8 <i>S</i> [*] ,9 R [*] ,10 <i>R</i> [*] ,1 1 <i>R</i> [*]	3	3.2	0.3	0.0	0.0	0.00	
					5	1	0%	0%	%	
		31b	a <i>S</i> [*] ,8 <i>S</i> [*] ,9 R [*] ,10 <i>R</i> [*] ,1 1 <i>R</i> [*]	5	3.2	0.2	0.0	0.0	0.00	
					1	3	0%	0%	%	
		31c	a <i>R</i> [*] ,8 <i>S</i> [*] ,9 R [*] ,10 <i>R</i> [*] ,1 1 <i>S</i> [*]	8	2.3	0.3	0.0	0.0	0.00	
					5	0	0%	0%	%	
		31d	a <i>S</i> [*] ,8 <i>S</i> [*] ,9 R [*] ,10 <i>R</i> [*] ,1 1 <i>S</i> [*]	9	2.0	0.2	0.0	0.0	0.00	
					6	3	5%	0%	%	
		31e	a <i>R</i> [*] ,8 <i>S</i> [*] ,9 R [*] ,10 <i>S</i> [*] ,1 1 <i>R</i> [*]	11	1.7	0.3	0.0	0.0	0.00	
					7	0	0%	0%	%	
		31f	a <i>S</i> [*] ,8 <i>S</i> [*] ,9 R [*] ,10 <i>S</i> [*] ,1 1 <i>R</i> [*]	11	3.1	0.2	0.0	0.0	0.00	
					6	8	0%	0%	%	
		31g	a <i>R</i> [*] ,8 <i>S</i> [*] ,9 R [*] ,10 <i>S</i> [*] ,1 1 <i>S</i> [*]	13	1.8	0.1	0.0	3.5	0.00	
					2	8	2%	3%	%	
		31h	a <i>S</i> [*] ,8 <i>S</i> [*] ,9 R [*] ,10 <i>S</i> [*] ,1 1 <i>S</i> [*]	5	4.5	0.3	0.0	0.0	0.00	
					9	5	0%	0%	%	
		31i	a <i>R</i> [*] ,8 <i>S</i> [*] ,9 S [*] ,10 <i>R</i> [*] ,1 1 <i>R</i> [*]	9	2.4	0.2	0.0	0.0	0.00	
					7	9	0%	0%	%	
		31j	a <i>S</i> [*] ,8 <i>S</i> [*] ,9 S [*] ,10 <i>R</i> [*] ,1 1 <i>R</i> [*]	9	2.4	0.2	0.0	0.0	0.00	
					4	8	0%	0%	%	
		31k	a <i>R</i> [*] ,8 <i>S</i> [*] ,9 S [*] ,10 <i>R</i> [*] ,1 1 <i>S</i> [*]	7	2.4	0.2	0.0	0.0	0.00	
					4	3	0%	0%	%	
		31l	a <i>S</i> [*] ,8 <i>S</i> [*] ,9 S [*] ,10 <i>R</i> [*] ,1 1 <i>S</i> [*]	1	3.6	0.2	0.0	0.0	0.00	
					9	8	0%	0%	%	
		31m	a <i>R</i> [*] ,8 <i>S</i> [*] ,9 S [*] ,10 <i>S</i> [*] ,1 1 <i>R</i> [*]	10	1.7	0.2	12.	0.0	0.00	
					6	8	02	0%	%	
							%			
		31n	a <i>S</i> [*] ,8 <i>S</i> [*] ,9	4	2.2	0.3	0.0	0.0	0.00	



	S*,10S*,1 1R*		7	2	1%	0%	%	
31o	aR*,8S*,9 S*,10S*,1 1S*	13	1.9	0.1	87.	96.	100.	aS,8R,9 R,10R,1 1R
31p	aS*,8S*,9 S*,10S*,1 1S*	8	2.9	0.3	0.0	0.0	0.00	
			7	0	0%	0%	%	

^a ¹³C MAE = (Σ[|δ_{exp} - δ_{calcd}|])/n, summation through n of the absolute error values (difference of the absolute values between corresponding experimental and ¹³C chemical shifts), normalized to the number of the chemical shifts. Chemical shift data reported were produced using the “multi standard” approach, using TMS as reference compound for sp³ ¹³C atoms, and benzene for sp² ¹³C atoms; . ^b ¹H MAE = (Σ[|δ_{exp} - δ_{calcd}|])/n, summation through n of the absolute error values (difference of the absolute values between corresponding experimental and ¹H chemical shifts), normalized to the number of the chemical shifts. Chemical shift data reported were produced using the “multi standard” approach, using TMS as reference compound for sp³ ¹H atoms, and benzene for sp² ¹H atoms. **DP4+ probabilities** This set of data was produced using only TMS as reference compound, and then sp³/sp² atoms were differently treated following the “multi-standard” approach flagging them in the DP4+ Excel file. ^d**The absolute configurations** of compounds **29-31** were determined after comparison of the experimental and predicted ECD spectra. Starting from the identified absolute configurations of **29-31**, we also predicted the ECD spectra of aR,8R,9S,10R-**29** and aR,8R,9R,10R,11R-**31**, namely the atropisomers differing from (aS,8R,9S,10R)-**29** and (aS,8R,9R,10R,11R)-**31** for the inversion of the axis of chirality. Their predicted CD spectra showed a poor superposition with the experimental curves and an opposite behaviour if compared with those of aS,8R,9S,10R-**29** and aS,8R,9R,10R,11R-**31**, then suggesting that the ECD transitions are strongly affected by the geometry of the biphenyl moiety and corroborating the aS axial chirality for the investigated compounds.

The results highlighted the slight accordance between ¹³C/¹H MAEs related to the possible isomers of **29** and **31** also when using the data arising from the “multi-standard” approach, then determining the uncertainty to unambiguously assign the relative configurations (table 2.6). For these reasons, we also relied on the recently introduced DP4+ approach²³, that emerged as a new powerful tool for the correct stereochemical assignment of organic compounds. In particular, the relative configurations of compounds **29** and **31** were predicted selecting the stereoisomers with the highest DP4+ probability (all data DP4+, namely combining both ¹³C/¹H NMR chemical shift data) (table 2.6). The results confirmed the 8S*,9R*,10S* configuration for compounds **29** and **30**, the same as was reported for carpinontriol B¹⁸. This was corroborated by the perfect

agreement between experimental and calculated ${}^3J_{9,10}$ ($J_{\text{exp}}=10.1$ Hz, $J_{\text{calc}}=10.2$ Hz). The data further suggest the axial chirality, permitting assignment of the $aR^*,8S^*,9R^*,10S^*$ -**29** and **-30** relative configurations. Moreover, the 1D ${}^1\text{H}$ NMR spectra at various temperatures of compound **29**, in $\text{DMSO-}d_6$, have been acquired, focusing on the protons of the diphenyl moieties (fig. 2.22).

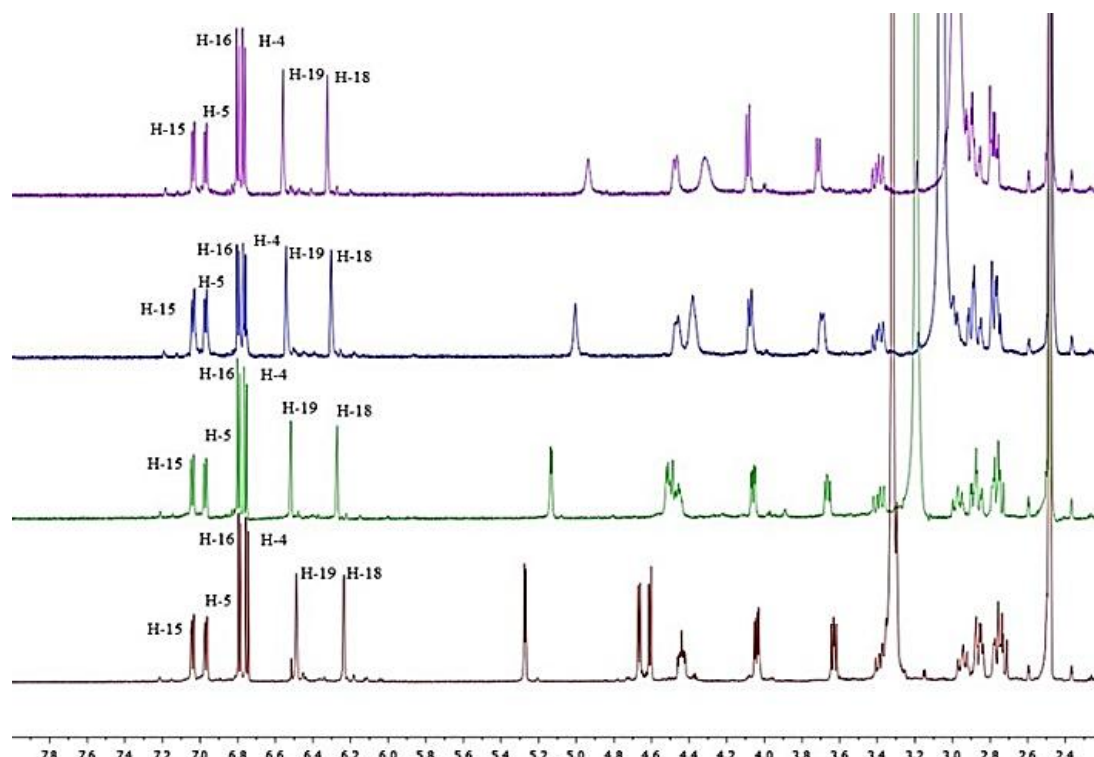


Figure 2.22. ${}^1\text{H}$ NMR spectra (600 MHz, DMSO) of compound **29** at 298 K (red), 323 K (green), 353 K (blue) and 373 K (purple).

As can be observed in the ${}^1\text{H}$ NMR spectra of carpinontriol B (fig. 2.22), the resonances of H-4, H-5, H-15, H-16, H-18, and H-19 showed no significant changes in their chemical shifts over a range of temperatures (298–373 K), a finding in agreement with a high rotational barrier, hence confirming the presence of atropisomers.

Concerning compound **31**, this procedure led to identification of the **31o** isomer showing the lowest MAEs and the highest DP4+ probability. We then proposed

$aR^*,8S^*,9S^*,10S^*,11S^*$ -**31** as relative configuration, that was further corroborated by the good agreement between experimental and predicted $^3J_{10-11}$ ($J_{\text{exp}}= 5.6$ Hz, $J_{\text{calc}}= 5.1$ Hz). Once the most probable relative configurations of **29** and **31** were identified.

Absolute configurations of the diarylheptanoids 29-31

In collaboration with Prof. Giuseppe Bifulco (Department of Pharmacy, University of Salerno), the absolute configurations of compounds **29-31** were assigned by comparing the calculated and experimental ECD spectra of the two enantiomers²⁴⁻²⁶. Starting from the selected conformers related to the isomers of **29** and **31** (**29c**, **31o**), QM calculations at the TDDFT MPW1PW91/6-31g(d,p) level were performed in EtOH IEFPCM to reproduce the experimental solvent environment. As shown in figure 2.23., the comparison of calculated and experimental ECD curves permitted assignment of the absolute configurations of **29-31** as ($aS,8R,9S,10R$)-**29** and **-30**; ($aS,8R,9R,10R,11R$)-**31**.

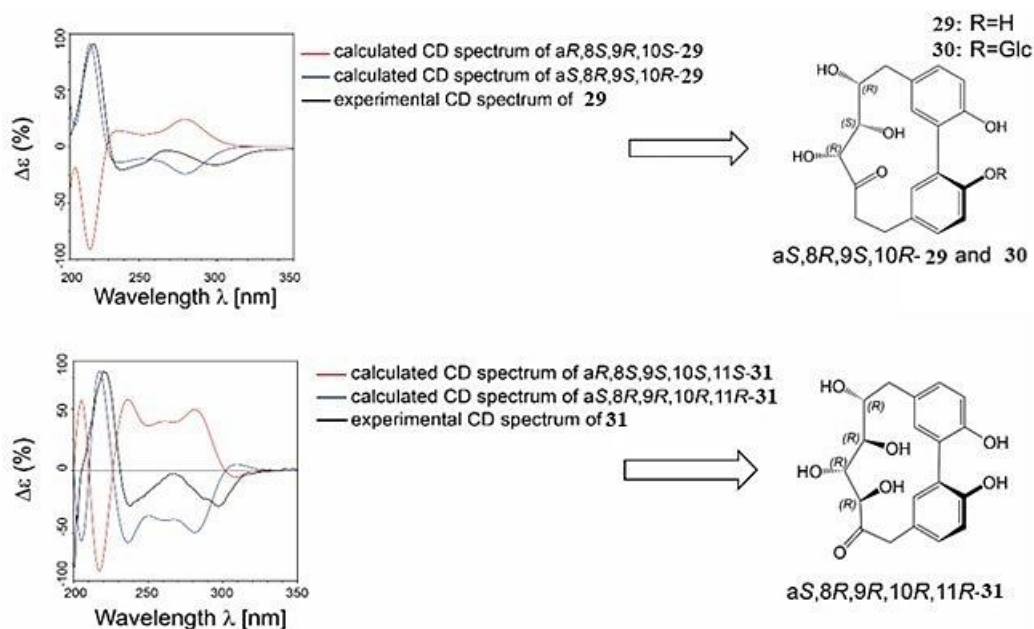


Figure 2.23. Comparison of the experimentally ECD spectra with the TDDFT-predicted curves of compounds **29** and **31**.

In addition, giffonin I (**9**), myricetin 3-*O*- α -L-rhamnopyranoside¹⁰ (**17**), kaempferol 3-*O*- α -L-rhamnopyranoside¹⁰ (**19**), kaempferol 3-*O*-(4''-*trans*-*p*-coumaroyl)- α -L-rhamnopyranoside¹⁰ (**20**), citric acid (**32**),²⁷ 1-methyl citrate²⁷ (**33**), trimethyl citrate²⁷ (**34**), 3,5-dicaffeoylquinic acid²⁸ (**35**), and were isolated from the green leafy covers of *C. avellana* (fig. 2.24).

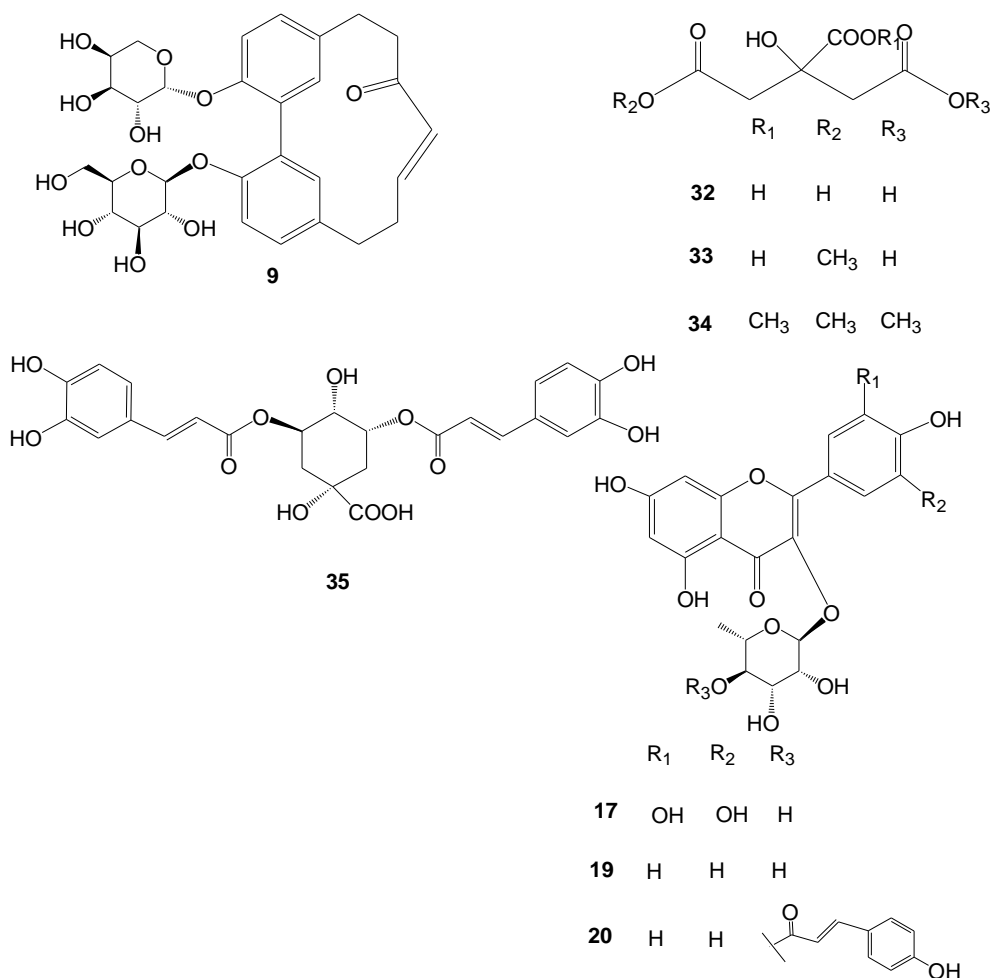


Figure 2.24. compounds isolated from the green leafy covers of *C. avellana*.

Interestingly, the aglycone moiety of giffonin I (**9'**) shows no stereogenic centers in the macrocyclic ring but its biphenyl moiety also possesses an axis of chirality. After performing an extensive conformational search at the MM level, the conformers were submitted to an optimization of the geometries at the QM level. In order to assess the possible interconversion between the *aR* and *aS* atropisomers of **9'** (**9'a** and **9'b**, respectively; fig. 2.25), the rotational barrier predicting the energy of the transition state was computed and showed a $\Delta G^\ddagger = 17.1$ kcal/mol value which may be compatible with an interconversion between the two atropisomers¹⁹.

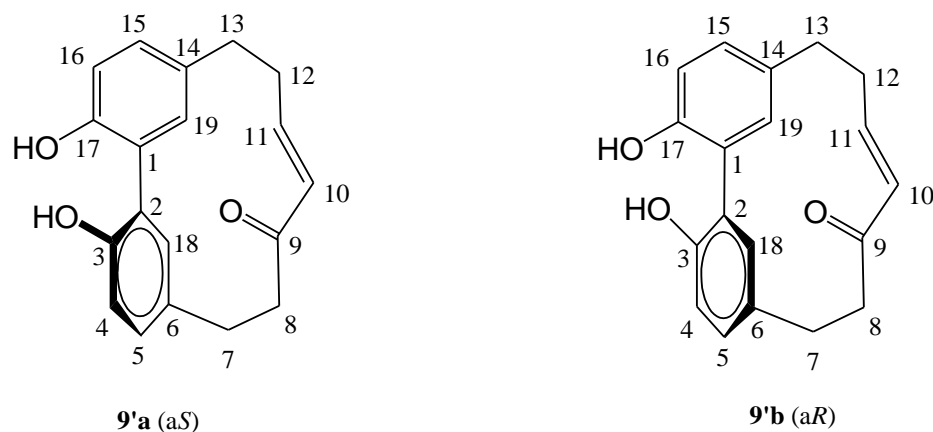


Figure 2.25. Chemical structures of the two possible atropisomers of **9'**, named **9'a-b**.

These data were corroborated by the experimental ECD spectrum of **9'** with the absence of Cotton effects near 220 nm (fig. 2.26).

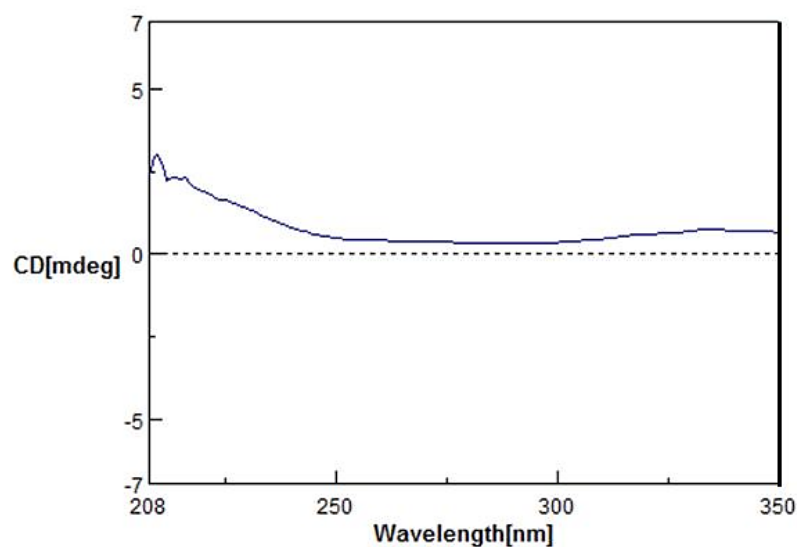


Figure 2.26. CD spectrum of the aglycone of compound **9**.

2.2.3. Biological assay

Cytotoxic activity

The cytotoxic activity of compounds isolated from the green leafy covers of *C. avellana* was tested against two cancer cell lines including A549 (human lung adenocarcinoma) and DeFew (human B lymphoma). In the range 10-100 μM , the compounds did not show a significant reduction of the cell number (data not shown), in agreement with the absence of cytotoxicity previously reported for giffonins A-P.

Evaluation of antioxidant activity of MeOH extract of green leafy covers and pure compounds by TBARS assay.

On the basis of the antioxidant activity shown by giffonins isolated from the MeOH extract of *C. avellana* cv. Tonda di Giffoni leaves, in collaboration with

Prof. Beata Olas, the antioxidant activity of the MeOH extract of the green leafy covers of *C. avellana* and of the isolated compounds was evaluated for their potential protective properties against oxidative damages (lipid peroxidation) induced by H_2O_2 and $\text{H}_2\text{O}_2/\text{Fe}^{2+}$ in human plasma. In particular, all compounds isolated by MeOH extract of leafy covers, except compounds **9**, and **19-20**, which were tested previously; were tested. So, the activity of compounds **17**, **29-35** was compared to that of the well-known antioxidant curcumin. Compounds and curcumin were tested at doses ranging from 0.1 to 100 μM . Compounds **29** and **31** at 10 μM reduced both H_2O_2 and $\text{H}_2\text{O}_2/\text{Fe}^{2+}$ induced lipid peroxidation by more than 30 %, hence were more active than curcumin (fig. 2.27 and table 2.7). Compound **35** exhibited a protective action against oxidative stress induced by H_2O_2 or $\text{H}_2\text{O}_2/\text{Fe}^{2+}$, similar to that shown by curcumin, while weaker activity was displayed by compounds **30**.

Table 2.7. Inhibitory Effects of Compounds **17** and **29-35** (10 μ M; 30 min) and curcumin (10 μ M; 30 min) on Plasma Lipid Peroxidation Induced by H_2O_2 or H_2O_2/Fe^{2+} .

compound	Inhibition of lipid peroxidation induced by H_2O_2 (%)	Inhibition of lipid peroxidation induced by H_2O_2/Fe^{2+} (%)
17	44.4 \pm 8.4 (p<0.05)	34.1 \pm 6.9 (p<0.05)
29	32.2 \pm 7.7 (p<0.05)	24.4 \pm 6.7 (p<0.05)
30	14.7 \pm 4.3 (p<0.05)	23.3 \pm 7.9 (p<0.05)
31	33.3 \pm 9.9 (p<0.05)	14.4 \pm 6.1 (n.s.)
32	n.s.*	n.s.*
33	n.s.*	n.s.*
34	n.s.*	n.s.*
35	24.2 \pm 6.7 (p<0.05)	25.5 \pm 9.9 (p<0.05)
curcumin	21.1 \pm 7.9 (p<0.05)	22.9 \pm 5.1 (p<0.05)

* not significant

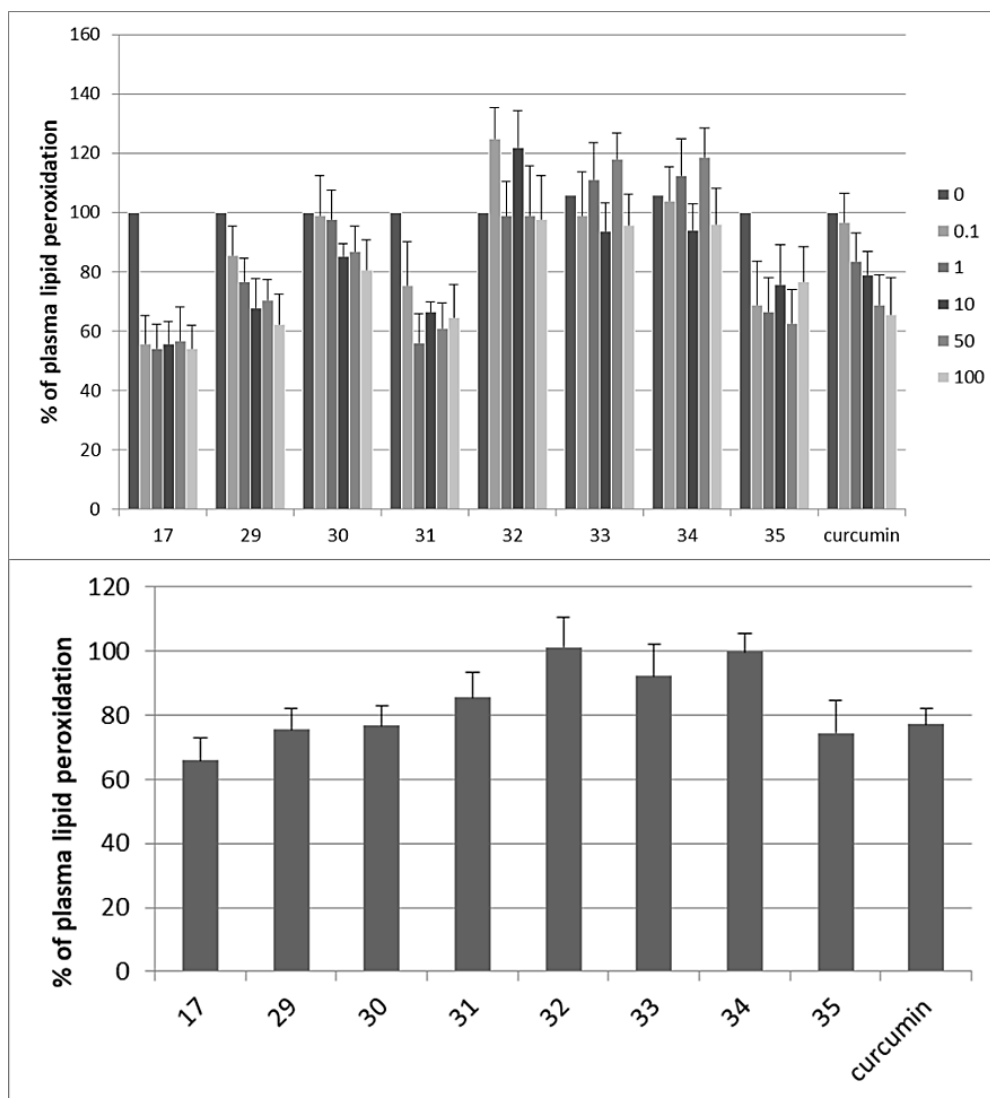


Figure 2.27. (A). The effects of MeOH extract (0.1 – 100 µg/mL; 30 min), tested compounds (0.1 – 100 µM; 30 min) and curcumin (0.1 – 100 µM; 30 min) on plasma lipid peroxidation induced by H₂O₂. The results are representative of 5-9 independent experiments, and are expressed as means ± SD. The effect of five different concentrations of tested compounds (0.1, 1, 10, 50 and 100 µM) and tested extract (0.1, 1, 10, 50 and 100 µg/mL) was statistically significant according to ANOVA I test ($p < 0.05$). (B). The effects of MeOH extract (10 µg/mL; 30 min), tested compounds (10 µM; 30 min) and curcumin (10 µM; 30 min) on plasma lipid peroxidation induced by H₂O₂/Fe²⁺. The results are representative of 6-9 independent experiments, and are expressed as means ± SD. The statistical significances were confirmed with the paired Student's t-test ($p < 0.05$, $p < 0.005$).

Evaluation of antimicrobial activity of MeOH extract of green leafy covers and pure compounds by halo assay.

On the basis of the antimicrobial activity reported for hazelnut tree leaves and for some diarylheptanoid derivatives²⁹⁻³¹, in collaboration with Dr. Filomena Nazzaro (ISA, CNR, Avellino), the antimicrobial activity of the MeOH extract *C. avellana* green leafy covers and of isolated compounds (**9**, **17**, **19-20** and **29-35**) was evaluated against the Gram-positive strains *Bacillus cereus* and *Staphylococcus aureus*, and the Gram-negative strains *Escherichia coli* and *Pseudomonas aeruginosa* by halo assay.

With halo test, approximately one million cells from a single strain are spread over an agar plate using a sterile swab, then incubated in the presence of the antimicrobial object (in our case MeOH extract and pure compounds). If the bacterial or fungal strain is susceptible to the antimicrobial agent, then a zone of inhibition appears on the agar plate (fig. 2.28). If it is resistant to the antimicrobial agent, then no zone is evident.

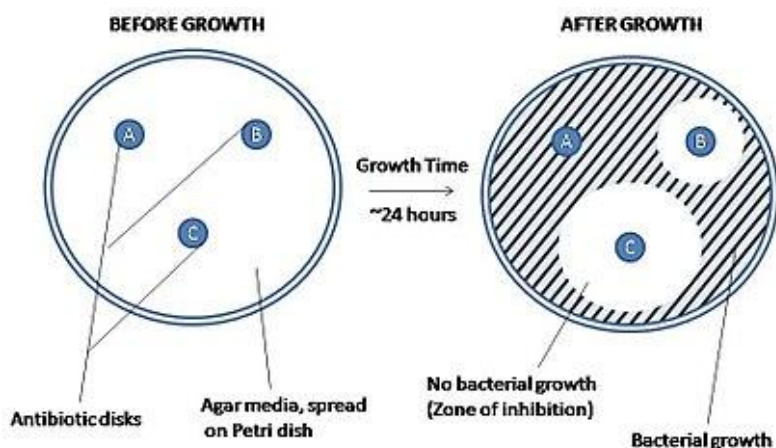


Figure 2.28.

Among compounds isolated from *C. avellana* green leafy covers, the most active compounds were **29** and **31**. In particular, carpinontriol B (**29**) proved efficacy at

10 µg/disk (tables 2.8 and 2.9), with the exception of *S. aureus*, in respect of which 40 µg/disk were needed to obtain an inhibition halo (tables 2.8 and 2.9). At 40 µg/disk both compounds caused the formation of zones of inhibition completely comparable to those obtained with tetracycline at 7 µg/disk used as positive control (table 2.8). Giffonin T (**30**) showed weaker antimicrobial activity, and only against *B. cereus* (4313), *P. aeruginosa*, and *S. aureus*, at 40 µg/disk (table 2.9).

Table 2.8. Antimicrobial Activity of compounds **29-31** and **20** and MeOH extract of leafy covers of *C. avellana* cv. Tonda di Giffoni.

	10 µg/disk					20 µg/disk					40 µg/disk				
	EC	BC 4384	BC 4313	PA	SA	EC	BC 4384	BC 4313	PA	SA	EC	BC 4384	BC 4313	PA	SA
20	3 (0) ^c	5(0) ^c	2.33 (0.57) ^c	0(0) ^c	5 (0) ^c	4.33 (0.57)	5 (0) ^c	3.33 (0.57) ^c	0(0) ^c	6.67 ^a (0.57)	8.66 (0.57)	9.67 (0.57)	5.33 (0.57)	9.67 (0.57)	10.67 (0.57) ^b
29	9.33 (0.57) ^b	5(0) ^c	5(0) ^c	4.67 (0.57)	0(0) ^c	9.67 (0) ^b	5 (0) ^c	5(0) ^c	4.67 ^c (0.57)	0 (0) ^c	11.67 (1.15)	10.66 (0.57)	10.66 ^a (0.57)	10.67 ^a (0.57)	5.67 (0.57)
30	0(0) ^c	0(0) ^c	0(0) ^c	0(0) ^c	0(0) ^c	0(0) ^c	0(0) ^c	0(0) ^c	0(0) ^c	0(0) ^c	0(0) ^c	0(0) ^c	5 (0) ^c	9 (0) ^c	11.3 (0.57)
31	4.67 (0.57) ^c	5.67 (0.57) ^c	5.67 (0.57) ^c	5 (0) ^c	6.33 (0.57)	10(0) ^b	9.67 (0.57)	9.67 (0.57) ^a	8.67 ^b (0.57)	10 ^b (0)	10.33 (0.57)	11.33 (0.57)	10.67 ^a (0.57)	10 (0) ^a	10.67 (0.57)
MeOH	0(0) ^c	0(0) ^c	0(0) ^c	0(0) ^c	0(0) ^c	0(0) ^c	0(0) ^c	0(0) ^c	0(0) ^c	0(0) ^c	0(0) ^c	0(0) ^c	0(0) ^c	5.67 (0.57)	10 (0) ^b (0.57)
	EC	BC 4384	BC 4313	PA	SA										
DMSO	0(0) ^c	0(0) ^c	0(0) ^c	0(0) ^c	0(0) ^c										
Tetracycline (7 µg/disk)	12.67 (1.15) ^a	8.67 (0.57) ^a	10.33 (0.57) ^a	9.67 (1.67) ^a	11.33 (0.57) ^a										

Data are expressed in mm. Results are shown as the mean \pm SD (n = 3). Means followed by different letters in each column differ significantly to Dunnett's multiple comparisons test, at the significance level of $p < 0.05$. EC: *Escherichia coli*; BC 4384: *Bacillus cereus* DSM 4384; BC 4313: *Bacillus cereus* 4313; PA: *Pseudomonas aeruginosa*; SA: *Staphylococcus aureus*. Tetracycline (7 µg/disk) and DMSO were used as positive and negative control, respectively. ^c: $p < 0.0001$; ^d: $p < 0.001$; ^e: $p < 0.001$; ^b: $p < 0.005$; ^a: $p < 0.05$.

Table 2.9. Antimicrobial Activity of compounds **9**, **17**, **19**, and **32-35** at 40 µg/disk.

	EC	BC 4384	BC 4313	PA	SA
9	10 (0) ^b	0(0) ^e	5 (0) ^e	4.67 ^e	10 (0) ^b
17	9.67 ^a (0.57)	0(0) ^e	0(0) ^e	5 (0) ^e	6.33 (0.57) ^d
19	10(0) ^b	5(0) ^e	0(0) ^e	4(0) ^e	10.33 (0.57) ^b
32	10.67 (0.57) ^b	0(0) ^e	10 (0)	9.33 ^a	10.67 (0.57) ^b
33	10(0) ^b	0(0) ^e	5.67 ^e	0(0) ^e	10.67 (0.57) ^b
34	11.33 (0.57) ^a	0(0) ^e	0(0) ^e	6.67 ^e	11.33 (0.57) ^a
35	8.33 (0.57) ^c	0(0) ^e	0(0) ^e	0(0) ^e	6.67 (0.57) ^d

Data are expressed in mm. Results are shown as the mean \pm SD (n = 3). Means followed by different letters in each column differ significantly to Dunnett's multiple comparisons test, at the significance level of $p < 0.05$. EC: *Escherichia coli*; BC 4384: *Bacillus cereus* DSM 4384; BC 4313: *Bacillus cereus* 4313; PA: *Pseudomonas aeruginosa*; SA: *Staphylococcus aureus*. Tetracycline (7 µg/disk) and DMSO were used as positive and negative control, respectively. ^e: $p < 0.0001$; ^d: $p < 0.001$; ^c: $p < 0.001$; ^b: $p < 0.005$; ^a: $p < 0.05$.

The different behaviour of compounds **29-31** was confirmed by evaluation of the minimal inhibitory concentration (MIC) (table 2.10), which evidenced a stronger activity of carpinontriol B (**29**) and giffonin U (**31**) on almost all strains tested (except against *S. aureus*). Giffonin I (**9**) was effective against almost all the tested strains at 40 µg/disk. The antimicrobial activity shown by the kaempferol derivatives **19** and **20** as well as by myricetin 3-*O*- α -L-rhamnopyranoside (**17**) was in agreement with those reported by Cushnie and Lamb³². The antimicrobial activity of citric acid (**32**), 1-methyl citrate (**33**), and trimethyl citrate (**34**) confirmed the capability of this class of compounds to inhibit the growth of microorganisms such as *E.coli*³³.

Table 2.10. Minimal Inhibitory Concentration (MIC, $\mu\text{g}/\text{disk}$) of compounds **29-31** and of MeOH extract of leafy covers of *C. avellana* cv. Tonda di Giffoni.

Microorganism	29	30	31	MeOH extract
<i>Bacillus cereus</i> 4313	4 μg	30 μg	5 μg	50 μg
<i>Bacillus cereus</i> 4384	4 μg	50 μg	5 μg	50 μg
<i>Escherichia coli</i>	10 μg	50 μg	10 μg	100 μg
<i>Pseudomonas aeruginosa</i>	10 μg	30 μg	10 μg	30 μg
<i>Staphylococcus aureus</i>	30 μg	30 μg	30 μg	30 μg

2.3. LC-MS profiling highlights Hazelnut (cultivar Tonda di Giffoni PGI) shells as a byproduct rich in antioxidant phenolics.

C. avellana shells



Hazelnut shells represent more than 50% of the total nut weight. They are composed of about 30% hemicelluloses, 27% celluloses and 43% lignin, so they are mainly utilized as a low-value heat source.

The hazelnut shells represent one of the major byproducts (about 42% of the total biomass) producing a big amount of waste material available at very low cost. Actually, hazelnut shells are mostly used as heating source upon burning and for the mulch.

In order to achieve deeper insight into the chemical composition of the shell of *C. avellana* cv. Tonda di Giffoni and to highlight the occurrence of biologically active compounds, a phytochemical investigation was carried out.

2.3.1 Results and discussion

Qualitative analysis of MeOH extract of C. avellana, cv. Tonda di Giffoni shells.

To determine the total phenol content of the MeOH extract of *C. avellana* shells, the Folin-Ciocalteu method was carried out. The phenolic content was 340.44 µg/mg extract and expressed as gallic acid equivalent. Moreover, a significant concentration-dependent free-radical scavenging activity evaluated by DPPH ($EC_{50} = 54.30$ µg/mL) and by TEAC assay (TEAC value = 1.42 mg/ml) correlated to the high phenolic content, as already suggested by Shahidi¹.

To correlate the phenolic content to the chemical composition of the MeOH extract, a preliminary plant metabolite profiling was performed by LC-ESI/LTQOrbitrap/MS/MSⁿ analysis, in negative ionization mode. LC-

ESI/LTQOrbitrap/MS/MSⁿ analysis using the “data dependent scan” mode in which the MS software selects precursor ions corresponding to the most intense peaks in LC-MS spectrum, were carried out. A careful analysis of the multistage mass spectra of the main peaks suggested the presence of sixteen phenolic compounds (fig. 2.29), corresponding to phenylpropanoids (**36-38**), neolignans (**39-45** and **47**) characterized by two phenylpropanoid units linked by a bond other than a β,β' -bond, flavonoid glycosides (**20** and **24**), and diarylheptanoid derivatives (**16**, **29** and **46**).

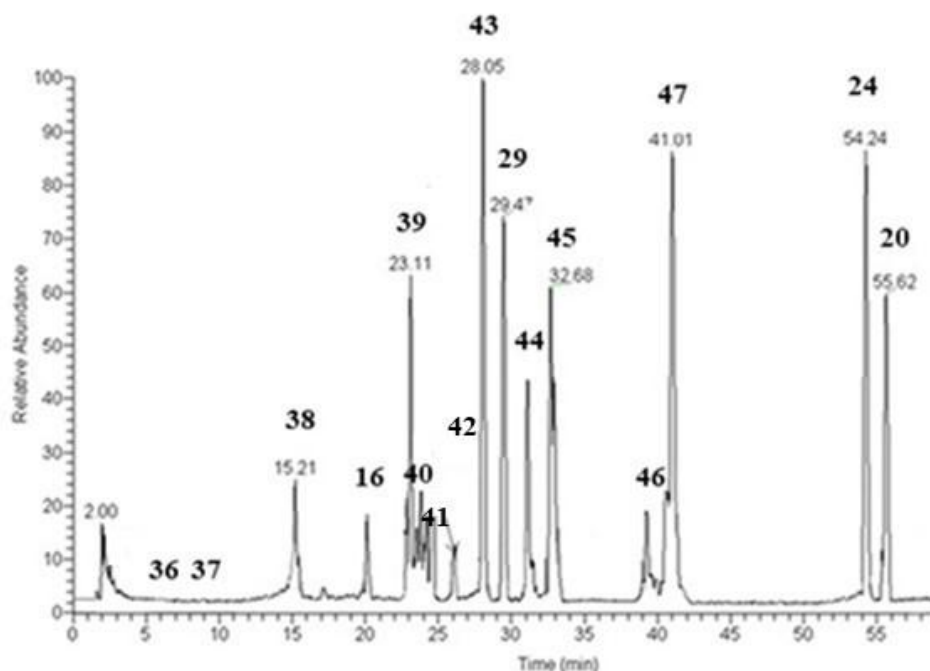


Figure 2.29. LC-ESI/LTQOrbitrap/MS profile (negative ion mode) of the MeOH extract of *C. avellana* shells has led to the isolation of sixteen compounds: 2,3-dihydroxy-1-(4-hydroxy-3-methoxyphenyl)-propan-1-one (**36**), 1-(4-hydroxy-3-methoxy)-1,2,3-propanetriol (**37**), threo-1,2-bis(4-hydroxy-3-methoxyphenyl)-1,3-propanediol (**38**), giffonin P (**16**), erythro-(7*S*,8*R*)-guaiacylglycerol- β -*O*-4'-dihydroconiferyl alcohol (**39**), ficusal (**40**), erythro-(7*R*,8*S*)-guaiacylglycerol- β -*O*-4'-dihydroconiferyl alcohol (**41**), *ent*-cedrusin (**42**), erythro-(7*S*,8*R*)-guaiacylglycerol- β -coniferyl aldehyde ether (**43**), carpinontriol B (**29**), ceplignan (**44**), dihydrodehydrodiconiferyl alcohol (**45**), giffonin V (**46**), balanophonin (**47**), kaempferol 3-*O*-(4''-cis-*p*-coumaroyl)- α -L-rhamnopyranoside (**24**), kaempferol 3-*O*-(4''-trans-*p*-coumaroyl)- α -L-rhamnopyranoside (**20**).

Compounds **39** and **41** in High Resolution Mass Spectrometry showed a pseudomolecular ion at m/z 377, that submitted to fragmentation gave a principal daughter ion at m/z 329 amu due to the loss of two methyl groups and a water

molecule; similarly, compounds **40**, **45** and **47** were characterized by [(M-30)-H]⁻ fragment ions at *m/z* 299, 329, 325 amu, respectively.

The formic acid adduct of compound **43** showed in the LC-ESI/LTQOrbitrap/MS/MSⁿ spectrum a principal precursor [(M⁺ HCOOH) H]⁻ ion at *m/z* 419 amu, whose fragmentation pattern was highly informative about the presence of a neolignan moiety; in the tandem LC-MS experiments a peak at *m/z* 195 amu originated by neutral loss of 224 amu attributed to the cleavage of the β O-linkage and the contemporary loss of a molecule of water leading to a deprotonated 1-(4-hydroxy-3-methoxy)-prop-2-ene-1,2diol was evident.

Compounds **29** and **46** were characterized by the same fragmentation pattern, very similar to that already described for alnusone. Infact the main peaks at *m/z* 269 and 253 respectively, were typical fragmentation of diarylheptanoids compounds due to the neutral moiety loss of 74 amu, this was explained by the rearrangement of the deprotonated compound and the subsequent opening of the diarylhepatonid cycle by the cleavage of the linkage between carbons 7 and 8. A subsequent cleavage of the linkage between carbons 10 and 11 originated a very intense [(M-74)-H]⁻ fragment ion ascribable to the neutral loss of an hydroxy-propan-2-one unit; for this reason these compounds were tentatively identified as diarylheptanoids.

Finally, compounds **24** and **20** showed both a pseudomolecular ion [M-H]⁻ at *m/z* 577 and submitted to fragmentation gave the same fragment ion at *m/z* 285 ascribable to the loss of a deoxyhexose and a p-coumaroyl units.

Some of the main peaks were tentatively attributed according to the accurate masses, characteristic fragmentation patterns, and retention times and “KNAPsAcK” database. MS information does not allow to discriminate among structural isomers or stereoisomers. Thus it is worthwhile to establish the truly chemical structure of naturally occurring molecules. Moreover, with the aim to quantify pure compounds occurring in the hazelnut shells and also evaluate their

activity, the phytochemical investigation of the hazelnut shell extract was carried out. Compounds **16**, **20**, **24**, **29** and **36-47** were isolated by size exclusion chromatography (SEC) of the MeOH extract, followed by further purification steps by reversed-phase HPLC-RI and their structures were unambiguously elucidated by NMR experiments and Circular Dichroism (CD) spectra, with ESI-MS and high resolution ESI-MS analysis.

The molecular formula of compound **46** was established as C₁₉H₂₀O₅ by ESI/LTQORBITRAP/MS (*m/z* 327.1232 [M-H]⁻, calcd for C₁₉H₁₉O₅, 327.1227) and the ¹³C NMR data. The IR spectrum showed bands at 3440, 2935, 1715 cm⁻¹, the latter suggesting the presence of a ketocarbonyl group³⁴. The ¹H and ¹³C NMR spectra of **46** showed signals ascribable to a diarylheptanoid moiety. In particular, the ¹H NMR spectrum (fig. 2.30 and table 2.11) showed signals attributable to two aromatic rings as ABX systems, at δ 7.10 (dd, *J* = 8.2, 1.8 Hz), 7.07 (dd, *J* = 8.2, 1.8 Hz), 6.84 (d, *J* = 8.2 Hz), 6.83 (d, *J* = 1.8 Hz), 6.81 (d, *J* = 8.2 Hz), and 6.49 (d, *J* = 1.8 Hz), as well as to two protons linked to oxymethine carbons at δ 3.84 (bs) and 3.82 (m).

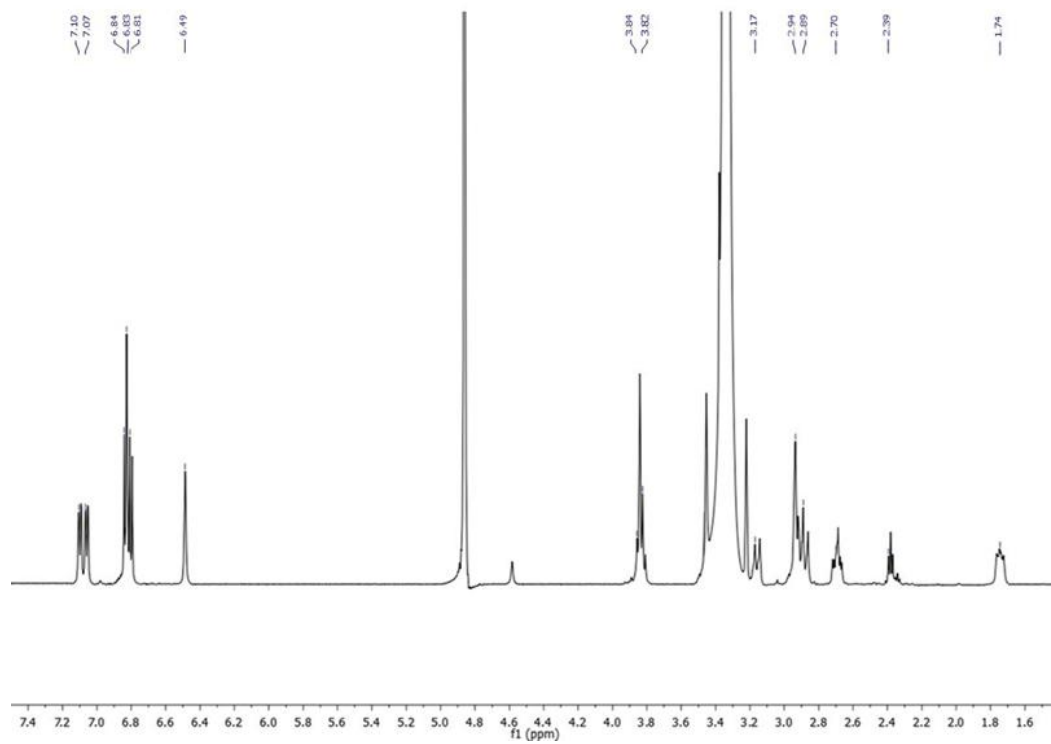


Figure 2.30. ^1H NMR spectrum (600 MHz, CD_3OD) of giffonin V (**46**).

Table 2.11. ^1H NMR and ^{13}C NMR data of compound **46** (CD_3OD).

46		
	δ_{C}	δ_{H} (<i>J</i> in Hz)
1	127.2	-
2	127.1	-
3	151.8	-
4	116.2	6.81 d (8.2)
5	130.6	7.07 dd (8.2, 1.8)
6	130.8	-
7	27.7	2.94 m
8	31.6	2.70, 1.74, m
9	69.1	3.82, m
10	82.5	3.84, bs
11	214.4	-
12	34.2	2.39 t (7.4)
13	24.6	3.17 dd (16.0, 7.4), 2.89 dd (16.0, 7.4)
14	131.2	-
15	129.1	7.10 dd (8.2, 1.8)
16	116.3	6.84 d (8.2)
17	151.0	-
18	135.3	6.49 d (1.8)
19	134.0	6.83 d (1.8)

A detailed analysis of 2D-NMR experiments (HSQC, HMBC and COSY) led to assign the two hydroxy groups to C-9 (δ 69.1) and C-10 (δ 82.5) of the heptanoid chain. The position of the keto group was assigned to C-11 by HMBC (fig 2.32) correlations between the proton signals of H-9 (δ 3.82) and H-13 (δ 2.89), with the carbon resonance at δ 214.4. The coupling constant between H-9 and H-10 was not observed, probably due to the gauche dihedral angle.

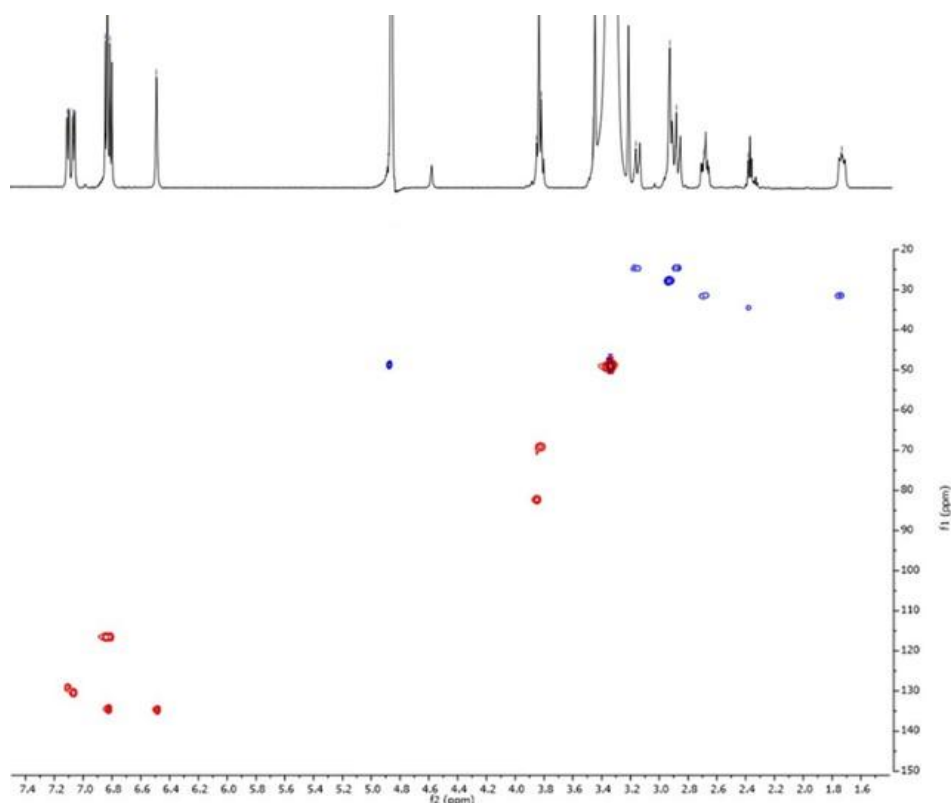


Figure 2.31. HSQC spectrum (CD_3OD) of giffonin V (**46**).

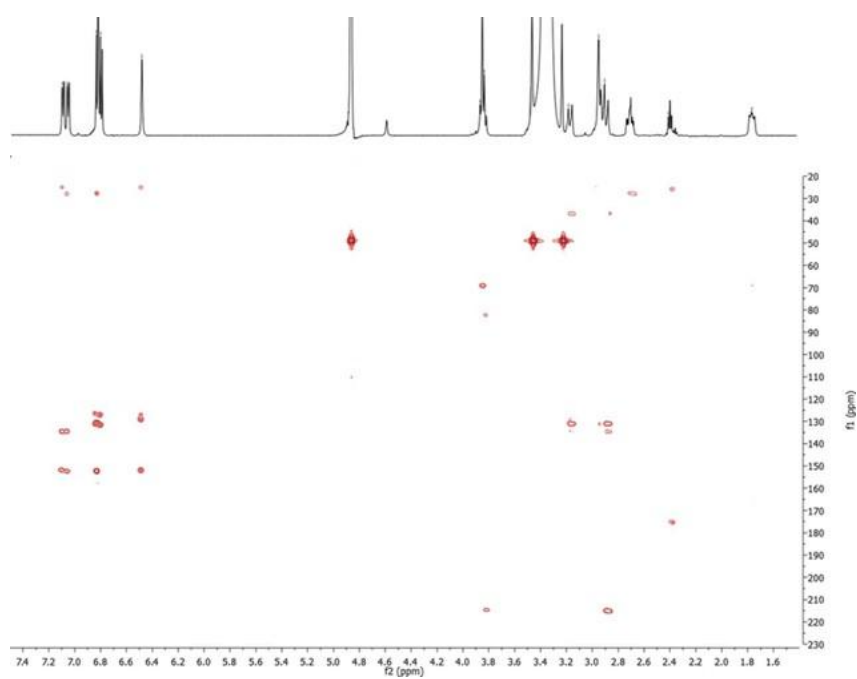


Figure 2.32. HMBC spectrum (CD_3OD) of giffonin V (**46**).

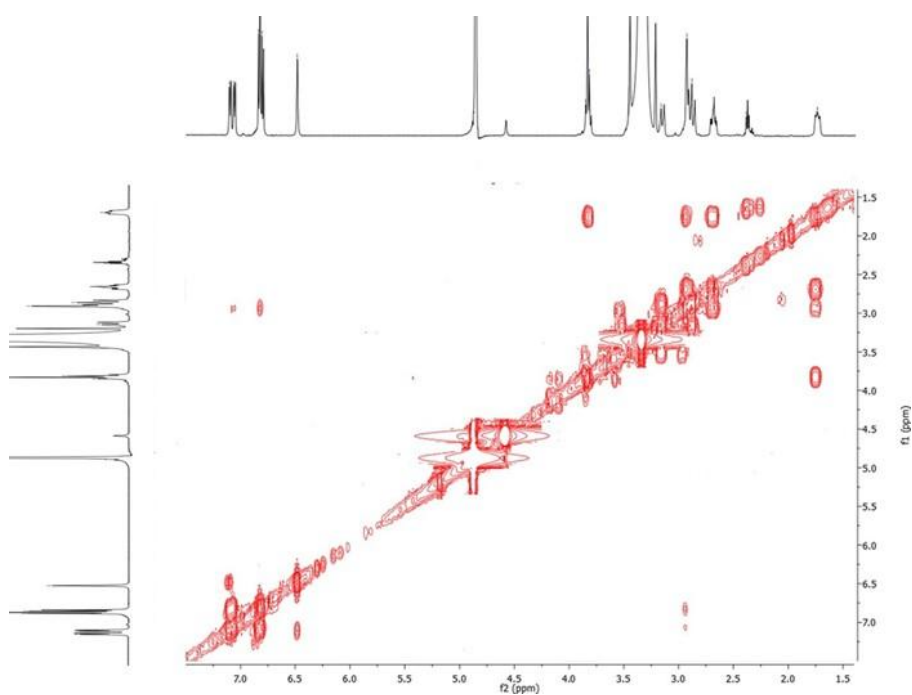


Figure 2.33. COSY spectrum (CD_3OD) of giffonin V (**46**).

To determine the relative configuration of giffonin V, ROESY experiment has been carried out. In particular ROESY spectra (fig. 2.34) highlighted the correlations between the proton signals H-10 (δ 3.84) and H-9 (δ 3.82) with the proton signals H-18 (δ 6.49), H-19 (δ 6.83), and H₂-8 (δ 2.70 and 1.74); These results indicated that the two hydroxy groups at C-9 and C-10 were located in the same orientation.

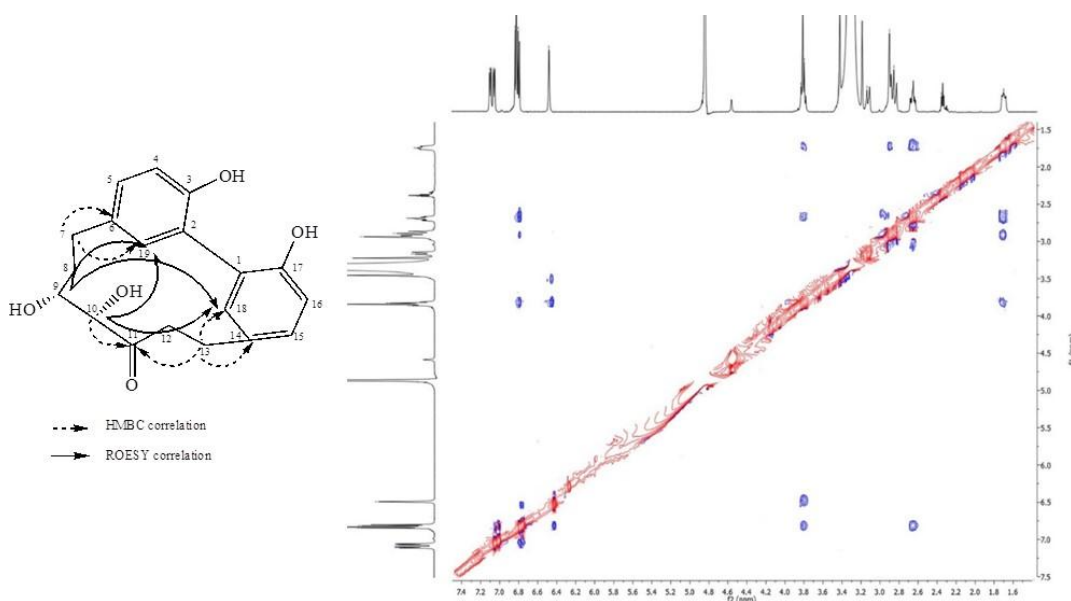


Figure 2.34. ROESY spectrum (CD₃OD) of giffonin V (**46**).

Thus, the structure of **46** was assigned as shown in figure 2.35, and named giffonin V (fig. 2.34).

Compounds **40**, **42**, **44**, **45**, and **47** have been established as dihydrobenzofuran neolignans according to 1D and 2D-NMR experiments. Since isomers are of widespread interest in chemistry and biochemistry, because can possess different biological activities, the truly chemical structure of compounds **40**, **42**, **44**, **45**, and **47** was assessed by NMR experiments along with CD analysis. The C-7/C-8 relative configuration of dihydrobenzofuran neolignans was assigned on the basis of the literature data, reporting a *trans* configuration with the coupling constant

between H-7/H-8 of 6.6 Hz, and a *cis* configuration with the coupling constant between H-7/H-8 of 8.4 Hz³⁵. In detail, for compounds **40**, **42**, **44**, **45**, and **47**, the coupling constant of 6.1 Hz between H-7 and H-8 suggested the C-7/C-8 *trans* relative configuration. Therefore, the isolated compounds have been established as ficusal³⁶ (**40**), *ent*-cedrusin³⁷ (**42**), ceplignan³⁸ (**44**), dihydrodehydrodiconiferyl alcohol³⁹ (**45**) and balanophonin⁴⁰ (**47**). To establish the absolute configuration, CD experiments have been carried out. Literature data reported in the CD spectrum a negative Cotton effect at 282 nm for the *7R,8S* configuration while a positive Cotton effect at 282 nm for the *7S,8R* configuration⁴¹. On the basis of these observation, the positive Cotton effect at 283 nm for compound **44** allowed us to establish a *7S,8R* configuration while a negative Cotton effect at 283 nm for compounds **40**, **42**, **45** and **47** permitted us to assign a *7R,8S* configuration.

The remaining isolated compounds were identified by analysis of their NMR spectroscopic data in comparison to those reported in literature as 2,3-dihydroxy-1-(4-hydroxy-3-methoxyphenyl)-propan-1-one⁴² (**36**), 1-(4-hydroxy-3-methoxy)-1,2,3-propanetriol⁴³ (**37**), threo-1,2-bis(4-hydroxy-3-methoxyphenyl)-1,3-propandiol⁴⁴ (**38**), giffonin P (**16**), erythro-(*7S,8R*)-guaiacylglycerol- β -*O*-4'-dihydroconiferyl alcohol⁴⁵ (**39**) and erythro-(*7R,8S*)-guaiacylglycerol- β -*O*-4'-dihydroconiferyl alcohol⁴⁵ (**41**), erythro-(*7S,8R*)-guaiacylglycerol- β -coniferyl aldehyde ether⁴⁶ (**43**), carpinontriol B¹⁸ (**29**), kaempferol 3-*O*-(4''-*cis-p*-coumaroyl)- α -L-rhamnopyranoside (**24**), kaempferol 3-*O*-(4''-*trans-p*-coumaroyl)- α -L-rhamnopyranoside (**20**) (fig 2.35).

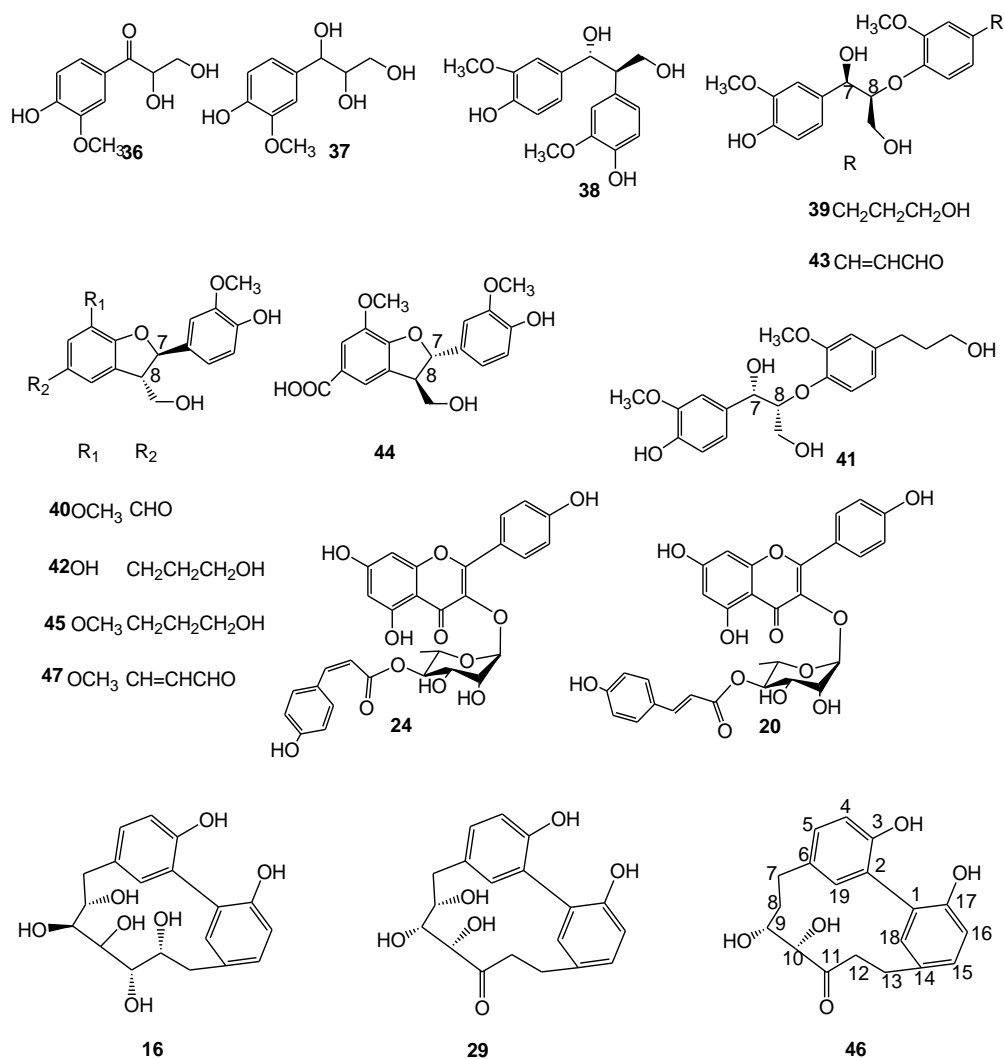


Figure 2.35. Compounds isolated from *C. avellana* shells.

Quantitative analysis of the MeOH extract of C. avellana, cv. Tonda di Giffoni shells.

The main compounds occurring in the MeOH extract of *C. avellana* shells, erythro-(7*S*,8*R*)-guaiacylglycerol- β -*O*-4'-dihydroconiferyl alcohol (**39**), ficusal (**40**), erythro-(7*R*,8*S*)-guaiacylglycerol- β -*O*-4'-dihydroconiferyl alcohol (**41**), erythro-(7*S*,8*R*)-guaiacylglycerol- β -coniferyl aldehyde ether (**43**), carpinontriol B

(**29**), dihydrodehydrodiconiferyl alcohol (**45**), giffonin V (**46**), balanophonin (**47**), kaempferol 3-*O*-(4''-cis-*p*-coumaroyl)- α -L-rhamnopyranoside (**24**) and kaempferol 3-*O*-(4''-trans-*p*-coumaroyl)- α -L-rhamnopyranoside (**20**), were quantified by LC-ESI/QqQ/MS/MS using a very accurate and sensitive tandem mass spectrometric technique such as MRM. Compounds **16**, **36-38**, **42** and **44** were not quantified, since their amount in the MeOH extract of *C. avellana* shells was found below the LOQ of the applied method.

On the basis of the transitions selected for MRM experiments, the amount (mg/100 g dry weight) of each compound in the MeOH extract of *C. avellana* shells was determined (tables 2.12 and 2.13).

The quantitative results highlight that indicated compounds occurred in the extract in concentration ranging from 6.4 to 83.3 (mg/100 g), with erythro-(7*S*-8*R*)-guaiacylglycerol- β -*O*-4'-dihydroconiferyl- alcohol (**39**) exhibiting the highest and kaempferol 3-*O*-(4''-trans-*p*-coumaroyl)- α -L-rhamnopyranoside (**20**) the lowest concentrations, respectively. The new compound giffonin V (**46**) occurred in concentration of 24.8 mg/100 g of *C. avellana* shells MeOH extract (table 1.13).

Table 2.12. Retention times (R_t), molecular formula, $[M-H]^-$, $[M+HCOOH]^-$, Δ ppm, characteristic product ions (m/z), amount (mg/100g dry weight) of compounds occurring in the MeOH extract of *C. avellana* shells quantified by LC-ESI/QqQ/MS/MS and identified by LC-ESI/LTQOrbitrap/MS/MS^a.

n°	Compound	R_t (min)	Molecular Formula	$[M-H]^-$	$[M+HCOOH]^-$	Δ ppm	Characteristic product ions (m/z)
36	2,3-dihydroxy-1-(4-hydroxy-3-methoxyphenyl)propan-1-one	5.68	C ₁₁ H ₁₄ O ₇		257.0661	1.99	-
37	1-(4-hydroxy-3-methoxy)-1,2,3-propanetriol	7.49	C ₁₁ H ₁₄ O ₇		257.0662	2.37	-
38	threo-1,2-bis(4-hydroxy-3-methoxyphenyl)-1,3-propandiol	15.22	C ₁₇ H ₂₀ O ₆	319.1180	365.1232	1.12	271
16	giffonin P	20.12	C ₁₉ H ₂₂ O ₇	361.1283		0.31	241, 271, 301, 343
39	erythro-(7 <i>S</i> ,8 <i>R</i>)-guaiacylglycerol- β - <i>O</i> -4'-dihydroconiferyl alcohol	23.10	C ₂₀ H ₂₆ O ₇	377.1595		0.08	329, 195, 165
40	ficusal	23.84	C ₁₈ H ₁₈ O ₆	329.1025		1.57	269, 209, 239, 167, 299
41	erythro-(7 <i>R</i> ,8 <i>S</i>)-guaiacylglycerol- β - <i>O</i> -4'-dihydroconiferyl alcohol	24.51	C ₂₀ H ₂₆ O ₇	377.1594		-0.16	329, 195, 165
42	<i>ent</i> -cedrusin	25.51	C ₁₉ H ₂₂ O ₆	345.1350	391.1337	1.37	327, 315
43	erythro-(7 <i>S</i> ,8 <i>R</i>)-guaiacylglycerol- β -coniferyl aldehyde ether	27.27	C ₂₁ H ₂₄ O ₉	373.1284	419.1335	-0.43	373, 325, 177, 195
29	carpinontriol B	29.47	C ₁₉ H ₂₀ O ₆	343.1181		1.53	269, 283, 299, 313, 325
44	ceplignan	31.11	C ₁₈ H ₁₈ O ₇	345.0974	391.1025	1.48	193, 151, 315, 221
45	dihydrodehydrodiconiferyl alcohol	32.70	C ₁₉ H ₂₀ O ₆	359.1495	405.1546	1.49	135, 177, 329, 341
46	giffonin V	38.91	C ₁₉ H ₂₀ O ₅	327.1227		-0.06	253, 283, 241, 271
47	balanophonin	41.02	C ₂₀ H ₂₀ O ₆	355.1182		1.62	337, 281, 249, 325, 219

Chapter 2

24	kaempferol 3- <i>O</i> -(4"- cis- <i>p</i> -coumaroyl)- α - L-rhamnopyranoside	54.24	C ₃₀ H ₂₆ O ₁₂	577.1334	-1.13	431, 285
20	kaempferol 3- <i>O</i> -(4"- trans- <i>p</i> -coumaroyl)- α -L- rhamnopyranoside	55.61	C ₃₀ H ₂₆ O ₁₂	577.1335	- 1.03	431, 285

* Values mean of triplicates for each sample.

**Not detected (ND) compounds.

Table 2.13. Quantitative data of *C. avellana* shells extract (MRM, negative ion mode), MRM transitions, Limits of detection (LODs), limits of quantification (LOQs) in ng mL⁻¹ and amount (mg/100g shells ±SD) of compounds isolated by shells.

Compound name	MRM transition	R ²	Regression line	LOQ (ng mL ⁻¹)	LOD (ng mL ⁻¹)	mg/100g shells ±SD*
erythro-(7 <i>S</i> ,8 <i>R</i>)-guaiacylglycerol-β- <i>O</i> -4'-dihydroconiferyl- alcohol (39)	377→329	0.990	Y=0.331x+0.0467	18.0	3.5	83.3±1.8
ficusal (40)	329→299	0.996	Y=0.143x+0.0054	12.0	3.0	72.2±5.4
erythro-(7 <i>R</i> ,8 <i>S</i>)-guaiacylglycerol-β- <i>O</i> -4'-dihydroconiferyl- alcohol (41)	377→329	0.989	Y=0.107x 0.0010	18.0	3.5	55.3±5.2
erythro-(7 <i>S</i> ,8 <i>R</i>)-guaiacylglycerol-β-coniferyl aldehyde ether (43)	419→195	0.987	Y=1.53x+0.6100	18.0	3.0	33.2±1.0
carpinontriol B (29)	343→269	0.997	Y=0.206x+0.0074	15.0	2.5	22.3±1.4
dihydrodehydrodiconiferyl alcohol (45)	359→329	0.991	Y=0.209x+0.0122	12.0	3.0	57.3±8.7
giffonin V (46)	327→253	0.990	Y=0.142x-0.0004	15.0	3.0	24.8±3.0
balanophonin (47)	355→325	0.993	Y=1.06x+0.0823	15.0	2.5	11.8±1.6
kaempferol 3- <i>O</i> -(4"- <i>cis-p</i> -coumaroyl)-α- <i>L</i> -rhamnopyranoside (24)	577→285	0.981	Y=2.86x + 0.196	10.0	2.5	9.8±1.0
kaempferol 3- <i>O</i> -(4"- <i>trans-p</i> -coumaroyl)-α- <i>L</i> -rhamnopyranoside (20)	577→285	0.996	Y=1.93x +0.0251	10.0	2.5	6.4±1.4

Evaluation of antioxidant activity by TEAC assay.

The antioxidant activity of each compounds was tested by TEAC assay and expressed as TEAC value, defined as the concentration of Trolox solution with antioxidant potential equivalent to a 1 mM concentration of the test sample⁴⁷ (table 2.14), and compared to that of quercetin 3-*O*-β-*D*-glucopyranoside. The results showed that compounds **24** and **20** exhibited the higher free-radical-scavenging activity similar to that shown by quercetin 3-*O*-β-*D*-glucopyranoside suggesting that the presence of coumaroyl moiety improves the radical-

scavenging capacity. The other compounds showed a free-radical-scavenging activity in the range of 0.54-0.87 mM. In detail, diarylheptanoids (**16**, **29** and **46**), possessing similar chemical features characterized by the presence of two phenolic groups showed a weak radical-scavenging capacity as well as compound **38**. Lower antioxidant activity was observed for other compounds due to the presence of methoxy functions, even if compounds **40** and **43** contribute to the antioxidant activity of the extract due to their reasonable amount in the extract.

Table 2.14. Free radical scavenging activities of compounds isolated, and of the MeOH extract of *C. avellana* shells in the TEAC assay.

Compound	TEAC value (mM± SD)
16	0.86 ± 0.01
20	1.43± 0.01
24	1.39± 0.02
29	0.82± 0.07
36	0.79 ± 0.01
37	0.76 ± 0.01
38	0.87 ± 0.01
39	0.65 ± 0.01
40	0.51 ± 0.01
41	0.66 ± 0.01
42	0.82± 0.02
43	0.54± 0.01
44	0.65± 0.01
45	0.60± 0.02
46	0.85± 0.06
47	0.61± 0.01
Quercetin 3- <i>O</i> -β-D-glucopyranoside	1.54 ± 0.01
	TEAC value (mg/mL ± SD)
MeOH extract	1.42 ± 0.02

2.3.2. Biological assay

Cytotoxicity activity of the MeOH extract of C. avellana shells and of compounds isolated.

Some neolignans are reported as promising chemopreventive compounds able to reverse, inhibit or prevent the development of cancer and to affect molecular events implicated in inflammation; the cytotoxic activity of the MeOH extract of *C. avellana* shells and of compounds isolated was tested against two cancer cell lines including A549 (human lung adenocarcinoma) and HeLa cells (human epitheloid cervix carcinoma). The MeOH extract (at 500 µg/mL and 250 µg/mL) and the tested compounds, in a range of concentrations between 12.5 and 100 µM, did not cause a significant reduction of the cell number (data not shown). The cytotoxic activity of MeOH extract and of compounds isolated was also tested against a human normal cell line, HaCat cells (human normal skin keratinocyte). The results showed the absence of a significant cytotoxicity at tested concentration.

2.4. Conclusion

This investigation afforded six new diarylheptanoids, in particular cyclic diaryletherheptanoids giffonins Q-S isolated by male flowers, and cyclic diarylheptanoids giffonins T-U isolated by green leafy covers and giffonin V isolated by shells. The absence of cytotoxicity evaluated on the selected human cancer cell lines and also on human normal cell line (HaCat) along with the antioxidant activity exerted by giffonins and flavonoids show the potential benefits of *C. avellana* byproducts as a rich source of phenolic compounds with antioxidant activity and highlight as, in addition to hazelnuts “Tonda di Giffoni”,

also other no eatable parts could represent interesting source of phytochemicals with health benefits.

2.5. Experimental section

Plant material

C. avellana L. shells and green leafy covers, cv. Tonda di Giffoni were collected at Giffoni, Salerno, Italy in August 2014, while the male flowers were collected in January 2015; they have been identified by V. De Feo (Department of Pharmacy, University of Salerno, Italy). A voucher specimen has been deposited in this Department.

Qualitative analysis

Qualitative LC-MS was performed using a Thermo Scientific Accela HPLC system (Thermo Scientific, Germany) equipped with a C₁₈ reversed-phase (RP) column at a flow rate of 0.2 µl/min and coupled to a LTQ-Orbitrap XL mass spectrometer. Linear gradient elution was carried out by using water with 0.1% formic acid as eluent A and acetonitrile as B.

The instrument was calibrated using the manufacturer's calibration standards. The scan was collected in the Orbitrap at a resolution of 30 000 in a m/z range of 200–1500 amu. The m/z of each identified compound was calculated to 4 decimal places and measured with a mass accuracy < 2ppm. The source voltage was -4.0 kV and capillary voltage -35 kV, the tube lens offset -126 V and the capillary temperature was set at 280 °C, the auxiliary gas was set at 20 (arbitrary units) and the sheath gas at 10 (arbitrary units). In full LC-ESIMS experiments Total Ion Current (TIC) profile was produced by monitoring the intensity of all the ions produced and acquired in every scan during the chromatographic run. In order to

get structural information, Data Dependent experiments were performed by acquiring MS² spectra of the most intense ions produced during the acquisition.

- LC-ESI/LTQOrbitrap/MS/MSⁿ gradient for *MeOH extract of flowers and green leafy covers*. X-Terra MS C18 5 μ m:(2.1 x 250 mm;; Waters, Milford, MA) was used for *HPLC-ESI-Orbitrap MS*. The HPLC gradient started at 5% (B) hold for 5 min and after 45 min, %B was at 100% holding it for 5 min before returning back to the starting percentage.

- LC-ESI/LTQOrbitrap/MS/MSⁿ gradient for *MeOH extract of shells*. Atlantis T3 5 μ m RP C18 column (150mmx2.1mm i.d.) was used for LC-ESI/LTQOrbitrap/MS/MSⁿ. The HPLC gradient started at 5% (B) hold for 5 min and after 6 min, %B was at 15%, after 60 min % (B) at 50 %, after 10 min at 100% holding it for 8 min before returning back to the starting percentage.

Extraction and isolation procedures

Extraction and isolation of the MeOH extract of cv. Tonda di Giffoni flowers

The male flowers of *C. avellana*, cv. Tonda di Giffoni (1.125 Kg), were dried and extracted at room temperature using solvents of increasing polarity such as petroleum ether (4.4 L for 3 days, three times), CHCl₃ (4.5 L for 3 days, three times), and MeOH (2.9 L for 3 days, three times). After filtration and evaporation of the solvent to dryness in vacuo, 30 g of crude MeOH extract were obtained. The metanolic extract was dried under vacuum and subjected to n-butanol–water repartition to remove free sugars. The final butanolic fraction was dried under vacuum and 3 g were fractionated on a Sephadex LH-20 (Pharmacia) column (100 x 5 cm), using MeOH as mobile phase, affording 49 fractions (8 mL), monitored by TLC. Fractions 14-16 (14.1 mg) were chromatographed by semipreparative HPLC using MeOH-H₂O (2:3) as mobile phase (flow rate 2.5 mL/min) to yield compounds **26** (1.2 mg, t_R = 40.0 min), **27** (1.0 mg, t_R = 59.5 min) and **28** (1.1 mg,

$t_R = 66.0$ min). Fractions 17-19 (21.4 mg) were chromatographed by semipreparative HPLC using MeOH-H₂O (2:3) as mobile phase (flow rate 2.5 mL/min) to yield compounds **9** (1.2 mg, $t_R = 34.0$ min) and **22** (8.0 mg, $t_R = 24.0$ min). Fractions 20-24 (42.5 mg) were chromatographed by semipreparative HPLC using MeOH-H₂O (2:3) as mobile phase (flow rate 2.5 mL/min) to yield compounds **25** (10.1 mg, $t_R = 35.8$ min) and **21** (7.8 mg, $t_R = 14.3$ min). Fraction 28, 32 and 35 corresponded to compounds **19** (2.3 mg), **18** (2.7 mg), and **23** (2.1 mg), respectively. Fractions 39-43 were chromatographed by semipreparative HPLC using MeOH-H₂O (2:3) as mobile phase (flow rate 2.5 mL/min) to yield compounds **24** (11.0 mg, $t_R = 34.6$ min) and **20** (4.8 mg, $t_R = 35.4$ min).

Giffonin Q (26): Amorphous white solid; C₁₉H₁₈O₃; IR $\nu_{\text{max}}^{\text{KBr}}$ cm⁻¹: 3440, 2935, 1715, 1660; ¹H and ¹³C NMR (MeOH-*d*₄, 600 MHz) data, see table 2.1; ESI/LTQORBITRAP/MS m/z 293.1182 [M-H]⁻ (calcd for C₁₉H₁₇O₃, 293.1178).

Giffonin R (27): Amorphous white solid; C₁₉H₁₆O₃; IR $\nu_{\text{max}}^{\text{KBr}}$ cm⁻¹: 3440, 2940, 1725, 1665; ¹H and ¹³C NMR (MeOH-*d*₄, 600 MHz) data, see table 2.1; ESI/LTQORBITRAP/MS m/z 291.1026 [M-H]⁻ (calcd for C₁₉H₁₅O₃, 291.1021).

Giffonin S (28): Amorphous white solid; C₂₀H₁₈O₄; IR $\nu_{\text{max}}^{\text{KBr}}$ cm⁻¹: 3445, 2935, 1720, 1665; ¹H and ¹³C NMR (MeOH-*d*₄, 600 MHz) data, see table 2.1; ESI/LTQORBITRAP/MS m/z 321.1130 [M-H]⁻ (calcd for C₂₀H₁₇O₄, 321.1127).

Extraction and isolation of the MeOH extract of C. avellana, cv. Tonda di Giffoni green leafy covers

The green leafy covers of *C. avellana* L., cv. Tonda di Giffoni (535 g) were dried and extracted with *n*-hexane (2 x 4.4 L, 3 days each), CHCl₃ (2 x 4.6 L, 3 days each), and MeOH (3 x 4.6 L, 3 days each), to obtain 23.8 g of crude MeOH extract. The dried MeOH extract (3 g) was fractionated on a Sephadex LH-20 (Pharmacia) column (100 x 5 cm), using MeOH as mobile phase to afford 65

fractions (8 mL), monitored by TLC. Some of these fractions were further chromatographed by semipreparative HPLC using MeOH-H₂O (7:13) as mobile phase (flow rate 2.5 mL/min). Fractions 15-16 (37.0 mg) were purified by HPLC using MeOH-H₂O (9:11) to yield giffonin I (**9**) (32.5 mg, t_R = 16.2 min). Fractions 19-20 (23.9 mg) were purified by HPLC using MeOH-H₂O (7:13) to yield citric acid (**32**) (8.1 mg, t_R = 2.8 min), 1-methyl citrate (**33**) (2.5 mg, t_R = 4.0 min) and trimethyl citrate (**34**) (1.6 mg, t_R = 4.2 min). Fractions 41-44 (77.8 mg) were purified by HPLC using MeOH-H₂O (2:3) to obtain compounds **30** (1.3 mg, t_R = 6.4 min), **31** (5.1 mg, t_R = 9.8 min), carpinontriol B (**29**) (3.2 mg, t_R = 20.8 min), and kaempferol 3-*O*- α -L-rhamnopyranoside (**19**) (1.8 mg, t_R = 26.7 min). Fractions 47-48 (17.2 mg) were purified by HPLC using MeOH-H₂O (2:3) to obtain 3,5-dicaffeoylquinic acid (**35**) (1.6 mg, t_R = 8.0 min) and myricetin 3-*O*- α -L-rhamnopyranoside (**17**) (2.1 mg, t_R = 24.2 min). Fraction 55 (6.0 mg) corresponded to kaempferol 3-*O*-(4''-trans-*p*-coumaroyl)- α -L-rhamnopyranoside (**20**) (17.1 mg).

Giffonin T (**30**): amorphous white solid; $[\alpha]_D^{25}$ -6 (c 0.1 MeOH); IR (KBr) max 3425, 2930, 1713, 1665 cm⁻¹; ¹H and ¹³C NMR (MeOH-*d*₄, 600 MHz) data, table 2.5; ESI/LTQORBITRAP/MS [M-H]⁻ *m/z* 505.1717 (calcd for C₂₅H₂₉O₁₁, 505.1710).

Giffonin U (**31**): amorphous white solid; $[\alpha]_D^{25}$ -21 (c 0.1 MeOH); IR (KBr) max 3425, 2930, 1730, 1665 cm⁻¹; ¹H and ¹³C NMR (MeOH-*d*₄, 600 MHz) data, table 2.5; ESI/LTQORBITRAP/MS [M-H]⁻ *m/z* 359.1136 (calcd for C₁₉H₁₉O₇, 359.1131).

Compound 30' was obtained as an amorphous white solid after hydrolysis of **30** with 1 N HCl; $[\alpha]_D^{25}$ 0 (c 0.1 MeOH).

Extraction and isolation of the MeOH extract of C. avellana cv. Tonda di Giffoni shells

C. avellana L. shells, cv. Tonda di Giffoni (2.435 Kg), were dried and extracted with hexane and CHCl_3 at room temperature (6.4 L \times 3 days \times 2 times), and after with MeOH at room temperature (6.4 L for 3 days, three times).

The filtrate was concentrated under reduced pressure until elimination of MeOH to obtain 12.27 g crude extracts.

MeOH extract (3 g) was fractionated on a Sephadex LH-20 (Pharmacia) column (100 x 5 cm), using MeOH as mobile phase, affording 62 fractions (8 mL), monitored by Thin-layer chromatography (TLC). HPLC separations were carried out on a Waters 590 system equipped with a Waters R401 refractive index (RI) detector, a Waters XTerra Prep MSC18 column (300 x 7.8 mm i.d.), and a Rheodyne injector. by using mixtures of MeOH- H_2O in different percentages as mobile phase (flow rate 2.5 mL/min). Fractions 23-24 (447.7 mg) were purified using MeOH- H_2O (2:3) to yield compounds **39** (2.0 mg, $t_R = 15.2$ min) and **41** (1.3 mg, $t_R = 16.0$ min). Fractions 25-27 (441.9 mg) were purified using MeOH- H_2O (4:6) as mobile phase to yield compounds **37** (2.0 mg, $t_R = 2.3$ min), **38** (1.5 mg, $t_R = 6.4$ min), **43** (3.1 mg, $t_R = 20.8$ min) and **45** (14.8 mg, $t_R = 42.0$ min). Fraction 28 (131.3 mg) was chromatographed using MeOH- H_2O (4:6) to yield compound **42** (5.1 mg, $t_R = 15.6$ min). Fractions 30-32 (249.4 mg) were purified using MeOH- H_2O (2:3) as mobile phase to yield compound **36** (1.2 mg, $t_R = 4.5$ min). Fractions 35-42 (207.5 mg) were chromatographed by semipreparative HPLC using MeOH- H_2O (1:1) as mobile phase (flow rate 2.5 mL/min) to yield compounds **44** (2.1 mg, $t_R = 11.8$ min), **40** (3.5 mg, $t_R = 16.8$ min) and **47** (6.5 mg, $t_R = 23.5$ min). Fractions 43-44 (21.7 mg) were purified using MeOH- H_2O (2:3) to yield compound **16** (1.3 mg, $t_R = 12.0$ min). Fractions 52-53 (21.2 mg) were purified using MeOH- H_2O (1:1) to yield compounds **29** (6.5 mg, $t_R = 11.3$ min) and **46** (1.5 mg, $t_R = 25.8$ min). Fractions 55-60 were purified using MeOH- H_2O

(2:3) to yield compounds **24** (11.0 mg, $t_R = 34.6$ min) and **20** (4.8 mg, $t_R = 35.4$ min).

Giffonin V (**46**): amorphous white solid; (*c* 0.1 MeOH); IR (KBr) \max 3320, 2933, 1725, 1665 cm^{-1} ; ^1H and ^{13}C NMR (MeOH- d_4 , 600 MHz) data, table 2.11; ESI/LTQORBITRAP/MS $[\text{M-H}]^-$ m/z 329.1227 (calcd for $\text{C}_{19}\text{H}_{19}\text{O}_5$, 359.1222).

Computational Details of the compounds 29-31

Maestro 10.2³⁹ was used for generating the starting 3D chemical structures of all possible diastereoisomers of compounds **29**, **31**, and **9**. Calculations were not performed for compound **30**, since experimental data revealed that it differs from **29** only by the presence of a β -D-glucopyranosyl unit. Optimization of the 3D structures was performed with MacroModel 10.2³⁹ using the OPLS force field⁴⁰ and the Polak-Ribier conjugate gradient algorithm (PRCG, maximum derivative less than 0.001 kcal/mol).

In particular, for compound **29**, which has three stereogenic centers and an axis of chirality, eight possible diastereoisomers were considered:

- **29a** ($aR^*, 8S^*, 9R^*, 10R^*$), **29b** ($aS^*, 8S^*, 9R^*, 10R^*$),
- **29c** ($aR^*, 8S^*, 9R^*, 10S^*$), **29d** ($aS^*, 8S^*, 9R^*, 10S^*$),
- **29e** ($aR^*, 8S^*, 9S^*, 10R^*$), **29f** ($aS^*, 8S^*, 9S^*, 10R^*$),
- **29g** ($aR^*, 8S^*, 9S^*, 10S^*$), **29h** ($aS^*, 8S^*, 9S^*, 10S^*$);

For compound **31**, possessing four stereogenic centers and an axis of chirality, 16 diastereoisomers were considered:

- **31a** ($aR^*, 8S^*, 9R^*, 10R^*, 11R^*$), **31b** ($aS^*, 8S^*, 9R^*, 10R^*, 11R^*$),
- **31c** ($aR^*, 8S^*, 9R^*, 10R^*, 11S^*$), **31d** ($aS^*, 8S^*, 9R^*, 10R^*, 11S^*$),
- **31e** ($aR^*, 8S^*, 9R^*, 10S^*, 11R^*$), **31f** ($aS^*, 8S^*, 9R^*, 10S^*, 11R^*$),
- **31g** ($aR^*, 8S^*, 9R^*, 10S^*, 11S^*$), **31h** ($aS^*, 8S^*, 9R^*, 10S^*, 11S^*$),
- **31i** ($aR^*, 8S^*, 9S^*, 10R^*, 11R^*$), **31j** ($aS^*, 8S^*, 9S^*, 10R^*, 11R^*$),
- **31k** ($aR^*, 8S^*, 9S^*, 10R^*, 11S^*$), **31l** ($aS^*, 8S^*, 9S^*, 10R^*, 11S^*$),

- **31m** (aR*,8S*,9S*,10S*,11R*), **31n** (aS*,8S*,9S*,10S*,11R*),
- **31o** (aR*,8S*,9S*,10S*,11S*), **31p** (aS*,8S*,9S*,10S*,11S*)

Starting from the obtained 3D structures, exhaustive conformational searches at the empirical molecular mechanics (MM) level with Monte Carlo Multiple Minimum (MCMM) method (50000 steps) and Low Mode Conformational Search (LMCS) method (50000 steps) were performed, in order to allow a full exploration of the conformational space. Furthermore, molecular dynamics simulations were performed at 450, 600, 700, and 750 K, with a time step of 2.0 fs, an equilibration time of 0.1 ns, and a simulation time of 10 ns. A constant dielectric term of MeOH, mimicking the presence of the solvent, was used in the calculations to reduce artifacts.

For each diastereoisomer, all the conformers obtained from the conformational searches were minimized (PRCG, maximum derivative less than 0.001 kcal/mol) and compared. The “Redundant Conformer Elimination” module of Macromodel 10.2³⁹ was used to select non-redundant conformers, excluding those differing more than 21.0 kJ/mol (5.02 kcal/mol) from the most energetically favoured conformation and setting a 0.5 Å RMSD (root-mean-square deviation) minimum cut-off for saving structures. For compounds **29**, **31**, and **9'**, MM conformational searches produced both sets of atropisomers, that were manually separated after visual inspection once the hindered rotation along the biaryl axis was assessed by means of quantum mechanical (QM) calculations (vide infra). All the QM calculations were performed using Gaussian 09 software⁴¹.

The conformers were optimized at the QM level using the MPW1PW91 functional and the 6-31G(d) basis set.⁴² Experimental solvent effects (MeOH) were reproduced using the integral equation formalism version of the polarizable continuum model (IEFPCM).⁴³ After this step at the QM level, the optimized geometries were visually inspected in order to remove redundant conformers.

The perceived atropisomerism arising from the hindered rotation about the biphenyl axis was evaluated by computing the rotational energy barrier required for the interconversion between the (*aR**,*8S**,*9R**,*10R**) and (*aS**,*8S**,*9R**,*10R**) atropisomers of compound **29**, assuming that this system could be considered representative of all diastereoisomers. Specifically, the starting geometry model representing the transition state was built with the two phenyl moieties occupying the same plane, that was subsequently optimized at the QM level using the Berny algorithm and the MPW1PW91 functional and the 6-31G(d) basis set followed by vibrational frequency calculations (*TS*, *CalcAll*, *Freq* keywords for Gaussian calculations). Analysis of the vibrational frequencies showed that the optimized structure was correctly associated with the transition state, since the two phenyl moieties slightly moves along the biaryl axis producing the two different atropisomeric forms at each oscillation. Comparison of the energies between the lowest energy-associated conformer found for (*8S**,*9R**,*10R**)-**29** and the transition state confirmed the hindered rotation about the biphenyl axis (Results and Discussion). The different atropisomers could be differently treated for the subsequent calculations of the NMR parameters and for the computation of the CD spectra.

Following the same procedure, the energy of the transition state associated with the interconversion between (*aR*) and (*aS*) atropisomers of **9'** was computed.

The computation of the ^{13}C and ^1H NMR chemical shifts was performed on all the selected conformers for the different diastereoisomers of compounds **29** and **31**, using the MPW1PW91 functional and the 6-31G(d,p) basis set and MeOH IEFPCM. Final ^{13}C and ^1H NMR spectra for each of the diastereoisomers were built considering the influence of each conformer on the total Boltzmann distribution taking into account the relative energies. Calibrations of calculated ^{13}C and ^1H chemical shifts were performed following the multi-standard approach (MSTD).^{21, 22} In particular, sp^2 ^{13}C and ^1H NMR chemical shifts were computed

using benzene as reference compound,^{21, 22} while TMS was used for computing sp^3 ^{13}C and 1H chemical shift data.

A further set of data was produced using only TMS as reference compound, and it was subsequently used for the computation of the DP4+ probabilities.

Firstly, experimental and calculated ^{13}C and 1H NMR chemical shifts were compared computing the $\Delta\delta$ parameter:

$$\Delta\delta = |\delta_{\text{exp}} - \delta_{\text{calc}}|$$

where δ_{exp} (ppm) and δ_{calc} (ppm) are the $^{13}C/^1H$ experimental and calculated chemical shifts, respectively.

The mean absolute errors (MAEs) for all the considered diastereoisomers were computed using the following equation:

$$\text{MAE} = \frac{\sum(\Delta\delta)}{n}$$

defined as the summation (Σ) of the n computed absolute error values ($\Delta\delta$), normalized to the number of chemical shifts considered (n).

Furthermore, DP4+ probabilities related to all the stereoisomers of **29** and **31** were computed considering both ^{13}C and 1H NMR chemical shifts, and comparing them with the related experimental data. In particular, since the available DP4+ Toolbox (Excel file) for the DP4+ computation allows the setting of sp^3/sp^2 atoms following the “multi-standard” approach, we used the chemical shift data set obtained using TMS as reference compound.

For compounds **29c** and **31o** identified as the most probable diastereoisomer of **29** and **31**, respectively, Boltzmann-weighted prediction of J values was performed for the most energetically favoured conformers [energies associated with the QM optimization step, MPW1PW91/6-31g(d,p)], performing a two-step spin-spin calculations (*mixed* keyword for Gaussian calculations) using the MPW1PW91 functional and the 6-311+g(d,p) basis set.

Once the relative configurations of **29** and **31** were obtained, the prediction of ECD spectra were performed using all the conformers obtained from the DFT calculations, and performing QM calculations at the TDDFT (NStates=40) MPW1PW91/6-31g(d,p) level, in EtOH IEFPCM to reproduce the experimental solvent environment. The final ECD spectra for both the enantiomers related to the predicted stereoisomers of **29** and **31** (**29c**, and **31o**) were calculated considering the influence of each conformer on the total Boltzmann distribution taking into account the relative energies, and were graphically plotted using SpecDis software⁴⁴. In order to simulate the experimental ECD curve, a Gaussian band-shape function was applied with the exponential half-width (σ/γ) of 0.20 eV.

Determination of the Sugar Configuration.

The configurations of the sugar unit of glycosylate compounds were established after hydrolysis of each compounds with 1 N HCl, trimethylsilation, and determination of the retention times by GC operating under the reported experimental conditions³⁸.

LC-ESI/QqQ/MS and MS/MS method

Quantitative analysis were performed on an Agilent 1100 HPLC system (Agilent Technologies, Palo Alto, CA, USA) coupled to an API 2000 QqQ mass spectrometer (Applied Biosystems, Foster City, CA, USA). HPLC separation was conducted by an Atlantis T3 5 μ m RP C18 column (150mm \times 2.1mm i.d.) and coupled to an Applied Biosystems API2000 triple quadrupole instrument. HPLC separation was conducted by an Atlantis T3 5 μ m C18 reversed-phase (RP) column (2.1 x 150nm, Waters, Mildford, MA, USA) at a flow rate of 0.2 μ L/min. Linear gradient elution was carried out by using H₂O with 0.1% formic acid as eluent A and acetonitrile 0.1% formic acid as B. The HPLC gradient started at 5% B after 10 min % B was at 20%, changing from 20% B to 40% B in 18 min, from

40%B to 56%B in 4 min, from 56% B to 68% B in 10 min, from 68% B to 76% B in 16 min and finally from 76% B to 100% B in 6 min holding it for 5 min before returning back to the starting percentage.

The QqQ mass spectrometer was used in tandem MS mode with MRM. The instrument operated in the negative ion mode with specific parameters for each extract (table 2.15).

C. avellana extracts were diluted by using a solution of MeOH/water (50:50 V/V) and 10 μ L were injected in triplicate.

Table 2.15. LC–MS/MS conditions for quantitation of identified compounds by negative ion MRM.

condition	MeOH extract of flowers	MeOH extract of shells
declustering potential	-108 eV	-35 eV
focusing potential	-200 eV	-354 eV
entrance potential	-8 eV	-8 eV
collision energy	45%	33%
collision cell exit potential	-5 eV	-15 eV

Preparation of calibration curves

Stock solutions (1 mg/mL) of the external standards (ES) were prepared by dissolving compounds isolated by MeOH extracts of male flowers and shells in a solution of MeOH/water (50:50 V/V). Stock solutions were diluted with appropriate amounts of MeOH to give solutions containing 0.0015, 0.002, 0.005, 0.01, 0.020 $\mu\text{g}\mu\text{L}^{-1}$ of each standard.

Stock solutions (1 mg/mL) of the external standards (ES) were prepared by dissolving compounds in a solution of MeOH/water (50:50 V/V). Stock solutions were diluted with appropriate amounts of MeOH to give solutions containing 0.0010, 0.005, 0.025, 0.05, 0.1 $\mu\text{g}\mu\text{L}^{-1}$ of each standard.

To each standard solution was added an appropriate amount of internal standard (IS; apigenin) to yield a final concentration of 0.025 $\mu\text{g}\mu\text{L}^{-1}$ and 0.05 $\mu\text{g}\mu\text{L}^{-1}$ for quantitative analysis of MeOH extract of flowers and shells, respectively. Calibration curves were constructed by injecting 10 μL of each standard solution at each concentration level in triplicate. The ratios of the peak areas of the ES to those of the IS were calculated and plotted against the corresponding concentrations of the standard compounds using weighted linear regression to generate standard curves.

Cancer cell lines

Human alveolar basal carcinoma (A549), obtained from the European Collection of Cell Cultures (ECACC), HeLa cells (human epitheloid cervix carcinoma), DeFew (human B lymphoma) and HaCat cells (human normal skin keratinocyte), obtained from Cell Bank in GMP-IST (Genova, Italy) were cultured in Dulbecco's Modified Eagle's Medium - high glucose (DMEM) medium supplemented with 10% fetal bovine serum (Invitrogen), 1% penicillin/streptomycin and 2 mM L-glutamine (37°C, 5% CO₂).

Analysis of cell viability

A549 (5×10^3), HeLa (5×10^3), DeFew (5×10^3) and HaCat (5×10^3) cells were plated in 96-well microtiter plates and incubated for 48 h in the absence and in the presence of compounds (at concentrations of 12.5, 25, 50, 100 μ M). The viability of cells was determined by 3-(4,-5-dimethylthiazo-2-yl)-2,5-diphenyltetrazolium bromide (MTT) assay to detect functional mitochondria in living cells (Mosmann, 1983). 25 μ L of MTT (5 mg/mL) were added to each well and the cells were incubated for an additional 3 h. Thereafter, cells were lysed with 100 μ L of a solution containing 50% (v/v) N,N-dimethylformamide and 20% (w/v) sodium dodecyl sulfate (SDS) (pH 4.5) to allow solubilization of dark blue crystals. The optical density (OD) of each well was measured with a microplate spectrophotometer (Mutiscan Go, Thermo Fisher Scientific Inc. Waltham, MA, USA) equipped with a 620 nm filter. IC₅₀ values were calculated from cell viability dose-response curves and defined as the concentration resulting in 50% inhibition of cell survival at 48 h, compared to untreated cells.

TBARS assay and Lipid Peroxidation Measurement.

Reported in the section: general experimental procedures.

Statistical analysis

The statistical analysis was done by several tests. In order to eliminate uncertain data, the Q-Dixon test was performed. All the values in this study were expressed as mean \pm SD. The statistical analysis was performed with one-way ANOVA for repeated measurements. The statistically significant differences were also assessed by applying the paired Student's t-test.

Antimicrobial Activity.

The antibacterial activity of the MeOH extract of *C. avellana*, cv. Tonda di Giffoni leafy covers and of isolated compounds, was assayed by the inhibition halo test on agar plates⁴⁷ against *Bacillus cereus* (DSM 4313 and DSM 4384), *Staphylococcus aureus* DSM 25923, *Escherichia coli* DSM 8579, and *Pseudomonas aeruginosa* ATCC 50071, provided by Deutsche Sammlung von Mikroorganismen und Zellkulturen GmbH (DSMZ, Braunschweig, Germany). Each strain was incubated at 37 °C for 18 h in TY broth (Sigma-Aldrich, Milano, Italy). The microbial suspensions at 1×10^8 colony forming units (cfu)/mL were uniformly spread on the solid media plates ($\varnothing = 90$ -mm dishes). Sterile Whatman Grade 1 paper filter disks ($\varnothing = 5$ mm), previously impregnated with samples (final amount ranging from 10 to 40 μ g/ disk) and dried at room temperature for 60 minutes, were individually placed on the inoculated plates. Plates were then incubated at 37 °C for 24–48 h, depending on the strain. The activity of compounds was evaluated by measuring the diameter (in mm) of the inhibition zones around the disks. Sterile DMSO was used as negative control. Tetracycline (7 μ g/disk; Sigma-Aldrich, Milano, Italy) was the reference sample. The samples were tested in triplicate, and the results were expressed as the mean values \pm standard deviations.

Minimum Inhibitory Concentration.

The MIC values for the MeOH extract and carpinontriol B (**29**) and giffonins T-U (**30-31**) were evaluated by the resazurin microtiter-plate assay modified from Sarker and coworkers⁴⁸ (2007), as previously reported⁴⁹. It is based on the capability of microorganisms to lower the redox potential of the medium in which they are located as a result of their growth and metabolic activities. The addition of resazurin as a redox indicator displays, through its colour change (dark purple > colorless), the state of oxidation or reduction, thus the growth of bacteria. Samples, dissolved in DMSO, were pipetted in a multi-well with different volumes of Muller-Hinton broth (Sigma Aldrich, Milano, Italy). Two-fold serial dilutions were performed such that each well had 50 μL of the test material in serially descending concentrations. Thirty-five μL of $3.3\times$ strength isosensitised broth and 5 μL of resazurin indicator solution were added to a final volume/well of 240 μL . Finally, 10 μL of bacterial suspension was added to each well to achieve a concentration of about 5×10^5 cfu/mL. Ciprofloxacin (1 mg/mL in DMSO, Sigma) and DMSO were used as positive and negative controls, respectively. Plates were prepared in triplicate, and incubated at 37 °C for 24 h. The lowest concentration at which a color change occurred indicated the MIC value.

References

1. Shahidi, F.; Alasalvar, C.; Liyana-Pathirana, C. M., Antioxidant phytochemicals in hazelnut kernel (*Corylus avellana* L.) and hazelnut byproducts. *J Agr Food Chem* **2007**, *55*, 1212-1220.
2. Nagumo, S.; Kaji, N.; Inoue, T.; Nagai, M., Studies on the constituents of *Aceraceae* plants. XI. Two types of cyclic diarylheptanoid from *Acer nikoense*. *Chem. Pharm. Bull.* **1993**, *41*, 1255-7.
3. Mari, A.; Napolitano, A.; Masullo, M.; Pizza, C.; Piacente, S., Identification and quantitative determination of the polar constituents in *Helichrysum italicum* flowers and derived food supplements. *J. Pharm. Biomed. Anal.* **2014**, *96*, 249-255.
4. Mari, A.; Montoro, P.; D'Urso, G.; Macchia, M.; Pizza, C.; Piacente, S., Metabolic profiling of *Vitex agnus castus* leaves, fruits and sprouts: Analysis by LC/ESI/(QqQ)MS and (HR) LC/ESI/(Orbitrap)/MSn. *J. Pharm. Biomed. Anal.* **2015**, *102*, 215-221.
5. Mari, A.; Montoro, P.; Pizza, C.; Piacente, S., Liquid chromatography tandem mass spectrometry determination of chemical markers and principal component analysis of *Vitex agnus-castus* L. fruits (Verbenaceae) and derived food supplements. *J. Pharm. Biomed. Anal.* **2012**, *70*, 224-230.
6. Napolitano, A.; Akay, S.; Mari, A.; Bedir, E.; Pizza, C.; Piacente, S., An analytical approach based on ESI-MS, LC-MS and PCA for the quali-quantitative analysis of cycloartane derivatives in *Astragalus* spp. *J. Pharm. Biomed. Anal.* **2013**, *85*, 46-54.
7. Maldini, M.; Montoro, P.; Piacente, S.; Pizza, C., Phenolic compounds from *Bursera simaruba* Sarg. bark: Phytochemical investigation and quantitative analysis by tandem mass spectrometry. *Phytochemistry (Elsevier)* **2009**, *70*, 641-649.
8. Masullo, M.; Montoro, P.; Autore, G.; Marzocco, S.; Pizza, C.; Piacente, S., Quali-quantitative determination of triterpenic acids of *Ziziphus jujuba* fruits and evaluation of their capability to interfere in macrophages activation inhibiting NO release and iNOS expression. *Food Res. Int.* **2015**, *77*, 109-117.
9. Haug, L. S.; Thomsen, C.; Becher, G., A sensitive method for determination of a broad range of perfluorinated compounds in serum suitable for large-scale human biomonitoring. *J. Chromatogr. A* **2009**, *1216*, 385-393.
10. Iranshahi, M.; Chini, M. G.; Masullo, M.; Sahebkar, A.; Javidnia, A.; ChitsazianYazdi, M.; Pergola, C.; Koeberle, A.; Werz, O.; Pizza, C.; Terracciano, S.; Piacente, S.; Bifulco, G., Can Small Chemical Modifications of Natural Pan-inhibitors Modulate the Biological Selectivity? The Case of Curcumin Prenylated Derivatives Acting as HDAC or mPGES-1 Inhibitors. *J. Nat. Prod.* **2015**, *78*, 2867-2879.

11. Gulcernal, D.; Masullo, M.; Bedir, E.; Festa, M.; Karayildirim, T.; Alankus-Caliskan, O.; Piacente, S., Triterpene glycosides from *Astragalus angustifolius*. *Planta Med.* **2012**, *78*, 720-729.
12. Bifulco, G.; Dambruoso, P.; Gomez-Paloma, L.; Riccio, R., Determination of relative configuration in organic compounds by NMR spectroscopy and computational methods. *Chemical Reviews* **2007**, *107*, 3744-3779.
13. Di Micco, S.; Chini, M. G.; Riccio, R.; Bifulco, G., Quantum Mechanical Calculation of NMR Parameters in the Stereostructural Determination of Natural Products. *Eur. J. Org. Chem.* **2010**, 1411-1434.
14. Barone, G.; Duca, D.; Silvestri, A.; Gomez-Paloma, L.; Riccio, R.; Bifulco, G., Determination of the relative stereochemistry of flexible organic compounds by ab initio methods: Conformational analysis and Boltzmann-averaged GIAO C-13 NMR chemical shifts. *Chem. Eur. J.* **2002**, *8*, 3240-3245.
15. Barone, G.; Gomez-Paloma, L.; Duca, D.; Silvestri, A.; Riccio, R.; Bifulco, G., Structure validation of natural products by quantum-mechanical GIAO calculations of C-13 NMR chemical shifts. *Chem. Eur. J.* **2002**, *8*, 3233-3239.
16. Bassarello, C.; Bifulco, G.; Montoro, P.; Skhirtladze, A.; Kemertelidze, E.; Pizza, C.; Piacente, S., Gloriosols A and B, two novel phenolics from *Yucca gloriosa*: structural characterization and configurational assignment by a combined NMR-quantum mechanical strategy. *Tetrahedron* **2007**, *63*, 148-154.
17. Plaza, A.; Piacente, S.; Perrone, A.; Hamed, A.; Pizza, C.; Bifulco, G., Stemmosides C and D, two novel unusual pregnane glycosides from *Solenostemma argel*: structural elucidation and configurational study by a combined NMR-quantum mechanical strategy. *Tetrahedron* **2004**, *60*, 12201-12209.
18. Lee, J. S.; Kim, H. J.; Park, H.; Lee, Y. S., New diarylheptanoids from the stems of *Carpinus cordata*. *J Nat Prod.* **2002**, *65*, 1367-1370.
19. Bringmann, G.; Mortimer, A. J. P.; Keller, P. A.; Gresser, M. J.; Garner, J.; Breuning, M., Atroposelective synthesis of axially chiral biaryl compounds. *Angew Chem Int Edit* **2005**, *44*, 5384-5427.
20. Smyth, J. E.; Butler, N. M.; Keller, P. A., A twist of nature - the significance of atropisomers in biological systems. *Nat Prod Rep.* **2015**, *32*, 1562-1583.
21. Sarotti, A. M.; Pellegrinet, S. C., A Multi-standard Approach for GIAO (13)C NMR Calculations. *J. Org. Chem.* **2009**, *74*, 7254-7260.
22. Sarotti, A. M.; Pellegrinet, S. C., Application of the Multi-standard Methodology for Calculating H-1 NMR Chemical Shifts. *J. Org. Chem.* **2012**, *77*, 6059-6065.
23. Grimblat, N.; Zanardi, M. M.; Sarotti, A. M., Beyond DP4: an Improved Probability for the Stereochemical Assignment of Isomeric Compounds using

- Quantum Chemical Calculations of NMR Shifts. *J. Org. Chem.* **2015**, *80*, 12526-12534.
24. Nadmid, S.; Plaza, A.; Lauro, G.; Garcia, R.; Bifulco, G.; Mueller, R., Hyalachelins A-C, Unusual Siderophores Isolated from the Terrestrial Myxobacterium *Hyalangium minutum*. *Org. Lett.* **2014**, *16*, 4130-4133.
25. Masullo, M.; Bassarello, C.; Bifulco, G.; Piacente, S., Polyisoprenylated benzophenone derivatives from the fruits of *Garcinia cambogia* and their absolute configuration by quantum chemical circular dichroism calculations. *Tetrahedron* **2010**, *66*, 139-145.
26. Gong, J.; Sun, P.; Jiang, N.; Riccio, R.; Lauro, G.; Bifulco, G.; Li, T. J.; Gerwick, W. H.; Zhang, W., New Steroids with a Rearranged Skeleton as (h)P300 Inhibitors from the Sponge *Theonella swinhoei*. *Org. Lett.* **2014**, *16*, 2224-2227.
27. Talapatra, B.; Bhaumik, A.; Talapatra, S. K., 2-Hydroxy-1,2,3-propanetricarboxylic acid 2-methyl ester, a new natural product from *Rhus parviflora*: a simple achiral molecule having both enantiotopic and diastereotopic hydrogens. *Indian J. Chem., Sect. B* **1993**, *32B*, 1292-4.
28. Dall'Acqua, S.; Viola, G.; Piacente, S.; Cappelletti, E. M.; Innocenti, G., Cytotoxic Constituents of Roots of *Chaerophyllum hirsutum*. *J. Nat. Prod.* **2004**, *67*, 1588-1590.
29. Oliveira, I.; Sousa, A.; Valentao, P.; Andrade, P. B.; Ferreira, I. C. F. R.; Ferreres, F.; Bento, A.; Seabra, R.; Estevinho, L.; Pereira, J. A., Hazel (*Corylus avellana* L.) leaves as source of antimicrobial and antioxidative compounds. *Food Chem.* **2007**, *105*, 1018-1025.
30. Lv, H.; She, G., Naturally occurring diarylheptanoids. *Nat. Prod. Commun.* **2010**, *5*, 1687-1708.
31. Liu, F.; Zhang, Y.; Sun, Q.-Y.; Yang, F.-M.; Gu, W.; Yang, J.; Niu, H.-M.; Wang, Y.-H.; Long, C.-L., Diarylheptanoids and phenylphenalenones from *Musa itinerans* fruits. *Phytochemistry (Elsevier)* **2014**, *103*, 171-177.
32. Cushnie, T. P. T.; Lamb, A. J., Antimicrobial activity of flavonoids. *Int J Antimicrob Ag.* **2005**, *26*, 343-356.
33. Eswaranandam, S.; Hettiarachchy, N. S.; Johnson, M. G., Antimicrobial activity of citric, lactic, malic, or tartaric acids and nisin-incorporated soy protein film against *Listeria monocytogenes*, *Escherichia coli* O157 : H7, and *Salmonella gaminara*. *J Food Sci* **2004**, *69*, M79-M84.
34. Perrone, A.; Masullo, M.; Bassarello, C.; Bloise, E.; Hamed, A.; Nigro, P.; Pizza, C.; Piacente, S., Unusual cycloartane glycosides from *Astragalus eremophilus*. *Tetrahedron* **2008**, *64*, 5061-5071.
35. Kim, C. S.; Subedi, L.; Kim, S. Y.; Choi, S. U.; Kim, K. H.; Lee, K. R., Lignan glycosides from the twigs of *Chaenomeles sinensis* and their biological activities. *J Nat Prod.* **2015**, *78*, 1174-1178.

36. Li, Y.-C.; Kuo, Y.-H., Four new compounds, ficusal, ficusesquilignan A, B, and ficusolide diacetate from the heartwood of *Ficus microcarpa*. *Chem Pharm Bull.* **2000**, *48*, 1862-1865.
37. Kawamura, F.; Kawai, S.; Ohashi, H., Lignans causing photodiscoloration of *Tsuga heterophylla*: 8-hydroxy-oxomatairesinol from sapwood. *Phytochemistry* **2000**, *54*, 439-444.
38. Liang, S.; Ying, S.-S.; Wu, H.-H.; Liu, Y.-T.; Dong, P.-Z.; Zhu, Y.; Xu, Y.-T., A novel sesquiterpene and three new phenolic compounds from the rhizomes of *Acorus tatarinowii* Schott. *Bioorg Med Chem Lett.* **2015**, *25*, 4214-4218.
39. Fang, J. M.; Lee, C. K.; Cheng, Y. S., Lignans from leaves of *Juniperus chinensis*. *Phytochemistry* **1992**, *31*, 3659-61.
40. Warashina, T.; Nagatani, Y.; Noro, T., Further constituents from the bark of *Tabebuia impetiginosa*. *Phytochemistry* **2005**, *66*, 589-597.
41. Wang, Y.-H.; Sun, Q.-Y.; Yang, F.-M.; Long, C.-L.; Zhao, F.-W.; Tang, G.-H.; Niu, H.-M.; Wang, H.; Huang, Q.-Q.; Xu, J.-J.; Ma, L.-J., Neolignans and caffeoyl derivatives from *Selaginella moellendorffii*. *Helv. Chim. Acta.* **2010**, *93*, 2467-2477.
42. Baderschneider, B.; Winterhalter, P., Isolation and characterization of novel benzoates, cinnamates, flavonoids, and lignans from riesling wine and screening for antioxidant activity. *J Agric Food Chem.* **2001**, *49*, 2788-2798.
43. Della Greca, M.; Ferrara, M.; Fiorentino, A.; Monaco, P.; Previtiera, L., Antialgal compounds from *Zantedeschia aethiopica*. *Phytochemistry* **1998**, *49*, 1299-1304.
44. Li, X.; Cao, W.; Shen, Y.; Li, N.; Dong, X.-P.; Wang, K.-J.; Cheng, Y.-X., Antioxidant compounds from *Rosa laevigata* fruits. *Food Chem* **2012**, *130*, 575-580.
45. Huang, X.-X.; Zhou, C.-C.; Li, L.-Z.; Li, F.-F.; Lou, L.-L.; Li, D.-M.; Ikejima, T.; Peng, Y.; Song, S.-J., The cytotoxicity of 8-O-4' neolignans from the seeds of *Crataegus pinnatifida*. *Bioorg Med Chem Lett.* **2013**, *23*, 5599-5604.
46. Huang, X.-X.; Liu, Q.-B.; Zhou, L.; Liu, S.; Cheng, Z.-Y.; Sun, Q.; Li, L.-Z.; Song, S.-J., The antioxidant and tyrosinase-inhibiting activities of 8-O-4' neolignans from *Crataegus pinnatifida*. *Rec Nat.Prod.* **2015**, *9*, 305-311.
47. Pereira do Amaral, F.; Napolitano, A.; Masullo, M.; Campaner dos Santos, L.; Festa, M.; Vilegas, W.; Pizza, C.; Piacente, S., HPLC-ESIMSⁿ profiling, isolation, structural elucidation, and evaluation of the antioxidant potential of phenolics from *Paepalanthus geniculatus*. *J Nat Prod* **2012**, *75*, 547-556.
48. Riethmuller, E.; Alberti, A.; Toth, G.; Beni, S.; Ortolano, F.; Kery, A., Characterisation of diarylheptanoid- and flavonoid-type phenolics in *Corylus avellana* L. leaves and bark by HPLC/DAD-ESI/MS. *Phytochem. Anal. : PCA* **2013**, *24*, 493-503.

49. Kirmizibekmez, H.; Ariburnu, E.; Masullo, M.; Festa, M.; Capasso, A.; Yesilada, E.; Piacente, S., Iridoid, phenylethanoid and flavonoid glycosides from *Sideritis trojana*. *Fitoterapia* **2012**, *83*, 130-136.
50. Wachowicz, B., Adenine nucleotides in thrombocytes of birds. *Cell Biochem. Funct.* **1984**, *2*, 167-71.

Chapter 3

Multi-class polar lipid profiling of fresh and roasted hazelnut (*Corylus avellana* cv. Tonda di Giffoni) by LC-ESI/LTQOrbitrap/MS/MSⁿ

Introduction

Several research groups have reported the benefits of inclusion of nuts in the human diet¹. Noteworthy, among nut species, Food and Drug Administration (FDA) has recognized hazelnuts as “heart-healthy” foods by virtue of their nutritional and nutraceutical properties^{1, 2}. In particular, the hazelnut oil has proved to be able to decrease cholesterol levels in blood and to control adverse effects of hypertension, due to its fatty acid composition, rich in monounsaturated (MUFA) and polyunsaturated fatty acids (PUFA). The presence of these compounds might bring health benefits, protecting low density lipoprotein (LDL) from oxidation and decreasing plasma oxidized LDL levels. Moreover, hazelnut oil is a good source of α -tocopherol, that reduces the risk of chronic diseases, such as heart disease, type 2-diabetes, hypertension, and prevents some of the negative effects associated with ageing³. Currently in Italy there are two hazelnut varieties registered by the European Union with the special origin declaration of Protected Geographical Indication (PGI), “Nocciola del Piemonte” and “Nocciola di Giffoni”. The latter is the product of a *C. avellana* cultivar of Campania region (Tonda di Giffoni, ‘TG’). It is recognized as high quality hazelnut with good sensorial characteristics and interesting technological properties, and largely contributes to the production of the national crop, accounting for about one-third of the nut national crop⁴. Notwithstanding this and the significant lipid role in determining beneficial effects on human health, until now no comprehensive analysis is available about polar lipid composition of “Nocciola di Giffoni” hazelnut kernel.

3.1. Result and discussion

LC-MS analysis of fresh and roasted hazelnut (C. avellana cv. Tonda di Giffoni) by LC-ESI/LTQOrbitrap/MS/MSⁿ

Preliminarily, in order to highlight the presence of diarylheptanoids in the butanol extract of fresh and roasted hazelnut (*C. avellana* cv. Tonda di Giffoni) a plant metabolite profiling was performed by LC-ESI/LTQOrbitrap/MS analysis, in negative ionization mode. LC-MS analyses using previously isolated giffonins A-T as standards have been carried out, showing that giffonins M, P, Q and carpinontriol B occurred in the extract of fresh hazelnut in very little amount and giffonin P, Q and carpinontriol B resulted minor compounds in the extract of roasted hazelnut. All the other giffonins were not detected (table 3.1 and fig. 3.1).

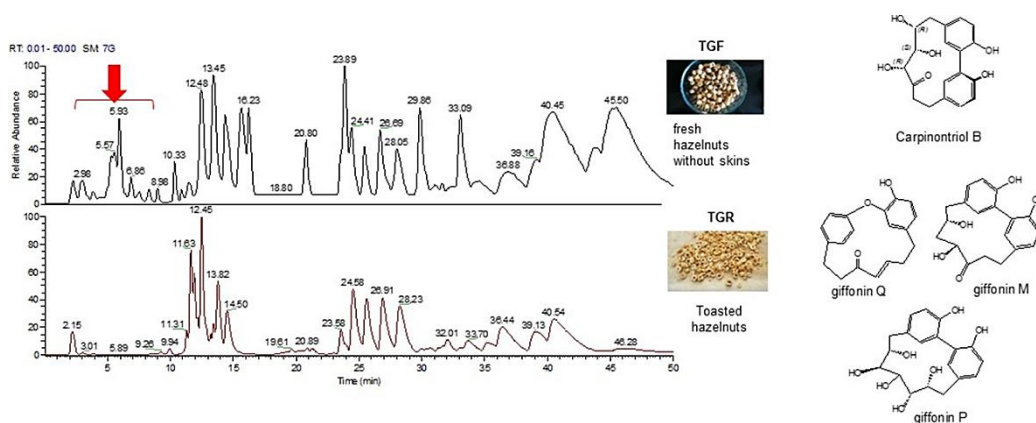


Figure 3.1. LC-ESI(Orbitrap)MS Base Peak chromatograms of the butanolic extract of *C. avellana* hazelnuts, toasted and fresh.

Table 3.1. Diarylheptanoids in fresh and roasted *C.avellana* cv. Tonda di Giffoni.

DIARYLHEPTANOIDS						Tonda di Giffoni	
Compound	R_t (min)	Molecular Formula	[M-H] ⁻ (m/z)	Δ ppm	Characteristic fragment ions	TGR	TGF
Carpinontriol B	3.83	C ₁₉ H ₁₉ O ₆	343,11874	3.27	Compare with standard	+	+
Giffonin M	5.20 ^a	C ₁₉ H ₁₉ O ₅	327,12314 ^a	1.34 ^a	Compare with standard	-	+
Giffonin P	6.12	C ₁₉ H ₂₁ O ₇	361,12845	0,75	Compare with standard	+	+
Giffonin Q	9.07 ^a	C ₁₉ H ₁₇ O ₃	293,11734 ^a	0,41 ^a	Compare with standard	+	+

LC-MS analysis of the butanol extract of *C.avellana* cv. Tonda di Giffoni highlighted the presence of m/z values corresponding to a wide range of polar lipids.

Polar lipids

Polar lipids are biomolecules distributed in different chemical classes (e.g. phospholipids, glycolipids, sphingolipids) according to the specific polar moiety ('head group') characterizing each class, in turn composed of various molecular species, structurally defined by fatty acids or other hydrocarbon portions varying in chain length and in saturation degree (fig. 3.2).

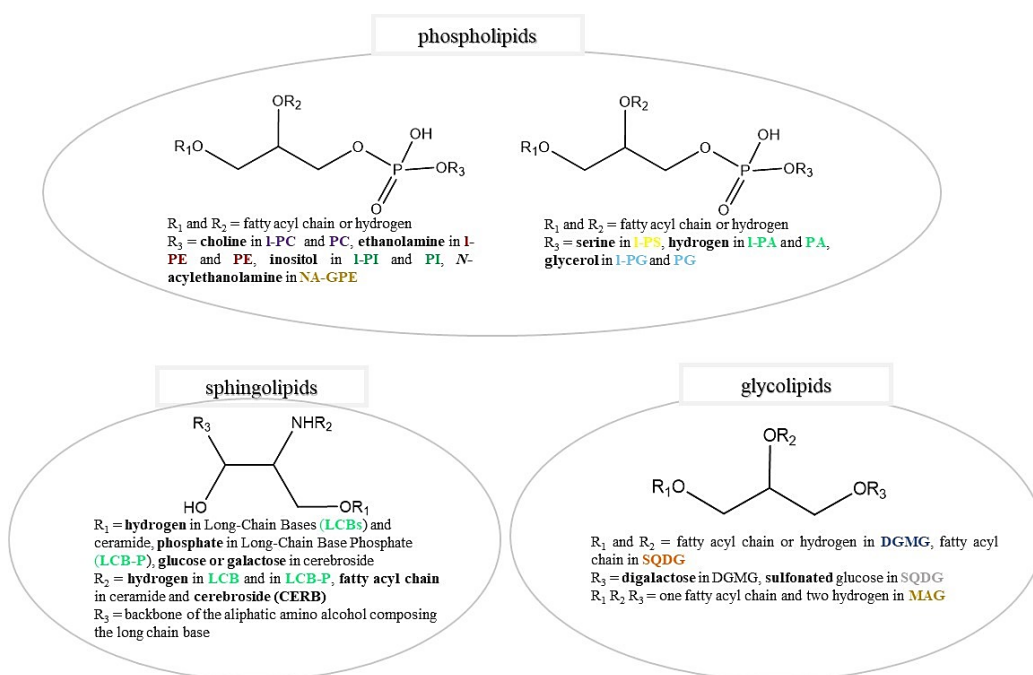


Figure 3.2. different class of polar lipids.

Polar lipids profiling by LC-ESI/LTQOrbitrap/MS/MSⁿ

Lipid profiling using mass spectrometry is emerging as a strategy allowing the analysis of a broad-range of lipid species in a single platform. Mass spectrometry (MS) can provide detailed information about lipid composition rapidly and with small amount of samples; extracts can be analysed directly and effectively even without pre-separation of the lipids into classes⁵. By using positive or negative electrospray ionization mode, each lipid compound provides singly charged molecular ion, most of the time sufficient on their own to allow unambiguous fatty acyl group identification. Infact the carbon number/double bond combination is strictly indicative of the nature of fatty acids composing the molecules. When the definition of fatty acids is ambiguous, or lipid species of the same mass (i.e. isobaric species) are contemporary present in the sample, liquid chromatography coupled to tandem mass spectrometry (LC-MS/MS) analysis can be resolute,

since in product ion experiments the head-group can undergo the neutral loss of the common head-group unit or yield a common product ion, in both cases allowing to promptly identify the lipid class.

Thereby, continuing our investigation on *C. avellana* cultivar Tonda di Giffoni hazelnut, we carried out this study with the aim to provide a detailed and comprehensive characterization of the polar lipids. More specifically, considering that roasting is a thermal process that could influence the chemical composition of hazelnut, and that hazelnuts are generally consumed after roasting, the *n*-butanol extracts of both fresh (TGF) and roasted (TGR) “Tonda di Giffoni” hazelnut kernels (without skin) were analysed by an analytical approach based on high-performance liquid chromatography coupled to multiple-stage linear ion-trap and orbitrap high-resolution mass spectrometry both negative and positive electrospray ionization mode (LC-ESI/LTQOrbitrap/MS/MSⁿ), in order to compare their lipid profil and to highlight the chemical changes occurring in hazelnut after thermal treatment.



LC-ESI/LTQOrbitrap/MS/MSⁿ analysis of the polar lipids of hazelnut kernels.

In order to obtain a multi-class polar lipid profiling of the *n*-butanol extract of fresh and roasted “Tonda di Giffoni” hazelnuts, an analytical approach based on high-performance liquid chromatography coupled to multiple-stage linear ion-trap and orbitrap high-resolution mass spectrometry (LC-ESI/LTQOrbitrap/MS/MSⁿ)

was applied. Considering the remarkable structural diversity of lipid classes, differing in their ionization capacity and producing polarity-dependent forms of molecular anions and cations, both negative and positive electrospray ionization were used. Moreover, to allow the analysis of lipid metabolites differing by size and polarity, two different types of chromatographic columns were used, a RP C18 and a RP C4 column, the latter in particular used to reduce the strong adsorption to the RP C18 stationary phase of high molecular weight lipids, such as phospholipids, obtaining a more effective detection and separation.

Using these conditions, a wide range of peaks corresponding to lipophilic metabolites ranging from oxylipins and long chain bases to intact high molecular weight lipids, such as phospholipids, sphingolipids, and glycolipids could be appreciated. In particular, for phospholipids and glycolipids the chromatographic step allowed the separation of structural isomers, corresponding to different distributions of unsaturations on the acyl chain, and regioisomers, characterized by a different positioning of the same acyl chain on the *sn*-1 and *sn*-2 positions of the glycerol backbone.

Identification of each TG hazelnut lipid compounds was based on chromatographic behavior, accurate mass measurements, consecutive MSⁿ analyses, and comparison with data in the literature. By this analytical approach, a total of 120 lipid compounds were tentatively identified from TGF and TGR hazelnut kernels.

Identification of Oxylipins

Oxylipins are a family of bioactive secondary metabolites deriving from the oxidative metabolism of essential PUFA, such as α -linolenic acid (ALA, 18:3 ω -3) and linoleic acid (LA, 18:2 ω -6)⁶. Oxylipins can be synthesized *in vivo* from their precursor fatty acids *via* oxygenase enzymes, or obtained through food or dietary oils. The oxidation of fatty acids in oils is nonenzymatic and is known to be

influenced by storage or processing conditions. However, enzymatic oxidation *via* lipoxygenase enzymes occurs during the oil extraction process, when the barrier integrity of the seed is compromised by homogenization⁷.

Oxylipins are reported in several seed oils of higher plants, such as soybean, corn, olive, canola, and ricinus, and in wheat flour. The best known of these metabolites is ricinoleic acid [12-HydroxyOctadec-9-MonoEnoic acid, 12-HOME (9)], which is the main constituent (up to 90%) of castor oil. Moreover, dienoic fatty acids with one hydroxy group [e.g. 9-HydroxyOctadec-10,12-DiEnoic acid, 9-HODE (10,12), and 13-HydroxyOctadec-9,11-DiEnoic acid, 13-HODE (9,11)] and dihydroxy fatty acids [e.g. 9,10-DiHydroxyStearic Acid (DHSA), 9,10-DHSA] have been described in a number of seed oils, and some of them have commercial value^{6,7}.

In plants, oxylipins serve as signal molecules in developmental processes (e.g., pollen formation) and in defense mechanisms (e.g., pathogenesis, wounding, and herbivores). Little is known about the role of ALA derived oxylipins in mammals, while LA derived oxylipins have proved to be involved in *in vivo* inflammatory cascades, pain perception, and skin barrier integrity⁷.

The careful study of full and tandem mass spectra acquired by LC-ESI/LTQOrbitrap/MS/MSⁿ analysis of both TGF and TGR hazelnut kernel extracts allowed to ascertain the presence of eight different oxylipin species (fig. 3.3).

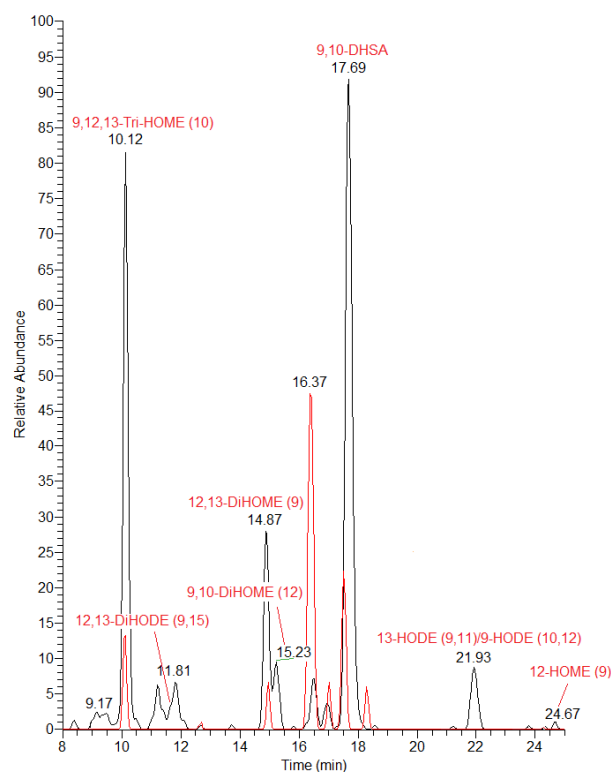


Figure 3.3. Extracted ion chromatograms of oxylipin ions from the LC-MS analysis of TGF (black plot) and TGR (red plot) extracts on Atlantis T3 column in ESI negative ion mode (Normalized level: TGF 1.4×10^5 ; TGR 1.0×10^4).

In agreement with literature data, they were tentatively identified on the basis of both their molecular formulae and characteristic product ions (table 3.2)^{6,7}.

Table 3.2. Oxylipins putatively identified in TG hazelnut kernel.

n°Compound	<i>R_t</i> (min)	Molecular Formula	[M-H] ⁻	Δ ppm	Characteristic product ions (m/z)	TGR	TGF
1 9,12,13-TriHOME (10)	10.15	C ₁₈ H ₃₄ O ₅	329,2327	1.27	314 (22), 311 (49), 293 (23), 291 (4), 229 (100), 211 (68), 199 (5), 197 (5), 183 (7), 171 (38)	+	+
2 12,13-DiHODE (9,15)	11.63	C ₁₈ H ₃₂ O ₄	311,2229	3.99	311 (48), 293 (13), 283 (6), 243 (10), 213 (37), 209 (22), 184 (75), 183 (100)	-	+
3 12,13-DiHOME (9)	14.87	C ₁₈ H ₃₄ O ₄	313,2376	0.87	295 (100), 277 (10), 183 (27)	+	+
4 9,10-DiHOME (12)	15.18	C ₁₈ H ₃₄ O ₄	313,2377	1.35	295 (82), 277 (11), 269 (17), 245 (21), 201 (100), 183 (20), 171 (32)	-	+
5 9,10-DHSA	17.64	C ₁₈ H ₃₆ O ₄	315,2533	1.09	297 (100), 279 (2), 201 (2), 187 (7), 171 (13)	+	+
6 13-HODE (9,11)	21.90	C ₁₈ H ₃₂ O ₃	295,2267	-0.07	277 (83), 233 (21), 195 (88), 179 (21), 171 (41), 99 (67)	-	+
7 9-HODE (10,12)					277 (100), 195 (10), 171 (22)		
8 12-HOME (9)	24.71	C ₁₈ H ₃₄ O ₃	297,2424	0.03	279 (4), 251 (25), 211 (5), 197 (15), 184 (30), 183 (100), 169 (2)	-	+

Calculated from the LC-MS analysis of TGF on Atlantis T3 column in negative ion mode. Characteristic ions for identification are in bold. Same as other tables. In round brackets relative intensities.

An elution order could be noted with oxylipins characterized by more hydroxy groups eluting before than oxylipins with a higher number of double bonds (i.e. TriHOME>DiHODE); furthermore in the frame of oxylipins with the same number of OH groups, those ones with a higher unsaturation degree eluted faster (i.e. DiHODE>DiHOME>DHSA) (fig. 3.1). Noteworthy, the thermal treatment of TG kernel hazelnuts by roasting seems to modify the oxylipin pattern, yielding a general decrease of oxylipin peaks in TGR and the disappearance of some species (fig. 3.3).

There are few reports about oxylipins in hazelnuts, mainly referring them in leaves and under glyceride forms in hazelnut derived fats and oils⁸. Thereby, to the best of our knowledge, this is the first report of these metabolites in hazelnuts.

Identification of phospholipids and N-acylglycerophosphoethanolamines (NA-GPEs).

Phospholipids (PL) are the main constituents of biological membranes and have important structural and functional properties. They are made up of several distinct moieties with different polar head groups (tables 3.3 and 3.4). Each phospholipid class consists of a mixture of many molecular species containing different combinations of fatty acids in the *sn*-1 and *sn*-2 positions on the glycerol backbone.

Phospholipids which are the main constituents of some foods are believed to have a diverse array of beneficial effects in the human body. For example, dietary phosphatidylserine (PS) has emerged as a brain-specific nutrient that ameliorates declining memory, while dietary phosphatidylcholine (PC) has shown to prevent the development of nonalcoholic fatty liver disease in rats fed with a high-fat diet. Moreover, phosphatidylethanolamine (PE) has shown to cause a decrease in serum cholesterol, and phosphatidylinositol (PI) has proved to promote cholesterol transport and excretion in rabbits and to affect cholesterol metabolism and absorption of PI in rats⁹.

Dietary phospholipids, known to be metabolized in the gastrointestinal lumen, are hydrolyzed into free fatty acids and lyso-phospholipids (l-PL) by pancreatic phospholipase A₂ (PLA₂) before absorption. l-PL are phospholipids in which only one of *sn*-1/*sn*-2 position of glycerol is fatty acylated; they are recognized as important cellular signaling molecules and are involved in important processes such as cell proliferation, cell survival, cell migration, diabetes, angiogenesis, inflammation, and cancer mediated by l-PL-specific G-protein coupled receptors¹⁰. Lyso-phospholipids are minor components in foodstuffs.

A challenge in identifying phospholipids by MS-based methods is that species from different structural classes may have the same masses. For example, exact

masses of molecular cations of PC and PE may overlap because their heteroatom compositions are the same (NO₈P).

This was the case of six compounds occurring in the positive LC-ESI/LTQOrbitrap/MS profile of the TGR kernel extract and showing a molecular formula with a NO₇P heteroatom composition that could correspond to lyso-forms of both PC and PE phospholipids. The analysis of the respective tandem mass spectra dispelled all doubts giving information on the nature of the headgroup. In fact in all cases a product ion at m/z 184 generated by the relative [M+H]⁺ pseudomolecular ion was detected and related to the presence of the phosphocholine moiety (table 3.3).

Table 3.3. 1-PC, PC, 1-PE, PE, 1-PI, PI, and NA-GPE putatively identified in TG hazelnut kernel.

R₁ and R₂ = fatty acyl chain or hydrogen
R₃ = choline in 1-PC and PC, ethanolamine in 1-PE and PE, inositol in 1-PI and PI, *N*-acylethanolamine in NA-GPE

n° Compound	R _i (min)	Molecular Formula	[M+H] ⁺	Δ ppm	[(M+FA)- H] ⁻	Δ ppm	Characteristic product ions (m/z)	TGR	TGF
<i>1-PC and PC</i>									
9	1-PC (18:1- 10)	11.83 ^a C ₂₆ H ₅₂ O ₈ NP	538,3493 ^a	- 1.88 ^a			520, 258, 184	+	-
10	1-PC (18:1- 20)	12.34 ^a C ₂₆ H ₅₂ O ₉ NP	554,3437 ^a	- 2.71 ^a			536, 520, 518, 394, 258, 184	+	-
11	1-PC (18:1- 20)	12.52 ^a C ₂₆ H ₅₂ O ₉ NP	554,3436 ^a	- 2.89 ^a			536, 520, 518, 394, 258, 184	+	-
12	1-PC (18:2)	15.15 ^a C ₂₆ H ₅₀ O ₇ NP	520,3380 ^a	- 3.37 ^a			502, 184	+	+
					564,3294 ^b	-0.43 ^b	504, 279; MS ³ (504): 279, 242, 224, 168		
13	1-PC (18:2)	15.77 ^a C ₂₆ H ₅₀ O ₇ NP	520,3379 ^a	- 3.49 ^a			502, 184	+	+
					564,3293 ^b	-0.56 ^b	504, 279; MS ³ (504): 279, 242, 224, 168, 153		
14	1-PC (16:0)	16.75 ^a C ₂₄ H ₅₀ O ₇ NP	496,3384 ^a	- 2.77 ^a			478, 184	+	-
					540,3292 ^b	-0.81 ^b	480, 255; MS ³ (480): 255, 242, 224, 168, 153		
15	1-PC (16:0)	17.69 ^a C ₂₄ H ₅₀ O ₇ NP	496,3383 ^a	- 2.87 ^a			478, 184	+	+
					540,3293 ^b	-0.58 ^b	480, 255; MS ³ (480): 255, 242, 224, 168, 153		
16	1-PC (18:1)	18.45 ^a C ₂₆ H ₅₂ O ₇ NP	522,3535 ^a	- 3.63 ^a			504, 184	+	+
					566,3452 ^b	-0.17 ^b	506, 281; MS ³ (506): 281, 242, 224, 168, 153		
17	1-PC (18:1)	19.44 ^a C ₂₆ H ₅₂ O ₇ NP	522,3535 ^a	- 3.59 ^a			504, 184	+	+
					566,3451 ^b	-0.27 ^b	506, 281; MS ³ (506): 281, 242, 224, 168, 153		
18	1-PC (18:0)	24.31 ^a C ₂₆ H ₅₄ O ₇ NP			568,3601 ^b	-1.36 ^b	508; MS ³ (508): 283, 242 , 224, 168, 153	+	-
19	1-PC (18:0)	25.95 ^a C ₂₆ H ₅₄ O ₇ NP			568,3603 ^b	-1.06 ^b	508; MS ³ (508): 283, 242 , 224, 168, 153	+	+
20	PC (18:2;18:2)	33.15 ^a C ₄₄ H ₈₀ O ₈ NP			826,5597 ^c	0.52 ^c	766; MS ³ (766): 504, 279	+	+
21	PC (16:0;18:2)	35.25 ^c C ₄₂ H ₈₀ O ₈ NP			802,5600 ^c	0.92 ^c	742; MS ³ (742): 504, 480, 462, 279, 255	+	+

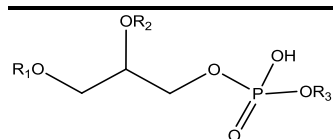
22	PC (18:2;18:1)	36.44 ^c C ₄₄ H ₈₂ O ₈ NP	828,5746 ^c	-0.39 ^c	768; MS ³ (768): 506, 504, 488, 486, 281, 279	+	+
23	PC (16:0;18:1)	39.13 ^c C ₄₂ H ₈₂ O ₈ NP	804,5750 ^c	0.12 ^c	744; MS ³ (744): 488, 480, 462, 281, 255	+	+
24	PC (18:1;18:1)	40.54 ^c C ₄₄ H ₈₄ O ₈ NP	830,5911 ^c	0.60 ^c	770; MS ³ (770): 506, 488, 281	+	+
<i>l</i>-PE and PE							
n° Compound	R _t (min)	Formula	[M-H] ⁻	Δ ppm	Characteristic ions	product	TGR TGF
25	l-PE (18:2)	14.78 ^b C ₂₃ H ₄₄ O ₇ NP	476,2766 ^b	-1.17 ^b	415, 279, 214, 196 , 153	+	-
26	l-PE (18:2)	15.32 ^b C ₂₃ H ₄₄ O ₇ NP	476,2770 ^b	-0.26 ^b	415, 279, 214, 196 , 153	+	+
27	l-PE (16:0)	16.15 ^b C ₂₁ H ₄₄ O ₇ NP	452,2768 ^b	-0.89 ^b	391, 255, 214, 196 , 153	+	-
28	l-PE (16:0)	17.01 ^b C ₂₁ H ₄₄ O ₇ NP	452,2764 ^b	-1.69 ^b	391, 255, 214, 196 , 153	+	+
29	l-PE (18:1)	17.79 ^b C ₂₃ H ₄₆ O ₇ NP	478,2923 ^b	-1.02 ^b	417, 281, 214, 196 , 153	+	+
30	l-PE (18:1)	18.74 ^b C ₂₃ H ₄₆ O ₇ NP	478,2924 ^b	-0.89 ^b	417, 281, 214, 196 , 153	+	+
31	l-PE (18:0)	24.67 ^b C ₂₃ H ₄₈ O ₇ NP	480,3079 ^b	-1.26 ^b	419, 283, 214, 196 , 153	+	-
32	PE (16:0;18:2-10)	22.25 ^c C ₃₉ H ₇₄ O ₉ NP	730,5023 ^c	0.79 ^c	712, 492, 474, 452, 295, 255	+	-
33	PE (18:2;18:1-10)	22.30 ^c C ₄₁ H ₇₆ O ₉ NP	756,5179 ^c	0.75 ^c	738, 494, 476, 297, 279	+	-
34	PE (16:0;18:2-20)	22.71 ^c C ₃₉ H ₇₄ O ₁₀ NP	746,4976 ^c	1.31 ^c	728, 710, 490, 472, 452, 434, 391, 311, 293, 255	+	-
35	PE (18:2-10;18:1)	22.80 ^c C ₄₁ H ₇₆ O ₉ NP	756,5185 ^c	1.14 ^c	738, 492, 478, 474, 295, 281	+	-
36	PE (18:2;18:1-20)	23.35 ^c C ₄₁ H ₇₆ O ₁₀ NP	772,5134 ^c	1.41 ^c	754, 736, 492, 476, 474, 313, 295, 279	+	-
37	PE (16:0;18:1-20)	23.94 ^c C ₃₉ H ₇₆ O ₁₀ NP	748,5139 ^c	2.08 ^c	730, 712, 510, 492, 452, 434, 391, 313, 295, 255	+	-
38	PE (18:1;18:1-20)	24.81 ^c C ₄₁ H ₇₈ O ₁₀ NP	774,5294 ^c	1.87 ^c	756, 738, 510, 492, 478, 460, 431, 417, 313, 295, 281	+	-
39	PE (18:2;18:2)	28.82 ^c C ₄₁ H ₇₄ O ₈ NP	738,5078 ^c	1.36 ^c	476, 458, 279	+	+
40	PE (16:0;18:2)	30.69 ^c C ₃₉ H ₇₄ O ₈ NP	714,5075 ^c	0.92 ^c	476, 458, 452, 434, 279, 255	+	+
41	PE (18:2;18:1)	32.01 ^c C ₄₁ H ₇₆ O ₈ NP	740,5232 ^c	0.99 ^c	478, 476, 460, 458, 281, 279	+	+
42	PE (16:0;18:1)	34.06 ^c C ₃₉ H ₇₆ O ₈ NP	716,5234 ^c	1.25 ^c	478, 460, 452, 434, 281, 255	+	+

43	PE (18:1; 18:1)	35.48 ^c	C ₄₁ H ₇₈ O ₈ NP	742.5391 ^c	1.33 ^c	504, 486, 478, 460, 281	+	+		
NA-GPE										
n° Compound	R _f	(min)	Formula	[M+H] ⁺	[M-H] ⁻	Δ ppm	Characteristic ions	product	TGR	TGF
44	NA-GPE (18:2)	24.94 ^d 12.46 ^e	C ₂₃ H ₄₄ O ₇ NP	478.2925 ^d		-0.64 ^d	460, 324, 306		+	+
					476.2771 ^e	1.33 ^c	402, 384, 278, 214, 171 , 153			
45	NA-GPE (18:1)	33.76 ^d 13.38 ^e	C ₂₃ H ₄₆ O ₇ NP	480.3070 ^d		-3.05 ^d	462, 326, 308		+	+
					478.2930 ^e	0.82 ^e	404, 386, 280, 214, 171 , 153			
l-PI and PI										
n° Compound	R _f	(min)	Formula	[M-H] ⁻	Δ ppm	Characteristic ions (m/z)	product	TGR	TGF	
46	l-PI (18:2- 1O)	12.95 ^b	C ₂₇ H ₄₉ O ₁₃ P	611.2819 ^b	-1.38 ^b	449, 431, 333, 315, 295, 277, 241 , 223		+	-	
47		13.36 ^b		611.2814 ^b	-2.08 ^b					
48		13.91 ^b		611.2813 ^b	-2.28 ^b					
49	l-PI (18:1- 1O)	14.69 ^b	C ₂₇ H ₅₁ O ₁₃ P	613.2963 ^b	-3.41 ^b	433, 333, 315, 297, 241 , 223		+	-	
50		15.32 ^b		613.2977 ^b	-1.12 ^b					
51	l-PI (18:1- 2O)	15.92 ^b	C ₂₇ H ₅₁ O ₁₄ P	629.2921 ^b	-1.84 ^b	611, 499, 449, 431, 333, 315, 313, 295, 241		+	-	
52		16.65 ^b		629.2926 ^b	-1.06 ^b					
53		17.19 ^b		629.2928 ^b	-0.76 ^b					
54	l-PI (18:2)	23.53 ^b	C ₂₇ H ₄₉ O ₁₂ P	595.2873 ^b	-0.84 ^b	415, 333, 315, 279, 241 , 223, 171		+	+	
55	l-PI (18:2)	25.26 ^b	C ₂₇ H ₄₉ O ₁₂ P	595.2874 ^b	-0.67 ^b	415, 333, 315, 279, 241 , 223, 171		+	+	
56	l-PI (16:0)	26.90 ^b	C ₂₅ H ₄₉ O ₁₂ P	571.2875 ^b	-0.51 ^b	409, 391, 333, 315, 255, 241 , 223, 171		+	+	
57	l-PI (16:0)	29.50 ^b	C ₂₅ H ₄₉ O ₁₂ P	571.2873 ^b	-0.87 ^b	409, 391, 333, 315, 255, 241 , 223, 171		+	+	
58	l-PI (18:1)	31.46 ^b	C ₂₇ H ₅₁ O ₁₂ P	597.3028 ^b	-1.07 ^b	435, 417, 333, 315, 281, 241 , 223, 171		+	+	
59	l-PI (18:1)	34.11 ^b	C ₂₇ H ₅₁ O ₁₂ P	597.3030 ^b	-0.75 ^b	435, 417, 333, 315, 281, 241 , 223, 171		+	+	
60	l-PI (18:0)	46.60 ^b	C ₂₇ H ₅₃ O ₁₂ P	599.3182 ^b	-1.42 ^b	437, 419, 333, 315, 283, 241 , 223		+	+	
61	PI (18:2- 2O;18:2)	16.55 ^c	C ₄₅ H ₇₉ O ₁₅ P	889.5074 ^c	0.12 ^c	609, 577, 447, 431, 311 , 293, 279		+	-	
62	PI (18:2- 2O;16:0)	17.19 ^c	C ₄₃ H ₇₉ O ₁₅ P	865.5079 ^c	0.68 ^c	703, 609, 553, 447, 311 , 297, 255 , 241		+	-	
63	PI (18:1- 2O;18:1)	17.28 ^c	C ₄₅ H ₈₃ O ₁₅ P	893.5389 ^c	0.37 ^c	731, 713, 629, 611, 579, 449, 315, 313 , 297, 281		+	-	

64	PI (18:2- 10;18:2)	18.42 ^c C ₄₅ H ₇₉ O ₁₄ P	873,5129 ^c	0,63 ^c	855, 711, 611, 593, 577, 449, 431, 415, 315, 295 , 297, 279	+	-
65	PI (18:2- 10;16:0)	19.29 ^c C ₄₃ H ₇₉ O ₁₄ P	849,5129 ^c	0,64 ^c	831, 687, 593, 553, 431, 391, 315, 295 , 255 , 241	+	-
66	PI (18:1;18:2- 10)	19.97 ^c C ₄₅ H ₈₁ O ₁₄ P	875,5283 ^c	0,31 ^c	713, 611, 593, 579, 431, 417, 315, 297, 295 , 281	+	-
67	PI (18:1- 10;16:0)	20.11 ^c C ₄₃ H ₈₁ O ₁₄ P	851,5286 ^c	0,67 ^c	689, 595, 571, 553, 433, 391, 315 297 , 255 , 241	+	-
68	PI (18:2- 10;18:2)	20.34 ^c C ₄₅ H ₇₉ O ₁₄ P	873,5129 ^c	0,62 ^c	611, 593, 577, 449, 431, 415, 315, 297, 295 , 279	+	-
69	PI (16:0;18:1- 20)	20.52 ^c C ₄₃ H ₈₁ O ₁₅ P	867,5235 ^c	0,66 ^c	849, 611, 571, 553, 535, 391, 315, 313 , 297, 295, 255 , 241	+	-
70	PI (18:1- 10;18:1)	20.75 ^c C ₄₅ H ₈₅ O ₁₄ P	877,5439 ^c	0,31 ^c	715, 613, 595, 579, 433, 417, 315, 297 , 281	+	-
71	PI (18:2- 10;16:0)	21.12 ^c C ₄₃ H ₇₉ O ₁₄ P	849,5129 ^c	0,62 ^c	831, 593, 571, 553, 431, 409, 391, 315, 297, 295 , 255 , 241	+	-
72	PI (18:2- 10;18:1)	21.75 ^c C ₄₅ H ₈₁ O ₁₄ P	875,5283 ^c	0,29 ^c	857, 713, 611, 593, 579, 431, 417, 315, 295 , 281	+	-
73	PI (18:3;18:2)	22.16 ^c C ₄₅ H ₇₇ O ₁₃ P	855,5023 ^c	0,53 ^c	595, 593, 577, 575, 433, 431, 415, 413, 315, 297, 279 , 277 , 241	+	+
74	PI (18:0;18:1- 10)	22.57 ^c C ₄₅ H ₈₅ O ₁₄ P	879,5598 ^c	0,58 ^c	717, 599, 595, 581, 433, 419, 315, 297 , 283	+	-
75	PI (16:1;18:2)	22.62 ^c C ₄₃ H ₇₇ O ₁₃ P	831,5021 ^c	0,40 ^c	813, 669, 577, 569, 551, 415, 389, 297, 279 , 253 , 241	+	+
76	PI (18:2;16:1)	22.98 ^c C ₄₃ H ₇₇ O ₁₃ P	831,5022 ^c	0,49 ^c	813, 577, 569, 551, 415, 389, 315, 297, 279 , 253 , 241	+	+
77	PI (18:2;18:2)	23.58 ^c C ₄₅ H ₇₉ O ₁₃ P	857,5177 ^c	0,26 ^c	595, 577, 433, 415, 315, 297, 279 , 241	+	+
78	PI (16:0;18:2)	24.58 ^c C ₄₃ H ₇₉ O ₁₃ P	833,5174 ^c	-0,09 ^c	577, 571, 553, 415, 391, 315, 297, 279 , 255 , 241	+	+
79	PI (18:1;18:2)	25.63 ^c C ₄₅ H ₈₁ O ₁₃ P	859,5334 ^c	0,35 ^c	597, 579, 435, 417, 315, 297, 281 , 279 , 241	+	+
80	PI (16:0;18:1)	26.91 ^c C ₄₃ H ₈₁ O ₁₃ P	835,5334 ^c	0,40 ^c	673, 579, 571, 553, 417, 391, 315, 297, 281 , 255 , 241	+	+
81	PI (18:1;18:1)	28.23 ^c C ₄₅ H ₈₃ O ₁₃ P	861,5492 ^c	0,53 ^c	699, 597, 579, 435, 417, 315, 297, 281 , 241	+	+
82	PI (18:0;18:1)	31.65 ^c C ₄₅ H ₈₅ O ₁₃ P	863,5647 ^c	0,36 ^c	599, 581, 437, 419, 315, 297, 283 , 281 , 241	+	+

a = Calculated from the LC-MS analysis of TGR on Atlantis T3 column in positive ion mode; b = Calculated from the LC-MS analysis of TGR on Atlantis T3 column in negative ion mode; c = Calculated from the LC-MS analysis of TGR on Simmetry C4 column in negative ion mode; d = Calculated from the LC-MS analysis of TGF on Atlantis T3 column in positive ion mode; e = Calculated from the LC-MS analysis of TGF on Simmetry C4 column in negative ion mode.

The 18-carbon (or 16-carbon) hydroxylated acyl chain is abbreviated, e.g., as 18:1-1O and 18:1-2O, to indicate one double bond equivalent and one or two oxygen atoms beyond the carbonyl group.

Table 3.4. l-PS, l-PA and PA, l-PG and PG putatively identified in TG hazelnut kernel.

R₁ and R₂ = fatty acyl chain or hydrogen

R₃ = serine in l-PS, hydrogen in l-PA and PA, glycerol in l-PG and PG

n°	Compound	R _t (min)	Molecular Formula	[M-H] ⁻	Δ ppm	Characteristic product ions (m/z)	TGR	TGF
<i>l-PS</i>								
83	l-PS (18:1)	23.12 ^a	C ₂₄ H ₄₆ O ₉ NP	522,2822 ^a	-0.79 ^a	504, 435 , 153	+	+
84	l-PS (18:1)	25.77 ^a	C ₂₄ H ₄₆ O ₉ NP	522,2825 ^a	-0.45 ^a	435 , 153	+	+
<i>l-PA and PA</i>								
85	l-PA (18:2)	32.42 ^b	C ₂₁ H ₃₉ O ₇ P	433,2349 ^b	-0.11 ^b	415, 279, 153 , 135	+	+
86	l-PA (18:2)	34.47 ^b	C ₂₁ H ₃₉ O ₇ P	433,2349 ^b	-0.05 ^b	415, 279, 153 , 135	+	+
87	l-PA (16:0)	41.95 ^b	C ₁₉ H ₃₉ O ₇ P	409,2347 ^b	-0.28 ^b	391, 255, 153	+	+
88	l-PA (18:1)	44.73 ^b	C ₂₁ H ₄₁ O ₇ P	435,2505 ^b	-0.16 ^b	417, 281, 153 , 135	+	+
89	l-PA (18:1)	47.69 ^b	C ₂₁ H ₄₁ O ₇ P	435,2503 ^b	-0.27 ^b	417, 281, 153 , 135	+	+
90	PA (18:2;18:2)	36.88 ^c	C ₃₉ H ₆₉ O ₈ P	695,4655 ^c	1.27 ^c	433, 415, 279	+	+
91	PA (16:0;18:2)	39.16 ^c	C ₃₇ H ₆₉ O ₈ P	671,4656 ^c	1.50 ^c	433, 415, 409, 391, 279 , 255	+	+
92	PA (18:1;18:2)	40.49 ^c	C ₃₉ H ₇₁ O ₈ P	697,4814 ^c	1.57 ^c	435, 433, 417, 415, 281 , 279	+	+
93	PA (16:0;18:1)	44.46 ^c	C ₃₇ H ₇₁ O ₈ P	673,4810 ^c	1.01 ^c	435, 417, 409, 391, 281 , 255	+	+
94	PA (18:1;18:1)	46.28 ^c	C ₃₉ H ₇₃ O ₈ P	699,4966 ^c	1.01 ^c	435, 417, 281	+	+
<i>l-PG and PG</i>								
95	l-PG (18:1)	13.09 ^c	C ₂₄ H ₄₇ O ₉ P	509,2887 ^c	1.30 ^c	417, 281, 245 , 227 , 153	+	+
96	l-PG (18:1)	13.36 ^c	C ₂₄ H ₄₇ O ₉ P	509,2885 ^c	1.08 ^c	417, 281, 245 , 227 , 153	+	+
97	PG (16:0;18:2)	30.42 ^c	C ₄₀ H ₇₅ O ₁₀ P	745,5023 ^c	1.16 ^c	671, 507, 489, 483, 465, 415, 391, 279 , 255	+	+
98	PG (18:1;18:2)	31.74 ^c	C ₄₂ H ₇₇ O ₁₀ P	771,5182 ^c	1.42 ^c	697, 509, 507, 491, 489, 417, 415, 281 , 279	+	+
99	PG (16:0;18:1)	33.70 ^c	C ₄₀ H ₇₇ O ₁₀ P	747,5176 ^c	0.69 ^c	567, 509, 491, 483, 465, 417, 391, 281 , 255	+	+
100	PG (18:1;18:1)	35.16 ^c	C ₄₂ H ₇₉ O ₁₀ P	773,5339 ^c	1.50 ^c	509, 491, 435, 417, 281	+	+

a = Calculated from the LC-MS analysis of TGR on Atlantis T3 column in negative ion mode; b = Calculated from the LC-MS analysis of TGF on Atlantis T3 column in negative ion mode; c = Calculated from the LC-MS analysis of TGR on Symmetry C4 column in negative ion mode

The fragmentation behaviour of each peak was in agreement with literature data, allowing to identify the 1-PC species reported in table 3.3 and here described for the first time in TG hazelnut kernel^{6, 11}. Unfortunately, the *sn*-1/*sn*-2 position of the acyl chain on the glycerol backbone could not be determined; notwithstanding this, it could be declared that likely both the lyso-forms occurred in the TGR extract, being present three couples of compounds sharing the same molecular formula two by two. Apparently, apart for the lack of the compounds eluted at 16.75 min, the TGF extract showed the same results, even though with a lower ion peak intensity (fig. 3.4).

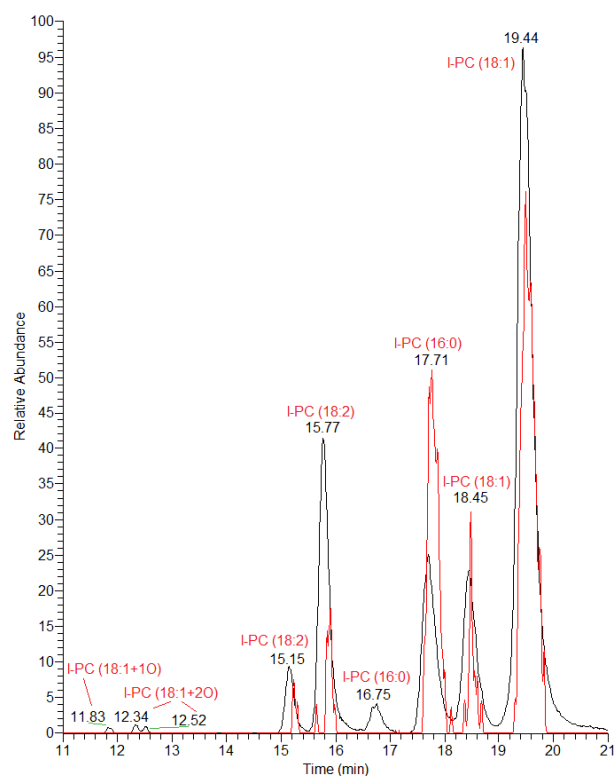


Figure 3.4. Extracted ion chromatograms of 1-PC ions from the LC-MS analysis of TGF and TGR extracts on Atlantis T3 column in ESI positive ion mode (Normalized level: TGR 1.5×10^7 ; TGF 1.5×10^5).

Noteworthy the analysis of the positive LC-ESI/LTQOrbitrap/MS/MSⁿ spectra highlighted, in the only TGR extract, the presence of three minor compounds belonging to the 1-PC class but showing molecular formulae characterized by NO₈P and NO₉P heteroatom composition, suggesting the presence of mono- and dihydroxylated fatty acid unit, respectively (fig. 3.4). In fact in all cases, in addition to the product ion at *m/z* 184 Da, main product ions originated by consecutive neutral losses of one or two water molecules from the [M+H]⁺ ion were present in the relative MS² spectrum, along with a common product ion at *m/z* 258 Da, corresponding to the phosphocholine-glycerol ion and originated by the neutral loss of the ketene form of the relative hydroxylated fatty acid (table 3.2). Once again, the regiospecificity of the relative acyl linkage could not be clearly assigned.

Noteworthy, 1-OH-PC species seem to be not present in TGF extract, allowing to suppose that the high roasting temperature have decreased the stability of hazelnut, mainly affecting the primary oxidation of lipids. This is in agreement with previous studies showing that high temperatures cause an increase in lipid oxidation rates².

To the best of our knowledge, this is the first report of 1-OH-PC species in hazelnut kernels, so far **9-11** being reported only in rice seed and jojoba seed meal¹².

Interestingly, the analysis of the LC-ESI/LTQOrbitrap/MS/MSⁿ spectra of both TGR and TGF extract acquired in negative ion mode on Symmetry C4 column displayed exclusively not hydroxylated PC species (table 3.3; fig. 3.5), characterized by molecular [(M+FA)-H]⁻ anions formed as adducts with formic acid, yielding a main [M-15]⁻ product ion in the MS² spectrum.

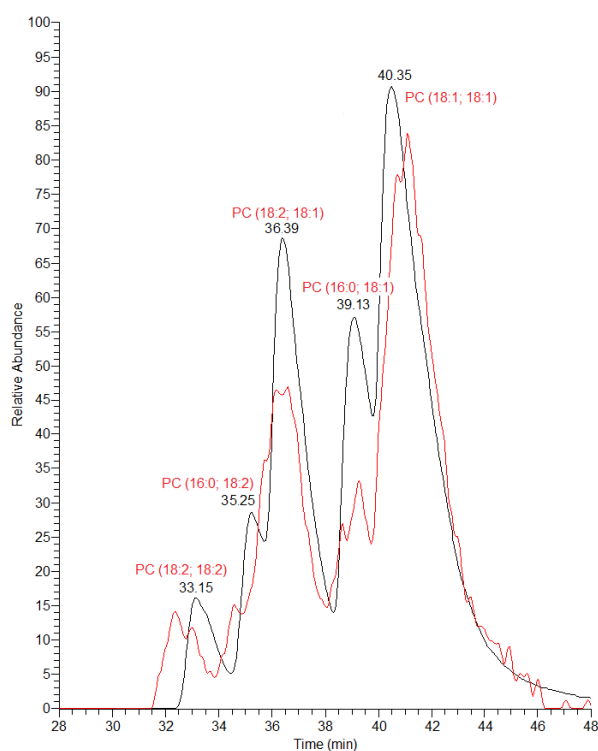


Figure 3.5. Extracted ion chromatograms of PC ions from the LC-ESI/LTQOrbitrap/MS analysis of TGF and TGR extracts on Symmetry C4 column in ESI negative ion mode (Normalized level: TGR 5.0×10^6 ; TGF 5.0×10^4).

The analysis of the MS^3 spectra obtained by this product ion allowed to identify the fatty acids, yielding the $[(M-15)-R_xCOOH]^-$ product ions along with the two R_xCOO^- anions and the product ions originated by the neutral loss of the ketene fatty acyl chain; the regiochemistry of the acyl chains could also be determined⁶. In this way, even though with an intensity difference, in both TGR and TGF kernel it could be appreciated the presence of five PC species (table 3.3), among which only **20-22** have already been described in hazelnut¹¹.

The analysis of negative MS^2 spectra allowed to ascertain, in both TGR and TGF extract, the presence of l-PE and PE species (table 3.3; fig. 3.6A-B).

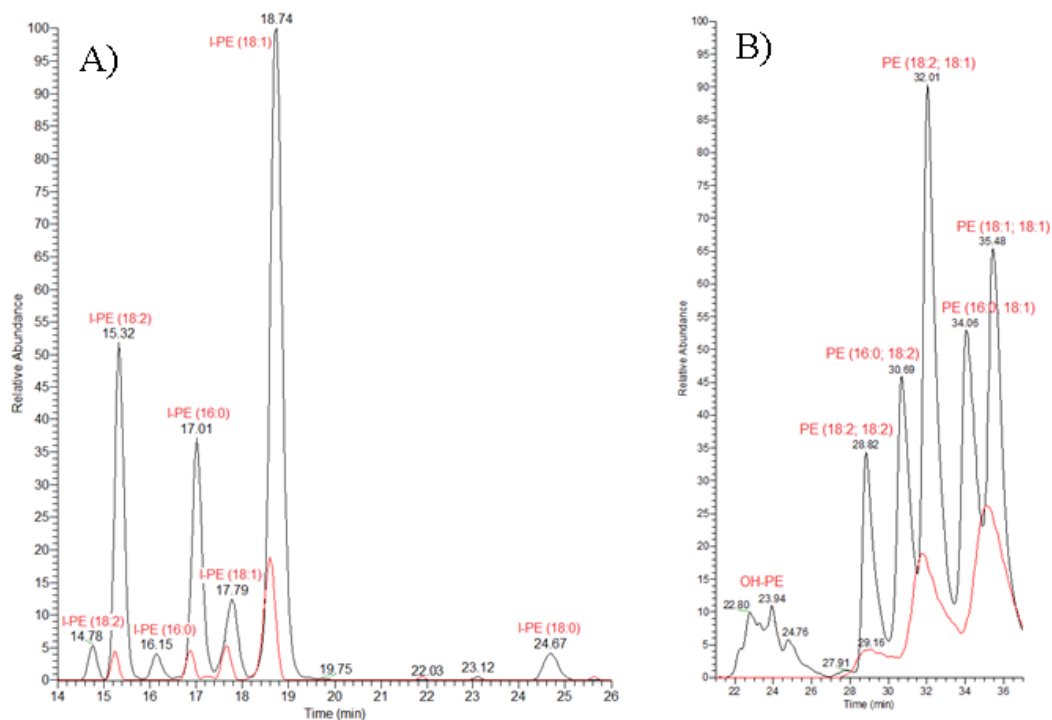


Figure 3.6. A) Extracted ion chromatograms of l-PE ions from the LC-MS analysis of TGF and TGR extracts on Atlantis T3 column in ESI negative ion mode. (Normalized level: TGR 1.2×10^6 ; TGF 1.2×10^5). B) Extracted ion chromatograms of PE ions from the LC-MS analysis of TGF and TGR extracts on Symmetry C4 column in ESI negative ion mode. (Normalized level: TGR and TGF 2.0×10^6).

Tandem mass spectra of l-PE were characterized by diagnostic product ions at m/z 214, 196 and 153 Da, corresponding to the glycerophosphatidylamine ion and to the mono-dehydrated forms of glycerophosphatidylamine and glycerol-phosphate ions, respectively, along with the abundant RCOO^- ion and the product ion obtained by neutral loss of ethanolamine from the $[\text{M-H}]^-$ ion (table 3.3). Analogously, the MS^2 spectra of PE species displayed minor¹¹ $[(\text{M-R}_x\text{COOH})\text{-H}]^-$, and $[(\text{M-R}_x=\text{CO})\text{-H}]^-$ product ions along with abundant carboxylate anions of *sn*-1 and *sn*-2 acyl residues (with $\text{R}_2\text{COO}^- > \text{R}_1\text{COO}^-$), each one originated by neutral loss of 197 Da (corresponding to the mono-dehydrated form of glycerol-

phosphatidylamine) from the $[(M-R_x=CO)-H]^-$ ion (table 3.3). Among the l-PE and the PE molecules detected, only PE **39-43** have been already described in hazelnut¹¹.

Once again, as well as for l-PC species, hydroxylated PE (OH-PE) species were detectable only in the TGR extract. Negative tandem mass spectra of compounds **32-38** were characterized by abundant R_xCOO^- anions, one of them being ascribable to a mono- or dihydroxylated unsaturated fatty acid, along with $[(M-R_xCOOH)-H]^-$ and $[(M-R_x=CO)-H]^-$ ions, and product ions formed by neutral loss of one or two water molecules¹³ (table 3.3; fig. 3.6B). The occurrence of OH-PE species in roasted hazelnut kernels is here reported for the first time, even though this class has been already described - along with other oxidized complex lipid species involving PC, PG, MGDG, and DGDG species - as lipid oxidation products with increased levels in plant under stress conditions like thermal treatment, hypoxia, light/darkness exposition, and wounding^{14, 15}. Nevertheless, to the best of our knowledge, oxidized complex PEs in which the oxylipin corresponds to 18:1-1O or 18:1-2O (**33, 36-38**) have not yet been reported so far (table 3.3).

The careful analysis of both positive and negative TGF and TGR LC-ESI/LTQOrbitrap/MS/MSⁿ spectra highlighted the presence of two compounds (**44-45**) showing the same molecular formula and the same NO_7P heteroatom composition of l-PE **25-26** and **29-30**, respectively, but displaying a different MS² fragmentation pattern and eluting at a later retention time (table 3.3; fig. 3.7). The comparison with literature data allowed to identify them as *N*-acylglycerophosphoethanolamines (NA-GPEs)¹⁶.

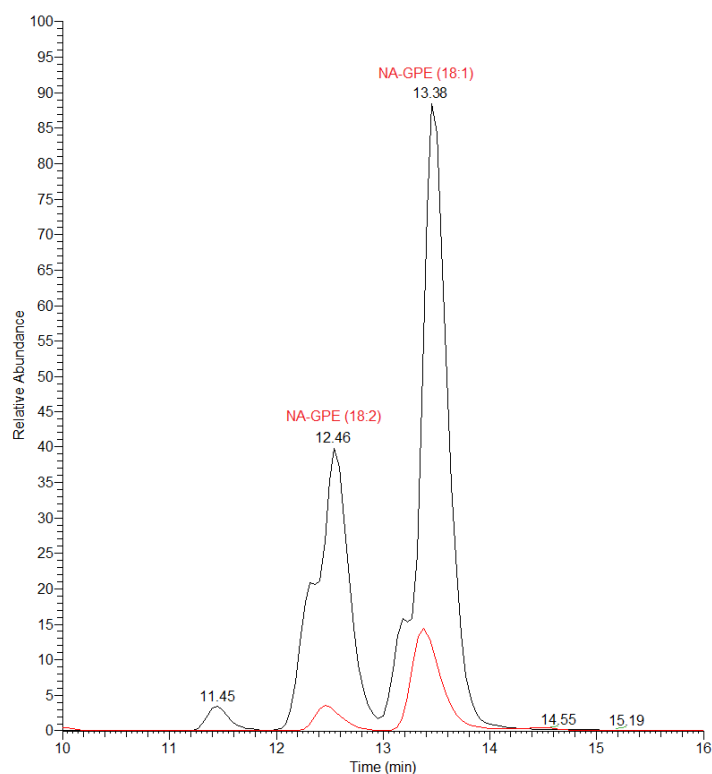


Figure 3.7. Extracted ion chromatograms of NA-GPE ions from the LC-MS analysis of TGF and TGR extracts on Symmetry C4 column in ESI negative ion mode. (Normalized level: TGR and TGF 4.0×10^6).

NAPEs are a widespread, albeit minor, class of membrane phospholipids found in both plants and animals, characterized by unusual structural features (a third fatty acid moiety amide-linked to the amino head group of PE) with bilayer-stabilizing properties. NA-GPEs have been reported as intermediate products of a NAPE-(phospholipase-D)-independent biosynthetic pathway in which both *O*-acyl chains of NAPE are eliminated, followed by hydrolysis of the phosphodiester bond of the resultant NA-GPE, to yield as final product the *N*-acylethanolamine (NAE)¹⁷. This latter gained wide recognition as evolutionarily conserved lipid mediator that modulates various physiological processes in eukaryotic cells, such as neuroprotection, cell proliferation, pain initiation, fertility, apoptosis and food

intake in animals, and responses to pathogens, plant development and germination in plants¹⁸. Among different NAEs, anandamide (*N*-arachidonoylethanolamine) has been well characterized since it exerts cannabimimetic actions as an endogenous agonist of cannabinoid receptors. Other NAEs that are inactive at cannabinoid receptors have also attracted attention because of their biological actions. In particular, *N*-palmitoylethanolamine and *N*-oleoylethanolamine have been extensively investigated owing to their anti-inflammatory and analgesic effects and anorexic effect, respectively¹⁷. Thereby, being NA-GPEs species natural precursors of NAEs, it is interesting to highlight their occurrence in hazelnut, as, at the best of our knowledge, they are so far never described in this nut.

The analysis of the LC-ESI/LTQOrbitrap/MS/MSⁿ spectra acquired for both TGR and TGF in negative ion mode on RP-C18 and RP-C4 columns highlighted the presence of l-PI and PI species, by showing the typical fragmentation pattern characterized by the diagnostic product ion at m/z 241 Da, corresponding to the dehydrated form of the inositol-phosphate, and by the [(M-162)-H]⁻ and [(M-180)-H]⁻ product ions formed by neutral loss of the inositol moiety (table 3.3). Product ions generated by neutral loss of one (in l-PI case) or two fatty acyl moieties, and one (in l-PI case) or two ketene fatty acyl moieties, along with the corresponding carboxylate anions (with R₁COO⁻ > R₂COO⁻ in the case of PI species) were also detectable (table 3.3)¹¹. Both roasted and fresh TG hazelnut kernels displayed the same l-PI (**54-60**) and PI (**73, 75-82**) species, here reported for the first time in hazelnut, among which **58-60**, **75-76**, and **81-82** never described before in plants (table 3.3; fig. 3.8A-B).

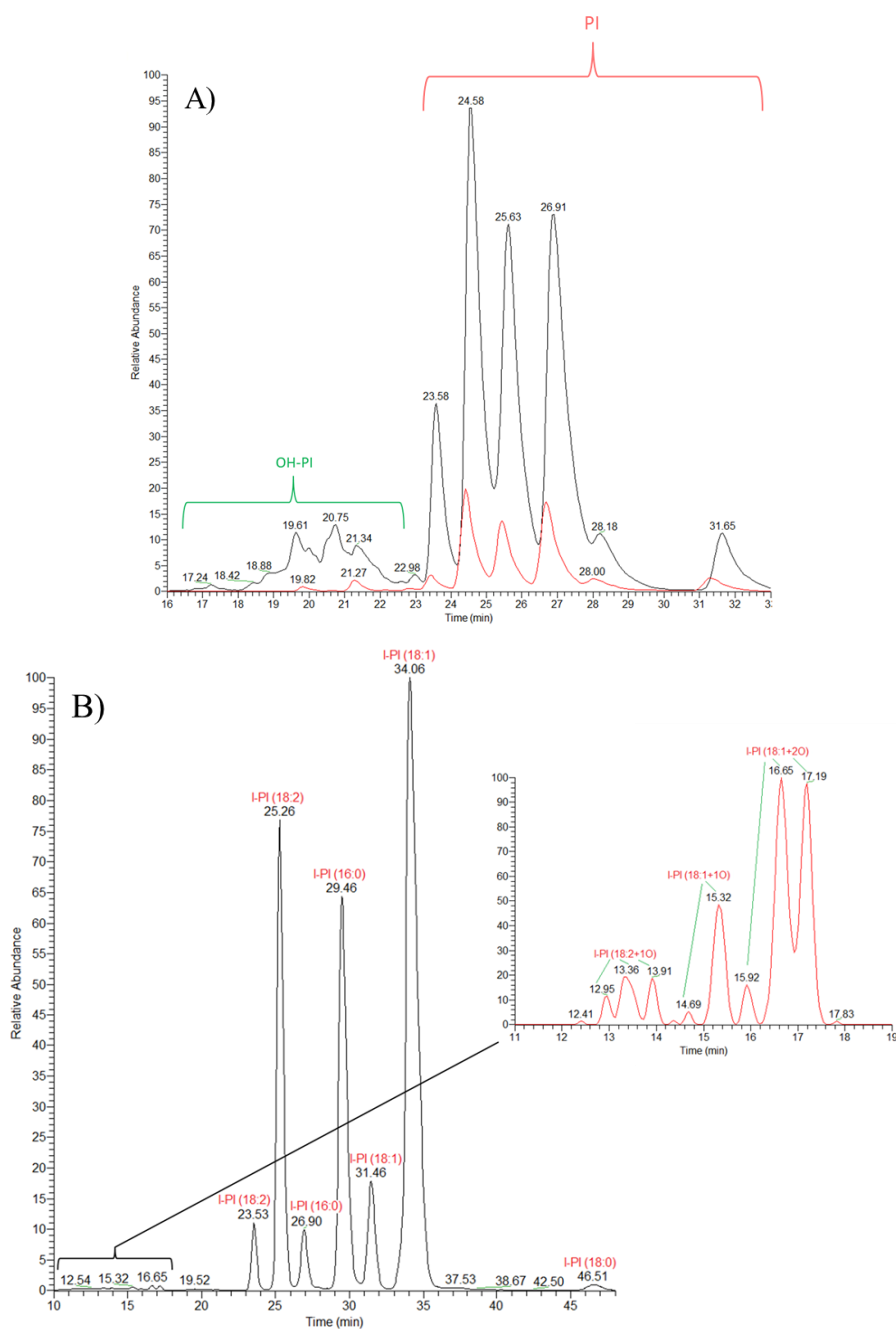


Figure 3.8. A) Extracted ion chromatograms of PI ions from the LC-MS analysis of TGF and TGR extracts on Symmetry C4 column in ESI negative ion mode (Normalized level TGR and TGF: 9.0×10^6). B) Extracted ion chromatograms of I-PI ions from the LC-MS analysis of TGR extract on Atlantis T3 column in ESI negative ion mode. (Normalized level: 6.7×10^6). Red plot = TGF; black plot = TGR.

l-PIs are small membrane-derived lipids. Increasing evidence supports a role for l-PIs as bioactive lipids. Indeed it is now well recognized that l-PIs are not merely intermediates in PIs metabolism without any informational function, but bioactive mediators *per se*. The first reports focusing on the biological activities of l-PIs in fact suggested that they were involved in stimulation of insulin release from pancreatic islets¹⁹. It was then suggested that l-PIs may play a significant role in the regulation of whole body metabolism. Moreover, PI holds a potential of becoming an important dietary supplement due to its biological effects, mainly related to improvement of lipid and cholesterol metabolism in animals and humans, manifested as a decrease of the blood cholesterol and lipids, and relief of the metabolic syndrome²⁰. On these bases it is important to underline the considerable number of l-PI and PI species occurring in TG hazelnut kernels.

Furthermore, a more careful analysis of negative LC-ESI/LTQOrbitrap/MS/MSⁿ spectra allowed to ascertain, such as for PE and l-PC species, the presence of oxidized forms of both l-PI and PI species only in TGR extract (table 3.3; fig. 3.8A-B). The contemporary presence of the diagnostic product ion at m/z 241 Da and of carboxylate anions corresponding to mono- or dihydroxylated fatty acyl chain, along with product ions generated by neutral loss of 162 Da due to the dehydrated inositol moiety, permitted to define the nature of these metabolites (table 3.3), however resulting as minor lipids (fig. 3.8A-B).

Generally the occurrence in plants of oxylipins esterified to complex lipids such as PI seems to be the result of a variety of abiotic and biotic stresses. For example, OH-PI species have been described to accumulate in *Arabidopsis* tissue following the so called hypersensitive response (HR), a strong resistance plant response to pathogenic effectors²¹. Interestingly, most of the OH-PI species observed in TGR (**64-68**, **70-72**, **74**) were also identified, at increased levels, in U87 cells, a human primary glioblastoma cell line, in response to the treatment with combined p53 gene- and chemotherapies, a treatment known to trigger apoptosis and cell cycle

arrest in cancer cells²². Accordingly with these results, the finding of hydroxylated 1-PI and PI species in TGR hazelnut kernels highlights hazelnut as a rich source of bioactive lipids with potential beneficial physiological activities and encourages their use in human nutrition.

Finally, the analysis of negative LC-ESI/LTQOrbitrap/MS/MSⁿ spectra of TGR and TGF allowed to identify in both extracts molecular species belonging to 1-PS, 1-PA, PA, 1-PG and PG classes, on the basis of diagnostic neutral losses of 87 or 92 and 74 Da from the [M-H]⁻ ion relative to 1-PS or 1-PG and PG species, respectively, and of the product ions at *m/z* 153 and 245 Da corresponding to the anhydrous form of the glycerolphosphate and to the glycerophosphoglycerol anion, typical of 1-PA, PA, 1-PG, and PG species (table 3.4; fig. 3.9, fig. 3.10A-B and fig. 3.11).

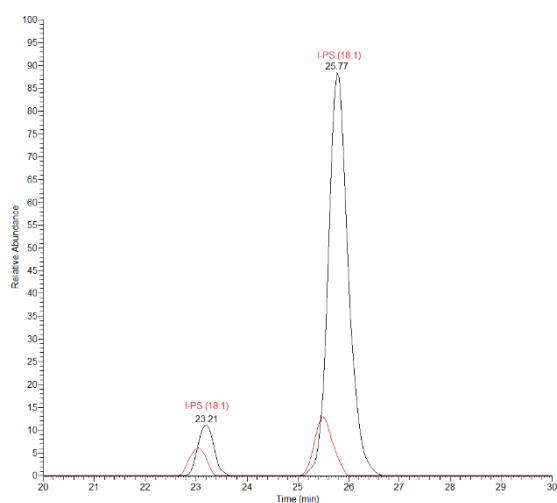


Figure 3.9. Extracted ion chromatograms of l-PS ions from the LC-MS analysis TGF (red plot) and TGR (black plot) extracts on Atlantis T3 column in ESI negative ion mode (Normalized level TGR and TGF: 1.5×10^5).

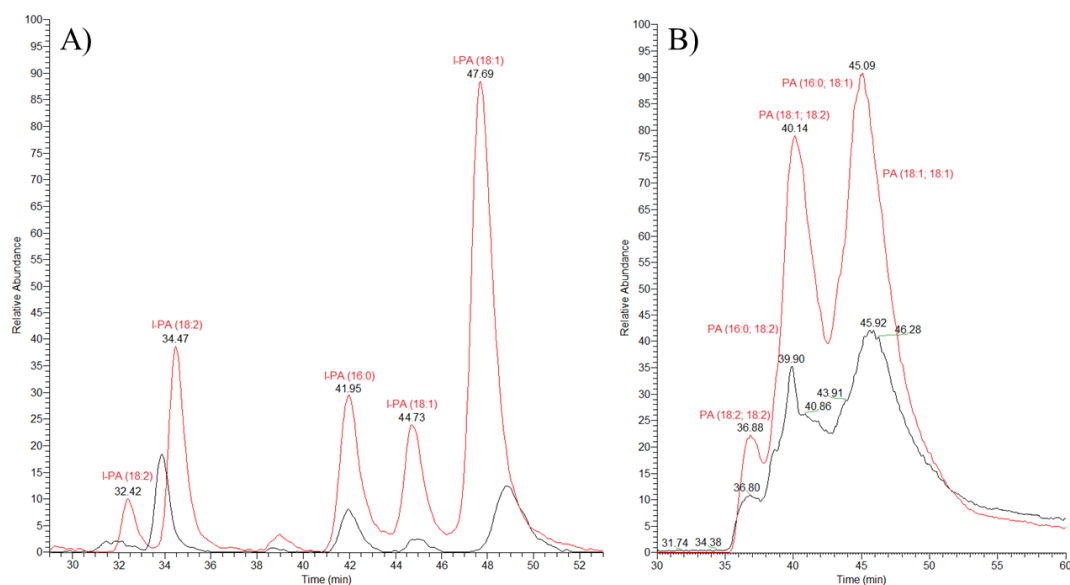


Figure 3.10. A) Extracted ion chromatograms of l-PA ions from the LC-MS analysis TGF and TGR extracts on Atlantis T3 column in ESI negative ion mode (Normalized level TGR and TGF: 5.0×10^5). B) Extracted ion chromatograms of PA ions from the LC-MS analysis TGF and TGR extracts on Symmetry C4 column in ESI negative ion mode (Normalized level TGR and TGF: 3.0×10^6). Red plot = TGF; black plot = TGR.

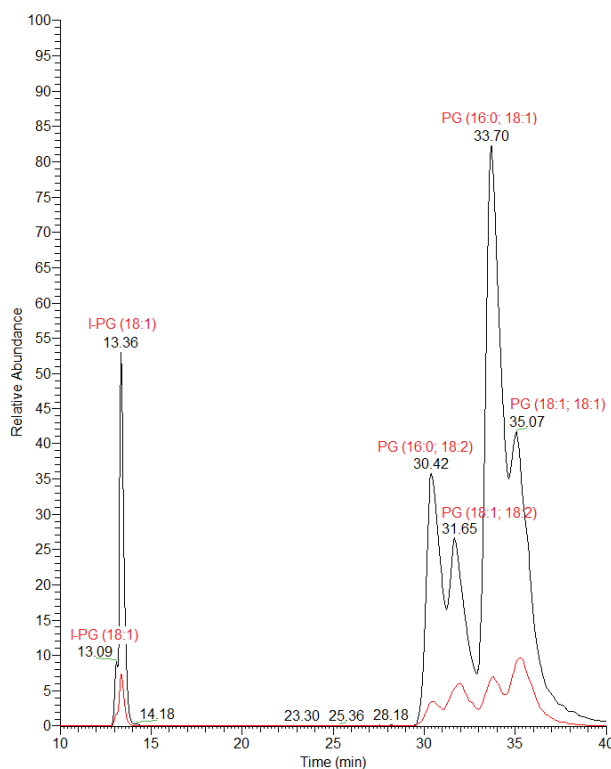


Figure 3.11. Extracted ion chromatograms of I-PG and PG ions from the LC-MS analysis TGF (red plot) and TGR (black plot) extracts on Symmetry C4 column in ESI negative ion mode (Normalized level TGR and TGF: 2.0×10^6).

The product ions relative to $R_x\text{COO}^-$, $[(M-R_x\text{CO}-92)\text{-H}]^-$, $[(M-R_x\text{COOH})\text{-H}]^-$, $[(M-R_x\text{CO})\text{-H}]^-$ and $[(M-74)\text{-H}]^-$ concurred to complete the fragmentation pattern of these phospholipid classes (table 3.4). Among these lipid species, I-PA and PA were more numerous than I-PG/PG and I-PS, and, unlike these latter, showed more intense peaks in TGF than in TGR extract (fig. 3.9, fig. 3.10A-B and fig. 3.11).

l-PA are the best studied lysophospholipid mediators. They play pivotal roles in physiological events including cell proliferation, survival, motility, cytoskeletal changes, and electrophysiological changes as well as pathophysiological processes that include autoimmune disease, fibrotic disease, cancer, inflammation, bone diseases, pain, metabolic syndrome, infertility, and hair loss¹⁰. For instance, l-PA was shown to prevent or restore gastrointestinal disorders, such as diarrhea and stomach ulcer⁹. Because l-PA can be formed from PA by digestive PLA₂, dietary PA can be considered a potential antiulcer phospholipid. l-PS has lipid mediator-like actions too, including stimulation of mast cell degranulation both *in vivo* and *in vitro*, suppression of proliferation of T lymphocytes and induction of neurite outgrowth. Thus, it is possible that l-PS serves as a lipid mediator and is involved in various pathophysiological processes through the l-PS receptors²³.

To the best of our knowledge, this is the first report describing the presence of these phospholipid species in hazelnut, although, for example, **85-89** were already reported in other plant seeds such as walnut²⁴.

Identification of Long-Chain Bases (LCBs), Long-Chain Base Phosphate (LCB-P), and Sphingolipids.

Sphingolipids are an ubiquitous class of lipids present in a variety of organisms including eukaryotes and bacteria. They are major structural lipids of biological membranes and perform additional essential functions as signalling molecules. Although there is considerable structural variation among the sphingolipids from different species, the basic building block of sphingolipids is an amino alcohol long chain base (LCB), which is composed predominantly of 18 carbon atoms²⁵. The LCB is characterized by the presence of a hydroxy group at C1 and C3 and an amine group at C2. The C18 sphinganine is the primary plant sphingolipid LCB from which any other derivative can be generated by subsequent hydroxylation and desaturation steps. Sphinganine (d18:0), 4-hydroxysphinganine (t18:0), *cis*

and *trans* isomers of 8-sphingenine (d18:1⁸), 4,8-sphingadienine (d18:2^{4,8}), and 4-hydroxy-8-sphingenine (t18:1⁸) are the most representative plant long-chain bases²⁵. The LCBs can also be phosphorylated (LCB-Ps) on primary hydroxy group of the LCB moiety as part of their metabolism.

The analysis of LC-ESI/LTQOrbitrap/MS/MSⁿ spectra of TGF *n*-butanol extract in ESI positive ion mode allowed to ascertain the presence of two LCBs (**101** and **102**) (fig. 3.12), showing an intense [M+H]⁺ pseudomolecular ion in the full scan spectrum (table 3.5).

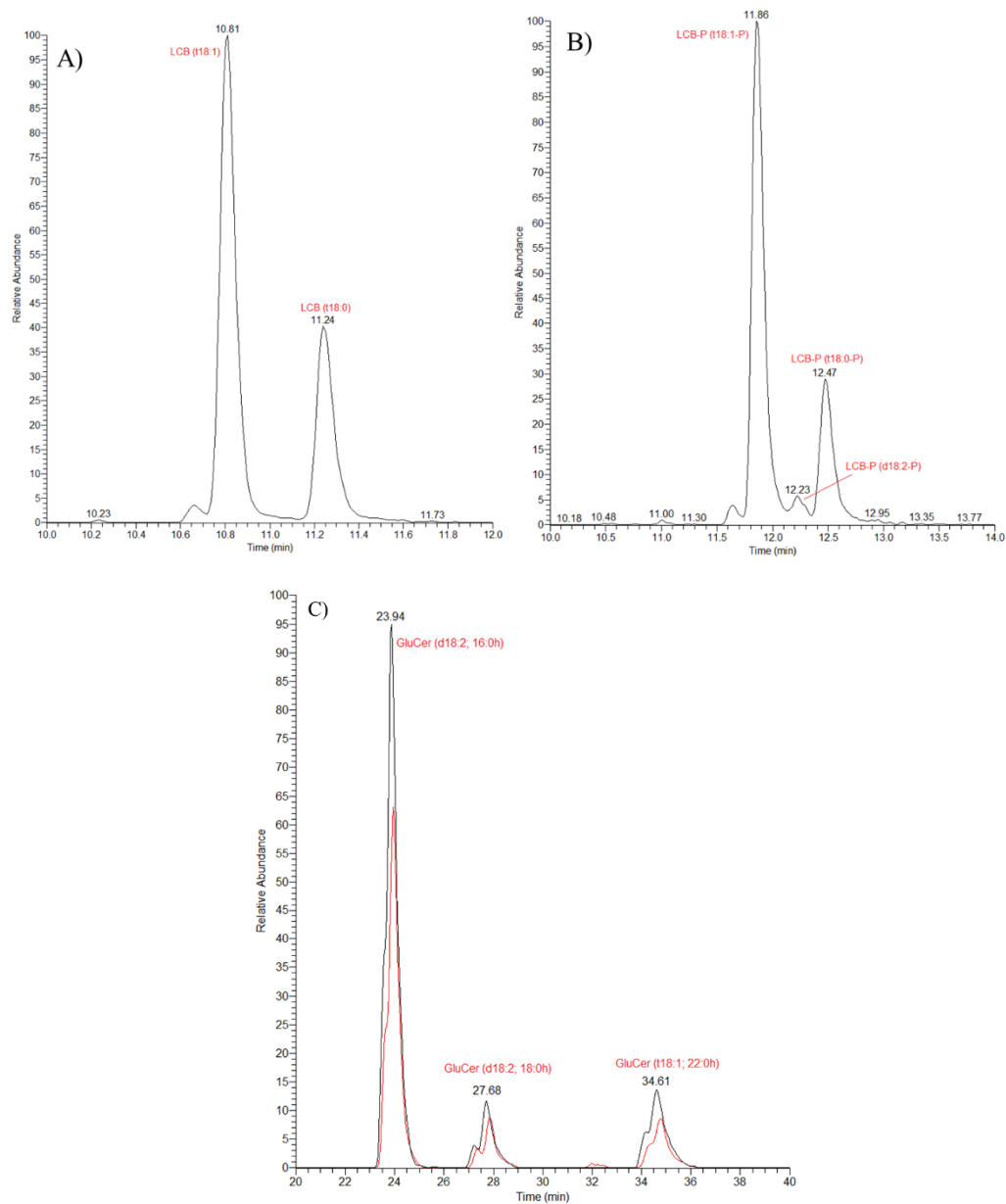
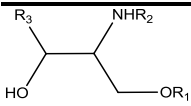


Figure 3.12. A) Extracted ion chromatogram of LCB ions from the LC-MS analysis of TGF extract on Atlantis T3 column in ESI positive ion mode (Normalized level: 1.0×10^7). B) Extracted ion chromatogram of LCB-P ions from the LC-MS analysis of TGF extract on Atlantis T3 column in ESI positive ion mode (Normalized level: 6.4×10^6). C) Extracted ion chromatograms of GluCer ions from the LC-MS analysis of TGF (red plot) and TGR (black plot) extracts on Symmetry C4 column in ESI negative ion mode (Normalized level TGR and TGF: 1.0×10^6).

Table 3.5. LCB, LCB-P and GlcCer putatively identified in TG hazelnut kernel.


R₁ = hydrogen in LCB and ceramide, phosphate in LCB-P, glucose or galactose in cerebroside
R₂ = hydrogen in LCB and in LCB-P, fatty acyl chain in ceramide and cerebroside
R₃ = backbone of the aliphatic amino alcohol composing the long chain base

n°	Compound	R _t (min)	Molecular Formula	[M-H] ⁻	Δ ppm	[M+H] ⁺	Characteristic product ions (m/z)	TGR	TGF
101	LCB (t18:1)	10.77 ^a	C ₁₈ H ₃₇ O ₃ N	-	4.96 ^a	316,2831 ^a	298, 280, 262, 245	-	+
102	LCB (t18:0)	11.21 ^a	C ₁₈ H ₃₉ O ₃ N	-	4.34 ^a	318,2989 ^a	300, 282, 264, 247	-	+
103	LCB-P (t18:1-P)	11.90 ^b	C ₁₈ H ₃₈ O ₆ NP	394,2352 ^b -	0.26 ^b	396,2491 ^a	378, 298, 280, 263, 262 377, 376, 348, 338, 314, 303, 282	-	+
104	LCB-P (d18:2-P)	12.26 ^b	C ₁₈ H ₃₆ O ₅ NP	376,2246 ^b -	0.18 ^b	378.2384 ^a	360, 280, 262, 245 359, 358, 341, 334, 327, 279, 224	-	+
105	LCB-P (t18:0-P)	12.52 ^b	C ₁₈ H ₄₀ O ₆ NP	396,2508 ^b -	0.33 ^b	398,2647 ^a	380, 300, 282, 265, 264 379, 378, 352, 350, 336, 312, 298, 284, 267, 255,225, 224	-	+
106	GlcCer (d18:2;16:0h)	23.94 ^c	C ₄₀ H ₇₅ O ₉ N	712,5369 ^c	1,50 ^c		550, 532, 271, 225; MS ³ (550): 532, 314, 312, 296, 271, 270, 253, 235, 225	+	+
107	GlcCer (d18:2;18:0h)	27.68 ^c	C ₄₂ H ₇₉ O ₉ N	740,5668 ^c	0,46 ^c		578, MS ³ (578): 560, 530, 342, 340, 324, 299, 298, 281, 253	+	+
108	GlcCer (t18:1;22:0h)	34.61 ^c	C ₄₆ H ₈₉ O ₁₀ N	814,6399 ^c	0,47 ^c		652; MS ³ (652): 634, 410, 398, 355, 354, 253	+	+

a = Calculated from the LC-MS analysis of TGF on Atlantis T3 column in positive ion mode; b = Calculated from the LC-MS analysis of TGF on Atlantis T3 column in negative ion mode; c = Calculated from the LC-MS analysis of TGR on Symmetry C4 column in negative ion mode. The nomenclature used to name LCBs consists of a first letter that is “d” for dihydroxylated bases or “t” for trihydroxylated ones, followed of two numbers separated by a colon, indicating the number of carbons and double bonds. In GlcCer nomenclature, the 2-hydroxylated fatty acids are indicated by the letter “h” added to their lipid number (i.e., 16:0h).

The MS² spectra of both LCBs were characterized by the presence of three main product ions originated by consecutive neutral losses of three water molecules, along with a minor product ion (at m/z 245 Da for **101**, and 247 Da for **102**, respectively) formed by neutral loss of an ammonia molecule from the totally dehydrated LCB molecule. This behaviour was consistent with trihydroxylated LCBs, likely 4-hydroxysphinganine (t18:0) and 4-hydroxy-8-sphinganine (t18:1⁸) (table 3.5)²⁶. Analogously, three different free LCB-P species differing for hydroxylation and unsaturation degree could be appreciated in TGF kernels. In fact, as shown in figure 3.12, compounds **103-105** could be assigned to LCB-P (t18:1-P), LCB-P (d18:2-P) and LCB-P (t18:0-P) species, respectively, on the basis of the careful analysis of the relative fragmentation pattern in the positive tandem mass spectrum, as supported by literature data (table 3.5)^{26, 27}. The analysis of the negative LC-ESI/LTQOrbitrap/MS and LC-ESI/LTQOrbitrap/MS/MSⁿ spectra acquired for these peaks confirmed this assignment (table 3.5).

Both LCB **101-102** and LCB-P **103-105** were not found in TGR and are here described for the first time in hazelnut species; in particular the free LCB-P (d18:2-P) has been described so far only in human and murine plasma and in *Drosophila melanogaster*²⁷.

Free LCBs are found in very small amounts in plants, mostly being in the form of complex sphingolipids such as ceramides and ceramide derivatives. To form a ceramide, the amine group of the LCB is acylated with a fatty acid, generally composed of 14-26 carbon atoms which are usually hydroxylated in the 2 position²⁵. Ceramide is the backbone of the sphingolipids detected in cells, and therefore the basic building block for the synthesis of more complex sphingolipids. The basic ceramide structure can be further modified through changes in chain length, methylation, hydroxylation and/or degree of desaturation of both the LCB and fatty acid moieties. Further modifications involve the

conjugation of the primary hydroxy group of the LCB moiety, resulting in a polar headgroup which can be a phosphoryl group (ceramide phosphates), mono- or pluri-hexose (glycosylceramides), and an inositol phosphate group.

The analysis of TGF and TGR extract on Symmetry C4 column in negative ion mode allowed to identify in both extracts three peaks yielding $[M-H]^-$ ions corresponding to molecular formulae of cerebrosides (**106-108**) (fig. 3.12C).

The multicollisional mass spectra of compounds **106-108** confirmed this claim, showing a fragmentation pattern typical of this molecular class, in particular all cerebrosides giving $[(M-162)-H]^-$ and $[(M-180)-H]^-$ product ions in their MS^2 spectra, along with anions of 2-hydroxy fatty acids (which can be used to determine the length of the fatty acyl chain moiety) in the MS^3 spectrum obtained from the relative $[(M-162)-H]^-$ ion, in agreement with literature data²⁵ (table 3.5). Unlike LCBs and LCB-Ps, the cerebroside distribution in TGF and TGR extract was about the same, suggesting that roasting treatment doesn't exert changes in the chemical composition of GlcCers. To our knowledge, although GlcCer **106** and **108** have already been described in hazelnut oil, this is the first report of **107** in hazelnut kernel²⁸.

Sphingolipids are found in many food products; it is estimated that individuals consume ~0.3 to 0.4 g/d. Little is known about the contribution of sphingolipids in the human diet, so there is not any nutritional requirement regarding them. However, studies with experimental animals pointed to a possible role of these lipids in the inhibition of colon carcinogenesis and improvements of the low-density versus high-density lipoprotein cholesterol balance, suggesting they are functional components of food²⁹.

This sphingolipid protective role may be the result of a turnover to bioactive metabolites, including LCBs (sphingosine and sphinganine) and ceramides, which inhibit proliferation and stimulate apoptosis. Sphingadienes (SDs), for example,

are growth-inhibitory LCBs that the enzymes at the brush border of the gut liberate from complex sphingolipids, thereby allowing SDs to be taken up into intestinal epithelial cells²⁹. It was recently demonstrated that SDs exert chemopreventive action in a mouse model of intestinal tumorigenesis. SDs are cytotoxic to colon cancer cells, promoting apoptosis and autophagy by inhibiting Akt (Protein Kinase B) activation, thereby derepressing conserved cell death pathways²⁹. Orally delivered SDs are poorly absorbed into the bloodstream, exhibit a low toxicity profile, and, unlike sphingolipids derived from mammalian sources are poorly converted to the oncogenic lipid sphingosine 1-phosphate (S1P). These features make SDs attractive for their potential utility in colon cancer chemoprevention strategies²⁹.

Although there are no studies on the biological effect of sphingolipids in nuts, investigations using human adenocarcinoma cell line (HT29 cells) found that the toxicities of soy and wheat ceramides were comparable to brain ceramides. Thereby, knowledge about the structures and concentrations of sphingolipids in nuts and their metabolic pathways in human body can become very important²⁸.

Identification of monoacylglycerols (MAG) and glycolipids (DGMG and SQDG)

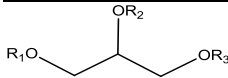
Among glycolipids, sulfolipids and galactolipids, species containing a sulfonic group and one (or two) galactose molecule(s), respectively, have been regarded as the predominant lipid components of the photosynthetic membrane in plants, algae and various bacteria³⁰.

Mono- and digalactosyldiacylglycerols, along with digalactosylmonoacylglycerols (MGDG, DGDG and DGMG) have been observed in significant levels in oat kernels and other seeds³¹. Various studies have shown that galactolipids exhibit specific biological properties including antiviral, antitumor, and anti-inflammatory activities. Additionally, they appear to play a role in the inhibition and promotion of cell growth and in protection against cell death³².

Moreover, monoacylglycerols (MAG) have been reported in plant tissues, in which the MAG product is believed to serve as a precursor for the synthesis of cutin polymers³³. This neutral lipid has long been recognized as a central molecule in lipid resynthesis from dietary fat in animals. MAG released by the action of pancreatic lipases is absorbed in the animal intestine and resynthesised into DAG by monoacylglycerol acyltransferase using fatty acyl-CoA as the acyl-donor³³. In addition, it is now recognized that 2-monoacylglycerols and 2-oleoylglycerol, in particular, have a signalling function in the intestines by activating a specific G-protein-coupled receptor GPR119, sometimes termed the 'fat sensor'. When stimulated, this causes a reduction in food intake and body weight gain in rats and regulates glucose-stimulated insulin secretion³⁴.

The LC-ESI/LTQOrbitrap/MS/MSⁿ analysis allowed to ascertain the presence of DGMG and MAG species in both TGF and TGR kernel (table 3.6).

Table 3.6. MAG, DGMG and SQDG putatively identified in TG hazelnut kernel.

n°	Compound	R _t (min)	Formula	[M-H] ⁻	Δ ppm	[M+H] ⁺	Characteristic product ions (m/z)	TGR	TGF
 <p>R₁ and R₂ = fatty acyl chain or hydrogen in DGMG, fatty acyl chain in SQDG R₃ = digalactose in DGMG, sulfonated glucose in SQDG R₁ R₂ R₃ = one fatty acyl chain and two hydrogen in MAG</p>									
DGMG									
109	DGMG (18:2)	14.05 ^a	C ₃₃ H ₅₈ O ₁₄	677.3743 ^a	0.07 ^a		415, 397, 323, 279, 235	+	+
110	DGMG (18:2)	14.69 ^a	C ₃₃ H ₅₈ O ₁₄	677.3735 ^a	- 1.09 ^a		415, 397, 323, 279, 235	+	+
111	DGMG (18:1)	16.60 ^a	C ₃₃ H ₆₀ O ₁₄	679,3889 ^a	- 1.59 ^a		415, 397, 281, 235	+	+
112	DGMG (18:1)	17.65 ^a	C ₃₃ H ₆₀ O ₁₄	679,3888 ^a	- 1.68 ^a		415, 397, 281, 235	+	+
SQDG									
113	SQDG (16:0; 18:1)	29.92 ^b	C ₄₃ H ₈₀ O ₁₂ S	819,5292 ^b	0.69 ^b		563, 555, 537, 281; MS ³ (563): 545, 519, 299, 225	+	+
114	SQDG (18:1; 18:1)	31.37 ^b	C ₄₅ H ₈₂ O ₁₂ S	845,5449 ^b	0.68 ^b		563, 281; MS ³ (563): 299, 225	+	+
115	SQDG (18:0; 18:1)	35.02 ^b	C ₄₅ H ₈₄ O ₁₂ S	847,5610 ^b	1.26 ^b		565, 563, 283, 281; MS ³ (563): 225	+	+
MAG									
116	MAG (16:0)	46.16 ^c	C ₁₉ H ₃₈ O ₄		- 4.09 ^c	331,2829 ^c	313, 281, 257	+	+
117	MAG (18:1)	47.19 ^c	C ₂₁ H ₄₀ O ₄		- 4.55 ^c	357,2983 ^c	339, 283, 265	+	+
118	MAG (18:1)	48.75 ^c	C ₂₁ H ₄₀ O ₄		- 4.88 ^c	357,2982 ^c	339, 283, 265	+	+
119	MAG (18:0)	54.42 ^c	C ₂₁ H ₄₂ O ₄		- 4.41 ^c	359,3140 ^c	341, 285, 267, 239	+	+
120	MAG (18:0)	55.76 ^c	C ₂₁ H ₄₂ O ₄		- 4.61 ^c	359,3139 ^c	341, 285, 267, 239	+	+

a = Calculated from the LC-MS analysis of TGR on Atlantis T3 column in negative ion mode; b = Calculated from the LC-MS analysis of TGR on Symmetry C4 column in negative ion mode; c = Calculated from the LC-MS analysis of TGF on Atlantis T3 column in positive ion mode.

In particular, in negative ion mode the analysis of the LC-ESI/LTQOrbitrap/MS/MSⁿ highlighted four peaks (**109-112**) characterized by [M-H]⁻ pseudomolecular ions whose molecular formula was referred to DGMG species (fig. 3.13).

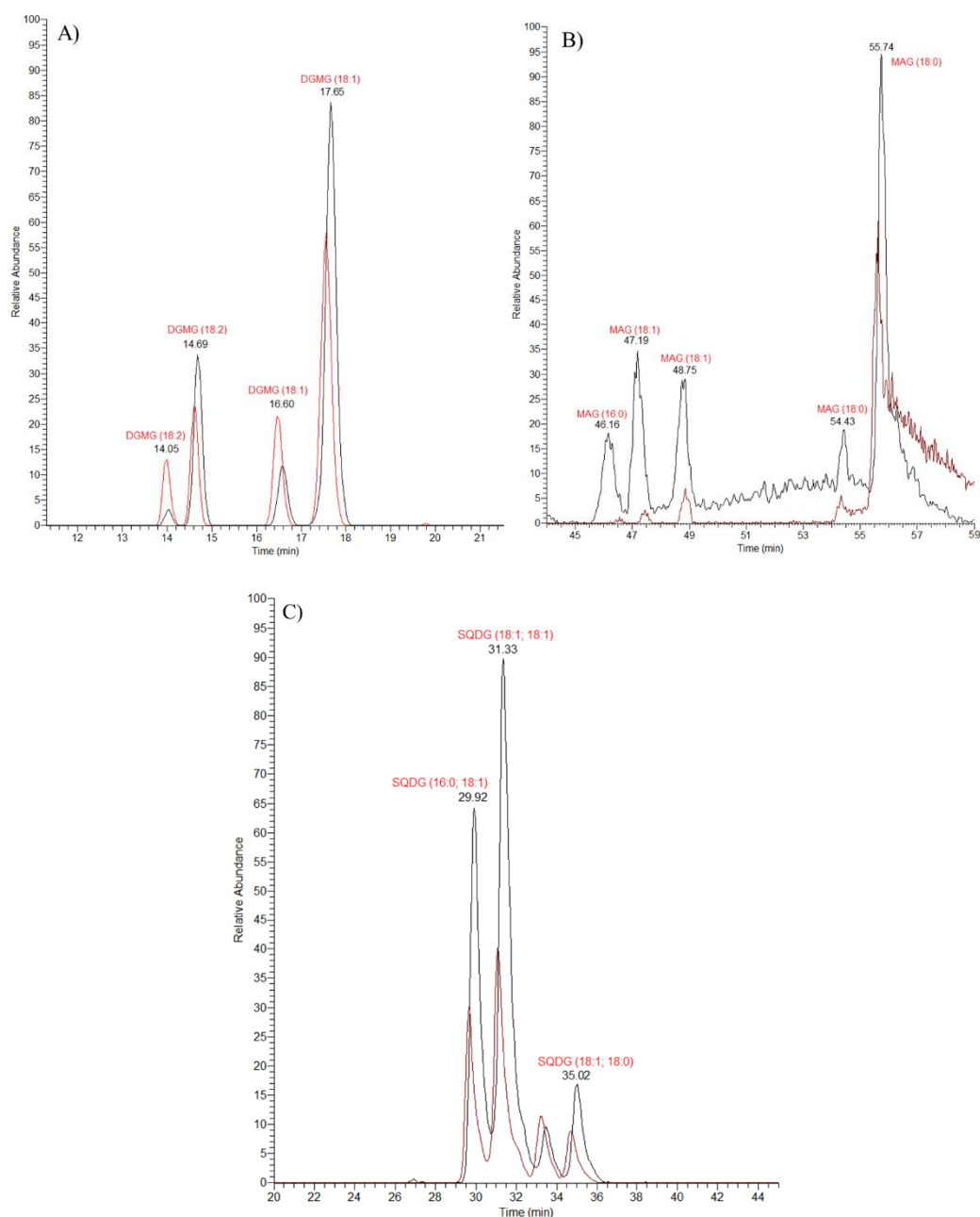


Figure 3.13. A) Extracted ion chromatograms of DGMG ions from the LC-MS analysis of TGF (red plot) and TGR (black plot) extracts on Atlantis T3 column in ESI negative ion mode (Normalized level TGR and TGF: 1.5×10^5). B) Extracted ion chromatograms of MAG ions from the LC-MS analysis of TGF (red plot) and TGR (black plot) extracts on Atlantis T3 column in ESI positive ion mode (Normalized level TGR and TGF: 2.0×10^6). C) Extracted ion chromatograms of SQDG ions from the LC-MS analysis of TGF (red plot) and TGR (black plot) extracts on Symmetry C4 column in ESI negative ion mode (Normalized level TGR and TGF: 3.0×10^5).

The MS² spectra of [M-H]⁻ ions from DGMGs showed as principal product ion the [(M-RCOOH)-H]⁻ ion due to the cleavage of the fatty acid attached to the *sn*-1 or *sn*-2 positions of the glycerol backbone, along with minor product ions corresponding to the RCOO⁻ ion. The [(M-RCOOH-162)-H]⁻ product ion originated by the loss of RCOOH and one anhydrous hexose moiety (belonging to the disaccharide unit linked to the *sn*-3 position of the glycerol), and the molecular ion without both the fatty acid and the glycerol moiety, also in the anhydrous form, were detectable (table 3.6)⁶. Thus DGMG species differing in degree of unsaturation and/or regiospecificity of the fatty acyl group were identified. They are here described for the first time in hazelnut and have been detected both in TGF and in TGR kernel, so indicating no influence of roasting.

The presence of MAG species was instead confirmed by the analysis of the positive MS² mass spectra produced by the [M+H]⁺ pseudomolecular ions of **116-120** (fig. 13B). In all cases, a predominant [(M-18)+H]⁺ product ion was present, originated by neutral loss of a water molecule, along with minor product ions as the [RCOOH+H]⁺ cation, accounting for the MAG fatty acid, and the [(RCOOH-92)+H]⁺ and [(RCOOH-74)+H]⁺ product ions formed by neutral loss of glycerol moieties³⁵. MAGs species in which oleic acid or palmitic acid was in *sn*-1 or *sn*-2 positions of glycerol backbone were already reported in hazelnut oil³⁶.

Sulfoquinovosyldiacylglycerols (SQDGs) are relatively abundant sulfolipids specifically associated with photosynthetic membranes of higher plants, mosses, ferns, algae and most photosynthetic bacteria³⁰. Their chemical structure is characterized by two fatty acyl moieties, with various degrees of unsaturation, linked to the glycerol backbone at *sn*-1 and *sn*-2 positions, and a polar head group represented by a sulfoquinovose molecule. In contrast to most naturally occurring sulfolipids, in which sulfur is involved in an ester linkage, SQDGs bear a sulfonic acid residue. Some SQDGs have been reported to exhibit a remarkable antiviral

activity, mainly against the human immunodeficiency virus (HIV-1), and are clinically promising as antitumor and immunosuppressive agents³⁰.

The careful study of the full LC-ESI/LTQOrbitrap/MS/MSⁿ spectra pointed to suggest the presence of three SQDGs species (**113-115**) in both TGF and TGR hazelnut extract, accordingly with their molecular formula containing a sulfur atom (table 3.6.; fig. 3-13C). The analysis of the corresponding MS² and MS³ allowed to define the nature of the corresponding acyl chains. Tandem mass spectrum of SQDG precursor ions clearly demonstrated a remarkable loss of neutral fatty acids from the relative pseudomolecular anion, clearly prevailing over ketene loss and carboxylate anion generation. In particular, in agreement with literature data, the regiochemical characterization of SQDG species could be based on the intensities of the [(M-R_xCOOH)-H]⁻ product ions (with [(M-R₁COOH)-H]⁻ > [(M-R₂COOH)-H]⁻)³⁰. Additionally, the SQDG identity could be confirmed by the analysis of the MS³ spectrum generated by the [(M-R₁COOH)-H]⁻/[(M-R₂COOH)-H]⁻ ions, characterized by the presence of the well-known fragment ion at *m/z* 225, for which a structure bearing an epoxydic bridge between carbon 1 and 2 of the quinovosylic ring has been recently proposed³⁰. Noteworthy, the three SQDGs found in both TGF and TGR kernels have never been described before in hazelnut; there are only few reports about them in a limited number of plant species³⁰.

3.2. Conclusion

In conclusion, the results of this study contribute to obtain a detailed and comprehensive profile of the polar lipids occurring in fresh and roasted hazelnut (cv. Tonda di Giffoni), highlighting the presence of many classes of lipids, ranging from the small oxylipins and long chain bases (LCBs and LCB-Ps) to the intact high molecular weight phospholipids (1-PC/PC, 1-PE/PE, 1-PI/PI, 1-PA/PA, 1-PG/PG, PS, and NA-GPEs), sphingolipids (GlcCers), and glycolipids (DGMG, MAG, SQDG). To the best of our knowledge, most of the polar lipids reported in this study are here described for the first time in hazelnut.

Noteworthy, our data suggest the presence of metabolite differences between fresh and roasted TG hazelnut kernels, in particular highlighting the higher levels in TGF of some lipid classes, such as LCB, LCB-P, and oxylipins, along with a good number of oxidized phospholipids in TGR. This remark points to suggest the high temperature of roasting treatment as a stress factor able to influence and modify the polar lipid profile of hazelnut kernels, mainly increasing oxidative processes in complex lipid species such as PC, PE, and PI. Apparently, no changes in the remaining phospholipid classes, in glycolipids, and in cerebrosides were detectable.

On the basis of the biological activities above cited for each class of lipids found in TG hazelnut kernels and their interesting effects on human health, our data support and encourage the use of PGI “Tonda di Giffoni” hazelnut kernels in human nutrition promoting it as a food rich of different classes of bioactive and healthy lipids with beneficial effects.

3.3. Experimental section

Samples

C. avellana L. hazelnuts, cv. Tonda di Giffoni, were collected at Giffoni, Salerno (Campania region, Italy), in August 2015, and identified by V. De Feo (Department of Pharmacy, University of Salerno, Italy). A voucher specimen has been deposited in this Department.

Preparation of Samples

C. avellana kernels were crushed by a knife and stored at room temperature for three days.

480.0 g of hazelnut kernels without skin were defatted with *n*-hexane and chloroform at room temperature (6.4 L × 3 days × 2 times), and after were extracted with MeOH at room temperature (6.4 L for 3 days, three times). After filtration, the methanolic extract was dried under vacuum and partitioned between *n*-hexane and MeOH to remove the non polar oily components (mainly triglycerides). The obtained MeOH extract was subjected to *n*-butanol–water partition to remove free sugars.

1.00 Kg of hazelnut kernels without skin were hot air roasted by using a laboratory electric oven at 170°C for 30 min; the roasted hazelnuts were extracted with the same procedure used for the fresh hazelnuts.

LC-ESI/LTQOrbitrap/MS/MSⁿ analysis of n-butanol extracts of fresh and roasted C. avellana kernels

The *n*-butanol extracts of both fresh and roasted kernels of *C. avellana* cv. Tonda di Giffoni cultivar were analyzed by a system of liquid chromatography coupled to electrospray ionization and high resolution mass spectrometry (LC-ESI/HRMS)

consisting of a quaternary Accela 600 pump and an Accela autosampler coupled to a LTQOrbitrap XL mass spectrometer (ThermoScientific, San Jose, CA), operating in both positive and negative electrospray ionization mode. Data were collected and analyzed by using the software provided by the manufacturer. The separation was carried out by using two different columns, an Atlantis T3 (RP-18, 2.1 x 150 mm, 5 μ m; Waters, Milford, MA) and a Symmetry 300 C-4 (RP-4, 3.5 μ m, 2.1mm \times 150mm; Waters, Milford, MA) column, in both cases by using a flow rate of 0.2 mL/min and a mobile phase consisting of a combination of A (0.1% formic acid in water, v/v) and B (0.1% formic acid in acetonitrile, v/v). On the Atlantis T3 column, a linear gradient from 15 to 60% B in 9 min, hold at 60% B for 5 min, from 60 to 65 % B in 10 min, hold at 65% B for 5 min, from 65 to 70% B in 10 min, from 70 to 100% B in 15 min, hold at 100% B for 6 min was used. On the the Symmetry C4 column, a linear gradient from 25 to 51% B in 10 min, from 51 to 60% B in 9 min, hold at 60% B for 5 min, from 60 to 64 % B in 8 min, hold at 64% B for 5 min, from 64 to 68% B in 8 min, hold at 68% B for 5 min, from 68 to 87% B in 19 min, from 87 to 100% B in 6 min, hold at 100% B for 5 min was used. The autosampler was set to inject 2 μ l of extract (0.5 mg/mL). In the negative ion mode, the following experimental conditions for the ESI source were adopted: sheath gas at 15 (arbitrary units), auxiliary gas at 5 (arbitrary units), source voltage at 3.5 kV, capillary temperature at 280 $^{\circ}$ C, capillary voltage at -48 V and tube lens at -176.47 V.

In the positive ion mode, the following experimental conditions for the ESI source were adopted: sheath gas at 15 (arbitrary units), auxiliary gas at 10 (arbitrary units), source voltage at 4.5 kV, capillary temperature at 280 $^{\circ}$ C, capillary voltage at 27 V and tube lens at 105 V. The mass range was from 200 to 1200 m/z with a resolution of 30000.

References

1. Shahidi, F.; Alasalvar, C.; Liyana-Pathirana, C. M., Antioxidant phytochemicals in hazelnut kernel (*Corylus avellana* L.) and hazelnut byproducts. *J Agr Food Chem* **2007**, *55*, 1212-1220.
2. Belviso, S.; Dal Bello, B.; Giacosa, S.; Bertolino, M.; Ghirardello, D.; Giordano, M.; Rolle, L.; Gerbi, V.; Zeppa, G., Chemical, mechanical and sensory monitoring of hot air- and infrared-roasted hazelnuts (*Corylus avellana* L.) during nine months of storage. *Food Chem.* **2017**, *217*, 398-408.
3. Alasalvar, C.; Shahidi, F.; Liyanapathirana, C. M.; Ohshima, T., Turkish Tombul hazelnut (*Corylus avellana* L.). 1. Compositional characteristics. *J. Agric. Food Chem.* **2003**, *51*, 3790-3796.
4. Petriccione, M.; Ciarmiello, L. F.; Boccacci, P.; De Luca, A.; Piccirillo, P., Evaluation of 'Tonda di Giffoni' hazelnut (*Corylus avellana* L.) clones. *Sci Hort.* **2010**, *124*, 153-158.
5. Welti, R.; Wang, X., Lipid species profiling: A high-throughput approach to identify lipid compositional changes and determine the function of genes involved in lipid metabolism and signaling. *Curr. Opin. Plant Biol.* **2004**, *7*, 337-344.
6. Geng, F.; Huang, X.; Majumder, K.; Zhu, Z.; Cai, Z.; Ma, M., Mass Spectrometry and Two-Dimensional Electrophoresis To Characterize the Glycosylation of Hen Egg White Ovomacroglobulin. *J. Agric. Food Chem.* **2015**, *63*, 8209-8215.
7. Richardson, C. E.; Hennebelle, M.; Otoki, Y.; Zamora, D.; Yang, J.; Hammock, B. D.; Taha, A. Y., Lipidomic Analysis of Oxidized Fatty Acids in Plant and Algae Oils. *J. Agric. Food Chem.* **2017**, *65*, 1941-1951.
8. Schwartz, D. P.; Rady, A. H., Quantitation and occurrence of hydroxy fatty acids in fats and oils. *J. Am. Oil Chem. Soc.* **1992**, *69*, 170-3.
9. Inoue, M.; Adachi, M.; Shimizu, Y.; Tsutsumi, T.; Tokumura, A., Comparison of Lysophospholipid Levels in Rat Feces with Those in a Standard Chow. *J. Agric. Food Chem.* **2011**, *59*, 7062-7067.
10. Kihara, Y.; Mizuno, H.; Chun, J., Lysophospholipid receptors in drug discovery. *Exp. Cell Res.* **2015**, *333*, 171-177.
11. Klockmann, S.; Reiner, E.; Bachmann, R.; Hackl, T.; Fischer, M., Food Fingerprinting: Metabolomic Approaches for Geographical Origin Discrimination of Hazelnuts (*Corylus avellana*) by UPLC-QTOF-MS. *J. Agric. Food Chem.* **2016**, *64*, 9253-9262.
12. Zhang, J.; Zhao, C.; Zeng, Z.; Luo, P.; Zhao, Y.; Zhao, J.; Li, L.; Lu, X.; Xu, G., Sample-directed pseudotargeted method for the metabolic profiling

analysis of rice seeds based on liquid chromatography with mass spectrometry. *J. Sep. Sci.* **2016**, *39*, 247-255.

13. Melo, T.; Silva, E. M. P.; Simoes, C.; Domingues, P.; Domingues, M. R. M., Photooxidation of glycated and non-glycated phosphatidylethanolamines monitored by mass spectrometry. *J. Mass Spectrom.* **2013**, *48*, 68-78.

14. Xie, L.-J.; Chen, Q.-F.; Chen, M.-X.; Yu, L.-J.; Huang, L.; Chen, L.; Wang, F.-Z.; Xia, F.-N.; Zhu, T.-R.; Wu, J.-X.; Yin, J.; Liao, B.; Shi, J.; Zhang, J.-H.; Aharoni, A.; Yao, N.; Shu, W.; Xiao, S., Unsaturation of very-long-chain ceramides protects plant from hypoxia-induced damages by modulating ethylene signaling in *Arabidopsis*. *PLoS Genet.* **2015**, *11*, e1005143/1-e1005143/33.

15. Narayanan, S.; Tamura, P. J.; Roth, M. R.; Prasad, P. V. V.; Welti, R., Wheat leaf lipids during heat stress: I. High day and night temperatures result in major lipid alterations. *Plant, Cell Environ.* **2016**, *39*, 787-803.

16. Guo, L.; Amarnath, V.; Davies, S. S., A liquid chromatography-tandem mass spectrometry method for measurement of N-modified phosphatidylethanolamines. *Anal. Biochem.* **2010**, *405*, 236-245.

17. Tsuboi, K.; Okamoto, Y.; Ikematsu, N.; Inoue, M.; Shimizu, Y.; Uyama, T.; Wang, J.; Deutsch, D. G.; Burns, M. P.; Ulloa, N. M.; Tokumura, A.; Ueda, N., Enzymatic formation of N-acylethanolamines from N-acylethanolamine plasmalogen through N-acylphosphatidylethanolamine-hydrolyzing phospholipase D-dependent and -independent pathways. *Biochim. Biophys. Acta, Mol. Cell Biol. Lipids* **2011**, *1811*, 565-577.

18. Coulon, D.; Bure, C., Acylphosphatidylglycerol (acyl-PG) or N-acylphosphatidylethanolamine (NAPE)? *J. Mass Spectrom.* **2015**, *50*, 1318-1320.

19. Yamashita, A.; Oka, S.; Tanikawa, T.; Hayashi, Y.; Nemoto-Sasaki, Y.; Sugiura, T., The actions and metabolism of lysophosphatidylinositol, an endogenous agonist for GPR55. *Prostaglandins Other Lipid Mediat.* **2013**, *107*, 103-116.

20. Damnjanovic, J.; Kuroiwa, C.; Tanaka, H.; Ishida, K.; Nakano, H.; Iwasaki, Y., Directing positional specificity in enzymatic synthesis of bioactive 1-phosphatidylinositol by protein engineering of a phospholipase D. *Biotechnol. Bioeng.* **2016**, *113*, 62-71.

21. Nilsson, A. K.; Johansson, O. N.; Fahlberg, P.; Steinhart, F.; Gustavsson, M. B.; Ellerstrom, M.; Andersson, M. X., Formation of oxidized phosphatidylinositol and 12-oxo-phytodienoic acid containing acylated phosphatidylglycerol during the hypersensitive response in *Arabidopsis*. *Phytochemistry* **2014**, *101*, 65-75.

22. He, H.; Emmett, M. R.; Nilsson, C. L.; Conrad, C. A.; Marshall, A. G., High mass accuracy and resolution facilitate identification of glycosphingolipids and phospholipids. *Int. J. Mass Spectrom.* **2011**, *305*, 116-119.

23. Uwamizu, A.; Inoue, A.; Suzuki, K.; Okudaira, M.; Shuto, A.; Shinjo, Y.; Ishiguro, J.; Makide, K.; Ikubo, M.; Nakamura, S.; Jung, S.; Sayama, M.; Otani, Y.; Ohwada, T.; Aoki, J., Lysophosphatidylserine analogues differentially activate three LysoPS receptors. *J. Biochem.* **2015**, *157*, 151-160.
24. Liu, F.; Zhang, Y.; Sun, Q.-Y.; Yang, F.-M.; Gu, W.; Yang, J.; Niu, H.-M.; Wang, Y.-H.; Long, C.-L., Diarylheptanoids and phenylphenalenones from *Musa itinerans* fruits. *Phytochemistry* **2014**, *103*, 171-177.
25. Napolitano, A.; Benavides, A.; Pizza, C.; Piacente, S., Qualitative on-line profiling of ceramides and cerebroside by high performance liquid chromatography coupled with electrospray ionization ion trap tandem mass spectrometry: The case of *Dracontium lorentense*. *J. Pharm. Biomed. Anal.* **2011**, *55*, 23-30.
26. Markham, J. E.; Jaworski, J. G., Rapid measurement of sphingolipids from *Arabidopsis thaliana* by reversed-phase high-performance liquid chromatography coupled to electrospray ionization tandem mass spectrometry. *Rapid Commun. Mass Spectrom.* **2007**, *21*, 1304-1314.
27. Narayanaswamy, P.; Shinde, S.; Sulc, R.; Kraut, R.; Staples, G.; Thiam, C. H.; Grimm, R.; Sellergren, B.; Torta, F.; Wenk, M. R., Lipidomic "Deep Profiling": An Enhanced Workflow to Reveal New Molecular Species of Signaling Lipids. *Anal. Chem.* **2014**, *86*, 3043-3047.
28. Alasalvar, C.; Pelvan, E., Fat-soluble bioactives in nuts. *Eur. J. Lipid Sci. Technol.* **2011**, *113*, 943-949.
29. Kumar, A.; Pandurangan, A. K.; Lu, F.; Fyrst, H.; Zhang, M.; Byun, H.-S.; Bittman, R.; Saba, J. D., Chemopreventive sphingadienes downregulate Wnt signaling via a PP2A/Akt/GSK3 β pathway in colon cancer. *Carcinogenesis* **2012**, *33*, 1726-1735.
30. Zianni, R.; Bianco, G.; Lelario, F.; Losito, I.; Palmisano, F.; Cataldi, T. R. I., Fatty acid neutral losses observed in tandem mass spectrometry with collision-induced dissociation allows regiochemical assignment of sulfoquinovosyl-diacylglycerols. *J. Mass Spectrom.* **2013**, *48*, 205-215.
31. Moreau, R. A.; Doehlert, D. C.; Welti, R.; Isaac, G.; Roth, M.; Tamura, P.; Nunez, A., The Identification of Mono-, Di-, Tri-, and Tetragalactosyl-diacylglycerols and their Natural Estolides in Oat Kernels. *Lipids* **2008**, *43*, 533-548.
32. Napolitano, A.; Carbone, V.; Saggese, P.; Takagaki, K.; Pizza, C., Novel galactolipids from the leaves of *Ipomoea batatas* L.: characterization by liquid chromatography coupled with electrospray ionization-quadrupole time-of-flight tandem mass spectrometry. *J. Agric. Food Chem.* **2007**, *55*, 10289-10297.
33. Petrie, J. R.; Shrestha, P.; Zhou, X.-R.; Mansour, M. P.; Liu, Q.; Belide, S.; Nichols, P. D.; Singh, S. P., Metabolic engineering plant seeds with fish oil-like levels of DHA. *PLoS One* **2012**, *7*, e49165.

34. Poursharifi, P.; Madiraju, S. R. M.; Prentki, M., Monoacylglycerol signalling and ABHD6 in health and disease. *Diabetes, Obes. Metab.* **2017**, *19*, 76-89.
35. Della Corte, A.; Chitarrini, G.; Di Gangi, I. M.; Masuero, D.; Soini, E.; Mattivi, F.; Vrhovsek, U., A rapid LC-MS/MS method for quantitative profiling of fatty acids, sterols, glycerolipids, glycerophospholipids and sphingolipids in grapes. *Talanta* **2015**, *140*, 52-61.
36. Paganuzzi, V., Monoglycerides in vegetable oils. Note IV: Raw oils of low unsaturation. *Riv. Ital. Sostanze Grasse* **1999**, *76*, 457-471.

Chapter 4

**Byproducts of *Castanea sativa* source of the Italian
PGI Product “Marrone di Roccadaspide”:
phytochemical investigation of leaves and shells**

Introduction



Castanea sativa Mill. (Fagaceae) is a deciduous tree growing in Southern Europe, especially in Mediterranean region¹. The fruit is a nut, commonly named chestnut or marron, which is collected in autumn. It represents a traditional basic food and can be processed into different elaborated and diversified food products².



From a nutritional point of view, chestnut can be used as an important source of dietary energy, due to its starch, carbohydrates and low fat content³. Cooked chestnuts are important in human health due to their applications as a component of gluten-free diets and as a source of essential fatty acids and phenolics, with a significant amount of polyphenols, gallic and ellagic acid, hydrolysable and condensed tannins⁴⁻⁸. Reports on chestnut by-products, such as leaf, shell and bur, revealed they can be considered a good source of phenolic compounds with marked biological activity, mainly antioxidant properties^{6,9}.

In Italy, one of the most famous chestnut is “Marrone di Roccadaspide”, a labeled PGI (Protected Geographical Indication) product of the Campania region, representing an important economic resource.

Generally, chestnuts are consumed raw or after cooking. They can be processed in various ways, at home or in agricultural industry, to improve the organoleptic properties (aroma, flavour, texture), digestibility of the fruits, and to make nutrients more bioavailable.

During industrial process a big amount of byproducts such as leaves, shells and burs is produced. As a part of an ongoing effort aimed at studying waste products of food plants, the phytochemical investigation of the MeOH extract of the byproducts of *C. sativa* cv. Marrone di Roccadaspide has been carried out with the aim to achieve deeper insight into the chemical composition of the by-

products of this important PGI product and to highlight the occurrence of biologically active phytochemicals.

.

4.1. Phenolics from *Castanea sativa* leaves and their effects on UVB-induced damage

C. sativa leaves

C. sativa leaves, used in traditional medicine for the treatment of cough, diarrhea and rheumatic conditions, showed the presence of phenolic compounds able to prevent oxidative stress-mediated diseases such as photoageing^{6,10}. In particular, the leaf extract from *C. sativa* was previously shown to exhibit *in vitro* scavenging activity against several reactive species detected in the skin after UV exposure, including O₂¹¹, as well as to determine a concentration-dependent protective effect against UV-mediated DNA damage in HaCaT cells. This effect was found to be related to a direct antioxidant effect (involving O₂) rather than activation of the endogenous antioxidant response coordinated by NRF₂¹².



These data prompted us to carry out a phytochemical investigation of the MeOH extract of *C. sativa* cv. Marrone di Roccadaspide leaves.

4.1.1. Results and discussion

Qualitative investigation of MeOH extract of C. sativa cv. Marrone di Roccadaspide leaves

The MeOH extract was fractionated by different chromatographic steps to afford seven main compounds (**1-7**). Their structures were established by the extensive use of 1D- and 2D-NMR experiments as crenatin¹³ (**1**), chestanin¹³ (**2**), gallic acid¹⁶ (**3**), crenatin¹⁴ (**4**), 5-*O-p*-coumaroylquinic acid¹⁵ (**5**), *p*-methoxygallic acid¹⁶ (**6**) and quercetin 3-*O*- β -D-glucopyranoside¹⁷ (**7**) (fig. 4.1).

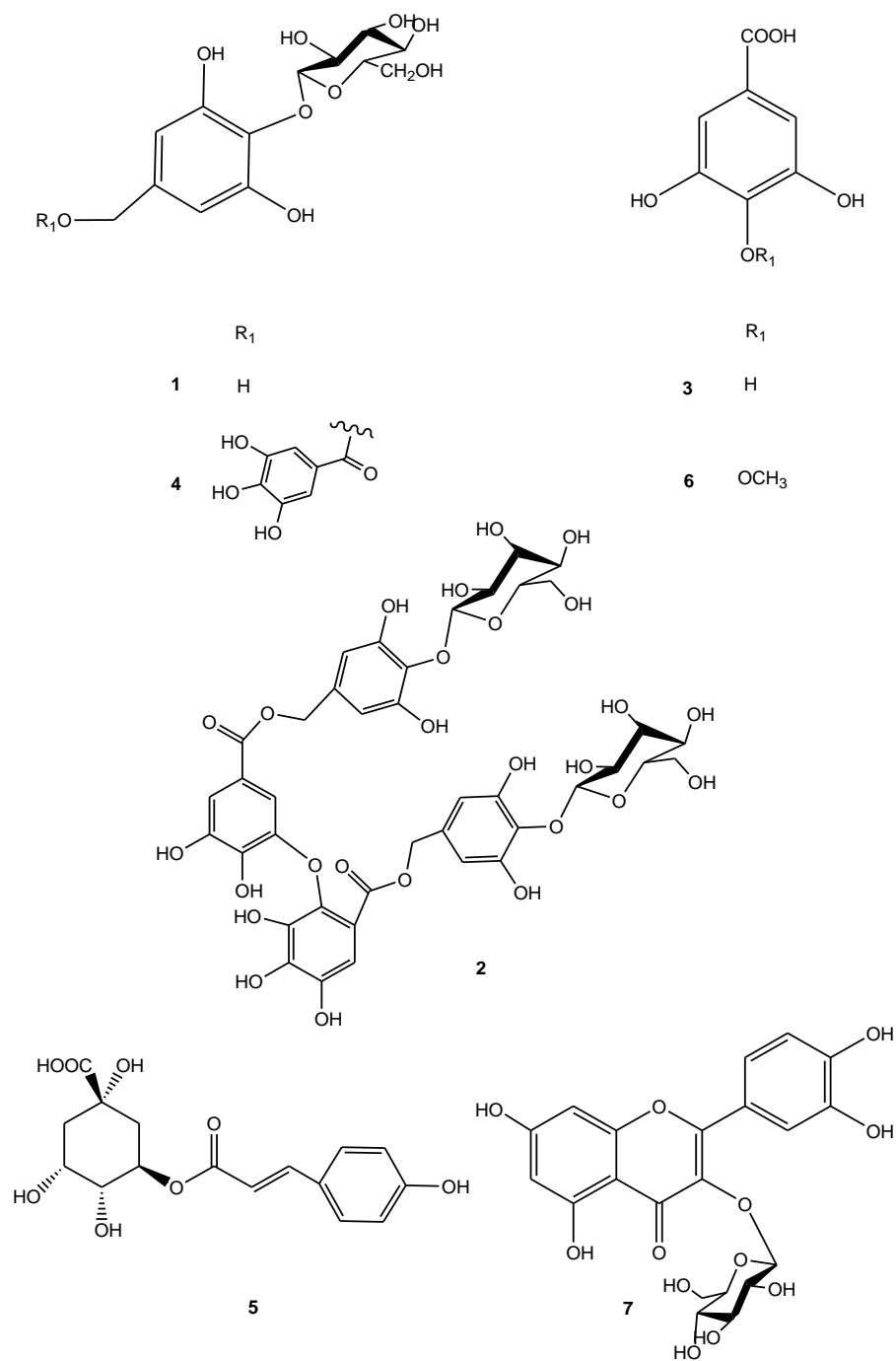


Figure 4.1. Compounds 1-7 isolated from *C. sativa* leaves.

Quantitative analysis of compounds 1-7

Compounds **1-7** were quantified by LC-ESI/QqQ/MS/MS. For quantitative purposes MRM (Multiple Reaction Monitoring) experiment was chosen, since among liquid chromatography tandem mass spectrometry analyses it can be considered a very accurate and sensitive technique¹⁸.

As reported in table 4.1, crenatin (**1**) showed a pseudomolecular ion $[M-H]^-$ at m/z 317; the loss of the glucose moiety, leading to the fragment ion $[(M-162)-H]^-$ at m/z 155, was the predominant fragmentation, thus this fragment ion was chosen for MRM analysis. Chestanin (**2**) showed a pseudomolecular ion $[M-H]^-$ at m/z 937 which gave a main fragment ion $[(M-470)-H]^-$ at m/z 467, due to the simultaneous loss of the glucose unit, the 3,4,5-trihydroxybenzyl alcohol unit and the galloyl unit (fig. 4.2).

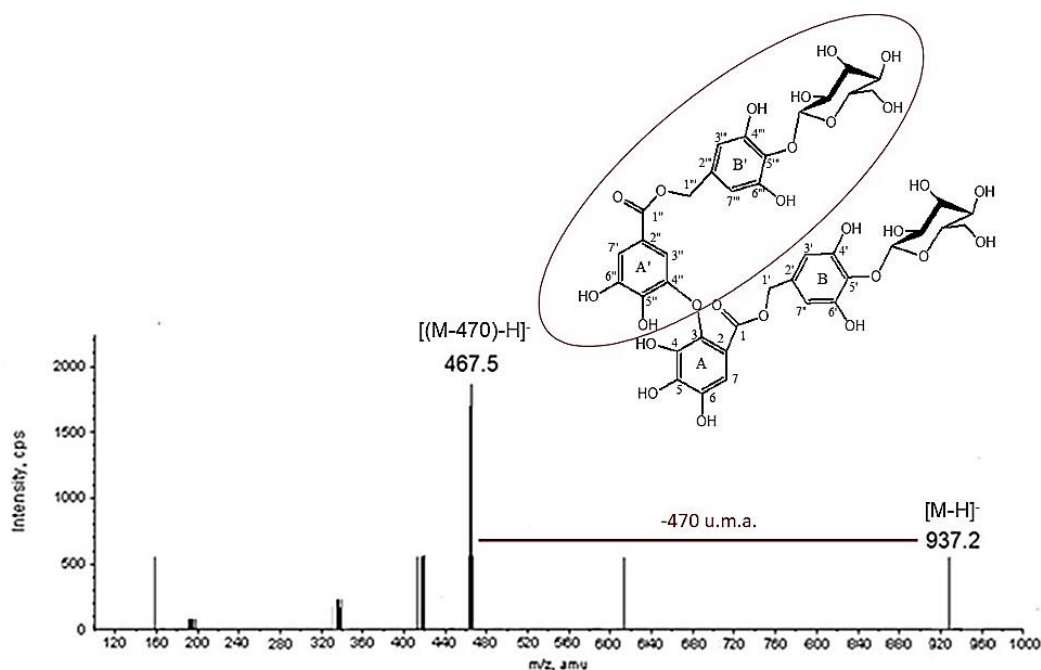


Figure 4.2. Negative ion LC-ESI/QqQ/MS/MS spectrum and proposed fragmentation pattern of chestanin (**2**) occurring in the MeOH extract of *C. avellana* leaves.

Similarly, cretanin (**4**) showed a pseudomolecular ion $[M-H]^-$ at m/z 469 and the MRM transition was characterized by the loss of both glucose and the 3,4,5-trihydroxybenzyl alcohol unit originating a very intense fragment ion $[(M-300)-H]^-$ at m/z 169 attributable to the galloyl moiety. Gallic acid (**3**) showed a pseudomolecular ion $[M-H]^-$ at m/z 169 and in the LC-MS/MS experiment a very intense fragment ion $[(M-44)-H]^-$ at m/z 125 due to the loss of a carbon dioxide unit; in the same way 4-methylgallic acid (**6**) showed a pseudomolecular ion $[M-H]^-$ at m/z 183 originating in the LC-MS/MS experiment a fragment ion at m/z 123 due to a neutral loss of 60 amu corresponding to carbon dioxide and methane molecules. 5-*p*-coumaroylquinic acid (**5**) showed a pseudomolecular ion $[M-H]^-$ at m/z 337, and quercetin 3-*O*- β -D-glucopyranoside (**7**) showed a pseudomolecular ion $[M-H]^-$ at m/z 463; both were characterized by very simple fragmentation patterns where the base peaks were produced by the neutral losses of 146 amu corresponding to a *p*-coumaroyl unit and of 162 amu corresponding to a glucose unit, respectively. On the basis of the above cited transitions selected for MRM experiments, the amount (mg/100 g dry weight) of each compound in the MeOH extract of *C. sativa* leaves was determined (table 4.1).

Table 4.1. Quantitative data of *C. sativa* leaves extract (MRM, negative ion mode). Seven-calibration points with six standards. MRM transitions, limits of detection (LODs), limits of quantification (LOQs).

Compound name	MRM transition	R ²	Regression line	LOQ (ng mL ⁻¹)	LOD (ng mL ⁻¹)	mg/100g leaves ±SD*
crenatin (1)	317→155	0.9931	Y = 0.0385x + 0.0131	25.0	8.0	17.52 ± 1.90
chestanin (2)	937→467	0.9913	Y = 0.0457x - 0.02030	10.0	2.5	33.28 ± 1.87
gallic acid (3)	169→125	0.9953	Y = 0.0082x + 0.0010	15.0	3.5	36.10 ± 3.88
cretanin (4)	469→169	0.9927	Y = 0.1310x - 0.02430	10.0	2.5	47.83 ± 1.26
5- <i>p</i> -coumaroylquinic acid (5)	337→191	0.9929	Y = 0.0406x + 0.0153	15.0	3.5	10.40 ± 1.00
4-methoxygallic acid (6)	183→123	0.9906	Y = 0.0167x + 0.00057	50.0	10.0	59.90 ± 0.86
quercetin 3- <i>O</i> -β-D-glucopyranoside (7)	463→301	0.9957	Y = 0.0232x + 0.0035	15.0	3.5	127.20 ± 3.37

The quantitative results highlight that compounds **1-7** occurred in the extract in concentration ranging from 10.40 to 127.20 (mg/100 g), with quercetin 3-*O*-β-D-glucopyranoside (**7**) exhibiting the highest and 5-*p*-coumaroylquinic acid (**5**) the lowest concentrations, respectively. Among crenatin (**1**), chestanin (**2**) and cretanin (**4**), this latter showed the highest amount (47.83 mg/100 g) comparable to that of 4-methylgallic acid (**6**) (59.90 mg/100 g).

Evaluation of antioxidant activities of compounds 1-7 by TEAC assay

The antioxidant activity of the MeOH extract and of compounds **1-7** were tested by the TEAC assay and expressed as TEAC value. The TEAC values of **1-7** and of *C. sativa* MeOH extract were compared to that of quercetin, used as reference compound (table 4.2). The results showed that the MeOH extract exhibited high free-radical-scavenging activity and among the tested compounds, gallic acid (**3**), cretanin (**4**), and quercetin 3-*O*-β-D-glucopyranoside (**7**) possessed a free-radical-scavenging activity (TEAC values = 1.46, 1.78 mM, and 1.53, respectively)

comparable to that shown by quercetin (TEAC value of 1.89 mM). Chestanin (**2**) showed the highest TEAC value (2.13 mM) suggesting that the presence of more galloyl moieties improves the radical-scavenging capacity.

Table 4.2. Free radical scavenging activities of compounds **1-7** and the MeOH extract of *C. sativa* leaves in the TEAC assay.

Compounds	TEAC value (mM± SD)
1	0.68 ± 0.002
2	2.13 ± 0.008
3	1.46 ± 0.005
4	1.78 ± 0.003
5	0.50 ± 0.003
6	1.03 ± 0.003
7	1.53 ± 0.002
quercetin	1.89 ± 0.002
	TEAC value (mg/mL ± SD)
MeOH extract	1.44 ± 0.012

4.1.2. Biological activity

Biological evaluation of compounds 1-7 on human keratinocytes

Previous reports have demonstrated that exposure of skin to UVB causes a wide variety of cellular damage to epidermal keratinocytes including DNA damage, oxidative stress, and immunotoxicity¹⁸. Thus the ability of compounds **1-7** isolated from the MeOH extract of *C. sativa* leaves to modulate the effects of UVB irradiation in immortalized keratinocytes has been investigated.

In collaboration with Dr. Anna Balato (University of Naples Federico II), a preliminary test to evaluate the effects of compounds **1-7** on cell viability was

carried out. Results revealed that compounds **1-7** didn't significantly affect viability respect to untreated control in HaCaT cell line. Moreover compounds **1-7** didn't alter viability after UVB treatment too (data not shown).

UVB can induce intracellular reactive oxygen species (ROS) generation, which activates cell signaling and stimulates transcription factor expression such as redox-sensitive transcription factor p53; it is also well documented an elevated nuclear p53 protein level after UVB treatment in HaCaT cell¹⁹. To assess if compounds **1-7** could interfere with the ratio of p53, protein band intensity relative to GAPDH was determined in the total cell extracts 24h after UVB treatment.

As shown, the obtained data demonstrated that treatment with compounds **1, 3, 4** and **5**, in different extent, diminished UVB-induced p53 expression in immortalized human keratinocytes (fig. 4.3).

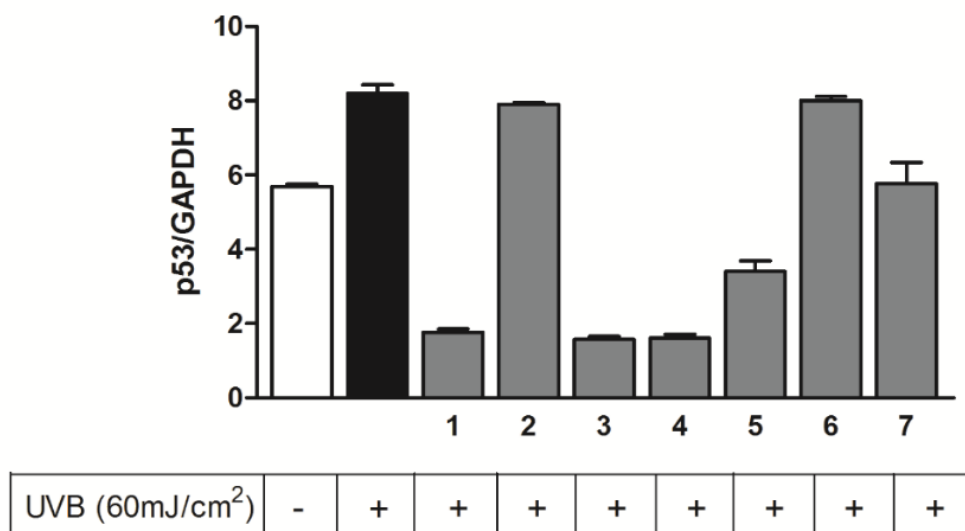


Figure 4.3. Effects of compounds **1-7** on UVB-induced p53 expression in immortalized human keratinocytes.

Notes: p53 protein analysis was assessed in cell lysates at 24h through western blot analysis. Incubation with **1-7** compounds for 2h was performed before UVB irradiation at 60 mJ/cm². The white and black bars represent, respectively, HaCat cells with just medium and HaCaT cells irradiated with UVB (60 mJ/cm²) without any compounds. Data were expressed as mean \pm SD of three independent experiments, each performed in triplicate.

Compounds **1**, **3** and **4** determined inhibition of p53/GAPDH ratio by more than 75% respect to control (HaCaT cells without any compounds, after UVB treatment). Compound **5** determined inhibition of p53/GAPDH ratio by more than 60% respect to control. Probably these compounds can scavenge or trap reactive oxygen species (ROS) formation that occur in response to UVB-induced DNA photodamage in surviving cells (fig. 4.3). It is interesting to note that simple methylation of gallic acid caused appreciable decrement in the activity (**6** vs **3**) while creatin (**1**) demonstrated a very interesting photoprotection property.

The obtained data are in agreement with Almeida *et al.*¹⁸ who reported that incubation of HaCaT with the extract of *C. sativa* caused no significant changes in

basal DNA damage, but significantly reduced the number of lesions generated by the singlet oxygen generating system²⁰, and extend the notion that this extract is able to reduce the effects of UVB irradiation, mainly due to crenatin (1), gallic acid (3), and crenatin (4).

The reasonable amount of gallic acid (3), and crenatin (4) found by LC-MS/MS analysis is interesting if we consider that they are the most active compounds in the extract. In conclusion, the above data reinforce the hypothesis that the extract of *C. sativa*, and the isolated compounds, might be an interesting option to prevent UV-induced/cell damage.

4.2. Evaluation of the biological activity of the MeOH extract of the different parts (leaves, burs, green burs, shells, chestnuts) of *C. sativa*, cv. Marrone di Roccadaspide.

During the PhD stage at the University of Veterinary and Pharmaceutical Sciences (Brno, Czech Republic), preliminary tests on the MeOH extract of *C. sativa* cv. Marrone di Roccadaspide byproducts and chestnuts have been carried out.

Cytotoxicity by WST-1 assay.

Preliminarily, the cytotoxicity of the extracts and their ability to inhibit proliferation were investigated by WST-1 assay using the cell lines THP-1 with the aim of finding a non-toxic concentration for subsequent *in vitro* experiments. The amount of formazan formed by reduction of the tetrazolium salt WST-1 corresponds directly to the number of viable cells with active mitochondrial reductases. Clearly non-toxic concentrations of the tested extracts were chosen for subsequent studies on cell cultures (5 µg/mL).

Evaluation of the inhibition of NF-κB activation

One of the most prominent among various known inflammatory pathways belongs to the transcription factor NF-κB (nuclear factor kappa-light-chain-enhancer of activated B cells).

NF-κB exists in the cytoplasm in an inactive complex bound to IκBα. Numerous stimuli activate NF-κB, mostly through the enzyme IκB kinase which phosphorylates the IκBα protein causing the dissociation of IκBα from NF-κB.

The activated NF-κB is then translocated into the nucleus, where it binds DNA and activates gene transcription. NF-κB regulates a wide variety of important target genes. Among the numerous target genes of NF-κB are those encoding

inflammatory and chemotactic cytokines such as interleukin-1 (IL-1), IL-2, IL-6, IL-8, and TNF (fig. 4.4).

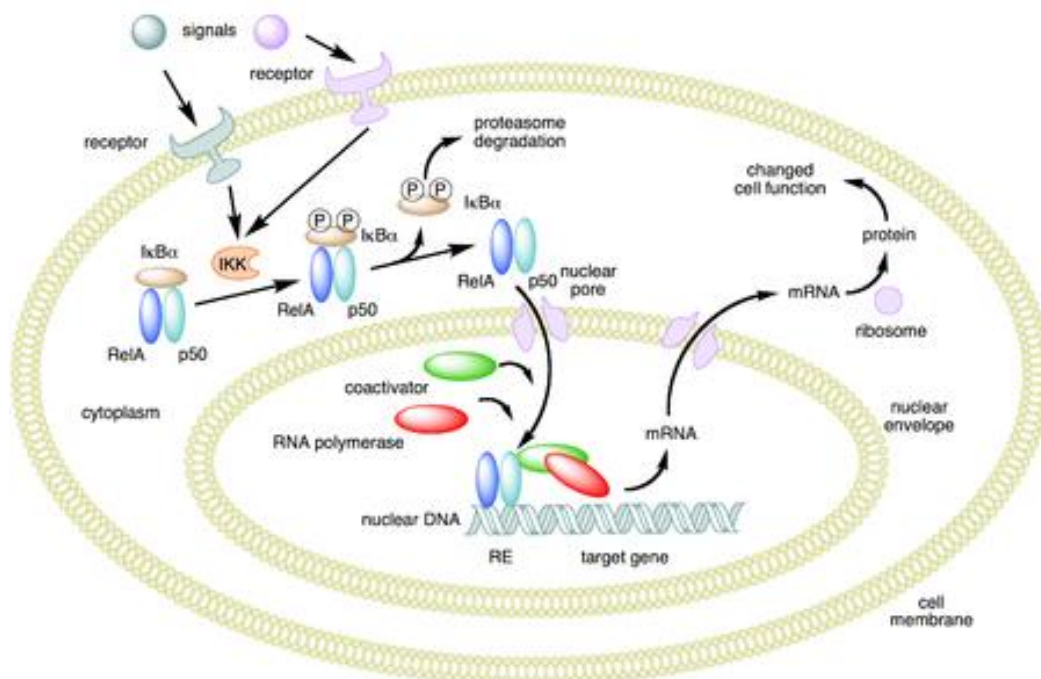


Figure 4.4. Mechanism of NF-κB action.

All the extracts showed the capacity to inhibit NF-κB activation. In particular, the best activity was displayed by MeOH extract of leaves which was more active than prednisone used as reference compound, while the MeOH extracts of burs and shells exhibited an activity comparable to reference (fig. 4.5).

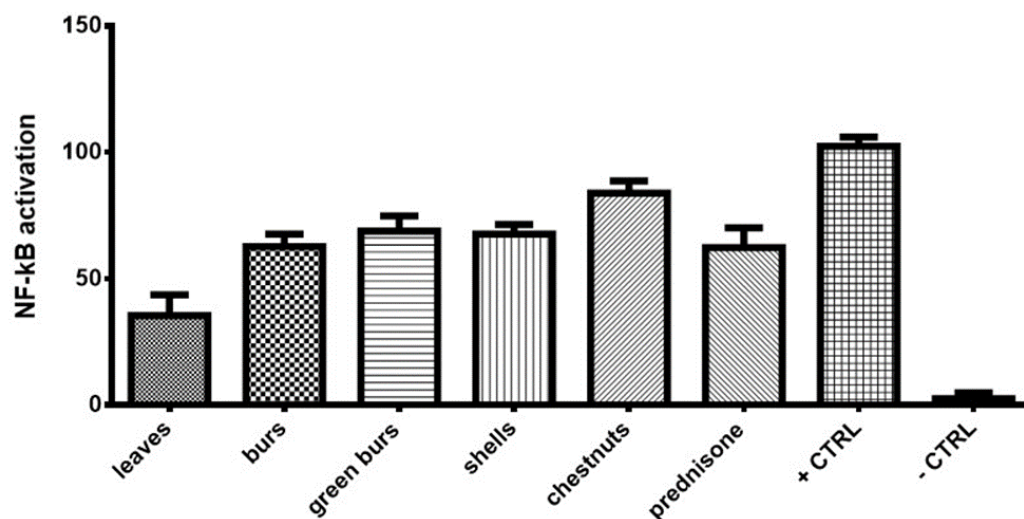


Figure 4.5. Effect of selected extracts on the nuclear translocation of NF- κ B.

Note: The results are expressed as mean \pm SE for three independent experiments. Significant difference in comparison to vehicle only treated cells ($p < 0.001$). + CTRL: cells+ LPS; -CTRL: only cells; prednisone: reference compound (1 μ M).

Evaluation of the influence of the extracts tested on the formation of ROS connected to pyocyanin.

The extracts were tested to evaluate the formation of ROS after stimulation of the THP-1 cells with pyocyanin. The extracts showed a strong antioxidant activity, in particular most of them showed an activity higher than quercetin, used as reference compound (fig. 4.6). In particular, the MeOH extract of “Marrone di Roccadaspide” shells (5 μ g/mL) reduced cellular ROS levels in a percentage of 83.91 ± 2.76 % of the control value ($p < 0.0001$), showing an antioxidant activity higher than quercetin (70.12 ± 3.14); therefore the *in vitro* antioxidant activity confirmed the strong antioxidant activity of the extract tested by DPPH ($EC_{50} = 23.80$ μ g/mL), and TEAC assay (3.00 mg/ml) assays (table 4.3).

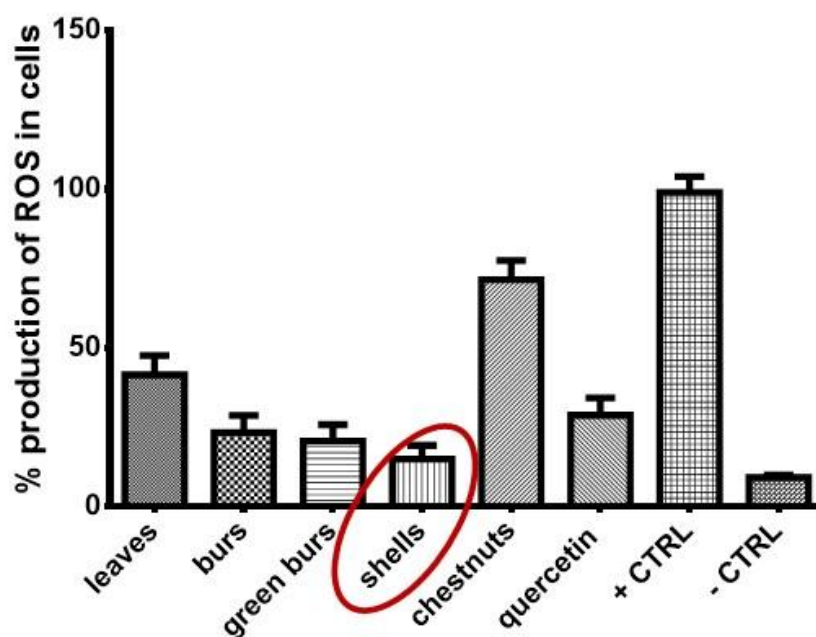


Figure 4.6. antioxidant activity of tested extracts by *in vitro* assay.

Note: The results are expressed as mean \pm SE for three independent experiments. Significant difference in comparison to vehicle only treated cells ($p < 0.001$). + CTRL: cells + pyocyanin; -CTRL: only cells; quercetin: reference compound (5 μ M).

Table 4.3. Antioxidant activity of extracts evaluated by ROS- Pyocyanin assay *in vitro*.

<i>C. sativa</i> MeOH extracts (5 μ g/mL)	inhibition of ROS induced by pyocyanin (%)
leaves	57.44 \pm 2.89**
burs	75.53 \pm 3.99**
green burs	78.27 \pm 3.99**
shells	83.91 \pm 3.99**
chestnuts	27.43 \pm 3.14**
Quercetin *	70.12 \pm 3.14**

* reference compound (5 μ M)

** $p < 0.0001$

4.3. Phytochemical investigation of MeOH extract of *C. sativa* cv. Marrone di Roccadaspide shells.

C. sativa shells



Chestnut is an achene, having a smooth and dark brown leathery pericarp. The peeling process generates a waste product, the shell, which represents 10 % of the weight of whole chestnut, which is often used as fuel.

4.3.1 Results and discussion

Phenolic content and antioxidant activity of MeOH extract of C. sativa shells

The MeOH extract of Marrone di Roccadaspide shells showed a high total phenolic content determined by the Folin-Ciocalteu method and expressed as gallic acid equivalent (871.80 mg GAE/g extract); moreover a significant concentration-dependent free-radical scavenging activity evaluated by DPPH ($EC_{50} = 23.80 \mu\text{g/mL}$), and by TEAC assay (3.00 mg/ml) correlated to the high phenolic content, as already suggested by Rodrigues²¹. and by antioxidant assay *in vitro* as previously reported.

LC-MS qualitative profile of the MeOH extract of C. avellana shells

To correlate the high phenolic content and the strong antioxidant activity to the chemical composition, the MeOH extract of *C. sativa* shells was investigated by an analytical approach based on high-performance liquid chromatography coupled to multiple-stage linear ion-trap and orbitrap high-resolution mass spectrometry (LC-ESI/LTQOrbitrap/MS), operating in negative ionization mode. The LC-ESI/LTQOrbitrap/MS profile showed more than eighty peaks (fig. 4.7), for each

of them both accurate molecular mass and molecular formula could be measured. The analysis of LC-MS/MS spectra of most ion peaks allowed to ascertain the occurrence in MeOH extract of *C. sativa* shells of metabolites mainly belonging to the tannin class, with a minor occurrence of flavonoids and phenolic derivatives, of which identity could be tentatively assigned according to literature data, homemade molecular database and chromatographic behaviour²².

In particular both classes of tannins, i.e. hydrolysable and condensed tannins, were detectable.

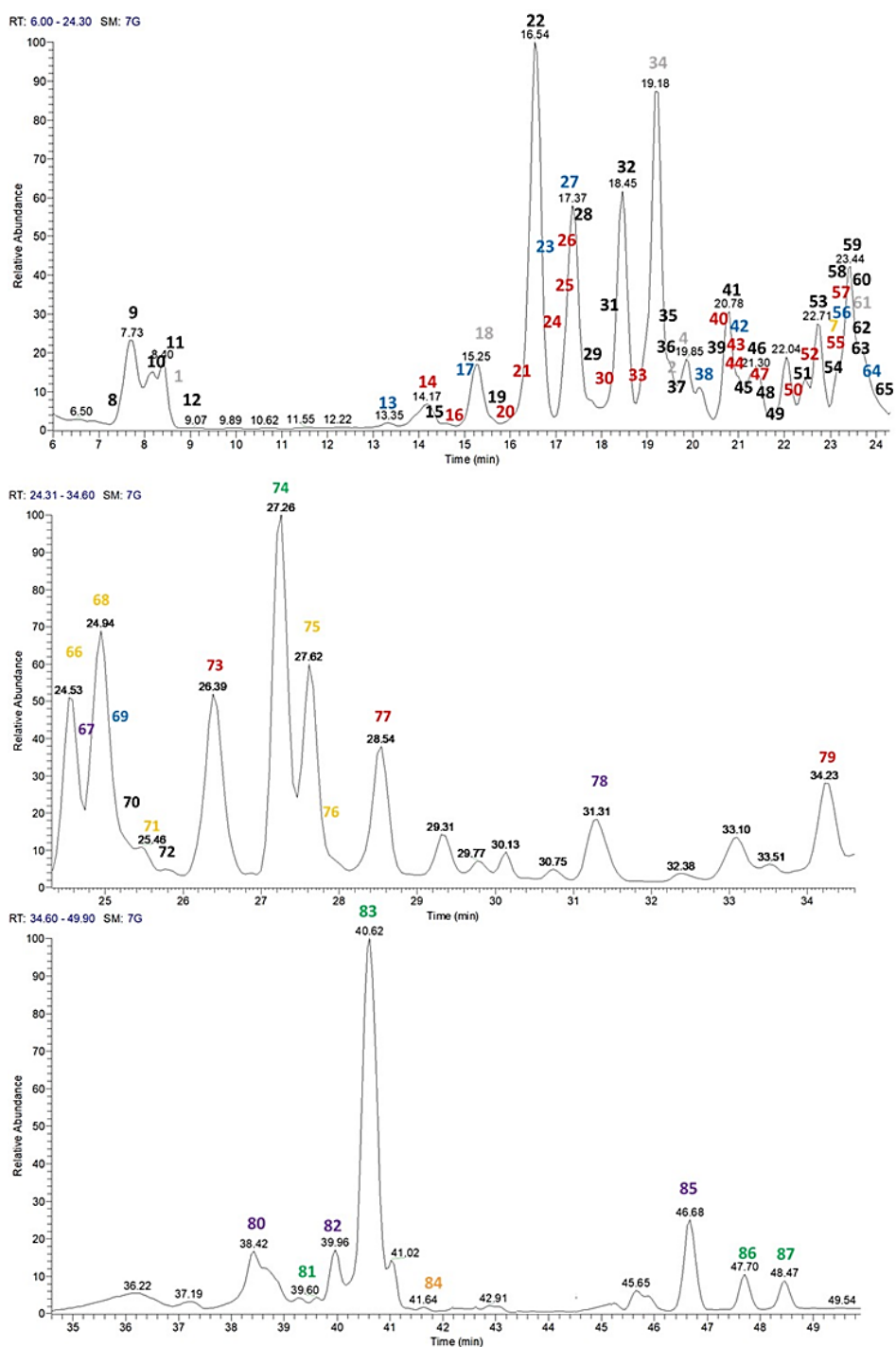


Figure 4.7. LC-ESI/LTQOrbitrap/MS profile (negative ion mode) of the MeOH extract of *C. sativa* shells.

Hydrolysable tannin class is composed of galloyl glucose derivatives, consisting of metabolites in which up to five gallic acid units can be esterified directly to D-glucose, and ellagitannins (ETs) such as hexahydroxydiphenoyl (HHDP) glucose derivatives, originated from pentagalloyl glucose by oxidative coupling (C-C coupling) of two (or more) neighboring galloyl groups, nonahydroxytriphenoyl (NHTP) derivatives, in which the HHDP group may be coupled with another galloyl group *via* a further C-C bond to form the NHTP group typical of C-glycosidic ET with an open glucose core, and flavanoellagitannins, complex combinations of C-glycosidic ETs and flavan-3-ol unit(s) (fig. 4.8).

Negative ion LC-ESI/LTQOrbitrap/MS spectra of hydrolysable tannins showed in most cases negative ions corresponding to the deprotonated molecule $[M-H]^-$ and to the doubly charged molecular ion $[M-2H]^{2-}$ according to the typical behaviour of ETs (table 4.4).

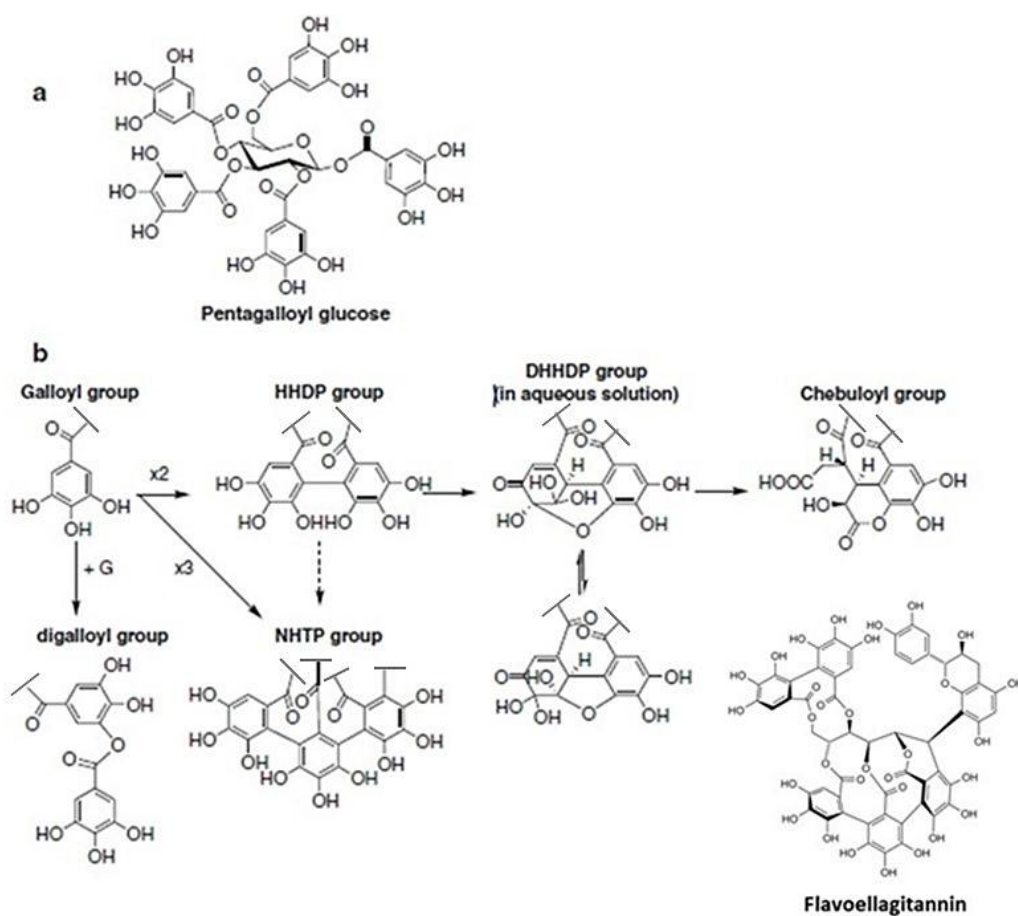


Figure 4.8. Pentagalloyl glucose (a) and gallotannins with the digalloyl group and different ellagitannin sub-structures by oxidative transformations (b).

Table 4.4. Retention times (R_t), molecular formula, $[M-H]^-$, $[M-2H]^{2-}$, Δ ppm, negative MS/MS values of compounds occurring in the MeOH extract of *C. sativa* shells identified by LC-ESI/LTQOrbitrap/MS/MSⁿ.

n°	Compound	R_t (min)	Molecular Formula	$[M-H]^-$	$[M-2H]^{2-}$	Δ ppm	Characteristic product ions (m/z)
1	crenatin*	8.51	C ₁₃ H ₁₈ O ₉	317.0870		1.04	299, 155
18	gallocatechin or epigallocatechin ²³	15.25	C ₁₅ H ₁₄ O ₇	305.0659		1.02	261, 221, 179, 165
34	catechin* ²²	19.18	C ₁₅ H ₁₄ O ₆	289.0711		1.54	245, 205, 179
2	chestanin*	19.74	C ₄₀ H ₄₂ O ₂₆	937.1875	468.0897	0.56	635, 634, 633, 467, 301
4	cretanin*	19.85	C ₂₀ H ₂₂ O ₁₃	469.0977		-0.01	317, 307, 169
61	(G)-cretanin ²⁴	23.60	C ₂₇ H ₂₆ O ₁₇	621.1085		-0.27	577, 469, 451, 317, 313
FLAVONOIDS							
7	quercetin 3- <i>O</i> - β -D- glucopyranoside* ²⁵	23.18	C ₂₁ H ₂₀ O ₁₂	463.0870		-0.13	317, 316, 301
66	syringetin 3- <i>O</i> - β -D- glucopyranoside* ²⁵	24.53	C ₂₃ H ₂₄ O ₁₃	507.1132		0.13	387, 345, 344, 179
68	isorhamnetin 3- <i>O</i> - β -D- glucopyranoside* ²⁶	24.94	C ₂₂ H ₂₂ O ₁₂	477.1028		0.18	357, 315, 314, 285
71	quercetin 3- <i>O</i> - α -L- rhamnopyranoside*	25.51	C ₂₁ H ₂₀ O ₁₁	447.09190		-0.67	301, 179, 151
75	isorhamnetin-hexoside ²⁷	27.62	C ₂₂ H ₂₂ O ₁₁	461.1077		-0.30	446, 357, 315, 314, 300, 285, MS3 (315): 300, 287, 256, 243 MS3 (314): 299, 285, 271,
76	isorhamnetin ²⁸	27.88	C ₁₆ H ₁₂ O ₇	315.0504		1.65	300, 297, 271, 229, 205, 165, 151, 137
84	kaempferol-di- <i>p</i> - coumaroyl- hexoside ²⁹	41.89	C ₃₉ H ₃₂ O ₁₅	739.16548		-0.37	593, 575, 453, 285
ELLAGIC ACID AND DERIVATIVES							
67	ellagic acid ³⁰	24.89	C ₁₄ H ₆ O ₈	300.9986		0.71	284, 257, 229, 201, 185, 145
78	methylellagic acid ³¹	31.36	C ₁₅ H ₈ O ₈	315.0139		0.41	300
80	dimethylellagic acid ³²	38.42	C ₁₆ H ₁₀ O ₈	329.0298		0.59	314, 299, 285; MS3(314): 299, 285
82	dimethylellagic acid ³²	39.96	C ₁₆ H ₁₀ O ₈	329.0297		0.56	314, 299, 285; MS3(314):

							299
85	trimethyllellagic acid ³³	46.67	C ₁₇ H ₁₂ O ₈	343.0453		0.51	328, 299, 297, 284, 275; MS3(328): 313, 299, 298, 297
HYDROLYSABLE TANNINS							
Ellagitannins							
8	NHHP-glucose (vescalin) ³⁴	6.96	C ₂₇ H ₂₀ O ₁₈	631.0561		-0.49	613, 587, 569, 551, 467, 441, 425
9	HHDP-glucose isomer ³⁴	7.73	C ₂₀ H ₁₈ O ₁₄	481.0610		-0.50	421, 301, 275
10	NHHP-glucose (castalin) ³⁴	8.09	C ₂₇ H ₂₀ O ₁₈	631.0562		-0.60	613, 587, 569, 551, 467, 441, 425
11	HHDP-glucose isomer ³⁴	8.47	C ₂₀ H ₁₈ O ₁₄	481.0612		-0.19	421, 301, 275
12	NHHP-HHDP-1-(C1- pentose)-deoxyglucose ³⁴	8.50	C ₄₆ H ₃₄ O ₃₀	1065.1042	532.0485	-0.81	MS ² (532): 523[M-2H- H ₂ O] ²⁻ , 514 [M-2H- 2H ₂ O] ²⁻ , 493 [M-2H-78] ²⁻ , 487 [M-2H- 90] ²⁻ , 465 [M- 2H-134] ²⁻ , 301, 249
15	NHHP-HHDP-glucose (castalagin) ³⁴	14.22	C ₄₁ H ₂₆ O ₂₆	933.0632	466.0274	0.34	MS ² (466): 631, 457 [M- 2H-H ₂ O] ²⁻ , 301
19	NHHP-Valoneoyl- glucose (castavalonic acid) ²³	15.61	C ₄₈ H ₃₀ O ₃₁	1101.0680	550.0300	-0.67	1057, 933, 931, 631, 587, 569, 449, 441, 425 MS ² (550): 933, 528 [M- 2H-44] ²⁻ , 465[M-2H- 170] ²⁻
22	NHHP-HHDP-glucose (vescalagin) ³⁴	16.54	C ₄₁ H ₂₆ O ₂₆	933.0622	466.0271	-0.71	915, 631, 613, 587, 425, 301
28	bis-HHDP-glucose isomer ²³	17.37	C ₃₄ H ₂₄ O ₂₂	783.0673	391.0299	-0.37	765, 481, 301, 275
29	HHDP-Valoneoyl- (acyclic)glucose isomer ³⁵	18.04	C ₄₁ H ₂₈ O ₂₇	951.0711	475.0324	-2.43	907, 783, 465, 453
31	galloyl-HHDP-glucose isomer ^{35 36}	18.25	C ₂₇ H ₂₂ O ₁₈	633.0722	316.0328	-0.06	481, 463, 301, 275, 257

Chapter 4

32	bis-HHDP-glucose isomer ²³	18.45	C ₃₄ H ₂₄ O ₂₂	783.0671	391.0298	-0.52	765, 721, 481, 301, 275
35	digalloyl-HHDP-glucose isomer ^{23 35}	19.48	C ₃₄ H ₂₆ O ₂₂	785.0832	392.0377	-0.01	633, 615, 483, 463, 331, 313, 301, 275
36	galloyl-bis-HHDP-(acyclic)glucose isomer ²³ (stachyurin)	19.59	C ₄₁ H ₂₈ O ₂₆	935.0770	467.0346	-1.48	917, 783, 633, 481, 301
37	NHTP/modified-Flavan/condensed-glucose (isomer) ^{37 24}	19.64	C ₄₁ H ₃₀ O ₂₂	873.1137		-0.90	829, 785, 767, 683, 583, 539
39	galloyl-bis-HHDP-flavan-(acyclic)glucose ^{38 39}	20.63	C ₅₆ H ₄₂ O ₃₂	1225.1553	612.0740	-1.86	MS ² (612): 935, 869, 633, 603, 467, 458, 433, 301, 289 MS ² (596): 1023, 903, 891, 601, 451, 301, 289
41	digalloyl-HHDP-glucose isomer ⁴⁰	20.78	C ₃₄ H ₂₆ O ₂₂	785.0833	392.0378	0.07	633, 615, 483, 463, 331, 313, 301, 275
45	HHDP-NHTP/modified-flavan-glucose (isomer) ⁴¹	21.25	C ₅₅ H ₃₈ O ₃₁	1193.1318	596.0611	0.43	1175, 1041, 1023, 903, 891, 849, 601, 587, 451, 421, 301, 289
46	HHDP-NHTP/modified-flavan/condensed-glucose (isomer) ⁴²	21.30	C ₅₆ H ₃₆ O ₃₃	1235.1052	617.0483	-0.23	1191, 1147, 1039, 901, 737, 639, 599, 415 MS2(617): 595 MS3(595): 573, 559, 478, 450, 301
48	bis-HHDP-flavan-(acyclic)glucose ³⁵	21.72	C ₄₉ H ₃₆ O ₂₇	1055.1341		-1.77	1037, 753, 463, 421, 301
49	HHDP-NHTP/modified-flavan/condensed-glucose (isomer) ⁴²	21.88	C ₅₆ H ₃₆ O ₃₃	1235.1008	617.0484	-3.79	MS2(617): 595, 573 MS3(595): 573, 551, 450, 301 MS3(573): 551, 497, 451, 323, 301, 287
51	galloyl-bis-HHDP-	22.45	C ₅₆ H ₄₂ O ₃₂	1225.1548	612.0744	-2.25	MS ² (612):

	flavan- (acyclic)glucose ³⁸						1055, 935, 783, 633, 603, 467, 458, 331, 301, 289
53	galloyl-bis-HHDP- flavan/condensed- (acyclic)glucose isomer ⁴³	22.71	C ₅₅ H ₃₈ O ₃₀	1177.1351	588.0639	-1.09	1133, 875, 831, 559, 301 MS ² (588): 875, 831, 559, 512 [M-2H- 152] ²⁻ , 301, 275
54	HHDP-depsidone- forming valoneoyl group-(acyclic)glucose ₃₅	22.82	C ₄₁ H ₂₆ O ₂₆	933.0623	466.0278	-0.64	915, 631, 481, 451, 301
58	HHDP- NHTP/modified- Flavan/condensed- glucose isomer ³⁷	23.44	C ₅₅ H ₃₆ O ₃₀	1175.1213	587.0561	0.39	1157, 1023, 873, 855, 829, 785, 767, 721, 677, 301
59	HHDP-depsidone- forming valoneoyl group-(acyclic)glucose ₃₅	23.44	C ₄₁ H ₂₆ O ₂₆	933.0621	466.0274	-0.84	915, 631, 481, 451, 301
60	galloyl-bis-HHDP- (acyclic)glucose isomer	23.44	C ₄₁ H ₂₈ O ₂₆	935.0781	467.0351	-0.40	917, 783, 633, 481, 301
62	trigalloyl-HHDP glucose ⁴⁴	23.70	C ₄₁ H ₃₀ O ₂₆	937.0939	468.0430	-0.18	785, 767, 741, 635, 633, 617, 465, 421 331, 313, 301
63	HHDP- NHTP/modified- Flavan/condensed- (acyclic)glucose isomer ³⁷	23.76	C ₅₅ H ₃₆ O ₃₀	1175.1207	587.0562	-0.03	1023, 873, 855, 829, 721, 677, 511, 301
65	HHDP-acyclic glucose derivative ⁴⁵	23.91	C ₃₆ H ₂₄ O ₂₂	807.0674	403.0298	-0.13	789, 505, 355, 311, 301, 275
70	galloyl-bis-HHDP- glucose isomer ³⁶	25.25	C ₄₁ H ₂₈ O ₂₆	935.0778		-0.80	783, 633, 451, 301
72	galloyl-bis-HHDP- glucose isomer ³⁶	25.97	C ₄₁ H ₂₈ O ₂₆	935.0783		-0.21	783, 633, 451, 301
Galloyl glucose derivatives							
13	digalloyl isomer ^{23, 40}	13.30	C ₂₀ H ₂₀ O ₁₄	483.0768		-0.13	331, 313, 169
17	digalloyl isomer ⁴⁰	15.09	C ₂₀ H ₂₀ O ₁₄	483.0767		-0.26	331, 313, 271, 169
23	dehydrated tergallic-c- glucoside ³⁷	16.80	C ₂₇ H ₁₈ O ₁₇	613.0459		-0.20	595, 523, 493, 299, 300

27	chesnatin ⁴⁶		17.37	C ₂₇ H ₂₆ O ₁₈	637.1031		-0.61	593, 467, 305
38	trigalloyl isomer ⁴⁰	glucose	20.11	C ₂₇ H ₂₄ O ₁₈	635.0875		-0.58	483, 465, 331, 313, 271, 211
42	trigalloyl isomer ⁴⁰	glucose	20.99	C ₂₇ H ₂₄ O ₁₈	635.0878		-0.09	483, 465, 331, 313, 271, 211
56	tetragalloyl isomer ⁴⁰	glucose	23.18	C ₃₄ H ₂₈ O ₂₂	787.0987	393.0453	-0.20	635, 617, 483, 465, 447, 295
64	tetragalloylglucose isomer ⁴⁰		23.81	C ₃₄ H ₂₈ O ₂₂	787.0980	393.0452	-1.13	635, 617, 483, 465, 447, 331, 295
69	pentagalloylglucose ⁴⁰		24.99	C ₄₁ H ₃₂ O ₂₆	939.1093	469.0506	-0.49	787, 769, 617, 599, 447, 277
CONDENSED TANNINS								
Proanthocyanidins								
14	GC-GC proanthocyanidin dimer ⁴⁷		14.17	C ₃₀ H ₂₆ O ₁₄	609.1235		-0.56	591, 483, 441, 423, 305
16	GC-GC-GC proanthocyanidin trimer ⁴⁷		14.69	C ₄₅ H ₃₈ O ₂₁	913.1812		-0.62	787, 727, 609, 577, 559, 541, 483, 441, 317, 305
20	GC-GC-GC proanthocyanidin trimer ⁴⁷		15.81	C ₄₅ H ₃₈ O ₂₁	913.1813		-1.00	727, 609, 577, 559, 483, 441, 423, 305
21	GC-GC-C proanthocyanidin trimer ²⁹		16.18	C ₄₅ H ₃₈ O ₂₀	897.1865		-0.90	771, 729, 711, 607, 593, 425, 407, 303, 289
24	GC-GC proanthocyanidin dimer ⁴⁷		16.85	C ₃₀ H ₂₆ O ₁₄	609.1237		-0.36	591, 483, 441, 423, 305
25	GC-GC-GC proanthocyanidin trimer ⁴⁷		17.01	C ₄₅ H ₃₈ O ₂₁	913.1819		-0.33	727, 609, 559, 483, 441, 423, 305, 303
26	C-C Proanthocyanidin dimer ⁴⁷		17.27	C ₃₀ H ₂₆ O ₁₂	577.1341		0.06	559, 451, 425, 407, 299, 289, 287
30	GC-GC-C proanthocyanidin trimer ⁴⁸		18.14	C ₄₅ H ₃₈ O ₂₀	897.1863		-1.10	771, 729, 711, 607, 593, 425, 407, 303, 289
33	C-C Proanthocyanidin dimer ⁴⁷		18.97	C ₃₀ H ₂₆ O ₁₂	577.1342		0.29	559, 451, 425, 407, 299, 289, 287
40	C-C-C Proanthocyanidin trimer ⁴⁸		20.16	C ₄₅ H ₃₈ O ₁₈	865.1971		-0.42	695, 577, 287
43	C-C-C(G) Proanthocyanidin trimer		21.04	C ₅₂ H ₄₂ O ₂₂	1017.2075		-0.92	999, 891, 865, 847, 771, 729,

Chapter 4

	gallate ⁴⁹					677, 577, 407
44	C-C-C-C proanthocyanidin tetramer ³²	21.04	C ₆₀ H ₅₀ O ₂₄	1153.2595	-1.13	1027, 1001, 983, 865, 739, 695, 577, 575, 449, 439, 407
47	C-C(G) proanthocyanidin dimer ^{50, 51}	21.46	C ₃₇ H ₃₀ O ₁₆	729.1448	-0.32	577, 559, 451, 425, 407, 289, 287
50	GC-C proanthocyanidin dimer ⁵⁴	22.24	C ₃₀ H ₂₄ O ₁₃	591.1135	0.24	573, 465, 453, 447, 439, 407, 301, 289, 245
52	C-C-C proanthocyanidin trimer ⁵²	22.51	C ₄₅ H ₃₈ O ₁₈	865.1967	-0.83	847, 739, 713, 695, 577, 575, 543, 451, 425, 407, 289, 287
55	C-C proanthocyanidin dimer ⁴⁷	22.87	C ₃₀ H ₂₆ O ₁₂	577.1344	0.60	559, 451, 425, 407, 299, 289, 287
57	C-C-C-C proanthocyanidin tetramer ⁵³	23.23	C ₆₀ H ₅₀ O ₂₄	1153.2615	0.45	1125, 1027, 1001, 983, 865, 739, 577, 575, 425, 407
73	C-C(G) proanthocyanidin dimer gallate ⁵⁰	26.39	C ₃₇ H ₃₀ O ₁₆	729.1441	-0.32	577, 559, 451, 425, 407, 289, 287
77	C-C proanthocyanidin dimer ⁵⁴	28.54	C ₃₀ H ₂₄ O ₁₂	575.1182	-0.30	539, 449, 437, 423, 407, 394, 393, 327, 289, 287, 285, 229
79	C-C-C proanthocyanidin trimer ⁵⁵	34.42	C ₄₅ H ₃₄ O ₁₈	861.1657	-0.50	833, 817, 735, 723, 709, 699, 680, 573, 529, 283
TRITERPENOIDS						
74	bartogenic acid 28- <i>O</i> - glucopyranoside*	27.26	C ₃₆ H ₅₆ O ₁₂	679.3682 1359.7 [2M-H] ⁻	-0.95	559, 517, 455
81	2- <i>epi</i> -bartogenic acid*	39.34	C ₃₀ H ₄₆ O ₇	517.3158	-0.35	487, 425
83	bartogenic acid*	40.62	C ₃₀ H ₄₆ O ₇	517.3163 1035.6 [2M-H] ⁻	0.71	499, 455, 437
86	Castanogenin or Ilexgenin A isomer ⁵⁶	47.70	C ₃₀ H ₄₆ O ₆	501.3208 1003.6 [2M-H] ⁻	-0.47	483, 455, 439, 421 MS3(439): 421, 395, 393, 379, 337
87	2 α ,19 α -dihydroxy-3-	48.47	C ₂₉ H ₄₄ O ₅	471.3104	-0.17	453, 425, 409

oxo-24-norolean-12-en- 28-oic acid*	943 [2M- H]
--	----------------

*Confirmed by comparison with isolated compound; GC = gallocatechin; ; C(G) = catechin gallate

The careful study of fragmentation pattern produced from hydrolysable tannins in MS/MSⁿ experiments allowed to tentatively assign their chemical structure considering that their fragmentation pathway is characterized by the presence of highly diagnostic product ions. Typical losses during fragmentation of ellagitannins are galloyl (152 Da), ellagic acid (302 Da), galloyl-glucose (332 Da), HHDP-glucose (482 Da), and galloyl-HHDP-glucose (634 Da).

So, for example the peak at 7.73 min corresponding to the [M-H]⁻ pseudomolecular ion at m/z 481.0610 could be assigned as HHDP-glucose based on its molecular weight and the presence of an intense product ion at m/z 301, corresponding to ellagic acid³⁴. Noteworthy, the same fragmentation pattern was exhibited by another peak, eluted at 8.47 min, that could be defined as a HHDP-glucose isomer (table 4.4). In fact, most of identified ETs in *C. sativa* shells extract occurred in several isomeric forms along the chromatogram (table 4.4).

Analogously, two [M-H]⁻ signals at m/z 785.0832 and 785.0833 were found (peaks **35** and **41**, respectively), with product ions at m/z 633 (M-H-152, loss of a galloyl unit), m/z 483 (M-H-302, loss of HHDP) and m/z 301. This fragmentation pattern corresponded to a digalloyl-HHDP-glucose structure^{23, 35, 40} (table 4.4).

Moreover, the structural features of HHDP- and NHTP-glucose derivatives determine that the molecular weights of HHDP and NHTP esters with the same number of galloyl units, such as galloyl-HHDP-glucose (molecular weight 634 Da) and NHTP-glucose (molecular weight 632 Da), differ by 2 Da. On this basis, the assignment of the peak at 16.54 min (**22**) as NHTP-HHDP-glucose³⁴ (m/z 933.0622) and of the peak at 19.59 min (**36**) as galloyl-bis-HHDP-(acyclic)glucose isomer²³ (m/z 935.0770) could be promptly hypothesized and successively confirmed by the analysis of the fragmentation pattern. In particular the tandem mass spectrum of **36** was characterized by a product ion at m/z 783, due to the neutral loss of a galloyl unit, a product ion at m/z 633, due to the neutral

loss of an ellagic acid unit, and a product ion at m/z 481, formed by the neutral loss of an ellagic acid from the degalloylated molecule (table 4.4 and fig. 4.9).

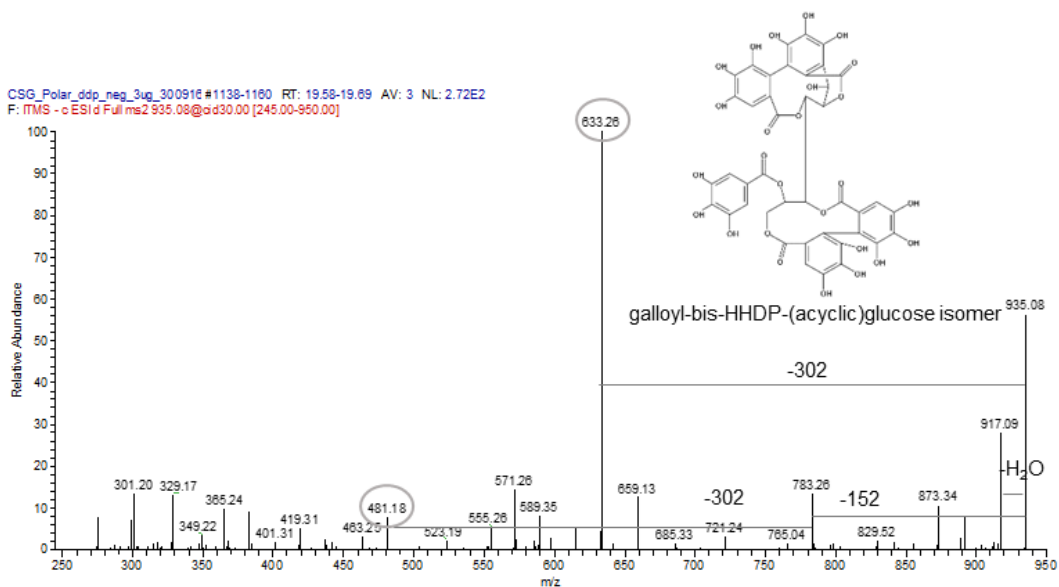


Figure 4.9. Negative LC-ESI/LTQ Orbitrap/MS/MSⁿ spectrum and proposed fragmentation pattern of compound **36**.

On the contrary, the MS² spectrum of **22** showed a main product ion at m/z 631, due to neutral loss of an ellagic acid unit, and a minor product ion at m/z 301, likely formed by the neutral loss of 330 Da (corresponding to the sugar core C-linked to a galloyl unit) as reported in figure 4.10.

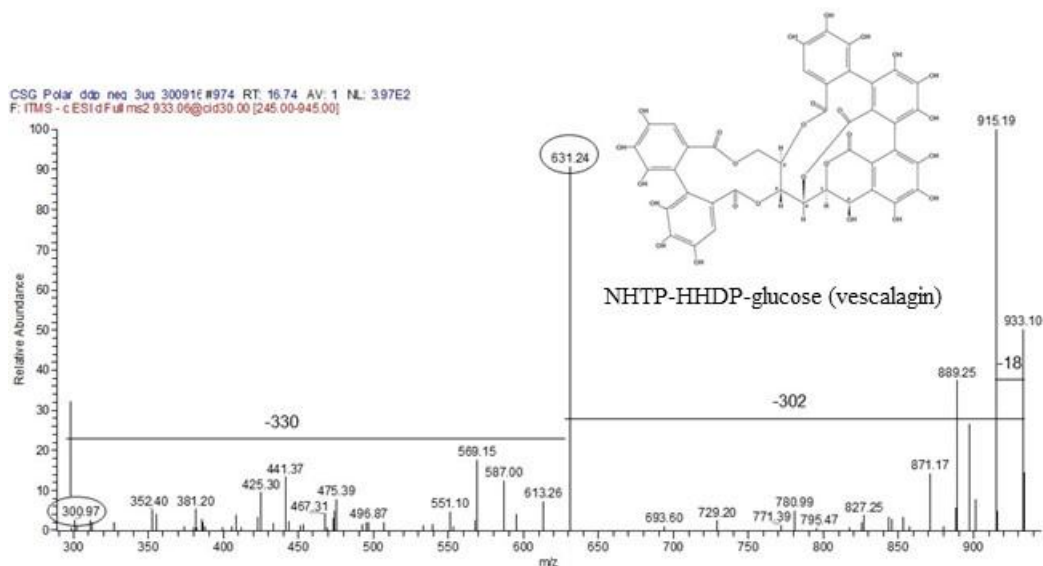


Figure 4.10. Negative LC-ESI/LTQOrbitrap/MS/MSⁿ spectrum and proposed fragmentation pattern of compound **22**.

However, both tandem mass patterns showed the presence of a product ion, respectively at m/z 917 for **36** and m/z 915 for **22**, due to the neutral loss of a water molecule, typical for ETs characterized by an acyclic sugar core. It is to be noted that NHTP-glucose derivatives have an acyclic glucose, while HHDP-glucose derivatives may have an acyclic glucose, but more commonly show cyclic glucose.

The loss of water can also be used to separate C-glycosidic ET isomer pairs, such as vescalagin and castalagin. They have the same molecular weight, but the former has β configuration and the latter α configuration at C-1 of the glucose unit. In LC-ESI/LTQOrbitrap/MS/MSⁿ spectrum, the loss of water is evidenced for the vescalagin-type ETs, but not for the castalagin-types; a phenomenon that can be explained by steric and intramolecular stabilization effects that have been

observed for these two epimers³⁴. Therefore, compound **22** could be tentatively assigned as vescalagin, while compound **15** as castalagin (table 4.4).

Other types of monomeric ETs, with more complex structures, show for example a valoneoyl group, consisting of an HHDP group supporting a galloyl group attached via C–O–C bond. This type of galloylation increases the molecular weight of an ET by 168 Da (170–2 Da), unlike the ester type galloylation that increases the molecular weight by 152 Da (170–18 Da). Thus, these two types of galloylation patterns may be differentiated on the basis of the molecular weight of the ET. This was the case of compound **29** showing in tandem mass spectrum a product ion at m/z 783, formed by the neutral loss of 168 Da, along with a product ion at m/z 907, originated by the neutral loss of a CO₂ molecule ([M-COOH]⁻), typical of the non-ester type galloylation that leaves the carboxylic acid group free³⁵ (table 4.4).

Finally, vescalagin-type ETs may also react with catechin/epicatechin units to form flavanoellagitannins, increasing the molecular weight of an ET derivative by 272 Da (290–18 Da); the catechin/epicatechin unit can be detected by a fragment ion at m/z 289 Da as well^{38,39} (table 4.4).

Condensed tannins, also known as proanthocyanidins (PAs), are oligomers and polymers of flavan-3-ol units such as afzelechin, epiafzelechin, catechin, epicatechin, galocatechin, and epigallocatechin. In PAs, three stereogenic carbons are present at C2, C3, and C4 of each benzopyran heterocyclic moiety. In the case of the couple catechin/epicatechin, if the 2,3 stereochemistry is *trans*, the monomer is designated as catechin, whereas if the 2,3 stereochemistry is *cis*, the monomer is designated as epicatechin. PAs are frequently galloylated, with the 3-OH being the most common site of galloylation.

In the B-type proanthocyanidins the flavan-3-ol units are linked through C4→C8 or C4→C6, respectively. A-Type proanthocyanidins have a second linkage through an ether bond at C2→O7. For all the PA compounds occurring in the

analyzed MeOH extract of *C. sativa* shells, the high-resolution mass data were in good agreement with the calculated molecular formulae, displaying a mass error minor than 5 ppm, thus confirming their elemental composition (table 4.4). B-type PAs and A-type PAs could be detected (e.g. the $[M-H]^-$ pseudomolecular ions at m/z 577 and 729, and at m/z 575 and 591, respectively) and promptly assigned on the basis of the fragmentation pathway corresponding to the well-known heterocyclic ring fission (HRF) and retro-Diels–Alder (RDA) fragmentation mechanisms, that give mainly information about the hydroxylation of the B-rings and the linkage-type between the two monomeric units, and by the quinonemethide (QM) fragmentation mechanism, defining the two monomeric units, especially the base unit¹⁵ (table 4.4)

Following these considerations, most of the peaks displayed in the LC-ESI/LTQOrbitrap/MS profile could be tentatively assigned (table 4.4); for compounds **74**, **81**, **83**, **86**, **87** a triterpenoid nature could be supposed by molecular formula but to unambiguously identify them, a more thorough phytochemistry investigation had to be performed.

Isolation and structural elucidation

In order to unambiguously ascertain the chemical structure of triterpenoids occurring in the LC-ESI/LTQOrbitrap/MS profile, the MeOH extract of *C. sativa* shells was subjected to size exclusion chromatography on Sephadex LH-20 and to further chromatographic separations by RP-IR/HPLC. Following this analytical approach, 12 compounds could be isolated and unambiguously identified by 1D- and 2D-NMR along with LC-ESI/LTQOrbitrap/MS/MSⁿ experiments. Compounds **1**, **2**, **4**, **7**, **34**, **66**, **68**, **71**, **74**, **81**, **83** and **87** were characterized by comparing the obtained NMR data with those reported in literature. In particular, compounds **7**, **34**, **66**, **68** and **71** were determined as flavonoids: quercetin 3-*O*- β -D-glucopyranoside (**7**), catechin²² (**34**), syringetin 3-*O*- β -D-glucopyranoside⁵⁷ (**66**),

isorhamnetin 3-*O*- β -D-glucopyranoside⁵⁸ (**68**), and quercetin 3-*O*- α -L-rhamnopyranoside²² (**71**) while compounds **74**, **81**, **83** and **87** were determined as triterpenoids: bartogenic acid 28-*O*- β -D-glucopyranosyl ester⁵⁹ (**74**), 2-epi-bartogenic acid⁶⁰ (**81**), bartogenic acid⁵⁶ (**83**) and 2 α ,19 α -dihydroxy-3-oxo-24-norolean-12-en-28-oic acid⁵⁶ (**87**). Interestingly, this is the first report describing the occurrence of triterpenoids compounds in MeOH extract of *C. sativa* shells (fig. 4.11).

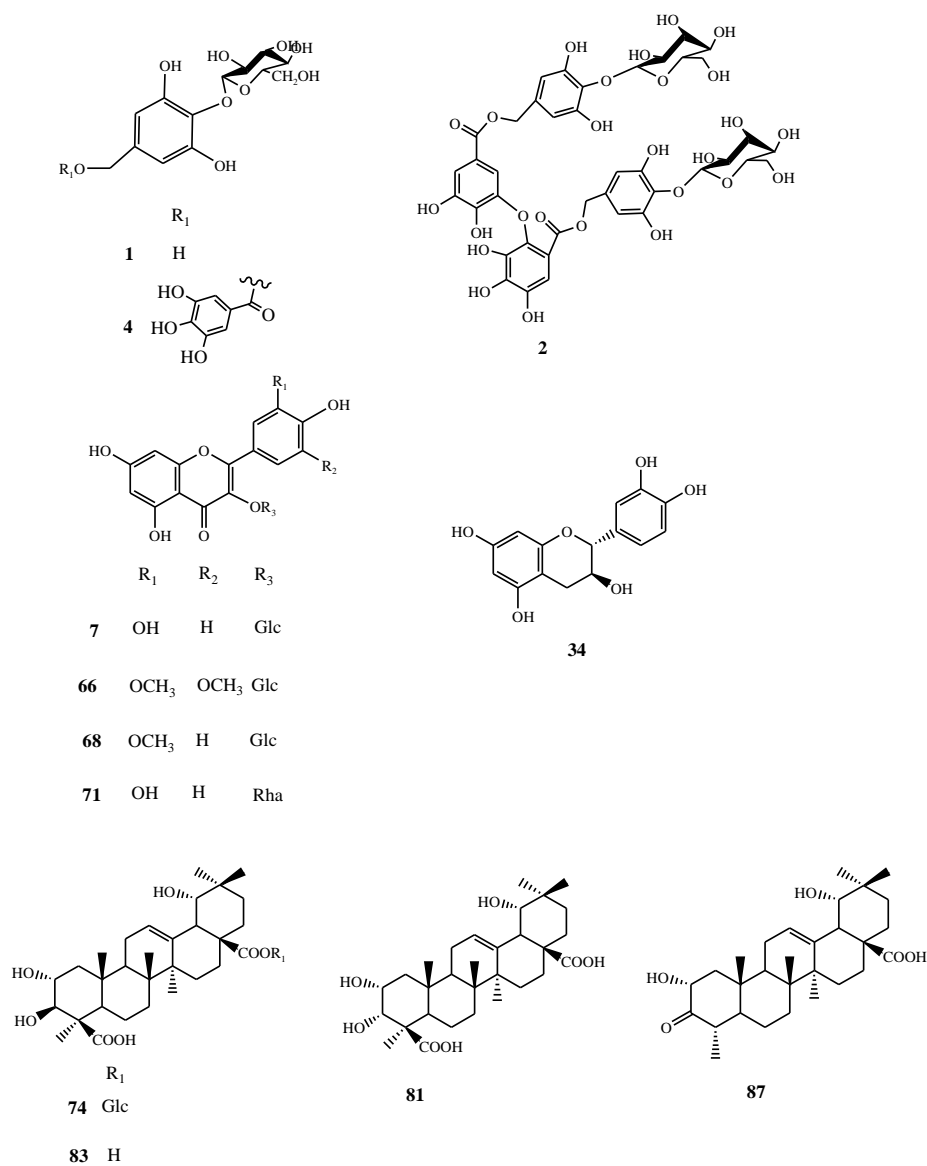


Figure 4.11. Compounds isolated from MeOH extract of *C. sativa* cv. Marrone di Roccadaspide shells.

Quantitative analysis by LC-ESI/QTrap/MS/MS

The amount of isolated compounds **34**, **66**, **68**, **71**, **74**, and **83**, occurring in the MeOH extract of *C. sativa* shells, ellagic acid (**67**), along with compounds **1**, **2**, **4**, and **7**, available in our laboratory as previously isolated from the MeOH extract of *C. sativa* leaves, were quantified by on liquid chromatography coupled to tandem mass spectrometry with ESI source and hybrid triple Quadrupole-linear ion Trap mass analyzer (LC-ESI/QTrap/MS/MS) instrument employed in MRM mode, a very sensitive and selective tandem mass spectrometry experiment. The MRM transitions reported in table 4.5 were chosen on the basis of the fragmentation pattern shown from each metabolite in own ESI/MSMS spectrum.

Table 4.5. Analytical parameters of the LC-ESI/QTrap/MS/MS method of *C. sativa* shells MeOH extract (MRM, negative ion mode).

Compound	MRM transition	R ²	Regression line	LOD (ng μL^{-1})	LOQ (ng μL^{-1})	mg/100g shells $\pm\text{SD}^*$
crenatin (1)	317→155	0.9955	Y=0.121x+0.0343	0.010	0.032	39.12±3.47
chestanin (2)	937→467	0.9971	Y=0.001x+0.00056	0.086	0.288	30.38±1.42
cretanin (4)	469→169	0.9966	Y=0.0353x+0.0009	0.013	0.043	40.45±2.63
quercetin 3-O- β -D-glucopyranoside (7)	463→301	0.9930	Y=3.52x+0.7220	0.006	0.021	1.63±0.02
catechin (34)	289→205	0.9924	Y=0.166x+0.0004	0.002	0.006	4.68±0.27
syringetin 3-O- β -D-glucopyranoside (66)	507→345	0.9913	Y=0.0355x+0.0157	0.050	0.168	20.47±0.37
ellagic acid (67)	301→284	0.9937	Y=0.071x+0.00285	0.016	0.055	55.92±0.51
isorhamnetin 3-O- β -D-glucopyranoside (68)	477→315	0.9977	Y=0.0168x+0.0016	0.066	0.221	36.02±2.63
quercetin-3-O- α -L-rhamnopyranoside (71)	447→301	0.9983	Y=1.74x +0.0193	0.006	0.020	0.57±0.01
bartogenic acid 28-O- β -D-glucopyranosyl ester (74)	679→517	0.9988	Y=0.010x+0.0010	0.036	0.120	58.06±2.03
bartogenic acid (83)	517→455	0.9920	Y=0.105x+0.0992	0.012	0.039	103.08±4.44

Therefore, for the $[M-H]^-$ pseudomolecular ion at m/z 317 (crenatin; **1**) the transition $317 \rightarrow 155$ was chosen for MRM analysis being the $[(M-162)-H]^-$ product ion at m/z 155, originated by the neutral loss of a glucose moiety, a main product ion. In turn, the $[M-H]^-$ pseudomolecular ion at m/z 937, corresponding to chestanin (**2**), showed a main $[(M-470)-H]^-$ product ion at m/z 467, due to the simultaneous loss of the glucose unit, the 3,4,5-trihydroxybenzyl alcohol unit and the galloyl unit. The mass tandem spectrum of the $[M-H]^-$ pseudomolecular ion at m/z 469 (cretanin; **4**) showed a very intense $[(M-300)-H]^-$ product ion at m/z 169, ascribable to the galloyl moiety and originated from the neutral loss of both the glucose unit and the 3,4,5-trihydroxybenzyl alcohol moiety. The flavonoids quercetin 3-*O*- β -D-glucopyranoside (**7**), syringetin 3-*O*- β -D-glucopyranoside (**66**), isorhamnetin 3-*O*- β -D-glucopyranoside (**68**), and quercetin 3-*O*- α -L-rhamnopyranoside (**71**), respectively corresponding to the $[M-H]^-$ pseudomolecular ions at m/z 463, 507, 477, and 447, yielded very simple fragmentation patterns in which the base peak was produced by the neutral loss of the sugar unit, respectively the glucose unit (neutral loss of 162 Da) for **7**, **66**, and **68**, and the rhamnose unit (neutral loss of 146 Da) for **71**. As MRM transition for ellagic acid (**67**) was chosen the $301 \rightarrow 284$ due to the neutral loss of the radical OH \cdot from the $[M-H]^-$ pseudomolecular ion at m/z 301. Catechin **28** ($[M-H]^-$ at m/z 289) showed a characteristic MS² product ion at m/z 205 due to the cleavage of the A-ring of flavan-3-ol. The $[M-H]^-$ pseudomolecular ion at m/z 679 of the triterpenoid bartogenic acid 28-*O*- β -D-glucopyranosyl ester (**74**), yielded a main product ion at m/z 517 formed by the neutral loss of the glucose moiety. The bartogenic acid (**83**) produced a main product ion at m/z 455 originated by neutral loss of both a carbon dioxide molecule (44 Da) and a water molecule (18 Da). Finally, on the basis of the above cited transitions selected for MRM experiments, the amount (mg/100 g dry weight) of each compound in the MeOH extract of *C. sativa* shells (table 1) was determined.

The quantitative results showed that compounds occurred in concentration ranges of 0.57-103.08 (mg/100 g). In particular, the triterpenoid bartogenic acid (**83**) exhibited the highest concentration, while the lowest concentration corresponded to quercetin 3-*O*- α -L-rhamnopyranoside (**71**).

4.4 Conclusions

With the aim to give a value to *C. sativa* cv. Marrone di Roccadaspide byproducts, a chemical and biological investigation of the MeOH extracts of leaves and shells has been carried out.

The phytochemical investigation of the MeOH extract of leaves highlighted the presence of phenolic and flavonoids compounds able to reduce UVB-induced p53 expression in HaCaT cell line. The obtained data are in agreement with Almeida *et al.*⁶¹ who reported that incubation of HaCaT with the extract of *C. sativa* caused no significant changes in basal DNA damage, but significantly reduced the number of lesions generated by the singlet oxygen generating system⁶², and extend the notion that this extract is able to reduce the effects of UVB irradiation, mainly due to crenatin (**1**), gallic acid (**3**), and cretanin (**4**). Therefore, the above data reinforce the hypothesis that the extract of *C. sativa* leaves, and the isolated compounds, might be an interesting option to prevent UV-induced/cell damage. Moreover, the antioxidant assay *in vitro* of the MeOH extracts of *C. sativa* byproducts has been evaluated.

Guided by the strong antioxidant activity exhibited by the MeOH extract of the shells, with the aim to achieve deeper insight into its chemical composition, the metabolite profile was obtained by an analytical approach based on high-performance liquid chromatography coupled to multiple-stage linear ion-trap and orbitrap high-resolution mass spectrometry (LC-ESI/LTQOrbitrap/MS/MSⁿ).

By this way the identification of several tannin derivatives, belonging to different chemical classes, such as hydrolysable tannins, comprising galloyl glucose derivatives and ellagitannins as hexahydroxydiphenoyl (HHDP) glucose derivatives, nonahydroxytriphenoyl (NHTP) derivatives with an acyclic glucose core, and flavanoellagitannins, along with condensed tannin proanthocyanidins, was obtained. Moreover, in order to unambiguously assign the chemical structure of the unknown compounds highlighted by the LC-ESI/LTQOrbitrap/MS/MSⁿ analysis, a phytochemical investigation was carried out. In this way 12 compounds, belonging to flavonoids, phenolic derivatives and triterpenoid classes have been isolated and unambiguously identified by 1D- and 2D-NMR experiments. Finally, by a LC-ESI/QTrap/MS/MS approach based on MRM experiments, 11 representative compounds have been quantified, showing *C. sativa* shells a rich source of antioxidative phenolics along with triterpenes, these latter never reported in *C. sativa* shells.

4.5 Experimental section

Plant material

The leaves of *Castanea sativa* Mill. cv. Marrone di Roccadaspide were collected at Roccadaspide, Salerno, in October 2014, while the shells were collected at Roccadaspide, Salerno, in October 2015, and identified by V. De Feo (Department of Pharmacy, University of Salerno, Italy). A voucher specimen has been deposited in this Department.

Extraction and isolation procedures

Extraction and isolation of the MeOH extract of C. sativa cv. Marrone di Roccadaspide leaves

The leaves of *C. sativa* (400 g) were dried and extracted at room temperature using solvents of increasing polarity such as petroleum ether (6 L for 3 days, three times), chloroform (6 L for 3 days, three times) and MeOH (6 L for 3 days, three times). After filtration and evaporation of the solvent to dryness in vacuo, 43.39 g of crude MeOH extract were obtained. The dried MeOH extract (3.0 g) was fractionated on a Sephadex LH-20 (Pharmacia) column (100 x 5 cm), using MeOH as mobile phase, affording 83 fractions (8 mL), monitored by TLC. Fractions 29–31 (25.1 mg) were chromatographed by semipreparative HPLC using MeOH–H₂O (1:3) as mobile phase (flow rate 2.5 mL/min) to yield compounds **3** (5.9 mg, t_R = 8.2 min) and **6** (1.4 mg, t_R = 26.0 min). Fractions 38–40 (28.5 mg) were chromatographed by semipreparative HPLC using MeOH–H₂O (3:7) as mobile phase (flow rate 2.5 mL/min) to yield compound **1** (1.1 mg, t_R = 5.2 min). Fractions 41–46 (43.0 mg) were chromatographed by semipreparative HPLC using MeOH–H₂O (5:5) as mobile phase (flow rate 2.5 mL/min) to yield compound **5** (2.2 mg, t_R = 5.8 min). Fractions 55–57 (36.1 mg) were chromatographed by semipreparative HPLC using MeOH–H₂O (3:7) as mobile phase (flow rate 2.5 mL/min) to yield compound **4** (11.8 mg, t_R = 24.3 min). Fractions 62–64 (12.0 mg) were chromatographed by semipreparative HPLC using MeOH–H₂O (3:7) as mobile phase (flow rate 2.5 mL/min) to yield compound **7** (1.3 mg, t_R = 12.2 min). Fractions 65–73 corresponded to compound **2** (52.2 mg).

Extraction and isolation of the MeOH extract of C. sativa cv. Marrone di Roccadaspide shells

C. sativa, cv. Marrone di Roccadaspide (404 g), shells were dried and extracted with petroleum ether and chloroform at room temperature (for 3 days, 2 times), and after with MeOH at room temperature (for 3 days, three times) to give 7.2 g of MeOH extract. The dried MeOH extract of *C. sativa* shells (3 g) was fractionated on a Sephadex LH-20 (Pharmacia) column (100 × 5 cm), using

MeOH as mobile phase, to afford 75 fractions (8 mL), monitored by TLC. Some of these fractions were further chromatographed by semipreparative HPLC using MeOH-H₂O as mobile phase (flow rate 2.5 mL/min). The phenolic and triterpenoid compounds were isolated by MeOH extracts shells in particular, fractions 14 and 15 (165.3 mg) were purified by HPLC using MeOH-H₂O (8-2) to obtain bartogenic acid 28-*O*-β-D-glucopyranosyl ester (**74**) (1.2 mg, *t_R* = 3.0 min). Fractions 19 and 20 (49.2 mg) were purified by HPLC using MeOH-H₂O (7-2) to obtain 2-epi-bartogenic acid (**81**) (2.1 mg, *t_R* = 6.2 min), bartogenic acid (**83**) (3.0 mg, *t_R* = 16.0 min), 2α,19α-dihydroxy-3-oxo-24-norolean-12-en-28-oic acid (**87**) (1.8 mg, *t_R* = 28.0 min). Fractions 29-32 (126.9 mg) were purified by HPLC using MeOH-H₂O (13:7) to obtain syringetin 3-*O*-β-D-glucopyranoside (**66**) (1.6 mg, *t_R* = 8.6 min) Fractions 33 and 34 (13.1 mg) were purified by HPLC using MeOH-H₂O (13:7) to obtain isorhamnetin 3-*O*-β-D-glucopyranoside (**68**) (1.6 mg, *t_R* = 8.6 min). Fractions 37-38 (13.1 mg) were chromatographed by semipreparative HPLC using MeOH-H₂O (3:7) as mobile phase (flow rate 2.5 mL/min) to yield crenatin (**1**) (1.1 mg, *t_R* = 5.2 min). Fractions 44-46 (14.7 mg) were chromatographed by semipreparative HPLC using MeOH-H₂O (3:7) as mobile phase (flow rate 2.5 mL/min) to yield cretanin (**4**) (11.8 mg, *t_R* = 24.3 min). Fractions 52-56 (45.8 mg) corresponded to catechin (**34**). Fractions 57-62 (12.0 mg) were chromatographed by semipreparative HPLC using MeOH-H₂O (3:7) as mobile phase (flow rate 2.5 mL/min) to yield quercetin 3-*O*-β-D-glucopyranoside (**7**) (1.5 mg, *t_R* = 12.2 min) and quercetin 3-*O*-α-L-rhamnopyranoside (**71**) (1.3 mg, *t_R* = 15.0 min). Finally, fractions 65-73 corresponded to chestanin (**2**) (52.2 mg). The configuration of the sugar units were established after hydrolysis with 1 N HCl, trimethylsilylation, and determination of the retention times by GC, as previously reported. The structures of these compounds were unambiguously elucidated by NMR spectroscopic.

Qualitative analysis

Qualitative LC-HRMS/MSⁿ analysis of MeOH extract of *C. sativa* shells was performed using a LC-ESI/LTQOrbitrap/MS/MSⁿ system consisting of a quaternary Accela 600 pump, an Accela autosampler, and LTQ Orbitrap XL mass spectrometer (ThermoScientific, San Jose, CA), operating in negative ionization mode. The separation was carried out by using a Synergi Polar column (RP-80A, 250 x 3.00 mm, 4µm; Phenomenex, Milano, Italy) at a flow rate of 0.2 mL/min and a mobile phase consisting of a combination of A (0.1% formic acid in water, v/v) and B (0.1% formic acid in acetonitrile, v/v). A linear gradient from 10 to 35% B in 20 min, held at 35% B for 5 min, from 35 to 55 % B in 12 min and from 55 to 100% B in 20 min, held to 100% B for 8 min was used. The autosampler was set to inject 6 µl of extract (0.5 mg/mL).

In the negative ion mode, the following experimental conditions for the ESI source were adopted: sheath gas at 15 (arbitrary units), auxiliary gas at 5 (arbitrary units), source voltage at 3.5 kV, capillary temperature at 280 °C, capillary voltage at -48 V and tube lens at -176.47 V.

The mass range was from 200 to 1500 *m/z* with a resolution of 30000. In order to get structural information, data-dependent experiments were performed by acquiring MS² spectra of the first and the second most intense ions from the HRMS scan event; moreover multiple-stage tandem mass (MSⁿ with n = 3, 4...) experiments on selected product ions were carried out. In both cases a normalization collision energy at 30%, a minimum signal threshold at 250, and an isolation width at 2.0 were used.

Quantitative analysis

For the quantitative analysis, mass spectrometer was used in Multiple Reaction Monitoring (MRM) mode, a very sensitive and selective tandem mass

spectrometry experiment that allows the selective isolation of the precursor ion in the first quadrupole Q1, its subsequent fragmentation in the collision cell, and the final monitoring of a selected product ion in the third quadrupole Q2, that in QTrap System can be operated in dual function, both as a quadrupole and Linear Ion Trap (LIT). In our MRM experiments it was always operated as a quadrupole.

LC-ESI/QqQ/MS/MS analyses of the MeOH extract of C. sativa leaves

Quantitative analysis (10 µg/mL of extract) were performed on an Agilent (Palo Alto, CA, USA) 1100 HPLC system equipped with an Atlantis T₃ 5 µm RP C18 column (150 mm×2.1 mm i.d.) and coupled to an Applied Biosystems API 2000 triple quadrupole instrument. Linear gradient elution was carried out by using 0.1% formic acid as eluent A and acetonitrile 0.1 % formic acid as B. The HPLC gradient started at 20% (B) for 5 min and returned 100% B in 45 min. Concerning with the ESI source conditions the instrument operated in the negative ion mode with declustering potential of -66 eV, focusing potential of -200 eV, entrance potential of -6 eV, collision energy of 35%, collision cell exit potential of -15 eV. The MeOH extract of *C. sativa* leaves was dissolved in MeOH and 10 µL injected in triplicate. For vitexin, used as internal standard, fragmentation reaction involving the loss of a neutral unit of 120 amu from the [M-H]⁻ ion at *m/z* 431.

LC-ESI/QTrap/MS/MS analysis of the MeOH extract of C. sativa shells

Quantitative analysis was performed on a Shimadzu HPLC system coupled to a hybrid triple quadrupole-linear ion trap (QTrap) 6500 LC-MS/MS System (SCIEX, Concord, Ontario (Canada) by using a Kinetex EVO 1.7 µm RP C18 column (Phenomenex, 100 × 2.1 mm), a flow rate of 0.23 mL/min, and a mobile phase consisting of a combination of A (0.1% formic acid in water, v/v) and B (0.1% formic acid in acetonitrile, v/v). A linear gradient from 10 to 35% B in 3.4 min, held at 35% B for 45 sec, from 35 to 55 % B in 2.4 min and from 55 to 100%

B in 3.4 min, held at 100% B for 2.36 min was used. The autosampler was set to inject 2 μL of extract (500 $\text{ng}/\mu\text{L}$).

Calibration and quantification

Stock solutions (1 mg/mL) of the external standards (ES)

- Compounds **1-7** isolated from MeOH extract of *C. sativa* leaves were prepared by dissolving each compound in MeOH. Stock solutions were diluted with appropriate amounts of MeOH to give 7 solutions containing 0.25, 0.5, 1, 2, 4, 5 and 6 $\mu\text{g}/\text{mL}$ of ES.
- Compounds **1, 2, 4, 7, 34, 66-68, 71, 74** and **83** isolated by MeOH extract of *C. sativa* shells were prepared by dissolving each compound in acetonitrile/water (70:30 V/V) was used. Stock solutions were diluted with appropriate amounts of acetonitrile to give 9 solutions containing 0.01, 0.05, 0.5, 1.0, 2.5, 5, 10, 25, 35 $\text{ng}/\mu\text{L}$ of each standard for shells. To each standard solution, as well as to the MeOH extract of *C. sativa* leaves and shells, an appropriate amount of internal standard, vitexin and resveratrol, respectively, was added to yield a final concentration of 1 $\mu\text{g}/\text{mL}$. Calibration curves were constructed by injecting each standard solution at each concentration level in triplicate. The ratios of the peak areas of the ES to those of the IS were calculated and plotted against the corresponding concentrations of the standard compounds using linear regression (least squares) to generate standard curves.

Determination of total phenolic content, determination of DPPH and TEAC radical scavenging activity.

Reported in the section: general experimental procedures.

*Biological assay: materials and methods**Cell Culture*

Immortalized human keratinocytes, HaCaT cells, were grown in Dulbecco's modified Eagle's medium (DMEM, GIBCO, Grand Island, NY) containing 10% fetal bovine serum (FBS, GIBCO, Grand Island, NY), 2 mM L-glutamine (GIBCO, Grand Island, NY) and antibiotics (100 IU/mL penicillin G, 100 µg/mL streptomycin, GIBCO, Grand Island, NY). Cells were cultured in a humidified incubator at 37°C with 5% CO₂. All derivatives (compounds **1-7**) were dissolved in dimethylsulfoxide (DMSO, Sigma-Aldrich, St. Louis, MO, USA) and diluted in DMEM to obtain treating concentrations of 5 µg/mL. The final concentration of DMSO in the medium was 0.5%.

HaCaT cells were plated onto 60 mm culture plates in 3 mL of fresh culture medium until they reached a confluence of about 70%, when the stimulation was performed. All samples (5 µg/mL in 0.5% DMSO) were added to the culture medium and cells were incubated for 2 h at 37 °C with 5% CO₂ prior to UVB irradiation.

UVB irradiation

HaCaT cells were washed and covered with 3 mL of phosphate-buffered saline (PBS 1X, GIBCO, Grand Island, NY) and irradiated with UVB 60 mJ/cm². The PBS was then replaced with the culture medium containing chemicals, and the cells were allowed to recover for 24h. As a source of UVB, six Philips TL12/60W fluorescent lamps (Philips, Eindhoven, The Netherlands) emitting UV light between 290 and 320 nm, with a peak at 300 nm, was used. The intensity of UVB irradiation, measured with a UV meter (Spectrolyne mod., Spectronics Corp., Westbury, NY, USA) was 0.8 mW/cm² at 15 cm distance. The optimal dose of UVB 60 mJ/cm² was determined by irradiating HaCaT as previously described .

Analysis of cell viability

Cell vitality was determined with the Trypan blue method. Twenty-four hours after treatment, cells were washed twice with PBS, incubated with trypsin/EDTA for 5 min. and centrifuged at 4000 rpm for 15 min. The cell pellet was resuspended in an appropriate volume of PBS, and 10 μ L of the cell suspension was combined with 20 μ L of Trypan blue solution. The mix was incubated for 5 min at room temperature and the number of unstained cells (vital cells) and the total number of cells (vital and not) were determined on the hemacytometer under a microscope (dead cells will take up the Trypan blue stain). The percentage of viable cells was determined dividing the number of unstained cells by the total number of cells.

Western blot analysis

Total cell extracts were prepared 24h after UV irradiation. Briefly, harvested cells were washed twice with ice-cold PBS 1X and lysed by radioimmunoprecipitation assay buffer with protease and phosphatase inhibitor cocktails (Sigma Chemical Co., St. Louis, MO, USA). Equal quantities of total proteins (20 μ g) were loaded on 10 % Bis–Tris NuPage denaturing gel (Invitrogen Life Technologies, Carlsbad, CA, USA) for electrophoresis. Gels were transferred to nitrocellulose membranes and were probed with anti-mouse p53 (DO-1): sc-126 monoclonal antibody (Santa Cruz Biotechnology, Santa Cruz, CA, USA). The immunodetection of proteins was performed with the use of the WesternDot™ 625 Western Blot Kit (Invitrogen Life Technologies, Grand Island, NY, USA). The detection step relies on a biotinylated secondary antibody and an interaction with a QdotR 625 streptavidin conjugate. Given that the QdotR 625 nanocrystal has a high extinction in the UV and blue wavelengths, proteins were detected using a Gel-Doc Imaging System. The intensity of the bands was expressed in volume-

adjusted intensity (intensity mm²). Normalization of total loaded proteins was obtained by immunodetection of GAPDH on the same blotted membrane with specific antibodies (Sigma-Aldrich, Oakville, ON, Canada). Ratios of p53 protein band intensity relative to GAPDH band intensity were calculated for each sample using the Quantity-One software (Bio-Rad, Hercules, CA, USA) provided with the UV detection system.

Cell Culture and Differentiation to Macrophages

The THP-1 human monocytic leukemia cell line was purchased from the European Collection of Cell Cultures (Salisbury, UK). Cells were cultured in RPMI 1640 medium (PAA) supplemented with antibiotics (100 U/ mL penicillin, 100 mg/mL streptomycin) (Sigma-Aldrich), 10% FBS (Sigma-Aldrich), and 2 mM L-glutamine (Sigma-Aldrich). Cultures were kept in an incubator at 37 °C in a water-saturated atmosphere of air containing 5% CO₂. Cells were passaged at approximately three-day intervals. Stabilized cells (3rd–15th passage) were split into microtitration plates to obtain a concentration of 500000 cells/mL, differentiation to macrophages was induced by phorbol myristate acetate (PMA) dissolved in dimethyl sulfoxide (DMSO) at a final concentration of 50 ng/mL, and the cells were incubated for 24 h. In comparison with monocytes, differentiated macrophages tend to adhere to the bottom of the cultivation plates. Unattached cells were washed out with PBS (PAA) and incubated with fresh complete RPMI medium, i.e., containing antibiotics and FBS but without PMA, for the next 24 h. The medium was then aspirated, and the cells were washed with PBS and cultivated for another 24 h in serum-free RPMI 1640 medium. These prepared macrophages were used for the detection of the inflammatory-like response.

Cytotoxicity Testing

THP-1 cells (floating monocytes, 500000 cells/mL) were incubated in 100 μ L of a serum-free RPMI 1640 medium and seeded into 96-well plates in triplicate at 37 $^{\circ}$ C. Measurements were taken 24 h after treatment with increasing concentrations of the test compounds dissolved in DMSO. Viability was measured by the cell proliferation reagent WST-1 (Roche, Basel, Switzerland) according to the manufacturer's manual. The amount of formazan created (which correlates to the number of metabolically active cells in the culture) was calculated as a percentage of the control cells, which were treated only with DMSO and were assigned as 100%.

Detection of Activation of the NF- κ B.

THP1-XBlueTM-MD2-CD14 cells were seeded in a serum-free medium (50 000 cells/100 μ L/well) into 96-well plate and were incubated for 2 hours. In the following step, the solutions of tested extracts were added at the final concentration of 5 μ g/mL and the standard antioxidant prednisone was added at the final concentration of 1 μ M. After 1 h of the incubation, the inflammatory response was induced by LPS [except of the control cells (- CTRL)].

Finally, The NF- κ B activation, through QUANTI-BlueTM, was measured 24 h after the LPS addition by Fluostar Omega Microplate Reader (BMG Labtech).

Detection of intracellular oxidative stress by ROS assay

THP1-XBlueTM-MD2-CD14 cells were seeded in a serum-free medium (50 000 cells/100 μ L/well) into a black 96-well plate and were incubated for 2 hours. In the following step, the solutions of tested compounds were added at the final concentration of 5 μ g/mL and the standard antioxidant quercetin was added at the final concentration of 5 μ M. After 30 minutes of the treatment of the cells with the compounds, pyocyanin was added in final concentration 100 μ M in each well (except in the group of negative control) and the cells were incubated for 30

minutes. After this incubation (DCFH-DA) 2'-7'-Dichlorodihydrofluorescein diacetate (5 $\mu\text{g/mL}$) was introduced into the cell medium of all the wells and the cells were incubated for the next 30 minutes. Finally, the intracellular fluorescence of the dichlorofluorescein product was measured by Fluostar Omega Microplate Reader (BMG Labtech) using the $\lambda(\text{ex./em.}) = 480/530$ nm.

Statistics

All statistical analyses were performed using GraphPad Prism 7.0 (San Diego, CA, USA). Data were analysed with two-tailed, *t*-test. Comparisons between groups were made using a one-way analysis of variance test, followed by the Bonferroni's multiple comparisons test. Values of $p < 0.05$ were considered significant.

References

1. Hadshiew, I. M.; Eller, M. S.; Gilchrest, B. A., Skin aging and photoaging: the role of DNA damage and repair. *Am J Contact Dermat.* **2000**, *11*, 19-25.
2. Nawwar, M.; Hussein, S.; Ayoub, N.; Hashim, A.; El-Sharawy, R.; Lindequist, U.; Harms, M.; Wende, K., Constitutive phenolics of *Harpephyllum caffrum* (Anacardiaceae) and their biological effects on human keratinocytes. *Fitoterapia* **2011**, *82*, 1265-1271.
3. Dinkova-Kostova, A. T., Phytochemicals as protectors against ultraviolet radiation: versatility of effects and mechanisms. *Planta Med.* **2008**, *74*, 1548-1559.
4. Afaq, F.; Mukhtar, H., Botanical antioxidants in the prevention of photocarcinogenesis and photoaging. *Exp. Dermatol.* **2006**, *15*, 678-684.
5. Hiermann, A.; Kedwani, S.; Schramm, H. W.; Seger, C., A new pyrrole alkaloid from seeds of *Castanea sativa*. *Fitoterapia* **2002**, *73*, 22-27.
6. Braga, N.; Rodrigues, F.; P. P. Oliveira, M. B., *Castanea sativa* by-products: a review on added value and sustainable application. *Nat. Prod. Res.* **2015**, *29*, 1-18.
7. Mendes De Vasconcelos, M. D. C. B.; Bennett, R. N.; Rosa, E. A. S.; Cardoso, J. V. F., Primary and Secondary Metabolite Composition of Kernels from Three Cultivars of Portuguese Chestnut (*Castanea sativa* Mill.) at Different Stages of Industrial Transformation. *J. Agric. Food Chem.* **2007**, *55*, 3508-3516.
8. Barreira, J. C. M.; Ferreira, I. C. F. R.; Oliveira, M. B. P. P.; Pereira, J. A., Antioxidant activities of the extracts from chestnut flower, leaf, skins and fruit. *Food Chem.* **2008**, *107*, 1106-1113.
9. Delgado, T.; Pereira, J. A.; Baptista, P.; Casal, S.; Ramalhosa, E., Shell's influence on drying kinetics, color and volumetric shrinkage of *Castanea sativa* Mill. fruits. *Food Res Int.* **2014**, *55*, 426-435.
10. Oliveira, I.; Sousa, A.; Valentao, P.; Andrade, P. B.; Ferreira, I. C. F. R.; Ferreres, F.; Bento, A.; Seabra, R.; Estevinho, L.; Pereira, J. A., Hazel (*Corylus avellana* L.) leaves as source of antimicrobial and antioxidative compounds. *Food Chem.* **2007**, *105*, 1018-1025.
11. Moure, A.; Conde, E.; Falqué, E.; Domínguez, H.; Parajó, J. C., Production of nutraceuticals from chestnut burs by hydrolytic treatment. *Food Res Int.* **2014**, *65*, Part C, 359-366.
12. Basile, A.; Sorbo, S.; Giordano, S.; Ricciardi, L.; Ferrara, S.; Montesano, D.; Castaldo Cobianchi, R.; Vuotto, M. L.; Ferrara, L., Antibacterial and allelopathic activity of extract from *Castanea sativa* leaves. *Fitoterapia* **2000**, *71*, S110-S116.
13. Almeida, I. F.; Pinto, A. S.; Monteiro, C.; Monteiro, H.; Belo, L.; Fernandes, J.; Bento, A. R.; Duarte, T. L.; Garrido, J.; Bahia, M. F.; Sousa Lobo,

- J. M.; Costa, P. C., Protective effect of *C. sativa* leaf extract against UV mediated-DNA damage in a human keratinocyte cell line. *J Photochem Photobiol B* **2015**, *144*, 28-34.
14. Kirmizibekmez, H.; Ariburnu, E.; Masullo, M.; Festa, M.; Capasso, A.; Yesilada, E.; Piacente, S., Iridoid, phenylethanoid and flavonoid glycosides from *Sideritis trojana*. *Fitoterapia* **2012**, *83*, 130-136.
15. Pereira do Amaral, F.; Napolitano, A.; Masullo, M.; Campaner dos Santos, L.; Festa, M.; Vilegas, W.; Pizza, C.; Piacente, S., HPLC-ESIMSⁿ Profiling, Isolation, Structural Elucidation, and Evaluation of the Antioxidant Potential of Phenolics from *Paepalanthus geniculatus*. *J. Nat. Prod.* **2012**, *75*, 547-556.
16. Montoro, P.; Teyeb, H.; Masullo, M.; Mari, A.; Douki, W.; Piacente, S., LC-ESI-MS quali-quantitative determination of phenolic constituents in different parts of wild and cultivated *Astragalus gombiformis*. *J. Pharm. Biomed. Anal.* **2013**, *72*, 89-98.
17. Lembo, S.; Balato, A.; Di Caprio, R.; Cirillo, T.; Giannini, V.; Gasparri, F.; Monfrecola, G., The Modulatory Effect of Ellagic Acid and Rosmarinic Acid on Ultraviolet-B-Induced Cytokine/Chemokine Gene Expression in Skin Keratinocyte (HaCaT) Cells. *Biomed Res Int.* **2014**.
18. Huang, Y. L.; Tanaka, T.; Matsuo, Y.; Kouno, I.; Li, D. P.; Nonaka, G. I., Two new phenolic glucosides and an ellagitannin from the leaves of *Castanopsis sclerophylla*. *Phytochem Lett.* **2012**, *5*, 158-161.
19. Xu, T. Y.; Wang, Z. H.; Lei, T. L.; Lv, C. N.; Wang, J.; Lu, J. C., New flavonoid glycosides from *Sedum aizoon* L. *Fitoterapia* **2015**, *101*, 125-132.
20. Chen, J.; Mangelinckx, S.; Ma, L.; Wang, Z. T.; Li, W. L.; De Kimpe, N., Caffeoylquinic acid derivatives isolated from the aerial parts of *Gynura divaricata* and their yeast alpha-glucosidase and PTP1B inhibitory activity. *Fitoterapia* **2014**, *99*, 1-6.
21. Rodrigues, F.; Santos, J.; Pimentel, F. B.; Braga, N.; Palmeira-de-Oliveira, A.; Oliveira, M. B. P. P., Promising new applications of *Castanea sativa* shell: nutritional composition, antioxidant activity, amino acids and vitamin E profile. *Food Funct.* **2015**, *6*, 2854-2860.
22. D'Urso, G.; Maldini, M.; Pintore, G.; d'Aquino, L.; Montoro, P.; Pizza, C., Characterisation of *Fragaria vesca* fruit from Italy following a metabolomics approach through integrated mass spectrometry techniques. *LWT-Food Sci. Technol.* **2016**, *74*, 387-395.
23. Moilanen, J.; Sinkkonen, J.; Salminen, J. P., Characterization of bioactive plant ellagitannins by chromatographic, spectroscopic and mass spectrometric methods. *Chemoecology* **2013**, *23*, 165-179.
24. Nonaka, G.; Ishimaru, K.; Mihashi, K.; Iwase, Y.; Ageta, M.; Nishioka, I., Tannins and Related-Compounds .63. Isolation and Characterization of

Mongolicain-a and Mongolicain-B - Novel Tannins from *Quercus* and *Castanopsis* Species. *Chem Pharm Bull.* **1988**, *36*, 857-869.

25. De Rosso, M.; Tonidandel, L.; Larcher, R.; Nicolini, G.; Dalla Vedova, A.; De Marchi, F.; Gardiman, M.; Giust, M.; Flamini, R., Identification of new flavonols in hybrid grapes by combined liquid chromatography-mass spectrometry approaches. *Food Chem.* **2014**, *163*, 244-251.

26. Barros, L.; Alves, C. T.; Duenas, M.; Silva, S.; Oliveira, R.; Carvalho, A. M.; Henriques, M.; Santos-Buelga, C.; Ferreira, I. C. F. R., Characterization of phenolic compounds in wild medicinal flowers from Portugal by HPLC-DAD-ESI/MS and evaluation of antifungal properties. *Ind Crop Prod.* **2013**, *44*, 104-110.

27. Ablajan, K.; Tuoheti, A., Fragmentation characteristics and isomeric differentiation of flavonol *O*-rhamnosides using negative ion electrospray ionization tandem mass spectrometry. *Rapid Commun. Mass Spectrom.* **2013**, *27*, 451-460.

28. Ji, S.; He, D.-d.; Wang, T.-y.; Han, J.; Li, Z.; Du, Y.; Zou, J.-h.; Guo, M.-z.; Tang, D.-q., Separation and characterization of chemical constituents in *Ginkgo biloba* extract by off-line hydrophilic interaction \times reversed-phase two-dimensional liquid chromatography coupled with quadrupole-time of flight mass spectrometry. *J. Pharm. Biomed. Anal.* **2017**, *146*, 68-78.

29. Lin, L.-Z.; Chen, P.; Harnly, J. M., New Phenolic Components and Chromatographic Profiles of Green and Fermented Teas. *J. Agric. Food Chem.* **2008**, *56*, 8130-8140.

30. Braunberger, C.; Zehl, M.; Conrad, J.; Fischer, S.; Adhami, H.-R.; Beifuss, U.; Krenn, L., LC-NMR, NMR, and LC-MS identification and LC-DAD quantification of flavonoids and ellagic acid derivatives in *Drosera peltata*. *J. Chromatogr. B: Anal. Technol. Biomed. Life Sci.* **2013**, *932*, 111-116.

31. Pfundstein, B.; El Desouky, S. K.; Hull, W. E.; Haubner, R.; Erben, G.; Owen, R. W., Polyphenolic compounds in the fruits of Egyptian medicinal plants (*Terminalia bellerica*, *Terminalia chebula* and *Terminalia horrida*): Characterization, quantitation and determination of antioxidant capacities. *Phytochemistry* **2010**, *71*, 1132-1148.

32. Zehl, M.; Braunberger, C.; Conrad, J.; Crnogorac, M.; Krasteva, S.; Vogler, B.; Beifuss, U.; Krenn, L., Identification and quantification of flavonoids and ellagic acid derivatives in therapeutically important *Drosera* species by LC-DAD, LC-NMR, NMR, and LC-MS. *Anal Bioanal Chem.* **2011**, *400*, 2565-76.

33. Kumar, S.; Chandra, P.; Bajpai, V.; Singh, A.; Srivastava, M.; Mishra, D. K.; Kumar, B., Rapid qualitative and quantitative analysis of bioactive compounds from *Phyllanthus amarus* using LC/MS/MS techniques. *Ind Crop Prod.* **2015**, *69*, 143-152.

34. Muccilli, V.; Cardullo, N.; Spatafora, C.; Cunsolo, V.; Tringali, C., alpha-Glucosidase inhibition and antioxidant activity of an oenological commercial tannin. Extraction, fractionation and analysis by HPLC/ESI-MS/MS and (1)H NMR. *Food Chem.* **2017**, *215*, 50-60.
35. Regueiro, J.; Sanchez-Gonzalez, C.; Vallverdu-Queralt, A.; Simal-Gandara, J.; Lamuela-Raventos, R.; Izquierdo-Pulido, M., Comprehensive identification of walnut polyphenols by liquid chromatography coupled to linear ion trap-Orbitrap mass spectrometry. *Food Chem.* **2014**, *152*, 340-348.
36. Boulekbache-Makhlouf, L.; Meudec, E.; Chibane, M.; Mazauric, J. P.; Slimani, S.; Henry, M.; Cheynier, V.; Madani, K., Analysis by high-performance liquid chromatography diode array detection mass spectrometry of phenolic compounds in fruit of *Eucalyptus globulus* cultivated in Algeria. *J Agric Food Chem.* **2010**, *58*, 12615-24.
37. Fernandes, A.; Sousa, A.; Mateus, N.; Cabral, M.; de Freitas, V., Analysis of phenolic compounds in cork from *Quercus suber* L by HPLC-DAD/ESI-MS. *Food Chem.* **2011**, *125*, 1398-1405.
38. Diaz-de-Cerio, E.; Gomez-Caravaca, A. M.; Verardo, V.; Fernandez-Gutierrez, A.; Segura-Carretero, A., Determination of guava (*Psidium guajava* L.) leaf phenolic compounds using HPLC-DAD-QTOF-MS. *J Funct Foods.* **2016**, *22*, 376-388.
39. Han, L.; Hatano, T.; Okuda, T.; Yoshida, T., Tannins of *Stachyurus* species. III. Stachyuranins A, B and C, three new complex tannins from *Stachyurus praecox* leaves. *Chem. Pharm. Bull.* **1995**, *43*, 2109-14.
40. Sanz, M.; Cadahia, E.; Esteruelas, E.; Munoz, A. M.; Fernandez de Simon, B.; Hernandez, T.; Estrella, I., Phenolic Compounds in Chestnut (*Castanea sativa* Mill.) Heartwood. Effect of Toasting at Cooperage. *J. Agric. Food Chem.* **2010**, *58*, 9631-9640.
41. Azevedo, J.; Fernandes, A.; Oliveira, J.; Bras, N. F.; Reis, S.; Lopes, P.; Roseira, I.; Cabral, M.; Mateus, N.; de Freitas, V., Reactivity of Cork Extracts with (+)-Catechin and Malvidin-3-*O*-glucoside in Wine Model Solutions: Identification of a New Family of Ellagitannin-Derived Compounds (Corklins). *J Agric Food Chem.* **2017**, *65*, 8714-8726.
42. Petit, E.; Lefeuvre, D.; Jacquet, R.; Pouysegue, L.; Deffieux, D.; Quideau, S., Remarkable biomimetic chemoselective aerobic oxidation of flavano-ellagitannins found in oak-aged wine. *Angew Chem Int Ed Engl.* **2013**, *52*, 11530-3.
43. Nonaka, G.; Nakayama, S.; Nishioka, I., Tannins and Related-Compounds .88. Isolation and Structures of Hydrolyzable Tannins, Phillyraeoidins-a-E from *Quercus-Phillyraeoides*. *Chem Pharm Bull.* **1989**, *37*, 2030-2036.
44. D'Urso, G.; Maldini, M.; Pintore, G.; d'Aquino, L.; Montoro, P.; Pizza, C., Characterisation of *Fragaria vesca* fruit from Italy following a metabolomics

approach through integrated mass spectrometry techniques. *LWT-Food Sci Technol.* **2016**, *74*, 387-395.

45. Omar, M.; Matsuo, Y.; Maeda, H.; Saito, Y.; Tanaka, T., New Metabolites of C-Glycosidic Ellagitannin from Japanese Oak Sapwood. *Org. Lett.* **2014**, *16*, 1378-1381.

46. Mato, M. C.; Mendez, J.; Vazquez, A., Polyphenolic auxin protectors in buds of juvenile and adult chestnut. *Physiol. Plant.* **1994**, *91*, 23-6.

47. Pereira, A.; Bester, M.; Soundy, P.; Apostolides, Z., Activity-guided isolation and identification of the major antioxidant and anticancer compounds from a commercial *Pelargonium sidoides* tincture. *Med. Chem. Res.* **2015**, *24*, 3838-3852.

48. Callemien, D.; Collin, S., Use of RP-HPLC-ESI(-)-MS/MS to differentiate various proanthocyanidin isomers in lager beer extracts. *J. Am. Soc. Brew. Chem.* **2008**, *66*, 109-115.

49. Fitzpatrick, D. F.; Fleming, R. C.; Bing, B.; Maggi, D. A.; O'Malley, R. M., Isolation and Characterization of Endothelium-Dependent Vasorelaxing Compounds from Grape Seeds. *J. Agric. Food Chem.* **2000**, *48*, 6384-6390.

50. Jimenez-Sanchez, C.; Lozano-Sanchez, J.; Gabaldon-Hernandez, J. A.; Segura-Carretero, A.; Fernandez-Gutierrez, A., RP-HPLC-ESI-QTOF/MS2 based strategy for the comprehensive metabolite profiling of *Sclerocarya birrea* (marula) bark. *Ind Crop Prod.* **2015**, *71*, 214-234.

51. Wang, Q.; Lu, Z.; Zhang, L.; Zhang, Q.; Wang, M.; Zhao, H.; Liu, Y.; Fu, S.; Huang, Z.; Xie, Z.; Yu, H.; Zhang, Z.; Gao, X., Applying characteristic fragment filtering for rapid detection and identification of ingredients in rhubarb by HPLC coupled with linear ion trap-Orbitrap mass spectrometry. *J. Sep. Sci.* **2017**, *40*, 2854-2862.

52. Sun, J.; Liu, X.; Yang, T.; Slovin, J.; Chen, P., Profiling polyphenols of two diploid strawberry (*Fragaria vesca*) inbred lines using UHPLC-HRMS(n). *Food Chem.* **2014**, *146*, 289-98.

53. Kapusta, I.; Janda, B.; Szajwaj, B.; Stochmal, A.; Piacente, S.; Pizza, C.; Franceschi, F.; Franz, C.; Oleszek, W., Flavonoids in horse chestnut (*Aesculus hippocastanum*) seeds and powdered wastewater byproducts. *J. Agric. Food Chem.* **2007**, *55*, 8485-8490.

54. Jaiswal, R.; Karar, M. G. E.; Gadir, H. A.; Kuhnert, N., Identification and Characterisation of Phenolics from *Ixora coccinea* L. (Rubiaceae) by Liquid Chromatography Multi-stage Mass Spectrometry. *Phytochem. Anal.* **2014**, *25*, 567-576.

55. Jaiswal, R.; Jayasinghe, L.; Kuhnert, N., Identification and characterization of proanthocyanidins of 16 members of the *Rhododendron* genus (Ericaceae) by tandem LC-MS. *J Mass Spectrom* **2012**, *47*, 502-15.

56. Hilbert, G.; Temsamani, H.; Bordenave, L.; Pedrot, E.; Chaher, N.; Cluzet, S.; Delaunay, J.-C.; Ollat, N.; Delrot, S.; Merillon, J.-M.; Gomes, E.; Richard, T., Flavonol profiles in berries of wild *Vitis* accessions using liquid chromatography coupled to mass spectrometry and nuclear magnetic resonance spectrometry. *Food Chem.* **2015**, *169*, 49-58.
57. Musa, A.; Al-muaikel, N. S.; Abdel-Bakky, M. S., Phytochemical and pharmacological evaluations of ethanolic extract of *Bassia eriophora*. *Pharma Chem.* **2016**, *8*, 169-178.
58. Arramon, G.; Saucier, C.; Colombani, D.; Glories, Y., Identification of triterpene saponins in *Quercus robur* L. and *Q. petraea* Liebl. heartwood by LC-ESI/MS and NMR. *Phytochem. Anal.* **2002**, *13*, 305-310.
59. Nguyen, T. D.; Nguyen, H. D.; Le, N. T., New flavonoid and pentacyclic triterpene from *Sesamum indicum* leaves. *Nat. Prod. Res.* **2016**, *30*, 311-315.
60. Chen, H.-D.; Yang, S.-P.; Liao, S.-G.; Zhang, C.-R.; Yue, J.-M., Three new 24-noroleanane triterpenoids from *Quercus aliena* var. *acuteserrata*. *Helv. Chim. Acta* **2006**, *89*, 1971-1977.
61. Ouyang, M. A.; Wein, Y. S.; Su, R. K.; Kuo, Y. H., Rhusemialins A-C, new cyclolignan esters from the roots of *Rhus javanica* var. *roxburghiana*. *Chem Pharm Bull.* **2007**, *55*, 804-7.
62. Szajwaj, B.; Moldoch, J.; Masullo, M.; Piacente, S.; Oleszek, W.; Stochmal, A., Amides and Esters of Phenylpropenoic Acids from the Aerial Parts of *Trifolium pallidum*. *Nat Prod Commun.* **2011**, *6*, 1293-1296.

General experimental procedures

Chromatographic method

Analytical Thin-layer chromatography (TLC) in direct phase was performed with sheets of silica gel laminated on glass 60 F254 of 0.25 mm (Merck). The revelation was carried out both with UV light at 254 and 366 nm and with the following detector electrospray: saturated solution of cerium sulphate in 65% sulfuric acid, followed by heating at 120 degrees for 15 minutes.

For Molecular Exclusion Chromatography, was used a resin of Sephadex LH-20 (25-100 mm Pharmacia), eluting with MeOH a constant flow of 1.2 mL / min. The size of the column used is 100x5 cm.

HPLC separations were carried out on a Waters 590 system equipped with a Waters R401 refractive index detector, a Waters XTerra Prep MSC18 column (300 x 7.8 mm i.d.), and a Rheodyne injector.

Chemical physics method

Optical rotations. Optical rotations were obtained on an Autopol IV (Rudolph Research Analytical) polarimeter.

Infrared spectroscopy. IR measurements were obtained on a Bruker IFS-48 spectrometer.

Electronic circular dichroism (ECD). Electronic circular dichroism spectra were obtained using a JASCO J-810 spectrometer.

Nuclear magnetic resonance spectroscopy (NMR). NMR experiments were performed on a Bruker DRX-600 spectrometer (Bruker BioSpin GmbH, Rheinstetten, Germany) equipped with a Bruker 5 mm TCI CryoProbe at 300 K. All 2D-NMR spectra were acquired in MeOH-*d*₄ (99.95%,) and standard pulse

sequences and phase cycling were used for Double Quantum Filter Homonuclear Correlation Spectroscopy (DQF-COSY), Heteronuclear Single-Quantum Correlation Spectroscopy (HSQC), and the Heteronuclear Multiple Bond Correlation (HMBC) spectra. The NMR data were processed using TOPSPIN 3.2 software. The Rotating-frame Overhauser Spectroscopy (ROESY) spectra were acquired with $t_{\text{mix}} = 400$ ms.

High Resolution Electrospray Ionisation Mass Spectrometry (HRESIMS). HRESIMS spectra were carried out using a Thermo Scientific Accela HPLC system (Thermo Scientific, Germany) equipped coupled to a LTQ-Orbitrap XL mass spectrometer. operating in negative and positive ion mode. The Orbitrap mass analyzer was calibrated according to the manufacturer's directions using a mixture of caffeine, methionine-arginine-phenylalanine-alanine-acetate (MRFA), sodium dodecyl sulfate, sodium taurocholate and Ultramark 1621. Data were collected and analyzed using the software provided by the manufacturer. In full LC-ESI/LTQOrbitrap/MS experiments Total Ion Current (TIC) profile was produced by monitoring the intensity of all the ions produced and acquired in every scan during the chromatographic run. In order to get structural information, Data Dependent experiments were performed. For the data-dependent scan, the first and the second most intense ions from the HRMS scan event were selected, in order to offer their tandem mass (MS^2) product ions with a normalization collision energy at 30%, a minimum signal threshold at 250, and an isolation width at 2.0; multiple-stage tandem mass (MS^n with $n = 3, 4, \dots$) experiments on selected product ions were carried out by the same collision energy.

Quantitative analysis

For quantitative analysis was used:

General experimental procedures

- an Agilent (Palo Alto, CA, USA) 1100 HPLC system coupled to an AB Sciex (AB Sciex, Foster City, CA, USA) API2000 triple quadrupole instrument.
- a Shimadzu HPLC system coupled to a hybrid triple quadrupole-linear ion trap (QTrap) 6500 LC-MS/MS System (SCIEX, Concord, Ontario (Canada))

Method validation for quantitative analysis

LC-ESI/QqQ/MS/MS method was validated according to the European Medicines Agency (EMA) guidelines relating to the validation of analytical methods, in particular precision, specificity, linearity, limit of quantification (LOQ) and limit of detection (LOD) were determined. Precision was evaluated at five concentrations for each compound through triplicate intra-day assays and inter-day assays over 3 days. Specificity was defined as the non-interference by other analytes detected in the region of interest. Linearity was evaluated by correlation values of calibration curves. The limit of quantification (LOQ; equivalent to sensitivity), defined as the lowest concentration of analyte that could be quantified with acceptable accuracy and precision, was estimated by injecting a series of increasingly diluted standard solutions until the signal-to-noise ratio was reduced to 10. The limit of detection (LOD) is defined as the concentration of analyte required to give a signal equal to the background (blank) plus three times the standard deviation of the blank.

Determination of total phenolic content

MeOH extracts have been analyzed according to the Folin-Ciocalteu (FC) colorimetric method. The extracts have been dissolved in MeOH to obtain a concentration of 0.5 mg/mL. Folin-Ciocalteu phenol reagent (0.5 mL) has been added to centrifuge tubes containing 0.5 mL of the extract. The content has been

General experimental procedures

mixed, and 1 mL of a saturated sodium carbonate solution has been added to each tube, followed by adjusting the volume to 10 mL with distilled water. The content in the tubes has been thoroughly mixed by vortex and kept at room temperature for 45 min (until the characteristic blue color developed) and then centrifuged at 3000 rpm for 5 min. Absorbance of the clear supernatant has been measured at 517 nm on a UV-visible spectrophotometer (Evolution 201, Thermo Fisher Scientific, Milan, Italy). A control without FC reagent and a blank with MeOH instead of sample have been included in the assay. The total polyphenol content has been expressed as gallic acid equivalents (GAE $\mu\text{mol}/\text{mg}$ extract, means \pm SD of three determinations) calculated by calibration curves ($y=0.0027x+0.0982$ $R^2 = 0.9929$).

Determination of DPPH Radical Scavenging Activity

The antiradical activity of extracts and vitamin C (positive control) has been determined using the stable 1,1-diphenyl-2-picrylhydrazyl radical (DPPH \cdot). An aliquot (37.5 μL) of the MeOH solution containing different amounts of the extract or vitamin C has been added to 1.5 mL of daily prepared DPPH \cdot solution (0.025 g/L in MeOH); the highest concentration employed was 75 $\mu\text{g}/\text{mL}$. An equal volume (37.5 μL) of the vehicle alone has been added to the control tubes. Absorbance at 517 nm has been measured on a UV-visible spectrophotometer (Evolution 201, Thermo Fisher Scientific, Milan, Italy) 10 min after starting the reaction. The DPPH \cdot concentration in the reaction medium has been calculated from a calibration curve (range = 5–36 $\mu\text{g}/\text{mL}$) analyzed by linear regression ($y = 0.2129x + 40.776$, $R_2= 0.95$). All experiments were carried out in triplicate.

Antioxidant activity (TEAC assay)

The antioxidant activity of the extracts and of the isolated compounds was determined by the Trolox Equivalent Antioxidant Capacity (TEAC) assay as

previously reported. The TEAC value is based on the ability of the antioxidant to scavenge the radical cation 2,2'-azinobis(3-ethylbenzothiazoline-6-sulfonate) ABTS^{•+} by spectrophotometric analysis.

The extracts have been diluted with MeOH to produce solutions of 250, 500, 750, 1.00 µg/mL; the isolated compounds were diluted with MeOH to produce solutions of 0.3, 0.5, 1, and 1.5 mM. The reaction has been initiated by the addition of 1.5 mL of diluted ABTS to 15 µL of each sample solution. Determinations have been repeated three times for each extract. The inhibition percentage of absorbance at 734 nm has been calculated for each concentration relative to a blank absorbance (MeOH) and has been plotted as a function of concentration of compound or standard 6-hydroxy-2,5,7,8-tetramethylchroman-2-carboxylic acid (Trolox). The TEAC value is defined as the concentration of a standard Trolox solution with the same antioxidant capacity as a 1 mg/mL of the tested extract.

TBARS assay: materials and methods

Dimethylsulfoxide (DMSO) and thiobarbituric acid (TBA), H₂O₂ were purchased from Sigma (St. Louis, MO., USA). All the other reagents were of analytical grade and were provided by commercial suppliers. Stock solution of tested compounds and tested plant extract were obtained in 50% DMSO. The final concentration of DMSO in samples was lower than 0.05% and in all the experiments its effects were determined.

Fresh human plasma was obtained from medication – free, regular donors at the blood bank (Lodz, Poland). Samples of human plasma were incubated with 1) the MeOH extract at the final concentrations of 0.1-100 µg/mL (30 min, at 37°C); 2) the MeOH extract at the final concentrations of 0.1-100 µg/mL plus 2 mM H₂O₂ (30 min, at 37°C); 3) the MeOH extract at the final concentration of 10 µg/mL

General experimental procedures

plus 4.7 mM H₂O₂/3.8 mM Fe₂SO₄/2.5 mM EDTA (30 min, at 37°C); 4) tested compounds and curcumin at the final concentrations of 0.1-100 μM (30 min, at 37°C); 5) tested compounds and curcumin at the final concentration of 0.1-100 μM plus 2 mM H₂O₂ (30 min, at 37°C); 6) tested compounds and curcumin at the final concentrations of 10 μM plus 4.7 mM H₂O₂/3.8 mM Fe₂SO₄/2.5 mM EDTA (30 min, at 37°C).

Lipid peroxidation measurement

Lipid peroxidation was quantified by measuring the concentration of TBARS. Incubation of plasma (control, tested compounds or extract - treated plasma) was stopped by cooling the samples in an ice-bath. Samples of plasma were transferred to an equal volume of 20% (v/v) cold trichloroacetic acid in 0.6 M HCl and centrifuged at 1200 x g for 15 min. One volume of clear supernatant was mixed with 0.2 volume of 0.12 M thiobarbituric acid in 0.26 M Tris at pH 7.0 and immersed in a boiling water bath for 15 min, then absorbance at 532 nm was measured⁵⁰. The TBARS concentration was calculated using the molar extinction coefficient ($\epsilon=156,000 \text{ M}^{-1}\text{cm}^{-1}$).

Conclusion

This project has been addressed to the definition of the chemical profile of selected PGI products of Campania region (*C.avellana* cv. Tonda di Giffoni and *C. sativa* cv. Marrone di Roccadaspide) and related byproducts with the aim to highlight the presence of phytochemicals with health benefits.

The phytochemical investigation of *C.avellana* cv. Tonda di Giffoni byproducts allowed us to isolate and characterize, by 1D and 2D NMR experiments, 22 new cyclized diarylheptanoids and diaryletherheptanoids, some of which highly hydroxylated, named giffonins A-V. Cyclized diarylheptanoids were characterized by a C-C bond between C-1 and C-2 positions of the two aromatic rings, while cyclized diaryletherheptanoids were characterized by an ether linkage between C-1 and C-17 of the two aromatic moieties. The MeOH extracts and some of isolated giffonins displayed the ability to prevent oxidative damages of human plasma lipids, induced by H₂O₂ and H₂O₂/Fe²⁺. Moreover, in order to highlight the compounds responsible of property attributed to hazelnut as “heart-healthy” food, a detailed characterization of the lipids occurring in fresh and roasted Tonda di Giffoni hazelnut was performed by LC-ESI/LTQOrbitrap/MS/MSⁿ. LC-MS analysis showed a wide range of compounds from oxylipins and long chain bases to phospholipids, sphingolipids, and glycolipids. Thereby, to the best of our knowledge, this work allowed to obtain the first accurate rationalization of the polar lipids of hazelnut kernels, some of these with known health benefits.

With the aim to achieve deeper insight into the chemical composition of *Castanea sativa* Mill. cv. Marrone di Roccadaspide, the phytochemical investigation of the leaves has been carried out; the phenolic compounds isolated were quantified by LC-ESI/QqQ/MS. Moreover, the ability of isolated compounds to protect HaCaT human keratinocytes from UVB-induced damage has been investigated.

Conclusion

During the PhD stage at the University of Veterinary and Pharmaceutical Sciences, preliminary tests to evaluate the ability of *C.sativa* extracts to inhibit *in vitro* reactive oxygen species formation and NF- κ B activation have been carried out. To explain the strong antioxidant activity of the MeOH extract of *C.sativa* shells, its metabolite profile by LC-ESI/LTQOrbitrap/MS/MSⁿ was carried out. LC-MS led to the identification of a wide range of compounds belonging to different chemical classes such as tannins, in particular hydrolysable tannins, ellagitannins derivatives and condensed tannins; moreover phenolic compounds and triterpenic derivatives were isolated and characterized by NMR and their quantitative determination was carried out by LC-ESI/QTrap/MS/MS.

The obtained results can be useful to enhance the use of byproducts which result waste products and represent a large amount of the total biomass, to protect the reputation of the regional foods and to promote rural and agricultural activity. Moreover, this work highlights that often only MS information is not sufficient to determine the complete profile of plant constituents and reinforces the notion that the combination of LC-MS and NMR analysis is a powerful tool to achieve the truly chemical structure of naturally occurring molecules in food plants.

Publication list

- Masullo, M.; **Cerulli, A.**; Olas, B.; Pizza, C. & Piacente, S. Giffonins A–I, Antioxidant Cyclized Diarylheptanoids from the Leaves of the Hazelnut Tree (*Corylus avellana*), Source of the Italian PGI Product “Nocciola di Giffoni”. *J. Nat. Prod.* **2015**, 78(1), 17-25.
- Masullo, M.; Cantone, V.; **Cerulli, A.**; Lauro, G.; Messano, F.; Russo, G.L.; Pizza, C.; Bifulco, G. & Piacente, S. Giffonins J–P, Highly Hydroxylated Cyclized Diarylheptanoids from the Leaves of *Corylus avellana* Cultivar Tonda di Giffoni. *J. Nat. Prod.* **2015**, 78(12), 2975-2982.
- Masullo, M.; Mari, A.; **Cerulli, A.**; Bottone, A.; Kontek, B.; Olas, B.; Pizza, C. & Piacente, S. Quali-quantitative analysis of the phenolic fraction of the flowers of *Corylus avellana*, source of the Italian PGI product "Nocciola di Giffoni": Isolation of antioxidant diarylheptanoids. *Phytochemistry*. **2016**, 130, 273-281
- **Cerulli, A.**; Lauro, G.; Masullo, M.; Cantone, V.; Olas, B.; Kontek, B.; Nazzaro, F.; Bifulco, & Piacente, S. Cyclic Diarylheptanoids from *Corylus avellana* Green Leafy Covers: Determination of Their Absolute Configurations and Evaluation of Their Antioxidant and Antimicrobial Activities. *J. Nat. Prod.* **2017**, 80, 1703–1713.
- **Cerulli, A.**; Masullo, M.; Mari, A.; Balato, A.; Filosa, R.; Lembo, S.; Napolitano A. & Piacente, S. Phenolics from *Castanea sativa* leaves and their effects on UVB-induced damage. *Natural Product Research*, **2017**, 1-6.
- Masullo, M.; **Cerulli, A.**; Mari, A.; de Souza Santos, C. C.; Pizza, C. & Piacente, S. LC-MS profiling highlights hazelnut (Nocciola di Giffoni

- PGI) shells as a byproduct rich in antioxidant phenolics. *Food Research International*, **2017**, 101 180–187.
- Napolitano, A; **Cerulli, A.**; Pizza, C. & Piacente, S. Multi-class polar lipid profiling in fresh and roasted hazelnut (*Corylus avellana* cultivar Tonda di Giffoni) by LC-ESI/LTQOrbitrap/MS/MSⁿ. *submitted*.
 - Santos de Souza, C., C.; Masullo, M.; **Cerulli, A.**; Mari, A.; Estevam, C. Dos Santos; Pizza, C.; Piacente, S.; Isolation of antioxidant phenolics from *Schinopsis brasiliensis* based on a preliminary LC-MS profiling. *Phytochemistry*, **2017**, 24, 45-51.
 - Mendes de Souza Mesquita, L.; da Rocha, C. Q.; Lima Affonso, L. H.; **Cerulli, A.**; Piacente, S.; Marucci Pereira Tangerina, M.; Gonçalves, Martins, M.B.; Vilegas, W. Phenolic Isomers from *Plantago catharinaea* Leaves: Isolation, Identification, Quantification and in vitro Antioxidant Activity. *Natural Product Communications*, **2017**, 12 (3).
 - Labed, F.; Masullo, M.; **Cerulli, A.**; Benayache, F.; Benayache, S.; Piacente, S. Chemical Constituents of the Aerial Parts of *Santolina chamaecyparissus* and Evaluation of Their Antioxidant Activity. *Natural Product Communications*, **2017**, 12 (10).

Acknowledgements

Firstly, I would like to express my sincere gratitude to my advisor Prof. Sonia Piacente for the continuous support during my PhD study and research, for her patience, motivation, enthusiasm, and immense knowledge. I could not have imagined having a better advisor and mentor for my PhD study.

A special thanks is also extended to Prof. Cosimo Pizza for his enormous knowledge and for his precious suggestions.

I would like to thank Prof. Milena Masullo and Dr. Assunta Napolitano, they represented for me an important help in all the time of research for their encouragement and insightful comments. Without their precious support would not be possible to conduct this research. Moreover, a special thanks to Prof. Paola Montoro for her important help and support.

My sincere thanks to Gilda and Alfredo, they are not only colleagues but very friends.

I would like to express my thanks to Dr. Jan Hosek, University of Veterinary and Pharmaceutical Sciences Brno, for offering me the opportunity to work for a short period in his research group.

Last but not the least, I would like to thank my parents and my sister, they represent my touchstone and my boyfriend Gianluca for his constant presence and immeasurable love.